[redacted]
[redacted]
TRAINING SCHOOL LIBRARY
AEC RESEARCH AND [redacted]
MARTIN MARIETTA ENERGY SYSTEMS LIBRARIES
3 4456 0360948 7

ORNL-1267
Progress

LABORATORY RECORDS
1954
DECLASSIFIED
CLASSIFICATION CHANGED TO: AEC-10, 9-55
BY AUTHORITY OF: 7-1-62
BY: [illegible]

METALLURGY DIVISION

QUARTERLY PROGRESS REPORT

FOR PERIOD ENDING JANUARY 31, 1952

CENTRAL RESEARCH LIBRARY
DOCUMENT COLLECTION
LIBRARY LOAN COPY
DO NOT TRANSFER TO ANOTHER PERSON
If you wish someone else to see this document, send in name with document and the library will arrange a loan.

OAK RIDGE NATIONAL LABORATORY
OPERATED BY
CARBIDE AND CARBON CHEMICALS COMPANY
A DIVISION OF UNION CARBIDE AND CARBON CORPORATION
UCC
POST OFFICE BOX P
OAK RIDGE, TENNESSEE

[redacted]
[redacted]

[redacted]

ORNL 1267

This document consists of 168 pages.

Copy 8 of 146 copies. Series A.

Contract No. W-7405-eng-26

METALLURGY DIVISION

QUARTERLY PROGRESS REPORT

for Period Ending January 31, 1952

J. H. Frye, Jr., Director

EDITED BY

W. H. Bridges

DATE ISSUED

AUG 12 1952

OAK RIDGE NATIONAL LABORATORY
operated by
CARBIDE AND CARBON CHEMICALS COMPANY
A Division of Union Carbide and Carbon Corporation
Post Office Box P
Oak Ridge, Tennessee

[redacted]

MARTIN MARIETTA ENERGY SYSTEMS LIBRARIES

3 4456 0360948 7

[redacted]

[redacted]

ORNL 1267
Progress

INTERNAL DISTRIBUTION

1. G. T. Felbeck (C&CCC)
2-3. Chemistry Library
4. Physics Library
5. Biology Library
6. Health Physics Library
7. Metallurgy Library
8-9. Training School Library
10. Reactor Experimental Engineering Library
11-14. Central Files
15. C. E. Center
16. C. E. Larson
17. W. B. Humes (K-25)
18. L. B. Emlet (Y-12)
19. A. M. Weinberg
20. E. H. Taylor
21. E. J. Murphy
22. E. D. Shipley
23. J. H. Frye, Jr.
24. F. C. VonderLage
25. R. C. Briant
26. J. A. Swartout
27. S. C. Lind
28. F. L. Steahly
29. A. H. Snell
30. A. Hollaender
31. M. T. Kelley
32. K. Z. Morgan
33. J. S. Felton
34. A. S. Householder
35. C. S. Harrill
36. C. E. Winters
37. D. S. Billington
38. D. W. Cardwell
39. E. M. King
40. A. J. Miller
41. D. D. Cowen
42. P. M. Reyling
43. W. H. Bridges
44. A. G. H. Andersen
45. L. K. Jetter
46. E. J. Boyle
47. W. D. Manly
48. C. D. Susano
49. W. W. Parkinson
50. R. J. Gray
51. B. S. Borie
52. D. C. Vreeland
53. D. E. Harpy
54. E. E. Stansbury
55. G. E. Smith
56. J. E. Cunningham
57. Anton Brasunas
58. R. S. Crouse
59. R. E. Adams
60. J. H. Erwin
61. J. O. Betterton, Jr.
62. L. D. Dyer
63. G. M. Adamson
64. E. S. Bomar
65. F. H. Eckert
66. R. B. Day
67. T. W. Fulton
68. W. J. Freeague
69. R. B. Oliver
70. P. Patriarca
71. J. T. Howe
72. T. H. Blewitt
73. W. E. Taylor
74. J. H. Crawford, Jr.

[redacted]

[redacted]

75. A. F. Cohen
76. J. C. Wilson
77. H. W. Savage
78. E. E. Hoffman
79. W. J. Leonard
80. J. A. Miller
81. J. M. Warde
82-85. Central Files (O.P.)

[redacted]

EXTERNAL DISTRIBUTION

86-93. Argonne National Laboratory
94-101. Atomic Energy Commission, Washington
102. Battelle Memorial Institute
103-106. Brookhaven National Laboratory
107-110. Carbide and Carbon Chemicals Company (Y-12)
111-112. Knolls Atomic Power Laboratory
113-114. General Electric Company, Richland
115-117. General Electric Company (ANPP)
118. Hanford Operations Office
119-122. Los Alamos
123. Massachusetts Institute of Technology (Kaufmann)
124-125. New York Operations Office
126. Patent Branch, Washington
127. Savannah River Operations Office, Wilmington
128-142. Technical Information Service, Oak Ridge
143-146. University of California Radiation Laboratory

[redacted]

[redacted]

Reports previously issued in this series are as follows:

ORNL-28	Period Ending March 1, 1948
ORNL-69	Period Ending May 31, 1948
ORNL-407	Period Ending July 31, 1949
ORNL-511	Period Ending October 31, 1949
ORNL-583	Period Ending January 31, 1950
ORNL-754	Period Ending April 30, 1950
ORNL-827	Period Ending July 31, 1950
ORNL-910	Period Ending October 31, 1950
ORNL-987	Period Ending January 31, 1951
ORNL-1033	Period Ending April 30, 1951
ORNL-1108	Period Ending July 31, 1951
ORNL-1161	Period Ending October 31, 1951

[redacted]

[redacted]

[redacted]

TABLE OF CONTENTS

	PAGE
SUMMARY	1
THORIUM RESEARCH PROGRAM	5
Development of Alloys	5
Mechanical Properties of Thorium	6
Fabrication	9
Rolling	9
Extrusion	10
SLUG PROBLEM	19
PREFERRED ORIENTATION AND ANISOTROPY IN METALS	21
FUNDAMENTAL STUDIES OF ALLOYING	39
Silver-Zirconium System	42
Indium-Zirconium System	47
Antimony-Zirconium System	47
Magnesium-Zirconium System	48
ANP PROGRAM	51
Static Corrosion	51
Low melting point alloy coolants	51
Corrosion by sodium-lead alloy coolants	51
Corrosion by fluorides	51
Temperature-dependence tests	60
Corrosion by sodium hydroxide	60
Dynamic Corrosion	63
Physical Metallurgy of Liquid Metal Corrosion	67
Seesaw tests	67
Standpipe tests	72

[redacted]

[redacted]

	PAGE
Physical Chemistry of Liquid Metals	72
Description of apparatus	74
Experimental procedure	76
Results	77
Conclusions	85
Future experiments	85
Structure of Liquid Lead and Bismuth	85
Experimental procedure and results	88
Analysis of diffraction patterns	88
Fabrication	93
Fuel elements	93
ARE control rod	97
Mechanical Properties of Metals	101
Thorium	101
Uranium	101
Inconel	105
Stainless steel	105
Welding Laboratory	105
Cone-arc welding	105
Brazing	111
Ceramics	116
HRP METALLURGY	119
HRE Control Rod	120
X-RAY LABORATORY	123
Low-Temperature X-Ray Diffraction	123
Service Work	126
METALLOGRAPHY LABORATORY	127
Metallography of Zirconium and Its Alloys	127
Remotely Controlled Polishing Unit	128
FUEL PLATE DEVELOPMENT FOR GENERAL ELECTRIC COMPANY	141

[redacted]

[redacted]

	PAGE
MTR FABRICATION	145
Fuel Unit and Control Element Fabrication	145
Cladding of Thorium with Aluminum	146
Service Work	146
Boral rolling	146
Uranium rolling	146

[redacted]

[redacted]

[redacted]

LIST OF FIGURES

FIGURE	TITLE	PAGE
1	Hardness of As-Arc-Cast Thorium-Carbon Alloys	11
2	Hardness of Thorium-Carbon Alloys After Homogenization for 24 hr in Vacuum at 950°C	11
3	Hardness of Thorium-Carbon Alloys After a Quench from 1600°C	12
4	Hardness of Thorium-Carbon Alloys After a Quench from 1500°C	12
5	Hardness of Thorium-Carbon Alloys After a Quench from 1400°C.	12
6	Hardness of Thorium-Carbon Alloys After a Quench from 1300°C	13
7	Hardness of Thorium-Carbon Alloys After a Quench from 1200°C	13
8	Hardness of Thorium-Carbon Alloys After a Quench from 1100°C	13
9	Hardness of Thorium-Carbon Alloys After a Quench from 1000°C	14
10	Hardness of Thorium-Carbon Alloys After a Quench from 800°C	14
11	Hardness of Thorium-Carbon Alloys After a Quench from 600°C	14
12	Hardness of Thorium-Carbon Alloys After a Quench from 400°C	14
13	Hardness of As-Cast Thorium-Oxygen Alloys	15
14	Hardness of Thorium-Oxygen Alloy After Homogenization at 950°C for 24 Hours	15
15	Cast Ingot of Ames Thorium Marked for Proper Cutting into Smaller Pieces for Rolling Investigation	16
16	Thorium Plate Cracked During Rolling	17
17	Diagram Showing the Orientation of the X-Ray Diffraction Specimen with Respect to the Principal Directions of a Section	22

[redacted]

[redacted]

[redacted]

FIGURE	TITLE	PAGE
18	Relationship Between Orientation of X-Ray-Diffraction Specimen with Respect to the Normal to the Reflecting Plane and the Position on the Stereographic Net	23
19	Special Goniometer and the Diffraction Specimen Mounted on a Horizontal X-Ray-Diffraction Spectrometer	24
20	Arrangement for Machining Spherical X-Ray-Diffraction Specimens	25
21	Preferred Arrangement for Machining Spherical X-Ray-Diffraction Specimens	25
22	Longitudinal Section of 1-in.-dia Extruded Thorium Rod in As-Extruded Condition Showing Deformed Grain Structure	30
23	Longitudinal Section of 1-in.-dia Extruded Thorium Rod in As-Extruded Condition Showing Completely Recrystallized Grain Structure	30
24	Longitudinal Section of 1-in.-dia Extruded Thorium Rod in As-Extruded Condition Showing Nearly Completely Recrystallized Grain Structure	30
25	Preferred Orientation Plot – (111) – 1-in.-dia Extruded Thorium Rod	31
26	Preferred Orientation Plot – (200) – 1-in.-dia Extruded Thorium Rod	31
27	Preferred Orientation Plot – (220) – 1-in.-dia Extruded Thorium Rod	32
28	Preferred Orientation Plot – (311) – 1-in.-dia Extruded Thorium Rod	32
29	Preferred Orientation Plot – (111) – 1-in.-dia Extruded Thorium Rod	33
30	Preferred Orientation Plot – (200) – 1-in.-dia Extruded Thorium Rod	33

[redacted]

[redacted]

[redacted]

FIGURE	TITLE	PAGE
31	Preferred Orientation Plot - (220) - 1-in.-dia Extruded Thorium Rod	34
32	Preferred Orientation Plot - (311) - 1-in.-dia Extruded Thorium Rod	34
33	Preferred Orientation Plot - (111) - 1-in.-dia Extruded Thorium Rod	35
34	Preferred Orientation Plot - (200) - 1-in.-dia Extruded Thorium Rod	35
35	Preferred Orientation Plot - (220) - 1-in.-dia Extruded Thorium Rod	36
36	Preferred Orientation Plot - (311) - 1-in.-dia Extruded Thorium Rod	36
37	Preferred Orientation Plot - (111) - 1-in.-dia Extruded Thorium Rod	37
38	Preferred Orientation Plot - (200) - 1-in.-dia Extruded Thorium Rod	37
39	Preferred Orientation Plot - (220) - 1-in.-dia Extruded Thorium Rod	38
40	Preferred Orientation Plot - (311) - 1-in.-dia Extruded Thorium Rod	38
41	Effect of Vacuum Pressure on Hardness and Weight Change of Zirconium Specimens Annealed for Two Days at 1000°C	40
42	Microstructure of Silver-Zirconium Alloy, 3.8 at. % Silver, Annealed 64 hr at 975°C, Showing Decomposed Beta Phase	44
43	Microstructure of Silver-Zirconium Alloy, 8.7 at. % Silver, Annealed 8 3/4 Days at 978°C, Showing Particles of Compound, Probably Ag_3Zr, Arranged in a Widmansatten Pattern on a Matrix of Decomposed Beta Phase	44

[redacted]

[redacted]

[redacted]

FIGURE	TITLE	PAGE
44	Microstructure of Silver-Zirconium Alloy, 0.77 at. % Silver, Annealed 12 Days at 802°C, Showing Two Eutectoid Areas in Alpha-Phase Matrix	45
45	Microstructure of Silver-Zirconium Alloy, 2.9 at. % Silver, Annealed 12 Days at 802°C, Showing Small, Dark Particles of Compound, Probably Ag_3Zr, in a Matrix of Decomposed Beta Phase	45
46*a*	Silver-Zirconium Alloy, 0.77 at. % Silver, Annealed 48 hr at 1011°C, Quenched from the Beta Region, Showing the Decomposed Beta Phase and the Acicular or Basket-Weave Structure Typical of the Zirconium Reaction $\beta \rightleftharpoons \alpha$ During Quenching	46
46*b*	Silver-Zirconium Alloy, 0.77 at. % Silver, Annealed 12 Days at 802°C, Quenched from the Alpha Region, Showing the Alpha Phase with a Small Amount of Eutectoid	46
47	Microstructure of a Zirconium Alloy Containing About 2.7 at. % Antimony in the As-Cast Condition	48
48	Zirconium-Magnesium Diffusion Couple Quenched After 5 Days at 762°C	49
49	Type-310 Stainless Steel Tested in 43% Sn-57% Bi Alloy for 100 hr at 816°C in Vacuum	52
50	Type-310 Stainless Steel Tested in 44.5% Pb-55.5% Bi Alloy for 100 hr at 816°C in Vacuum	52
51	Inconel Tested in 43% Sn-57% Bi for 100 hr at 816°C in Vacuum	53
52	Type-317 Stainless Steel Tested in 60% Bi-40% Cd for 100 hr at 816°C in Vacuum	53
53	Inconel Tested in Unpretreated Fluoride Mixture No. 14 for 100 hr at 816°C in Vacuum	56

[redacted]

[redacted]

[redacted]

FIGURE	TITLE	PAGE
54	Inconel Tested in Pretreated Fluoride Mixture No. 14 for 100 hr at 816°C in Vacuum	56
55	Type-309 Stainless Steel Tested in Unpretreated Fluoride Mixture No. 14 for 100 hr at 816°C in Vacuum	57
56	Type-309 Stainless Steel Tested in Pretreated Fluoride Mixture No. 14 for 100 hr at 816°C in Vacuum	57
57	Inconel Tested in Unpretreated Fluoride Mixture No. 14 Plus 2% Magnesium for 100 hr at 816°C in Vacuum	58
58	Type-309 Stainless Steel Tested in Unpretreated Fluoride Mixture No. 14 Plus 2% Magnesium for 100 hr at 816°C in Vacuum	58
59	Inconel Tested in Unpretreated Fluoride Mixture No. 14 Plus 2% Zirconium for 100 hr at 816°C in Vacuum	59
60	Type-309 Stainless Steel Tested in Fluoride Mixture No. 14 Plus 2% Zirconium for 100 hr at 816°C in Vacuum	59
61	Inconel Tested in Sodium Hydroxide for 100 hr at 816°C in Vacuum	62
62	Inconel Tested in 51% NaOH-49% NaCN for 100 hr at 816°C in Vacuum	62
63	Hot-Leg Section of Inconel Convection Loop After Circulating Fulinak at 1500°F for 500 Hours	66
64	Cold-Leg Section of Inconel Convection Loop After Circulating Fulinak at 1500°F for 500 Hours	66
65	Rocking Furnace used in Making Seesaw Tests	68
66	Typical Seesaw Test Specimen	68
67	Sectioned View of Nickel Tube Containing Sodium Hydroxide After 14,000 Cycles (117 hr) in Seesaw Unit	68

[redacted]

[redacted]

[redacted]

FIGURE	TITLE	PAGE
68	Nickel Crystal Observed on Wall of Cold End of Nickel Tube Containing Sodium Hydroxide (Fig. 67)	69
69	Polished Nickel Surface on Wall on Hot End of Nickel Tube (Fig. 67)	69
70	Nonmetallic Crystals Obtained from Cold End of Nickel Tube Containing Sodium Hydroxide	70
71	Metal Crystals Deposited on Comb-like Nickel Oxide Crystals in Cold End of Test SS-4a (Fig. 70)	70
72	Metal Crystals at the Surface of the Hot Zone Tube	71
73	Crystals in the Cold Zone	71
74	Sectional View of Thermal-Gradient Furnace for Standpipe Tests	73
75	Thermal Convection Loop	75
76	Nickel-Sodium Hydroxide Thermal Convection Loop No. 1	79
77	Nickel-Sodium Hydroxide Thermal Convection Loop No. 3	80
78	Nickel-Sodium Hydroxide Thermal Convection Loop No. 4	81
79	Hot Leg of Nickel-Sodium Hydroxide Loop No. 1 Showing Polished Surface	82
80	Polished Surface in Hot Leg of Nickel-Sodium Hydroxide Loop No. 1	84
81	Cross Section of Cold Leg of Nickel-Sodium Hydroxide Loop No. 1	84
82	Heavy Deposits in Top Cross Piece of Nickel-Sodium Hydroxide Loop No. 3	84
83	Inconel-Potassium Hydroxide Convection Loop No. 5	86

[redacted]

[redacted]

[redacted]

FIGURE	TITLE	PAGE
84	Surface of Hot Leg of Inconel-Potassium Hydroxide Loop No. 5	87
85	Surface of Cold Leg of Inconel-Potassium Hydroxide Loop No. 5	87
86	Surface of Untreated Section of Inconel-Potassium Hydroxide Loop No. 5	87
87	Intensity Curves for Liquid Lead	92
88	Intensity Curves for Liquid Bismuth	92
89	Distribution Curves for Liquid Lead	93
90	Distribution Curves for Liquid Bismuth	93
91	$W(R)$ Functions for Liquid Lead	94
92	$W(R)$ Functions for Liquid Bismuth	94
93	Transverse Section Through 1/4-in.-OD Tubes Prepared from Rolled Plate	96
94	Transverse Section Through 1/4-in.-OD Tube Prepared by Rubberstatic Pressing	97
95	Solid-Phase-Welding Test Equipment	99
96	Creep of Thorium	102
97	Creep Rate of Thorium	103
98	Stress-to-Rupture Plot for Normal Uranium	104
99	Creep Rate of Normal Uranium	106
100	Stress-to-Rupture Plot for Type-316 Stainless Steel	107
101	Schematic Diagram of Cone-Arc Welding Circuit	108

[redacted]

[redacted]

[redacted]

FIGURE	TITLE	PAGE
102	Iron Filing Pattern of the Magnetic Lines of Flux of a Permanent Alnico Magnet	110
103	Typical Heat Exchanger Component Fabricated by Brazing	112
104	As-Polished Nicrobrazed Slug Showing Various Intermetallics	114
105	As-Polished Nicrobrazed Slug After Corrosion Testing in Sodium Hydroxide for 100 hr at 1500°F	114
106	As-Polished Nicrobrazed Slug After Corrosion Testing in Unpretreated Fluoride Mixture No. 14 for 100 hr at 1500°F	115
107	Nicrobrazed Inconel Tube-To-Header Joints Corrosion Tested for 100 hr at 1500°F	115
108	Boral–Stainless Steel Interface of Thermally Cycled Sample	121
109	Low-Temperature Specimen Holder for High-Angle X-Ray Spectrometer	124
110	Low-Temperature Specimen Holder in Place on X-Ray Spectrometer	125
111	As-Cast Zirconium-Tungsten Alloy	131
112	Zirconium-Tungsten Alloy Heated at 800°C for 1 hr and Slowly Cooled	131
113	Zirconium-Tungsten Alloy Heated at 900°C for 1 hr and Slowly Cooled	131
114	Section Shown in Fig. 113	131
115	Zirconium-Tungsten Alloy Heated at 900°C for 1 hr and Slowly Cooled	132
116	Zirconium-Tungsten Alloy Heated at 900°C for 1 hr and Water Quenched	132

[redacted]

[redacted]

[redacted]

FIGURE	TITLE	PAGE
117	Zirconium-Tungsten Alloy Heated at 990°C for 4 1/2 hr, Slowly Cooled for 1 hr, and Water Quenched	132
118	As-Cast Zirconium-Tungsten Alloy (4.91 wt % W)	133
119	Zirconium-Tungsten Alloy (4.91 wt % W) Heated at 800°C for 1 hr and Slowly Cooled	133
120	Zirconium-Tungsten Alloy (4.91 wt % W) Heated at 900°C for 1 hr and Slowly Cooled	133
121	Zirconium-Tungsten Alloy (4.91 wt % W) Heated at 900°C for 1 hr and Water Quenched	133
122	As-Cast Zirconium-Tungsten Alloy (5.72 wt % W)	134
123	Zirconium-Tungsten Alloy (5.72 wt % W) Heated at 800°C for 1 hr and Slowly Cooled	134
124	Zirconium-Tungsten Alloy (5.72 wt % W) Heated at 900°C for 1 hr and Slowly Cooled	134
125	Zirconium-Tungsten Alloy (5.72 wt % W) Heated at 900°C for 1 hr and Water Quenched	134
126	Polishing Unit with Rotator for Holding Four Specimens; Specimen Mount with Steel Washer; Lead Shot for Weight Variation	135
127	Thinner, Applicator Gun, and Refill Cartridge	136
128	Inconel	137
129	Type-347 Stainless Steel After Corrosion Test	137
130	Inconel Tube Brazed to Copper	138
131	Mild Steel Showing Dark Pearlite Patches in a Matrix of Alpha Ferrite	138

[redacted]

[redacted]

[redacted]

FIGURE	TITLE	PAGE
132	Tungsten	139
133	Molybdenum with a Surface Layer of $MoSi_2$	139
134	As-Received Stainless Steel Sandwich	142
135	Effect of Hot Rolling on Stainless Steel Sandwich	142
136	Effect of Total Cold Reduction on Stainless Steel Sandwich	143
137	Stainless Steel Sandwich 30% Cold Worked Plus Annealed Plus 24% Cold Worked Plus Annealed Plus 17% Cold Worked	144
138	Transverse Section of an Alclad Thorium Sample Showing Thickness of Aluminum Cladding	147
139	Transverse Section of an Alclad Thorium Sample Showing Continuous Bond and Intermetallic Compound at Aluminum-Thorium Interface	147

[redacted]

[redacted]

[redacted]

LIST OF TABLES

TABLE	TITLE	PAGE
1	Hardness Values of Arc-Cast Thorium-Carbon Alloys	5
2	Hardness of Thorium-Carbon Alloys After Homogenization at 950°C for 24 Hours	6
3	Hardness of Thorium-Carbon Alloys After Quenching from Various Temperatures	7
4	Hardness of Arc-Cast Thorium-Oxygen Alloys	7
5	Hardness of Thorium-Oxygen Alloys After Homogenization at 950°C for 24 Hours	7
6	Tensile Test Data for Ames Remelted Thorium and Ames Virgin Thorium	8
7	Tensile Test Data for As-Cast Ames Thorium	9
8	Fabricating Conditions and Results of Examination of Extruded Thorium Rod	28
9	Weight Change and Hardness of Small Zirconium Specimens After Annealing for Two Days at 1000°C in Quartz Capsules Under Various Conditions	41
10	Hardness and Weight Changes in 2- to 3-g Specimens of Iodide-Deposited Zirconium That Were Degassed Only	42
11	Corrosion of Types-310 and -317 Stainless Steel and Inconel Tested in Various Low Melting Point Eutectic Alloys for 100 hr at 816°C in Vacuum	54
12	Corrosion of Types-316, -317, and -446 Stainless Steel Tested in Sodium-Lead Alloy for 100 hr at 816°C in Vacuum	55
13	Corrosion of Inconel and Type-309 Stainless Steel Tested in Fluoride Mixture No. 14 for 100 hr at 816°C in Vacuum	60

[redacted]

[redacted]

[redacted]

TABLE	TITLE	PAGE
14	Corrosion of Various Metals Tested in Fluoride Mixture No. 2 for 100 hr at 816°C in Vacuum	61
15	Temperature-Dependence Tests in Fluoride Mixture No. 2 for 100 hr in Vacuum	63
16	Corrosion of Various Metals Tested in Sodium Hydroxide and Sodium Hydroxide plus Additions for 100 hr at 816°C in Vacuum	64
17	Results of Preliminary Dynamic Screening Tests in Thermal Convection Loops	65
18	Summary of Test Conditions for Nickel-Sodium Hydroxide Loops	78
19	Summary of Neutron-Diffraction Runs for Determining the Structures of Liquid Lead and Liquid Bismuth	89
20	Dimensions and Constants Used	91
21	Core Compositions of Various Tubes	94
22	Summation of the Reduction Schedule	95
23	Results of Bonding Tests	100
24	Treatment of Pressed Boral Cores	121
25	Lattice Constants of Ammonium Bromide as a Function of Temperature	123
26	Analyses of a Blank Melt and Three Alloys of Tungsten	127
27	Hardness Values of a Blank Melt and Three Alloys of Tungsten	128

[redacted]

[redacted]

METALLURGY DIVISION QUARTERLY PROGRESS REPORT

SUMMARY

The program for developing thorium alloys has continued with further work being done to evaluate a series of carbon and oxygen alloys made with high-purity, iodide crystal-bar thorium. Both carbon and oxygen considerably increase the hardness of the iodide metal. Maximum observed hardness of the carbon alloys was found to be about Rockwell *B* 100 at 1% carbon. A maximum hardness of Rockwell *H* 70 was found in the carbon-oxygen series at about 0.3% oxygen. The hardness of the carbon and oxygen alloys was essentially unchanged after homogenization for 24 hr at 950°C. Quenching of the thorium-carbon alloys from various temperatures ranging from 1600 to 400°C appeared to produce definite changes in the hardness of the alloys. These changes in hardness seem to indicate increased solubility of the carbon at the higher temperatures.

Preliminary data on the mechanical properties of thorium made by remelting turnings of Ames metal indicate that the properties of this material are within the range of values obtained for virgin metal produced at Ames. The remelted metal shows a slightly higher impurity content, particularly carbon and nitrogen, than normal production of Ames metal, and this is reflected in a ductility slightly lower than usual.

Preferred orientation studies of extruded thorium show that very slow extrusions, 2.7 ft/min, produce material with a deformation texture. Specimens are being prepared to compare mechanical properties of this material with metal extruded at fast rates, 200 to 600 ft/min, which showed a recrystallization texture.

Tensile specimens of cast Ames thorium were tested and found to be comparable with extruded material, except for slightly less ductility. The cast material was used to start an investigation of rolling variables. There is some indication that the material given a preliminary breakdown at 1200°F is inferior to material given a breakdown at 1450°F. Cracking was encountered while rolling the material subsequent to the 1200°F preliminary rolling even though the metal can be cold rolled successfully if the 1200°F rolling is eliminated.

The triple-dip process previously used to can bonded Clinton slugs was discontinued since the complete elimination of the undesirable residual tin was difficult to achieve. The alpha-canning technique used by Argonne National Laboratory was adopted and with one refinement, the use of a flux over the duplex aluminum-silicon and lead bath, the method appears to be giving good results.

A method has been developed for making complete and quantitative texture studies with only one specimen and without complicated corrections. The use of a spherical specimen mounted in a modified goniometer of a Geiger-counter x-ray-diffraction spectrometer is unique. Analysis of the x-ray-diffraction data from spherical specimens of thorium indicates that extruded thorium rod developes a deformation texture similar to that developed by other face-centered cubic metals. The recrystallization texture differs in that there is no retention of either component of deformation texture and no [112] fiber texture development. The well-developed deformation texture leads to marked

anisotropy in mechanical properties of the rod, and it is presumed that the longitudinal mechanical strength of a rod with recrystallization texture will be less than one with deformation texture.

The fundamental study of alloying has begun with the investigation of the influence of zirconium on the valency of silver, cadmium, indium, tin, and antimony. These *B* subgroup solute elements extend along the same horizontal row of the periodic table as zirconium and are considered to have valencies of 1, 2, 3, 4, and 5, respectively. The preparation of the zirconium alloys is experimentally difficult. In particular, the appropriate container materials and atmospheres must be found for the vacuum-arc furnace used to prepare certain of the alloys and for the annealing furnaces.

Static corrosion tests with low melting point alloys have indicated that those containing tin are very corrosive, but 82% lead–18% cadmium alloy and 60% bismuth–40% cadmium might be contained in type-317 stainless steel. Two alloys of sodium and lead (50% Na and 80% Na) were tested with several stainless steels and with Inconel. No severe attack was found. Pretreated fluoride mixtures show less attack on type-309 stainless steel and Inconel than do unpretreated mixtures. Additions of magnesium metal to the fluoride mixture tend to increase corrosiveness, and additions of zirconium tend to lessen corrosion. The addition of 50% sodium cyanide to sodium hydroxide resulted in a change in the character of attack on type-316 stainless steel and Inconel. Additions to sodium hydroxide of zirconium, sodium carbonate, sodium metal, and sodium hydride were also tried and gave erratic results.

Thus far no material may be described as satisfactory in dynamic corrosion testing of fluoride mixtures at 1500°F. Preliminary dynamic screening tests are being made with thermal convection loops, which plug after a relatively short period of operation. The mechanism and nature of the plugging are to be determined.

The phenomenon of mass transfer (the removal of metal from one part of a system and deposition in another part) in materials containing molten media is under investigation. Since it seems necessary that a thermal gradient be present, two types of apparatus are being used by the Physical Metallurgy of Corrosion group in an attempt to gain a better understanding of the phenomenon and its mechanism. In the first apparatus tubes of various materials are partly filled with the transfer media under investigation. A temperature gradient is established between the ends, and the tube is rocked 20 deg above and below horizontal. For the second type of test a long tube is mounted vertically in a furnace so that a hot zone is produced in the center and cooler zones at either end. Thus far, nickel and Inconel have been used with sodium hydroxide and mixed fluorides.

In order to determine the role of oxygen in mass transfer, the Physical Chemistry group has operated small thermal convection loops under well-controlled conditions. Loops constructed of nickel and filled with sodium hydroxide produced mass transfer. The presence of oxygen increased corrosion and the presence of hydrogen may completely eliminate it. An Inconel loop containing potassium hydroxide produced no mass transfer or other corrosive effects when operated at a maximum of 715°C under a hydrogen atmosphere.

The structures of liquid lead and liquid bismuth have been studied by neutron diffraction. The results appear to be in excellent agreement with x-ray-diffraction results and superior to previous neutron-diffraction work. New details, which had not previously been reported, have been observed in the structure of these liquid metals.

The fabrication of tubular laminates for fuel elements by joining two semicircular plates and subsequently reducing the diameter by drawing shows some promise. Picture-frame techniques were used to prepare the powder-core plates for forming. A schedule of severe reductions produced only fair elements, and further work is necessary to determine the proper reduction schedule.

The creep testing of thorium, uranium, and Inconel continues. The testing of type-316 stainless steel is in abeyance pending the completion of the Inconel tests.

The Welding group is making further studies of the application and limitations of the cone-arc welding process for making tube-to-header joints. The cone-arc process involves the use of a magnetic field established about the welding arc in such a way as to make the arc rotate rapidly about the tip, which results in uniform fusion of the work. A comprehensive study of the welding variables, beginning with arc current, is under way. Since brazing is a possible fabrication technique for heat exchangers, a program has been started for evaluating various brazing alloys for high-temperature service. The continuous removal of oxide scale by dry hydrogen appears to be necessary for successful joining. Corrosion testing of joints brazed with Nicrobraz has been done in sodium hydroxide and in fluoride mixtures. Both media attack the brazing alloy and preferentially leach the boron. Other brazing alloys are being corrosion tested.

The procurement of personnel and equipment for the ceramics laboratory is essentially complete. A program has been established that is broad in scope and will encompass projects of immediate interest, as well as those with long-range objectives. A study of hafnia has started and experience has been gained in fabricating and processing it. A program for the development of ceramic coatings for stainless steel is well under way.

The Division has been asked to coordinate the metallurgical phases of the HRP. This will include evaluation of potential structural materials such as the stainless steels, titanium, zirconium, and other possible alternates; development of specifications and procedures for fabricating, welding, cladding, and lining these materials; metallurgical assistance to the HRP Corrosion Section; nondestructive testing; radiation damage studies; and a variety of metallographic and other service work.

A low-temperature specimen holder for use with the high-angle x-ray spectrometer has been completed. The possibility of a low-temperature transformation in thorium involving only a sudden change in lattice constant is being investigated. As yet no such change has been found. The specimen holder has also been used in the measurement of the tetragonal phase of ammonium bromide.

The laboratory has completed its portion of the joint program for the investigation of the metallography of zirconium and its alloys with the study of zirconium-tungsten alloys containing up to 5.72% tungsten.

An automatic polishing machine has been completed for the purpose of preparing metallographic specimens with radiation levels that are too high for use of the usual manual techniques. Tests have been made on polishing Inconel, type-347 stainless steel (after a corrosion test), copper, mild steel, tungsten, and molybdenum with very satisfactory results.

A suitable fuel element manufacturing process for the direct-cycle aircraft reactor is under development. Stainless steel sandwiches with a core of uranium oxide were used, and it was desired to roll these from 0.190 in. in thickness to 0.014 inch. The variables of rolling temperature, reduction per pass, and ratio of hot work to cold work for finishing to final dimensions were investigated and a rolling schedule evolved.

The fabrication of fuel and control rod elements for the MTR continues. Barring failure of outside vendors to meet their schedules, the initial loading units will be ready by March 1, 1952.

THORIUM RESEARCH PROGRAM

D. E. Hamby W. J. Fretague
R. E. Adams J. A. Milko

DEVELOPMENT OF ALLOYS

Work has continued on alloying carbon and oxygen with high-purity, iodide crystal-bar thorium. The methods of preparation and homogenization of the alloys were given in a previous report.[1] The homogenized samples were quenched from various elevated temperatures, 400 to 1600°C, to establish the solubility limit. The quenching procedure was as follows: The homogenized arc melts were cut into 1/4-in. cubes and placed on a circular, alundum block that was suspended by a tungsten wire in a vertical-tube Globar furnace. A calibrated platinum-to-platinum, 10% rhodium thermocouple was inserted with the specimens. The high-temperature refractory tube was closed on each end with rubber stoppers in which the necessary gas inlet and outlet lines were provided. A positive pressure (indicated by bubbling bottle) of argon, which had been purified by passing tank argon over zirconium chips at 800°C, was maintained over the specimens at all times. The specimens were held at the desired temperature for 15 min to ensure an equilibrium condition. The bottom stopper was removed, and immediately afterwards the tungsten wire was cut to allow the specimens to fall into a container of water for quenching. It was felt that this method yielded the structure at the particular temperature of interest and also a relative freedom from contaminants such as oxygen and nitrogen.

The hardness values for the as-arc-cast thorium-carbon alloys are shown in Table 1. It may be seen that the addition of carbon to iodide thorium increases the hardness markedly. The hardness of the 0.07% carbon alloy is approximately R_B 15, whereas the hardness of the 2.5% carbon alloy is R_B 108, an increase of about 90 points. It should be noted that the addition of 0.11% carbon (an amount frequently present in Ames thorium) to the iodide metal increased the hardness at least 50 points on the R_B scale. (Recent determinations of the hardness of iodide thorium showed R_H 52 to 55, which is less than R_B 1. More precise comparisons of hardness values are being made.)

TABLE 1

Hardness Values of As-Arc-Cast Thorium-Carbon Alloys

ALLOY NO.	CARBON (wt %)	HARDNESS		NUMBER OF DETERMINATIONS AVERAGED
		R_A	R_B*	
F-8	0.07	19	15	5
F-13	0.09	24	24	5
F-3	0.11	36	52	5
F-6	0.20	46	74	5
F-9	0.26	51	83	5
F-11	0.50	57	93	5
F-19	1.05		107	5
F-17	1.42		106	7
F-20	2.50		108	7

*Converted value.

(1) "Thorium-Alloy Development," *Metallurgy Division Quarterly Progress Report for Period Ending October 31, 1951*, ORNL-1161, p. 3.

The hardness data are shown graphically in Fig. 1, and it appears that maximum hardness is obtained with the addition of about 1% of carbon to the iodide thorium. The curve of Fig. 2 and data in Table 2 show that the homogenization treatment (950°C for 24 hr) had little, if any, effect on the hardness of the alloys.

TABLE 2

Hardness of Thorium-Carbon Alloys After Homogenization at 950°C for 24 Hours

ALLOY NO.	CARBON (wt %)	HARDNESS		NUMBER OF DETERMINATIONS AVERAGED
		R_A	R_B*	
F-8	0.07	22	20	17
F-13	0.09	29	36	20
F-3	0.11	37	54	19
F-6	0.20	45	72	24
F-9	0.26	49	79	25
F-11	0.50	57	93	14
F-19	1.05	63	104	12
F-17	1.42	66	108	13
F-20	2.50	65	107	9

*Converted value.

Hardness values are shown in Table 3 for the nine thorium-carbon alloys after quenching from various temperatures ranging from 400 to 1600°C. These data are shown graphically in Figs. 3 through 12. It may be noted that the hardness of any particular alloy increases noticeably as the quenching temperature is increased. Furthermore, alloys of 0.26% carbon and above develop high hardness values even after a quench from 800°C. No definite significance can be attached at this time to the inflection above 0.26% carbon of the curves of Figs. 3 through 9. Additional data are needed to determine whether the inflection has any particular significance.

As shown in Table 4 and Fig. 13, the addition of increasing amounts of oxygen to the iodide thorium increased the hardness from a low value of R_H 44 to a high value of R_H 94. It appears that maximum hardness is obtained at about 0.3%. An oxygen content of 0.013% (an amount nominally present in Ames thorium) seems to increase the hardness of iodide thorium by about 15 points. The 950°C homogenization treatment for 24 hr had no apparent effect on the alloys; this is evident by comparison of Figs. 13 and 14 and the data of Table 5. Metallographic specimens are being prepared and the data obtained will be correlated with the hardness data. X-ray determinations of lattice parameters will be made for the various alloys to establish the limits of solid solubility.

MECHANICAL PROPERTIES OF THORIUM

Ames Laboratory at Iowa State College has started reclaiming thorium turnings because of the recent urgent demand for thorium ingots. Two of the remelted ingots were received from Ames, and a program has been outlined to evaluate the remelted material as compared with virgin metal. Tests using remelted material of known composition and virgin material of similar analysis are planned. Both high- and low-purity virgin material will also be tested. At present available data on the remelted material consist of tensile test results on four specimens from a single billet. These data and a comparison with similar data on virgin material are given in Table 6. The averaged data presented for the virgin metal were obtained on annealed specimens taken from extruded rods.

TABLE 3

Hardness of Thorium-Carbon Alloys After Quenching from Various Temperatures

Average of five determinations

ALLOY NO.	CARBON (wt %)	QUENCHED FROM (°C)									
		1600	1500	1400	1300	1200	1100	1000	800	600	400
		HARDNESS (136° DPH, 10 kg load)									
F-8	0.07	112	99	99	98	100	89	94	80	82	70
F-13	0.09	120	97	99	93	98	93	89	84	88	83
F-3	0.11	144	131	124	126	120	119	112	110	124	99
F-6	0.20	192	168	153	153	142	142	143	140	131	129
F-9	0.26	198	185	179	176	171	163	161	160	150	133
F-11	0.50	237	245	250	252	259	265	246	218	201	205
F-19	1.05	350	394	412	335	335	410	264	291	287	270
F-17	1.42	412	433	385	470	415	424	379	325	284	290
F-20	2.50	440	421	472	477	401	448	406	393	253	259

TABLE 4

Hardness of Arc-Cast Thorium-Oxygen Alloys

ALLOY NO.	OXYGEN (wt %)	HARDNESS R_H	NUMBER OF DETERMINATIONS AVERAGED
F-34	0.006	44	6
F-32	0.013	52	5
F-30	0.022	63	5
F-26	0.050	67	5
F-36	0.080	69	5
F-28	0.120	72	5
F-38	0.240	79	5
F-40	0.440	82	5
F-42	0.770	83	10
F-48	1.500	87	5
F-24	2.000	94	5

TABLE 5

Hardness of Thorium-Oxygen Alloys After Homogenization at 950°C for 24 Hours

ALLOY NO.	OXYGEN (wt %)	HARDNESS R_H	NUMBER OF DETERMINATIONS AVERAGED
F-34	0.006	45	14
F-32	0.013	44	15
F-30	0.022	54	15
F-26	0.050	56	15
F-36	0.080	56	15
F-28	0.120	62	15
F-38	0.240	72	15
F-40	0.440	73	15
F-42	0.770	77	15
F-48	1.500	92	5
F-24	2.000	97	15

TABLE 6

Tensile Test Data for Ames Remelted Thorium and Ames Virgin Thorium

TYPE OF THORIUM	BILLET NO.	NUMBER OF SPECIMENS TESTED	YIELD POINT (psi)	TENSILE STRENGTH (psi)	REDUCTION IN AREA (%)	ELONGATION (%)	CARBON (wt %)	NITROGEN (wt %)
Remelt	MX-322	4	29,000	38,000	68	45	0.064	0.024
Virgin	A-323	4	15,400	25,300	75	51	0.046	0.010
Virgin	A-222	1	20,800	30,300	75	50	0.043	0.008
Virgin	A-223	1	22,100	30,500	71	52	0.041	0.007
Virgin	A-227	1	21,100	29,800	74	51	0.031	0.010
Virgin	A-231	4	27,500	34,500	73	50	0.060	0.009
Virgin	A-239	5	32,000	38,400	70	48	0.076	0.006

The properties of the single heat of remelted thorium are within the range of those obtained with the virgin material. Ductility of the remelted specimens is slightly less than for any of the virgin thorium but tensile test results show that it should be adequate for most purposes. Remelted thorium shows slightly higher impurity content, particularly nitrogen and carbon, both of which tend to make thorium harder and less ductile. A more complete evaluation of properties of the remelted thorium is in progress but no further data are available.

Preferred orientation studies of extruded thorium indicate that extrusions made at very slow rates (2.5 ft/min) retained a deformation texture typical of face-centered cubic metals. The actual texture is duplex (100) (113). Since extrusions made at greater speeds showed a recrystallization texture with some residual deformation, it is planned to repeat some of the tests with a very slow and a very fast extrusion of the same material under identical conditions. Specimens from these extrusions will be tested in the as-extruded condition to determine the effect of fabrication on the properties of Ames thorium. It had been assumed that all extrusions were fully recrystallized, since the material was hot worked at 750°C or higher.

Tensile test specimens were prepared from a cast sheet ingot of Ames thorium that is being used in a rolling investigation. The cast tensile specimens were intended as a means for evaluating the starting material. The cast ingot was cut into pieces suitable for rolling, and tensile test specimens were taken from the top, center, and bottom of the cast ingot in both longitudinal and transverse directions. Figure 15 shows the ingot with the pieces marked for proper cutting. The pieces marked C, D, E, F, J, K, N, O, R, and S were used to make the cast specimens.

The as-cast samples have been tested and the data are tabulated in Table 7. By comparison of data in Tables 6 and 7, it may be noted that the tensile strength of the as-cast metal is comparable with that of the extruded metal. However, as would be expected, the ductility is slightly less in the case of the cast metal.

TABLE 7

Tensile Test Data for As-Cast Ames Thorium

SPECIMEN NO.	PERCENTAGE OF ELONGATION IN 4 in.	TENSILE STRENGTH (psi)	ULTIMATE BREAKING STRENGTH (psi)	YIELD POINT (psi)	REDUCTION IN AREA (%)
C	44.6	30,500	53,900	18,100	59.0
D	48.2	30,300	51,700	20,000	59.7
E	44.6	30,000	48,500	19,800	54.7
F	43.6	30,100	48,500	20,400	54.9
J	42.8	29,900	48,500	20,200	54.9
K	44.6	29,800	49,900	20,500	55.3*
N	44.6	30,000	48,500	19,900	54.7
O	45.0	29,800	48,900	20,300	55.3
R	44.6	30,100	48,900	20,800	55.3
S	44.6	29,800	47,500	20,600	54.9

*Proportional limit, 14,570 psi; modulus of elasticity, 10.6×10^6.

FABRICATION

Rolling. An investigation of the effect of rolling variables on Ames thorium was initiated by using cast Ames ingots as starting material. The cast ingot marked for proper cutting is shown in Fig. 15. The larger pieces were used for rolling experiments and the smaller pieces were made into tensile test specimens for evaluating the as-cast material. The tensile test data for the cast material are given in the previous section "Mechanical Properties of Thorium."

The rolling study was started by hot rolling pieces at temperatures of 1450 and 1200°F. The pieces were rolled for 50% reduction at these temperatures and cut into eight pieces that were subsequently rolled to 1/8-in.-thick sheet at temperatures of 1450, 1200, and 400°F, and at room temperature. Thus, the finished samples were as follows:

1. rolled from 1 1/2-in. to 1/8-in. thickness at 1450°F;
2. rolled from 1 1/2-in. to 3/8-in. thickness at 1450°F and finished at room temperature to 1/8-in. thickness;
3. rolled from 1 1/2-in. to 3/4-in. thickness at 1450°F, rolled to 3/8 in. at 400°F, and finished at room temperature to 1/8-in. thickness;
4. rolled from 1 1/2-in. to 3/4-in. thickness at 1450°F and rolled to 1/8 in. at 400°F.

Specimens 5 through 8 were treated in the same way except that the breakdown temperature was 1200 rather than 1450°F. The same rolling schedule was followed for two sets of specimens, the only

difference being that one set was rolled straight through all passes. The second set was cross rolled; that is, after each pass through the rolls the plate was turned 90 deg. so that alternate passes were made in a direction perpendicular to the previous one.

The material rolled at 1450°F gave good rolling results even when finished at lower temperatures and at room temperature. However, the material with a 1200°F breakdown cracked when it was rolled at 400°F and lower. The crack was parallel to the rolling plane and midway between the two rolling faces. Typical failures of straight and cross rolling are shown in Fig. 16. It should be noted that this material can be rolled successfully if all the rolling is done at room temperature. The rolling is to be continued at other temperatures.

Extrusion. Die materials continue to be somewhat of a problem in the extrusion of thorium. Die inserts made from Super Cobalt steel have been used for routine extrusion work with fairly good results. One die 7/8 in. in diameter was used for approximately 25 extrusions without ill effects. However, a 5/8-in.-dia die made of the same material was used to extrude a 3-in.-dia billet 8 in. long at 800°C and was completely washed out by the same type of erosion as previously reported. The increased reduction ratio and a billet somewhat longer than usual apparently caused sufficient temperature rise to soften the die.

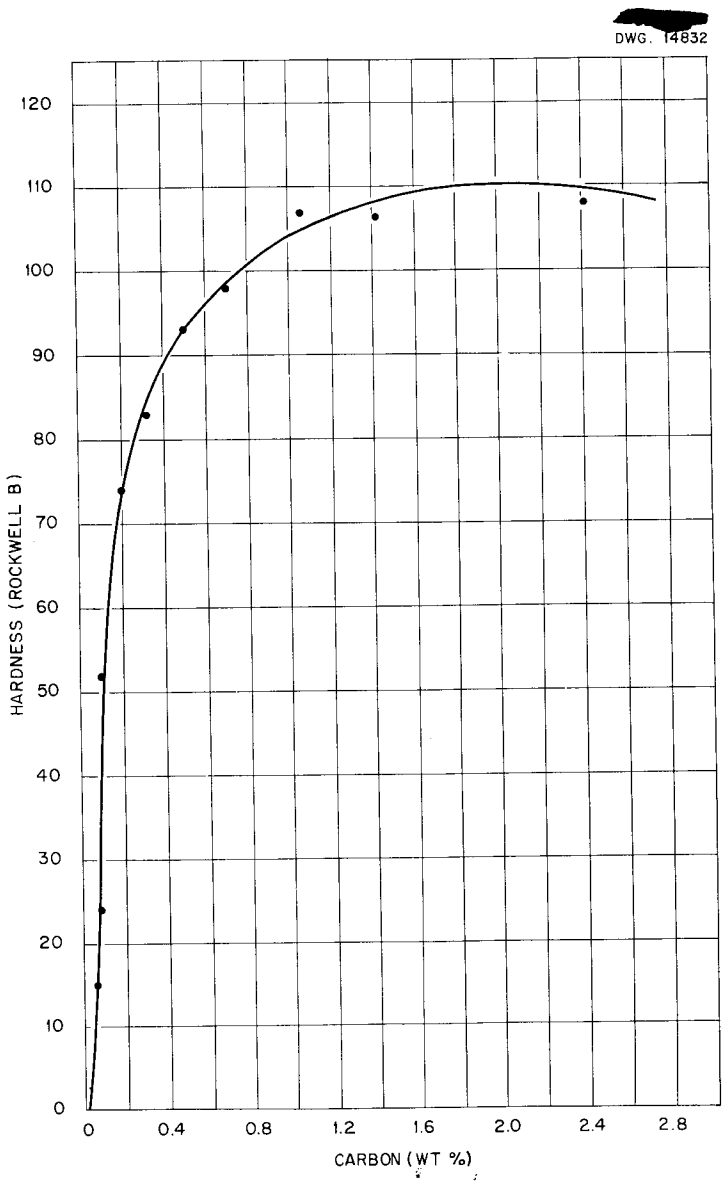

Fig. 1. Hardness of As-Arc-Cast Thorium-Carbon Alloys.

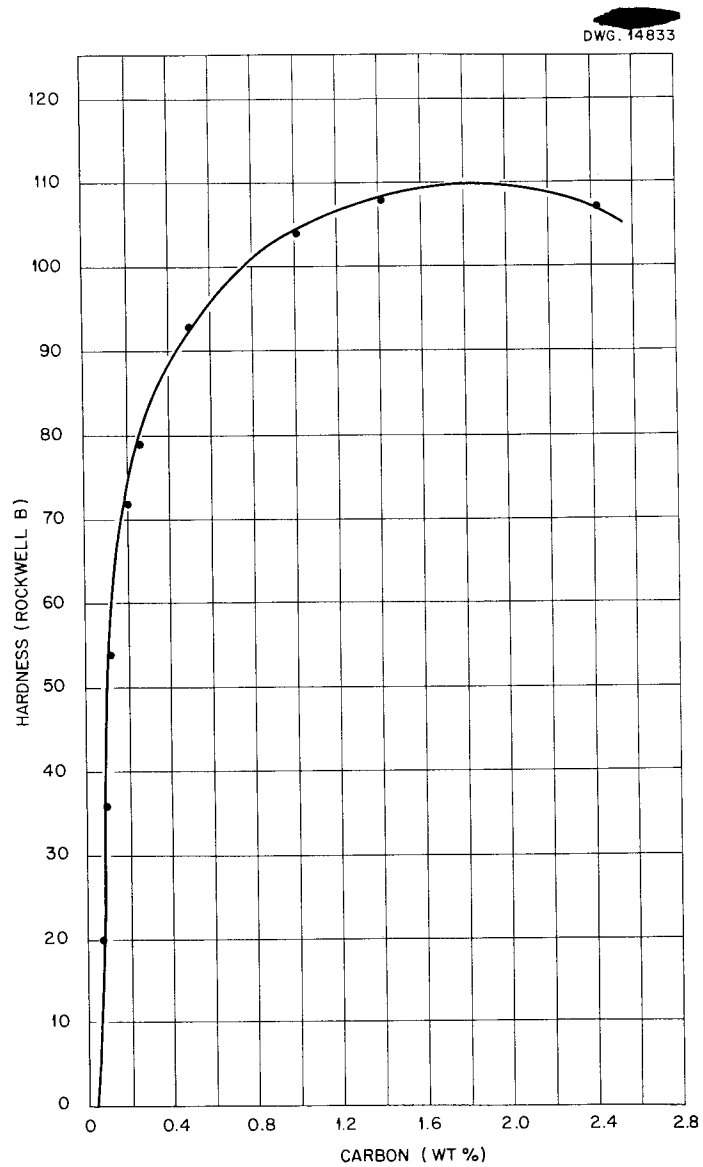

Fig. 2. Hardness of Thorium-Carbon Alloys After Homogenization for 24 hr in Vacuum at 950 °C.

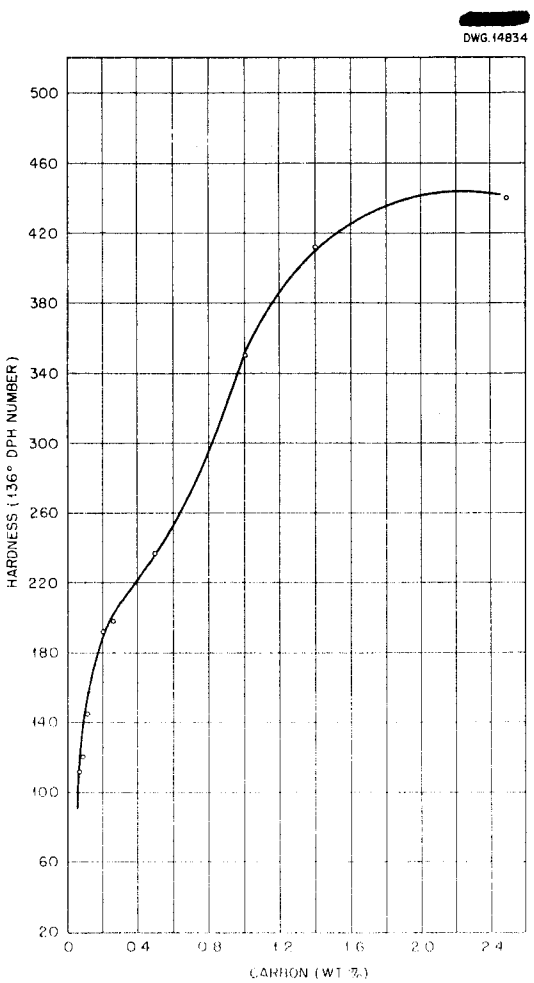

Fig. 3. Hardness of Thorium-Carbon Alloys After a Quench from 1600°C.

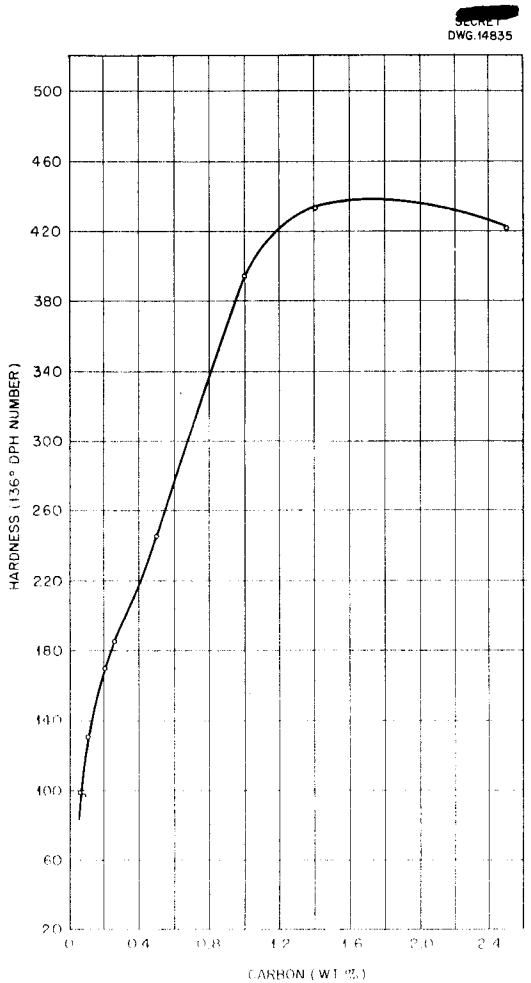

Fig. 4. Hardness of Thorium-Carbon Alloys After a Quench from 1500°C.

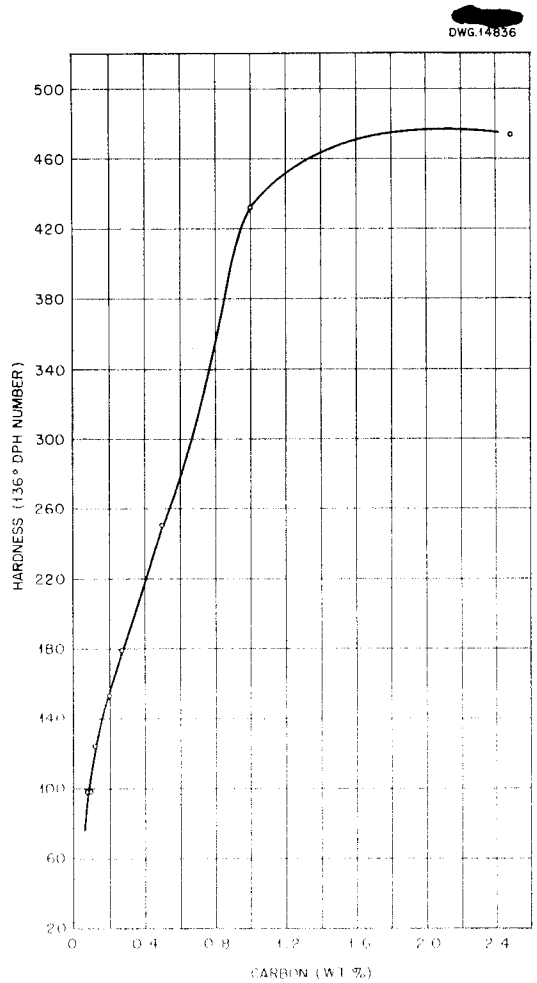

Fig. 5. Hardness of Thorium-Carbon Alloys After a Quench from 1400°C.

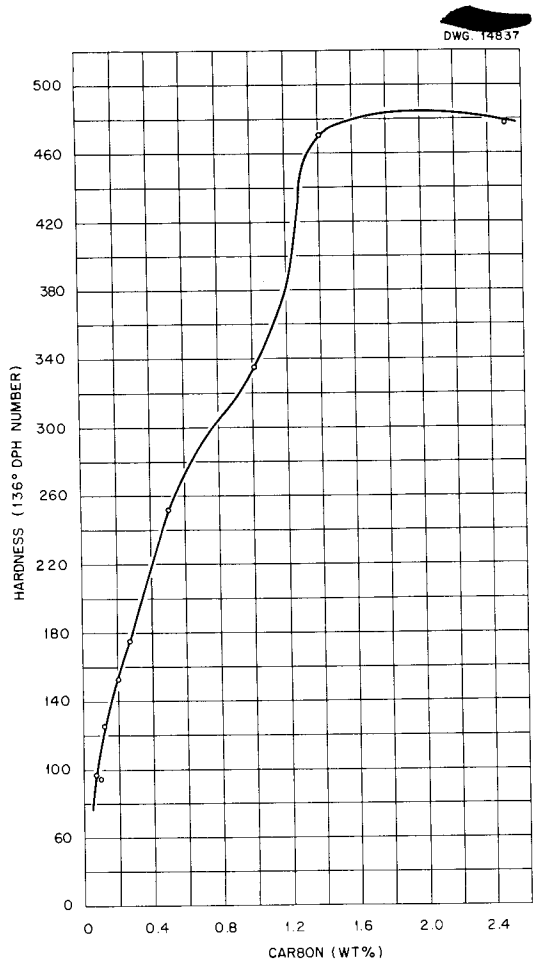

Fig. 6. Hardness of Thorium-Carbon Alloys After a Quench from 1300°C.

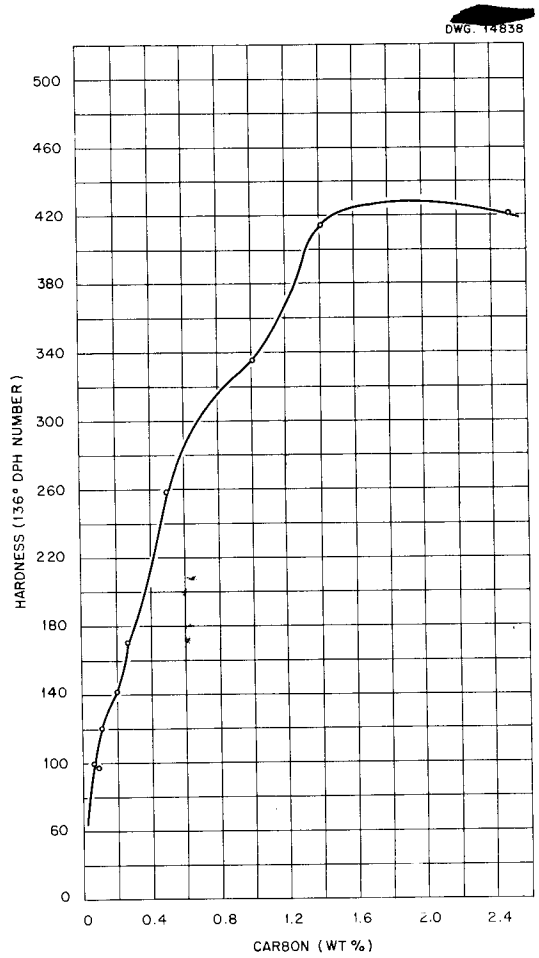

Fig. 7. Hardness of Thorium-Carbon Alloys After a Quench from 1200°C.

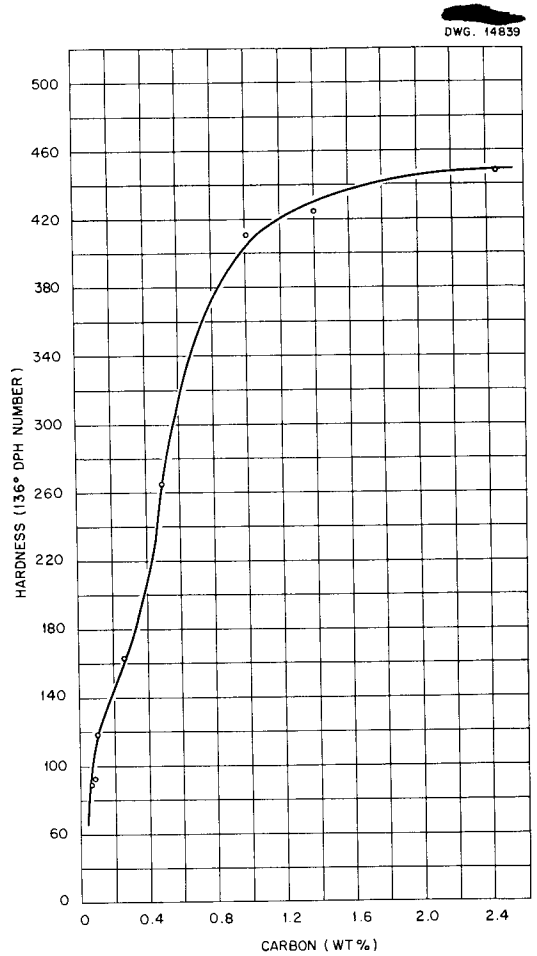

Fig. 8. Hardness of Thorium-Carbon Alloys After a Quench from 1100°C.

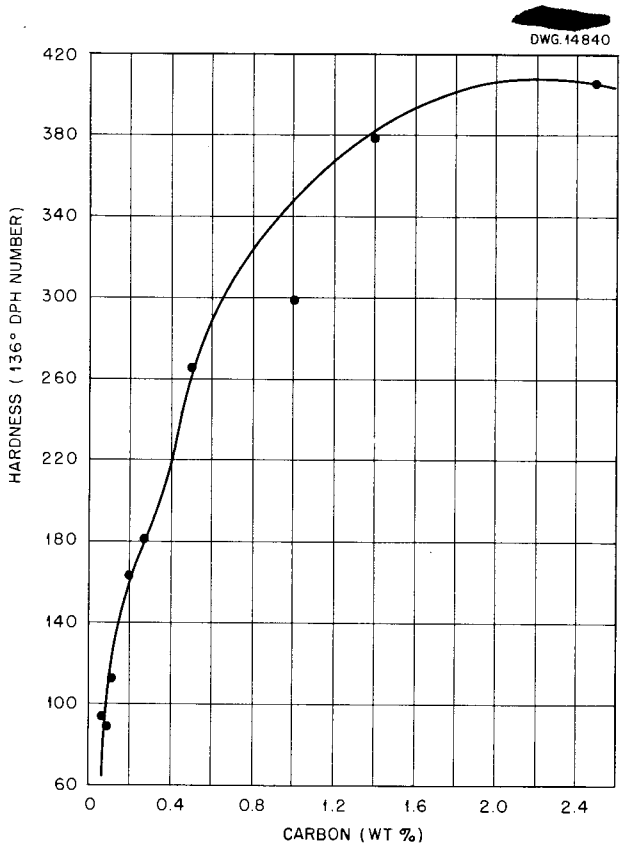

Fig. 9. Hardness of Thorium-Carbon Alloys After a Quench from 1000°C.

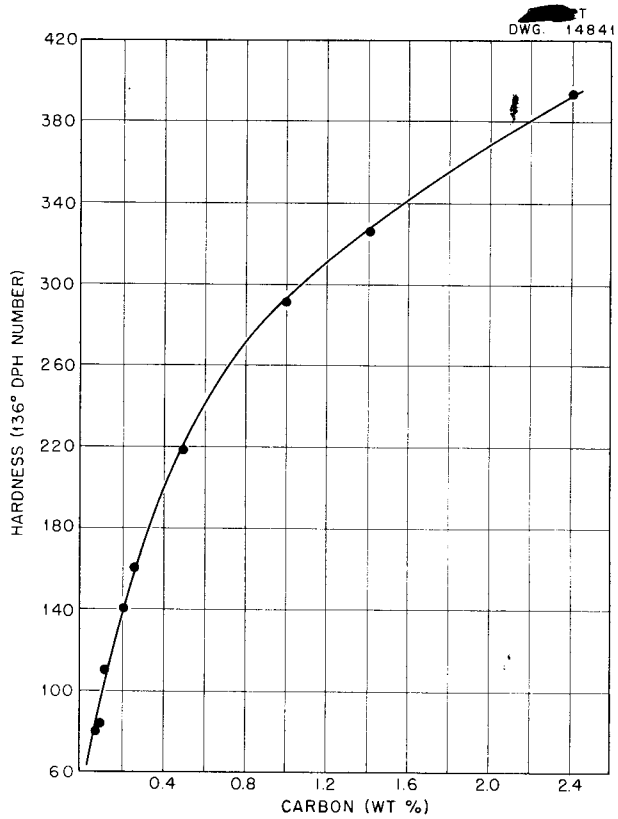

Fig. 10. Hardness of Thorium-Carbon Alloys After a Quench from 800°C.

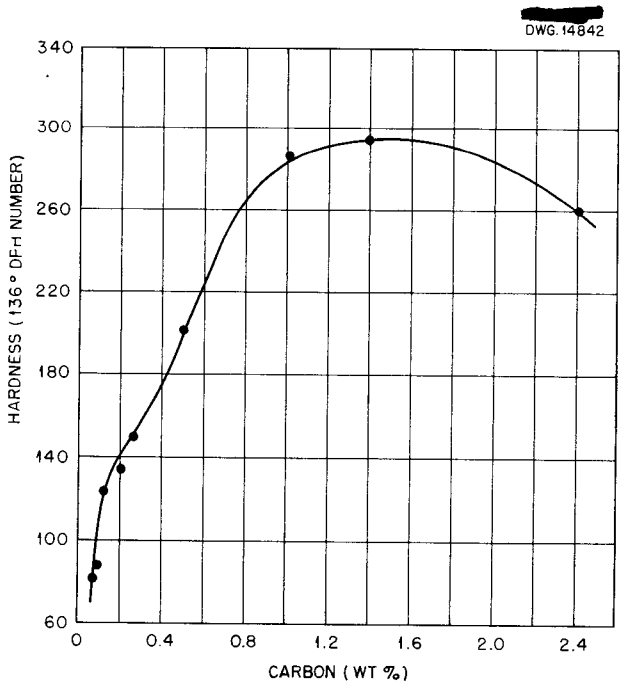

Fig. 11. Hardness of Thorium-Carbon Alloys After a Quench from 600°C.

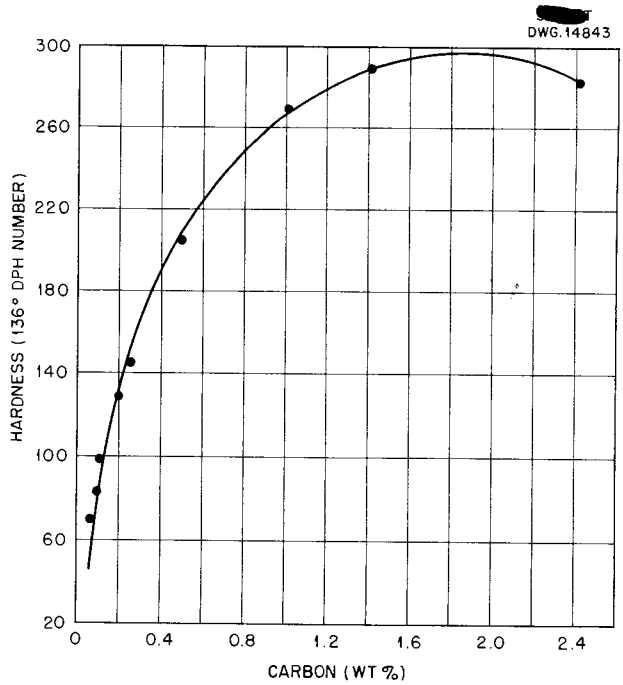

Fig. 12. Hardness of Thorium-Carbon Alloys After a Quench from 400°C.

[redacted]

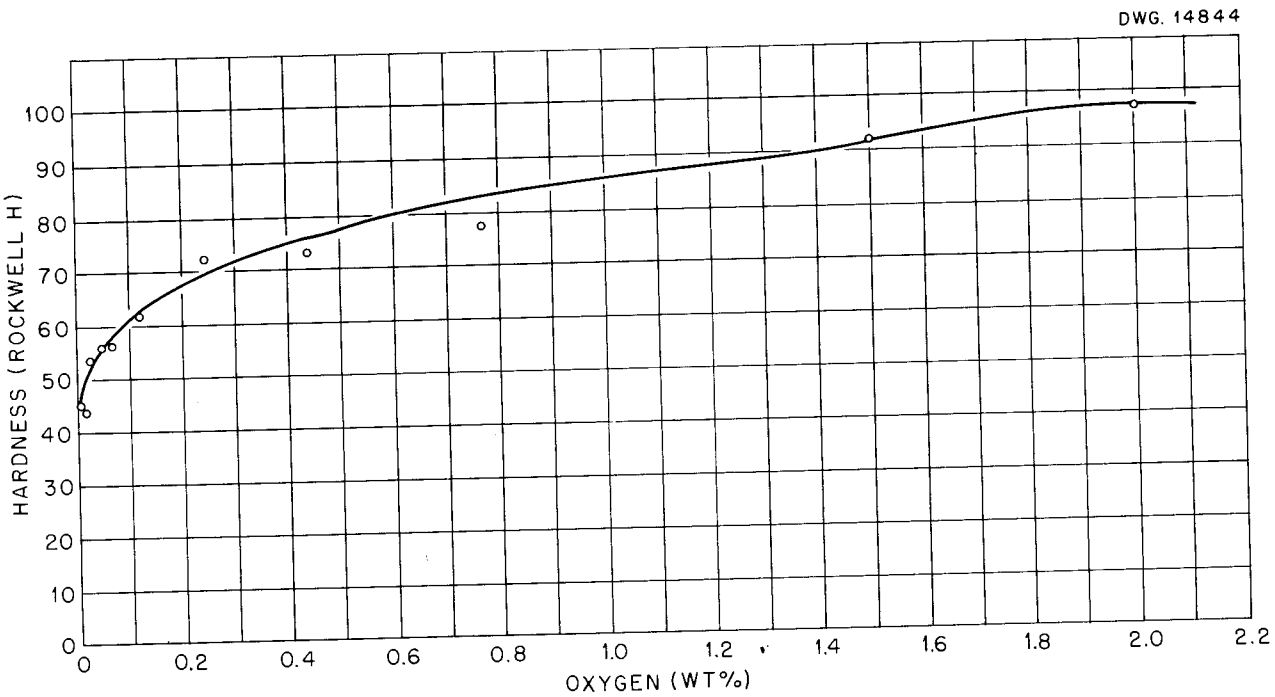

Fig. 13. Hardness of As-Cast Thorium-Oxygen Alloys.

[redacted]

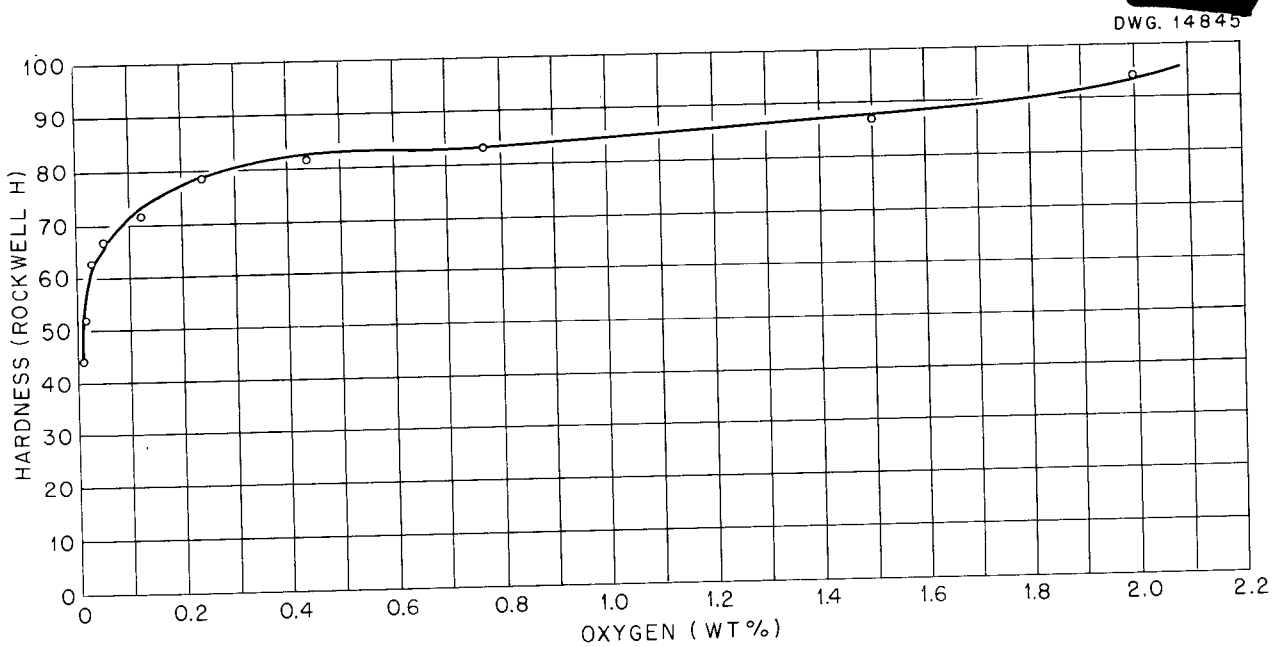

Fig. 14. Hardness of Thorium-Oxygen Alloy After Homogenization at 950°C for 24 Hours.

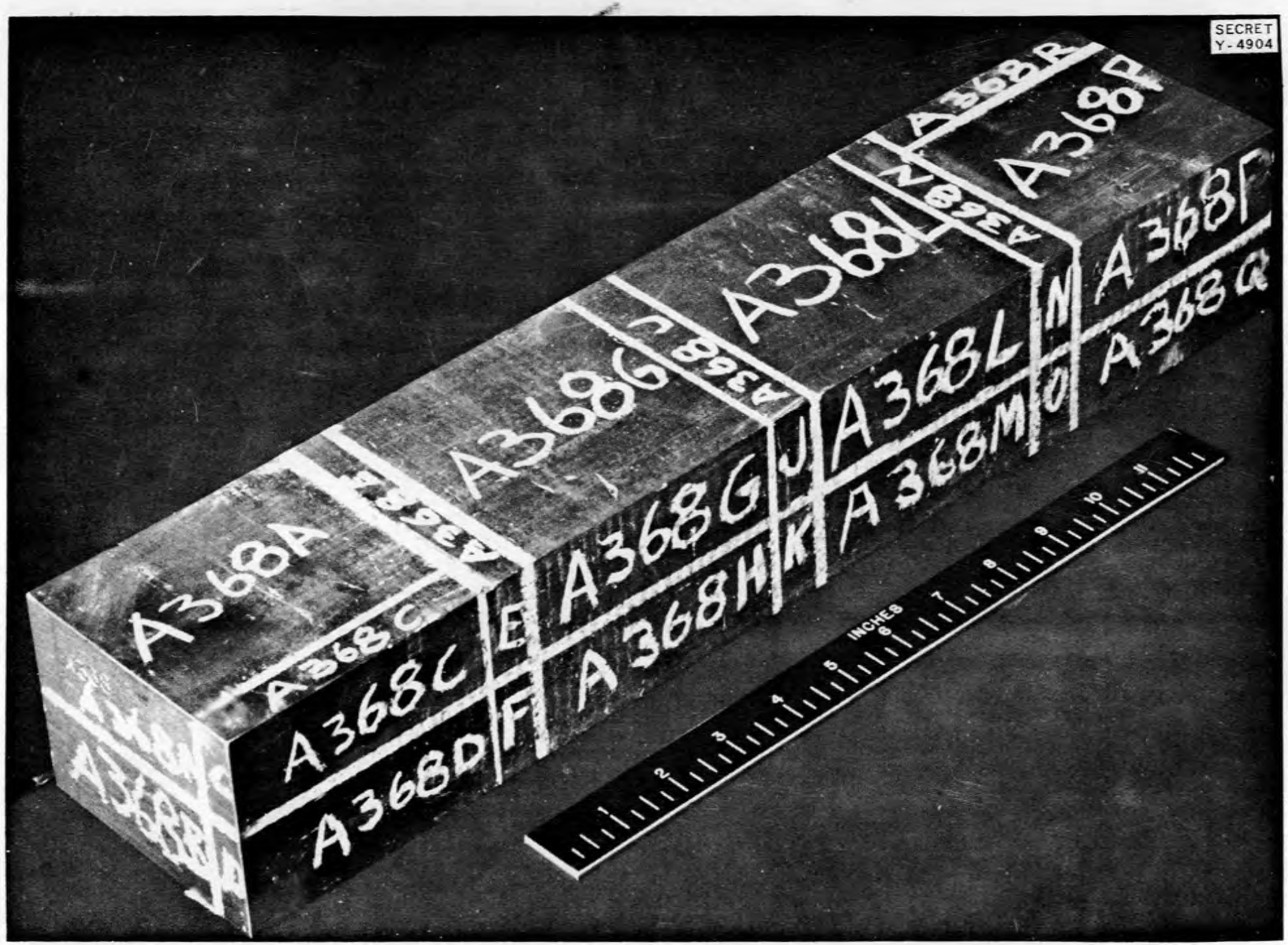

Fig. 15. Cast Ingot of Ames Thorium Marked for Proper Cutting into Smaller Pieces for Rolling Investigation.

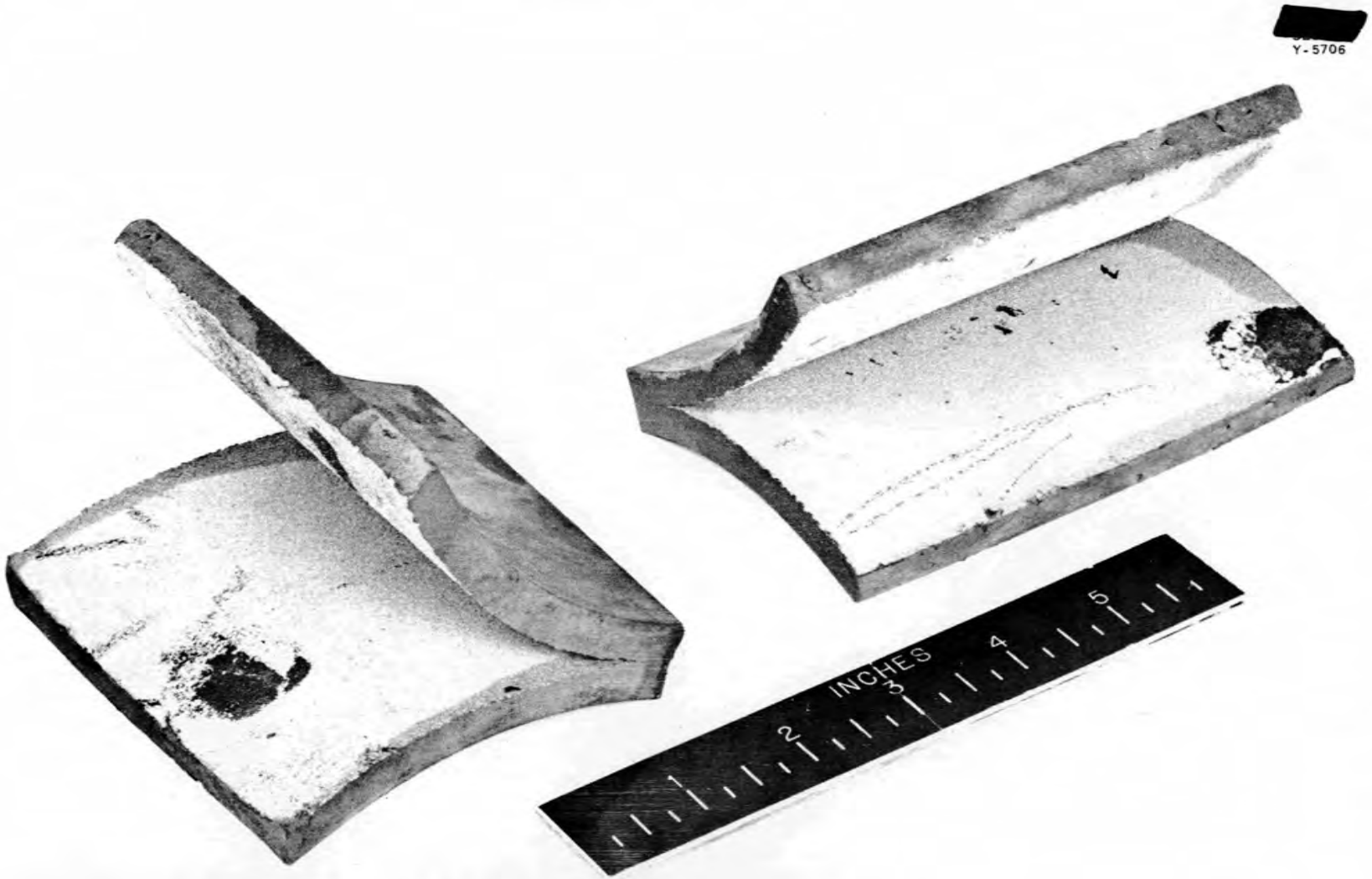

Fig. 16. Thorium Plate Cracked During Rolling.

SLUG PROBLEM

D. E. Hamby W. J. Fretague
R. E. Adams J. A. Milko

The bonded Clinton slugs produced by the triple-dip process were found to be unsuitable for use at temperatures as high as 350°C. The 400°C heat treatment for seven days that was adopted as a criterion for acceptance of the slugs resulted in considerable diffusion between the aluminum can and the uranium slug. As previously reported, a high concentration of tin was invariably associated with the diffusion pimples, and steps were taken to eliminate the tin. However, it was difficult, if not impossible, to completely eliminate the tin, and it was found that areas containing trace amounts of tin still resulted in diffusion pimples. In order to completely remove tin, the triple-dip process, which used a bronze-bath heat treatment followed by a tin dip, was discontinued.

The alpha-canning technique developed by Argonne National Laboratory was adopted for production of the bonded Clinton slugs. In this process the slugs are given a beta-heat treatment in a salt bath operated at 730°C, chemically cleaned in a nitric acid solution, rinsed, and dried. The slugs are then dipped in a duplex bath of lead and aluminum-silicon alloy. The slugs are preheated in the lead bath and raised into the aluminum-silicon layer above the lead and held for 3 min so that a compound layer of $U(Al\text{-}Si)_3$ is formed around the slug. The slugs are then transferred to another aluminum-silicon dip bath and held for an additional 3 min, after which the slugs are canned in an aluminum-silicon bath. The Argonne National Laboratory is experiencing some difficulty in wetting the slugs uniformly, and the same trouble was encountered here for the first few runs. It was felt that the surface condition was largely responsible for this, and steps were taken to prepare a clean surface prior to dipping in the duplex bath. Experimental lots of slugs were electropolished and canned and then stripped to determine the extent of wetting. The wetting was found to be fairly good. A larger lot of slugs that were canned and given the standard 400°C heat treatment proved to be bad; about 58% developed diffusion pimples. Since the location of the pimples could be correlated to the location of the rings on the handling tools, as mentioned in a previous report, the tools were redesigned to give a minimum of surface contact with the slugs, and a definite improvement of coating was noted.

The slugs are inserted into a hot tool immediately before immersion into the duplex bath, and there is a chance that some oxidation occurs and prevents proper wetting. For this reason, it was suggested that a flux over the duplex bath might be beneficial. A commercial aluminum flux (Eutector 190) was used over the duplex bath and a number of slugs were canned with only the usual nitric acid etch. The appearance of these slugs, when stripped, was unusually good. Since these improvements were noted on small lots of slugs, lots of 50 to 100 each were canned with variations of the normal procedure to further test the results. The use of a flux over the duplex bath seemed to be the significant change in the procedure, because six lots with a total of 455 slugs canned by using a flux over the bath showed no failures after seven days at 400°C. These slugs are being tested

for longer periods of time to prove that the diffusion problem has been eliminated. Control lots of 108 slugs that were canned without using a flux showed a total of 24 failures after the 400°C heat treatment. This rate of failure (22%) is equivalent to that found in slugs produced by the triple-dip process. Metallographic examination of the slugs canned by the preferred technique of using a flux over the bath showed that a continuous layer of $U(Al\text{-}Si)_3$ compound is formed on the uranium slug. Since it is this compound that acts as a barrier to excessive diffusion, it is necessary that a perfectly continuous layer be formed and maintained. This requirement seems to be most nearly fulfilled by the alpha-canning process with the aforementioned refinements. The lot of 455 slugs canned by this method has passed the 400°C heat treatment for three weeks without a single failure, and a production lot of 1000 slugs has passed the 400°C heat treatment for seven days without a failure.

PREFERRED ORIENTATION AND ANISOTROPY IN METALS

L. K. Jetter

A method using a Geiger-counter x-ray-diffraction spectrometer for accurate determination of the type and degree of preferred orientation in metals has been described briefly in previous reports.[1] The unique feature of the method is that a spherical diffraction specimen is used, and therefore complete and quantitative investigation of the texture can be made with only one specimen, without resort to complicated corrections of the observed intensities for variations in diffracting volume, absorption, and focusing. The experience gained with this method is now sufficient to permit more complete description of the equipment and the techniques found to facilitate its application.

Appended as an integral part of the spherical diffraction specimen is a cylindrical stem by which the specimen is mounted on the x-ray diffraction spectrometer. The specimen is machined so that the axis of the stem coincides with some principal direction (usually the longitudinal direction) of the section from which the specimen is taken and therefore serves to identify this direction. Reference marks (Fig. 17) are made on the cylindrical surface of the stem to identify the other principal directions (the transverse and the normal directions).

The diffraction specimen is mounted on the spectrometer by means of a special goniometer so that the longitudinal direction is in the plane of the incident and the diffracted x-ray beams – the plane of the spectrometer. The goniometer provides for rotation of the sphere about an axis in the spectrometer plane (the longitudinal direction) through angles designated α ($\alpha = 0$ when the transverse direction is in the spectrometer plane); it also provides for rotation of the sphere about an axis perpendicular to the spectrometer plane through angles designated ϕ ($\phi = 0$ when the longitudinal direction coincides with the normal to the diffracting plane). Both axes pass through the center of the sphere. The specimen thus can be oriented so that at least a hemisphere of the pole figure can be scanned. Figure 18 shows how the various orientations of the specimen, in terms of α and ϕ, are related to the stereographic net, with the plane of projection being the plane containing the longitudinal and transverse directions.

Since a spherical specimen when rotated about any axis through its center does not alter its geometry with respect to the incident and diffracted beams, there is no change in absorption or in focusing with change in orientation. Accordingly, the observed intensity of the diffracted beam for the various orientations of the sphere can be related directly to the portion of the irradiated volume properly oriented for diffraction. No variation in intensity with specimen orientation indicates random orientation, whereas observed variations in intensity reflect accurately the type and degree of preferred orientation in the material composing the specimen.

Figure 19 shows the special goniometer and the diffraction specimen mounted on a horizontal x-ray-diffraction spectrometer. The goniometer has a multiple base. The upper section,

(1) "Preferred Orientation and Anisotropy in Properties of Metals," *Metallurgy Division Quarterly Progress Reports*, ORNL-511, p. 66; ORNL-583, p. 37; and ORNL-827, p. 35.

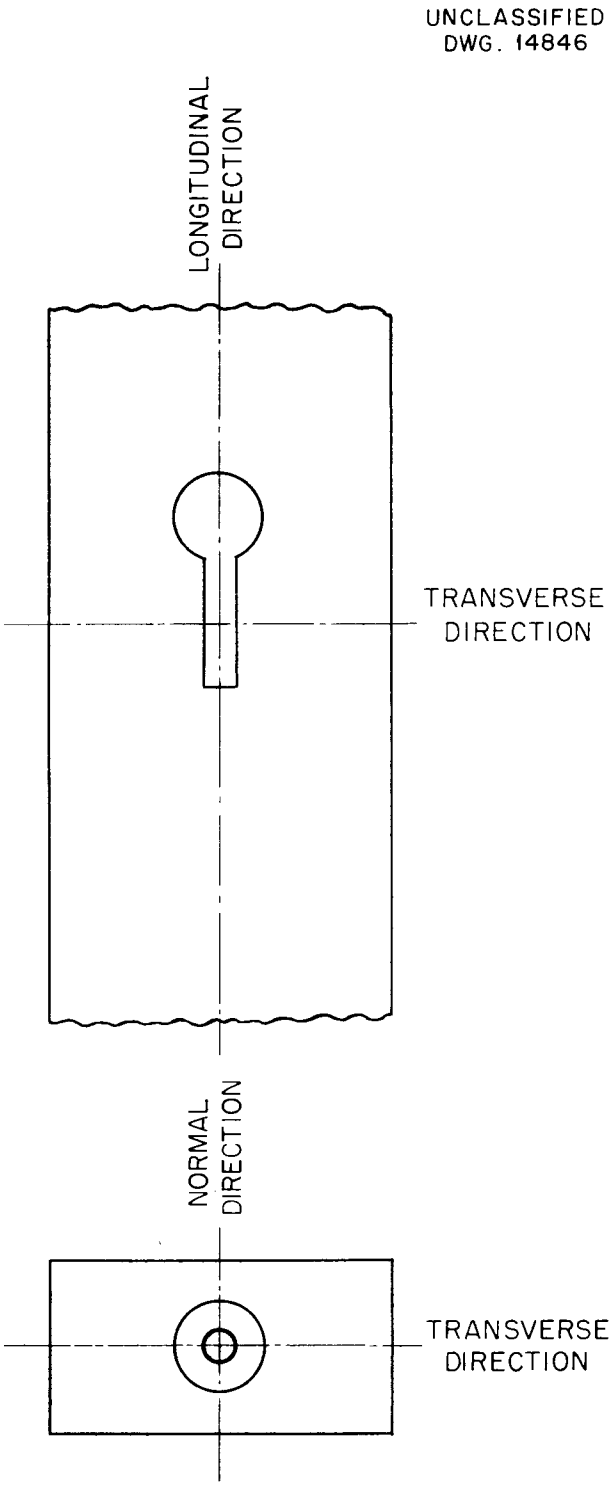

Fig. 17. Diagram Showing the Orientation of the X-Ray Diffraction Specimen with Respect to the Principal Directions of a Section.

which is dovetailed into the lower, can be moved linearly with respect to the lower section by means of a micrometer screw. The lower section is rigidly attached to the flange of the goniometer bushing of the spectrometer. The upper section supports an arm that can be rotated about a vertical axis; this arm in turn supports a horizontal spindle to which the specimen is attached by means of a chuck. With the aid of a toolmaker's microscope, the specimen is positioned so that the center of the sphere falls on the axis of rotation of the arm. A horizontally mounted, Bodine synchronous motor, with accessory gearing, provides for automatic rotation of the arm about its vertical axis. Another Bodine motor, mounted vertically, provides for automatic rotation of the spindle about its horizontal axis. By means of an eccentric, the latter motor also provides for oscillation of the arm about its vertical axis. Accordingly, the specimen can be subjected to five independent motions for its alignment and scanning.

1. Movement of the Geiger counter along the spectrometer arc through an angle 2θ rotates the specimen about the vertical axis through the center of the spectrometer arc through an angle θ (0 to 45 deg) and places the desired family of planes in position to diffract.

2. Rotation of the micrometer screw slides the upper section of the base over the lower, moves the specimen linearly in the direction of the normal to the diffracting plane, and positions the sphere in the incident beam.

3. Rotation or oscillation of the arm rotates the specimen about the vertical axis through the center of the sphere through angle ϕ (rotation from −15 to +105 deg with superimposed

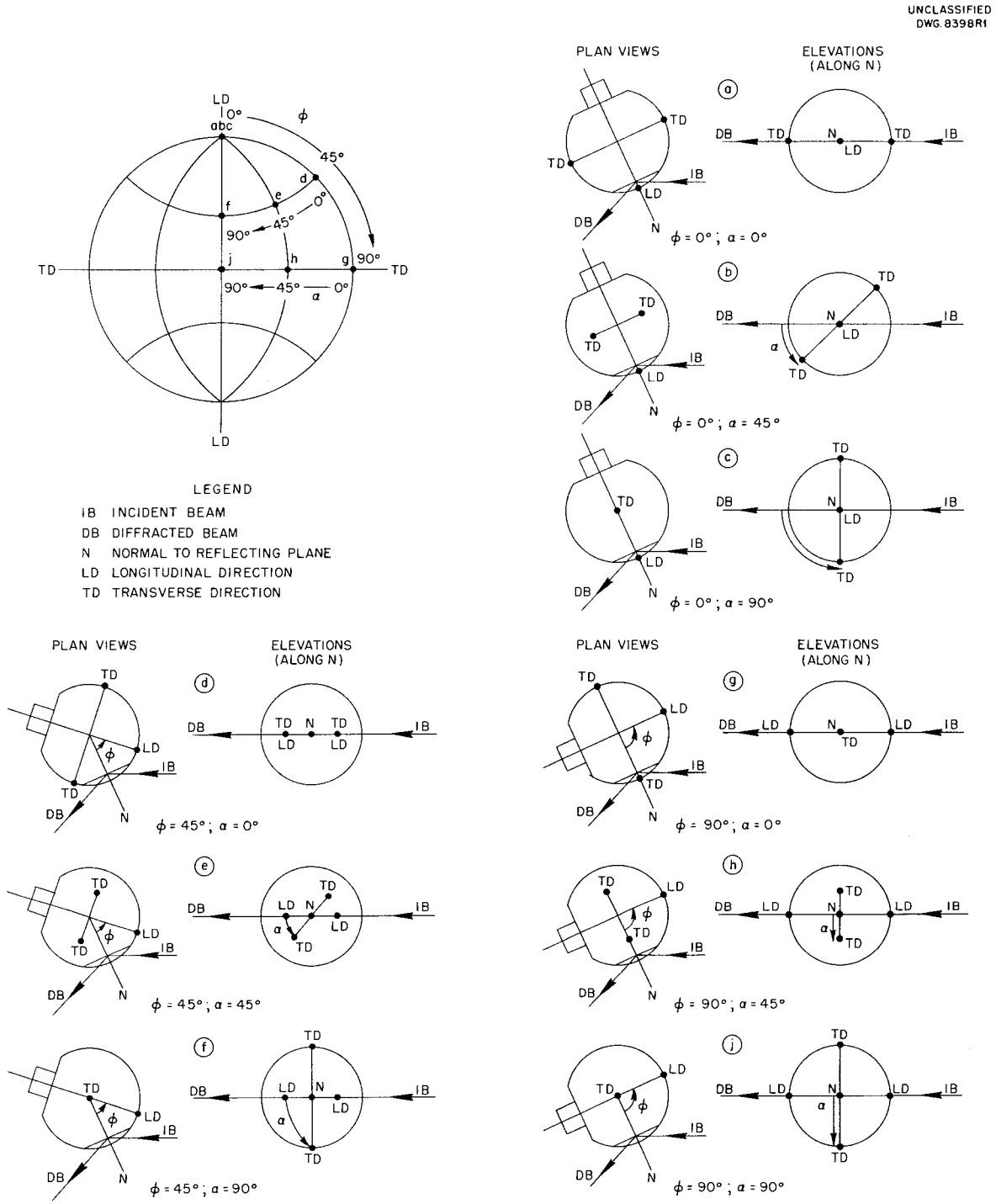

Fig. 18. Relationship Between Orientation of X-Ray-Diffraction Specimen with Respect to the Normal to the Reflecting Plane and the Position on the Stereographic Net.

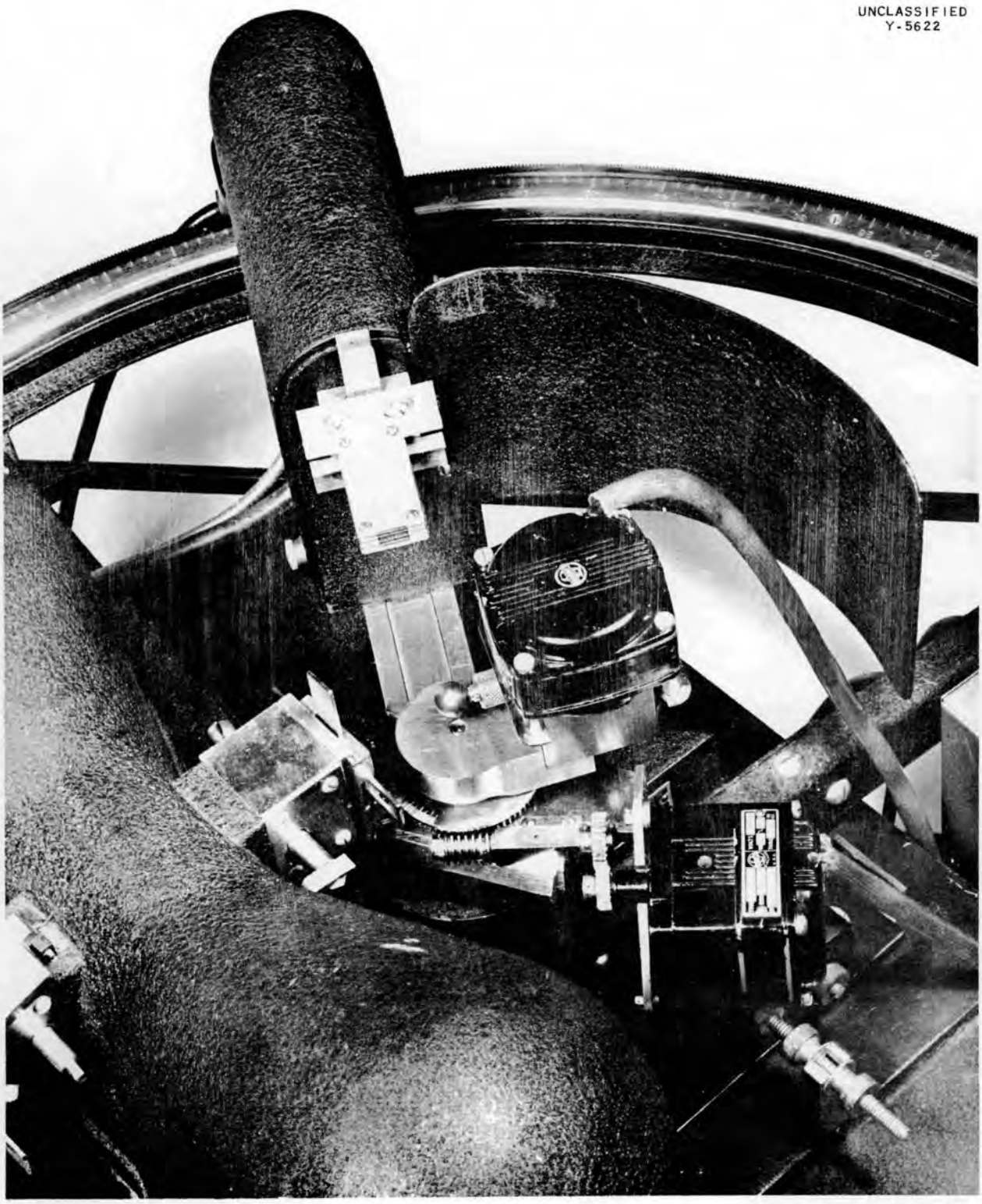

Fig. 19. Special Goniometer and the Diffraction Specimen Mounted on a Horizontal X-Ray-Diffraction Spectrometer.

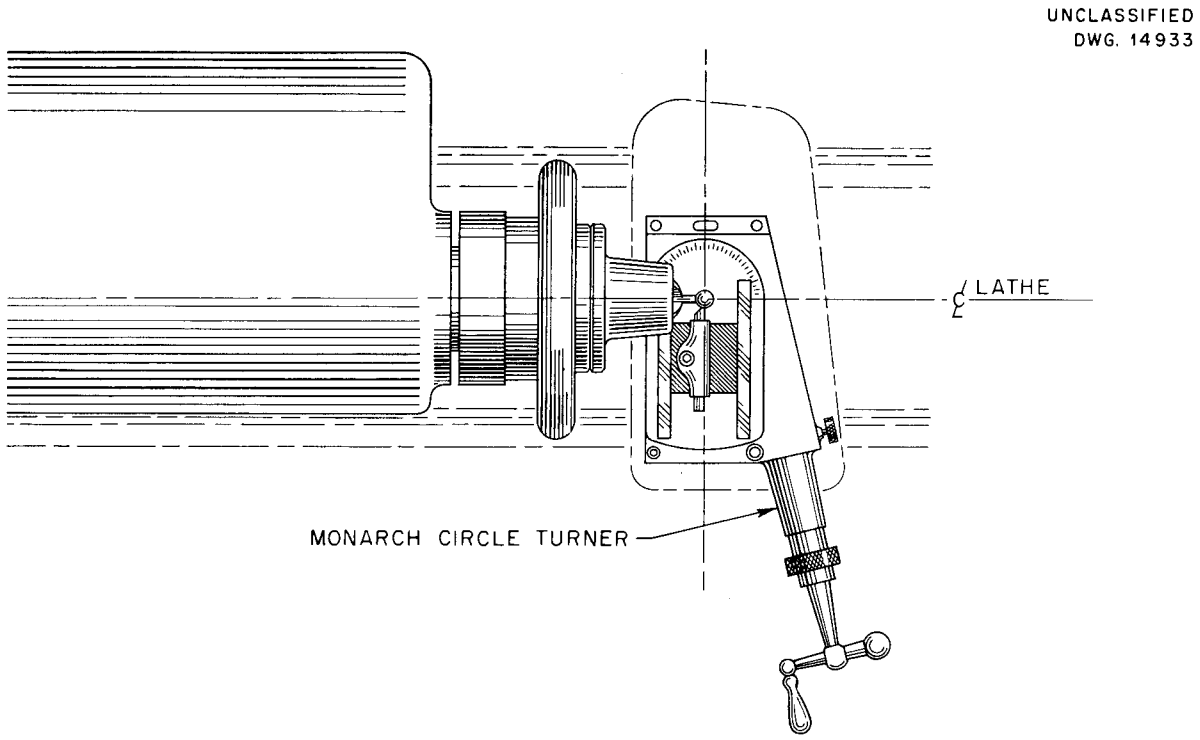

Fig. 20. Arrangement for Machining Spherical X-Ray-Diffraction Specimens.

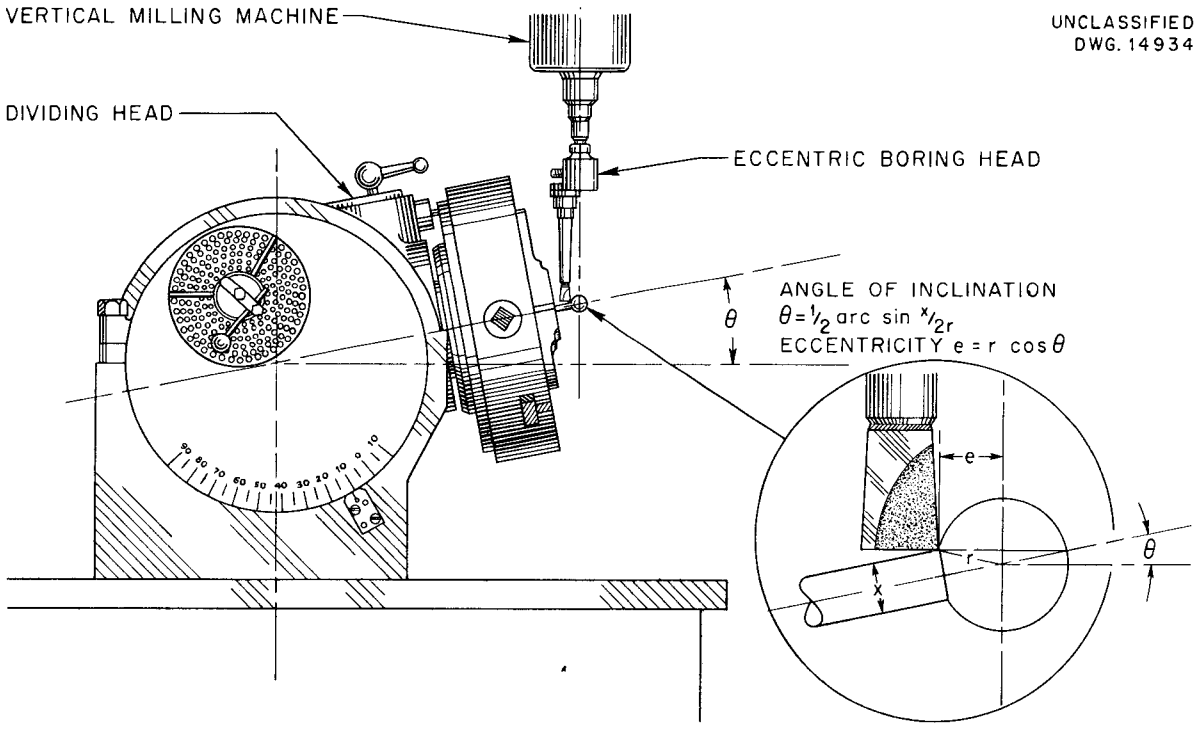

Fig. 21. Preferred Arrangement for Machining Spherical X-Ray-Diffraction Specimens.

oscillation up to 6 deg) and orients the sphere with respect to the incident beam.

4. Rotation of the spindle rotates the specimen about the horizontal axis through the center of the sphere through angle α (0 to 360 deg) and orients the sphere with respect to the incident beam.

5. Sliding the specimen in the chuck moves it linearly in the direction of the normal to the diffracting plane and positions the sphere on the vertical rotation axis of the arm.

In collaboration with the Research Shops, several techniques have been developed for machining the diffraction specimen. The most obvious technique involves the use of a lathe in conjunction with a circle turner, as illustrated in Fig. 20.

The preferred method, which is more complicated in theory but simpler in execution, involves the use of a vertical milling machine equipped with an eccentric boring head and a dividing head, as shown in Fig. 21. The stem of desired diameter x is first machined in a lathe. By means of the stem, the specimen is then mounted in the dividing head of the milling machine. The sphere is machined by rapidly rotating the eccentric cutter while slowly rotating the dividing head and slowly elevating the table of the milling machine. When the cutter just contacts the stem, the specimen is fully formed. The angle of inclination of the dividing head, θ, and the offset of the cutter, e, are calculated as follows:

$$\theta = \frac{1}{2} \text{arc sin} \frac{x}{2r} ,$$

$$e = r \cos \theta ,$$

where r is the desired radius of the sphere and x is the diameter of the stem.

The machined sphere is lapped to smoothness with diamond grit on a hollowed-out block of cast iron and then electroetched to remove the surface layer deformed by machining and lapping. The sphere is reduced in diameter approximately 0.010 in. by electroetching in a special setup employing a cathode of stainless steel in the form of a hollow sphere 4 in. in diameter. Conditions are adjusted so that etching occurs slowly, and sphericity of the specimen is maintained until nearly the desired amount of metal is removed; then the conditions are readjusted to give a rapid finishing etch that removes pitting and polishes the sphere. Specimens spherical to within 0.001 in. are obtained consistently with this technique.

A specimen that is as small in diameter as possible is used to minimize heterogeneity of texture. Spheres ranging down to 0.2 in. in diameter have been prepared in the manner described above. Other methods are available for preparing thin sections, which cannot be conveniently prepared in the manner described. For instance, a hemispherical end could be lapped on small diameter rod or wire. For sheet, a sphere might be machined from a compact made up of many layers of identical orientation.

The preferred orientation is determined by moving the Geiger counter along the spectrometer arc to the proper 2θ angle to receive the beam diffracted from the family of planes being considered. For a fixed value of α, the intensity of the diffracted beam is recorded on a Brown potentiometer recorder while the specimen is automatically rotated through ϕ (2.4

to 15.0 deg/min). This procedure is repeated for other values of α sufficient to scan at least a hemisphere. For materials exhibiting a fiber texture, the specimen may be rotated continuously and rapidly (360 rpm) through all values of α while it is rotated slowly through ϕ. For materials with coarse grain size, a rapid oscillation (71 cpm) may be superimposed upon the slow rotation through ϕ to improve the statistics. The counter slit is adjusted to as great a width as is consistent with clean separation of the diffraction lines and an adequate ratio of line-to-background intensity. The intensity of the diffracted beam has been found to be greatest when the specimen is positioned to intercept approximately three-fourths of the incident beam.

Samples of extruded thorium rod, described in a previous report,[2] were selected for determination of the type and degree of preferred orientation. The samples were taken 18 in. from the front end of rods 1 in. in diameter that had been extruded at various rates from 2.7 to 560 ft/min through a flat-face die at 800 to 850°C billet temperature. The billets were 3-in.-dia cast ingot of Ames thorium. The extruded lengths were water-spray quenched as they emerged from the die. The extrusion conditions are described in detail in Table 8.

Metallographic examination revealed that the rod extruded at the slowest rate (2.7 ft/min, sample A-239-C2) had a deformed grain structure, but all the others had completely or nearly completely recrystallized grain structures, as shown in Figs. 22, 23, and 24.

The preferred orientation was determined by the x-ray diffraction spectrometer technique described above. Examination was made on a Norelco Type-12021 Geiger-counter spectrometer using copper K-alpha radiation. The spherical diffraction specimens were 0.500 in. in diameter and machined so that the center line of the specimen coincided with that of the extruded rod. The specimen was rotated at 360 rpm about its longitudinal axis (the extrusion direction) during exposure.

Plots of the intensity of diffraction vs. the angle ϕ between the extrusion direction and the normal to the diffraction plane for various planes for each specimen are given in Figs. 25 through 40.

Analysis of these data revealed that the unrecrystallized sample (A-239-C2) had a duplex [111] - [100] fiber texture (the [111] component being predominant) but that the completely recrystallized sample (A-222-C) had a single [114] fiber texture. The other samples that were not completely recrystallized had a [114] fiber texture with a minor [100] component (Table 8). Figures 25 through 40 show the positions of the intensity maxima to be expected for the various diffracting planes for these preferred directions and the multiplicity of planes at each position.

These results indicate that extruded thorium rod develops a deformation texture similar to that developed by other face-centered cubic metals. The recrystallization texture, however, is somewhat different in that other metals either retain one or both the components of the deformation texture upon recrystallization or else develop a [112] fiber texture. It is presumed that the [100] component in the nearly completely recrystallized thorium rod

(2) "Thorium Research," *Metallurgy Division Quarterly Progress Report for Period Ending April 30, 1951*, ORNL-1033, p. 11.

TABLE 8

Fabricating Conditions and Results of Examination of Extruded Thorium Rod

X-RAY DIFFRACTION SPECIFICATION NO.	EXTRUSION SAMPLE NO.*	BILLET SIZE (diameter and length in inches)	BILLET TEMPERATURE (°C)	EXTRUSION RATE (ft/min)	DEGREE OF RECRYSTALLIZATION	TEXTURE
40	A-239-C2	3 by 4	850	2.7	None	[111] strong [100] strong
41	A-222-C	3 by 4	850	560.	Complete	[114] strong
42	A-231-B	3 by 8	800	32	Nearly complete	[114] strong [100] medium
43	A-231-A	3 by 8	800	31	Nearly complete	[114] strong [100] medium
44	A-239-B	3 by 6	850	> 400	Nearly complete	[114] strong [100] weak
45	A-239-A	3 by 6	850	> 400	Nearly complete	[114] strong [100] weak
46	A-239-D1	3 by 4 7/8	850	515	Nearly complete	[114] strong [100] medium
47	A-223-A	3 by 4 7/8	850	32	Nearly complete	[114] strong [100] medium

*Diameter of extruded rod, 1 in; extrusion ratio, 9:1; extrusion water quenched at die; samples taken 18 in. from front end of extruded length.

represents the unrecrystallized portion, since this texture is not present in the completely recrystallized sample. Apparently the growing recrystallized grains selectively absorb those deformed regions composing the [111] texture.

This well-developed deformation texture will impart marked anistropy to the mechanical properties of the rod. The yield and tensile strengths in the longitudinal direction, for instance, will be much higher than those at 45 deg to the longitudinal direction or in the transverse direction – a consequence of the low resolved shear stress on the slip planes under applied stress in the longitudinal direction and the relatively high shear stress under applied stress in either of the other directions. Similar considerations lead to the prediction that the longitudinal mechanical strength of the rod with the deformation texture will be greater than that of the rod with the recrystallization texture, aside from any effect from differences in degree of strain hardening.

Fig. 22. Longitudinal Section of 1-in.-dia Extruded Thorium Rod in As-Extruded Condition Showing Deformed Grain Structure. Met. spec. 3916; sample A-239-C2-40; etched with acetic-perchloric acid. 200X.

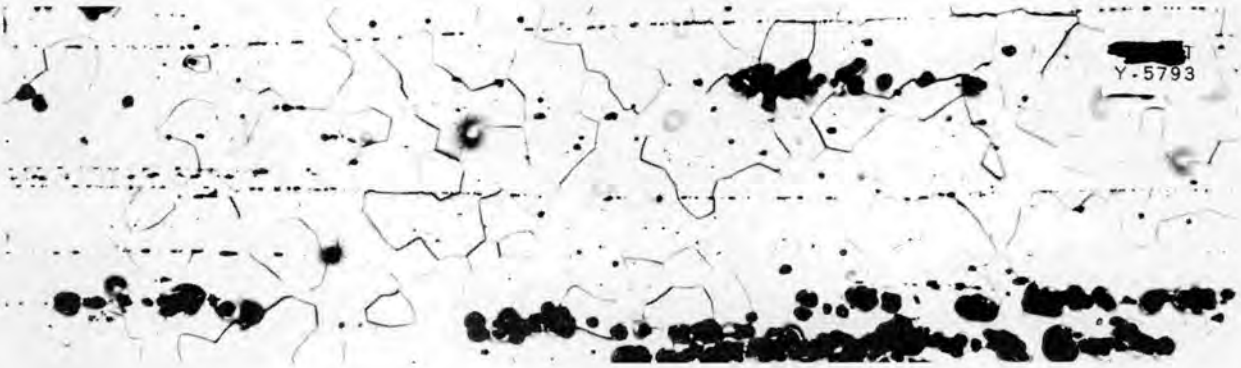

Fig. 23. Longitudinal Section of 1-in.-dia Extruded Thorium Rod in As-Extruded Condition Showing Completely Recrystallized Grain Structure. Met. spec. 3917; sample A-222-C-41; etched with acetic-perchloric acid. 200X.

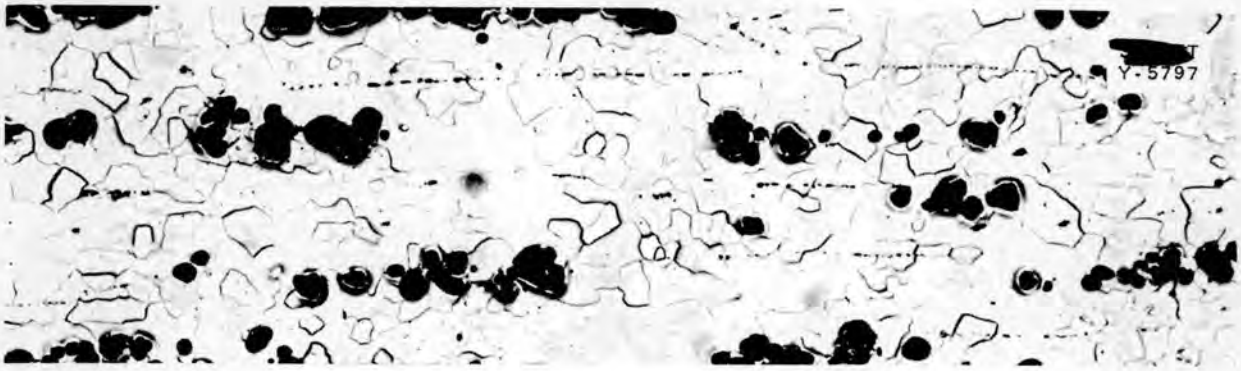

Fig. 24. Longitudinal Section of 1-in.-dia Extruded Thorium Rod in As-Extruded Condition Showing Nearly Completely Recrystallized Grain Structure. Met. spec. 3921; sample A-239-D1-46; etched with acetic-perchloric acid. 200X. This structure is also representative of samples A-231-B-42, A-231-A-43, A-239-B-44, A-239-A-45, A-233-A-47.

[redacted]

DWG. 14847

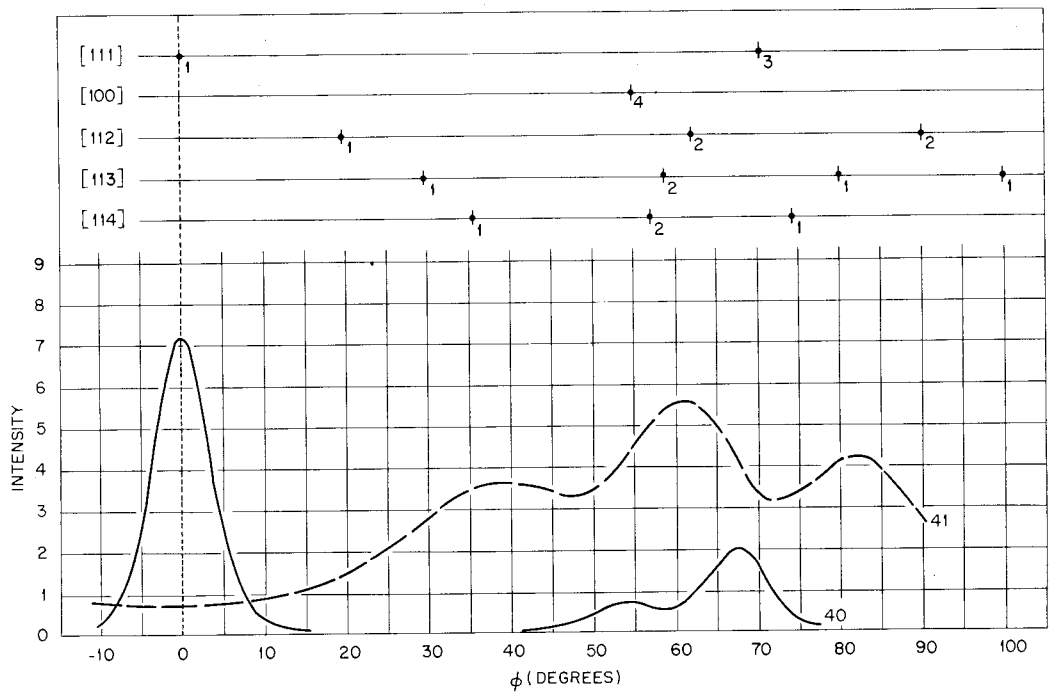

Fig. 25. Preferred Orientation Plot - (111) - 1-in.-dia Extruded Thorium Rod.

[redacted]

DWG. 14848

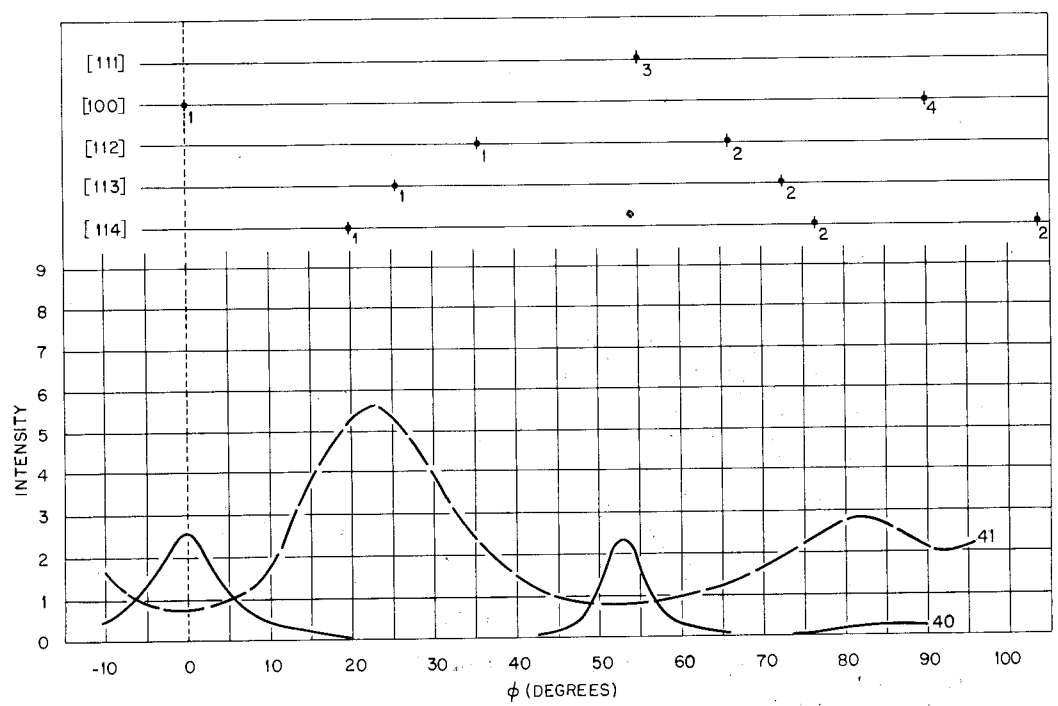

Fig. 26. Preferred Orientation Plot - (200) - 1-in.-dia Extruded Thorium Rod.

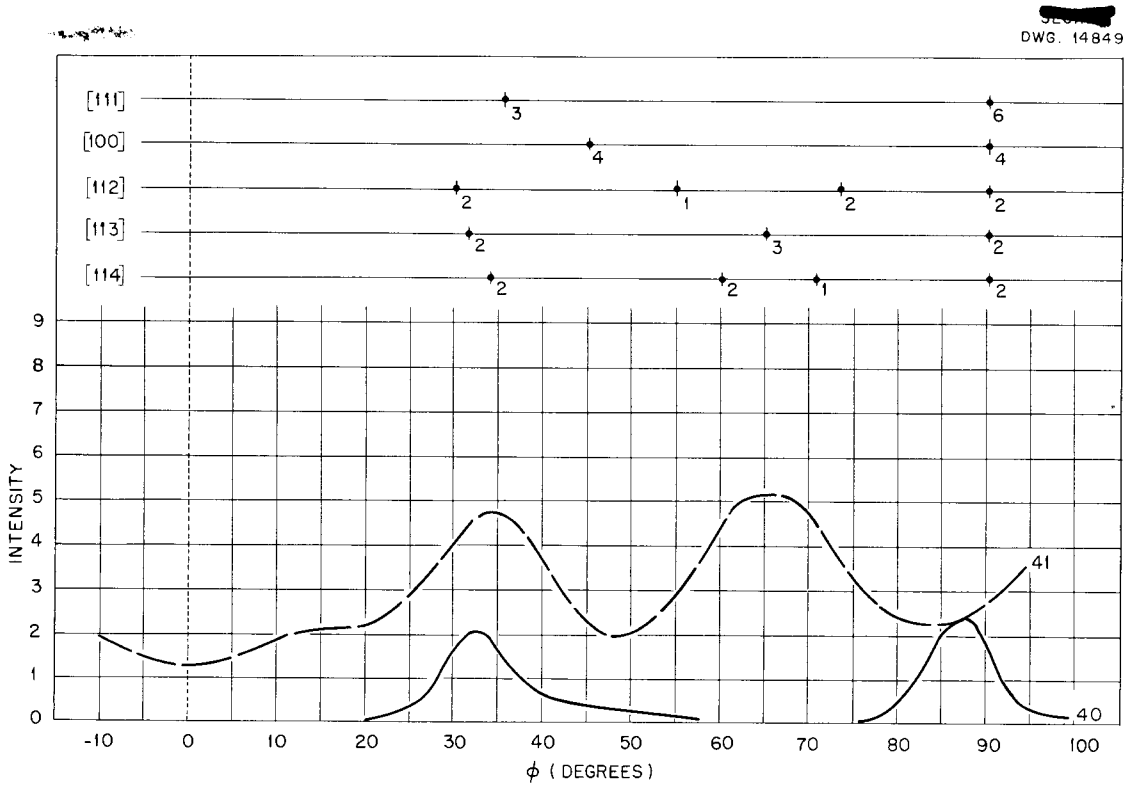

Fig. 27. Preferred Orientation Plot - (220) - 1-in.-dia Extruded Thorium Rod.

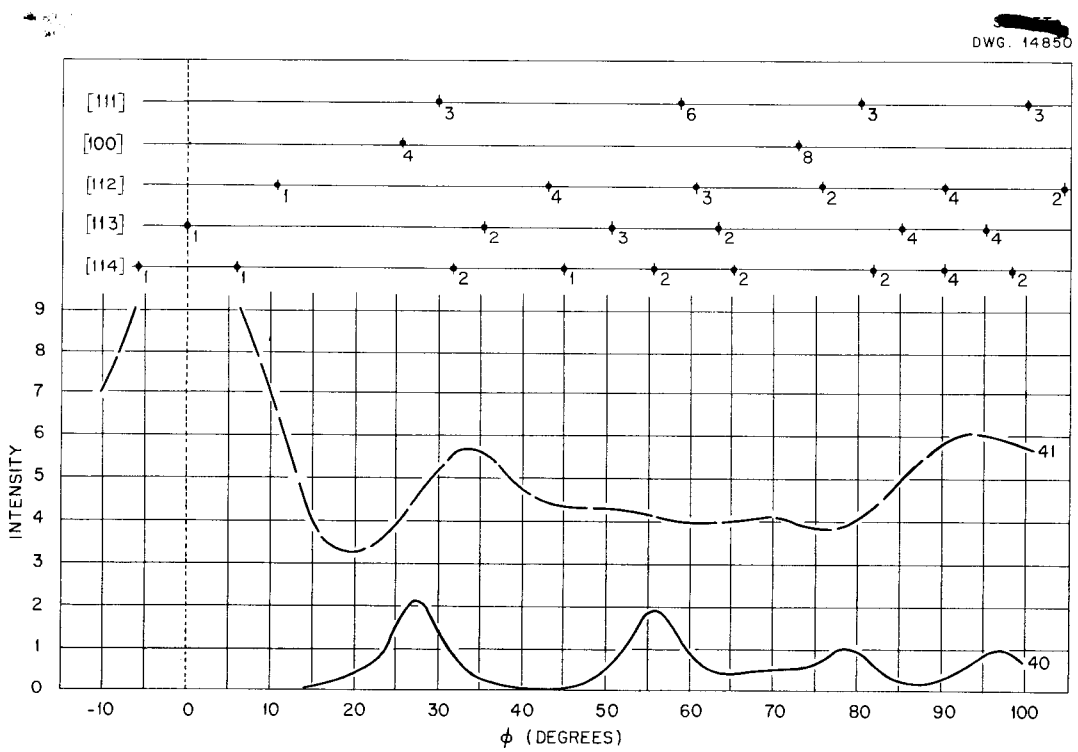

Fig. 28. Preferred Orientation Plot - (311) - 1-in.-dia Extruded Thorium Rod.

[redacted]

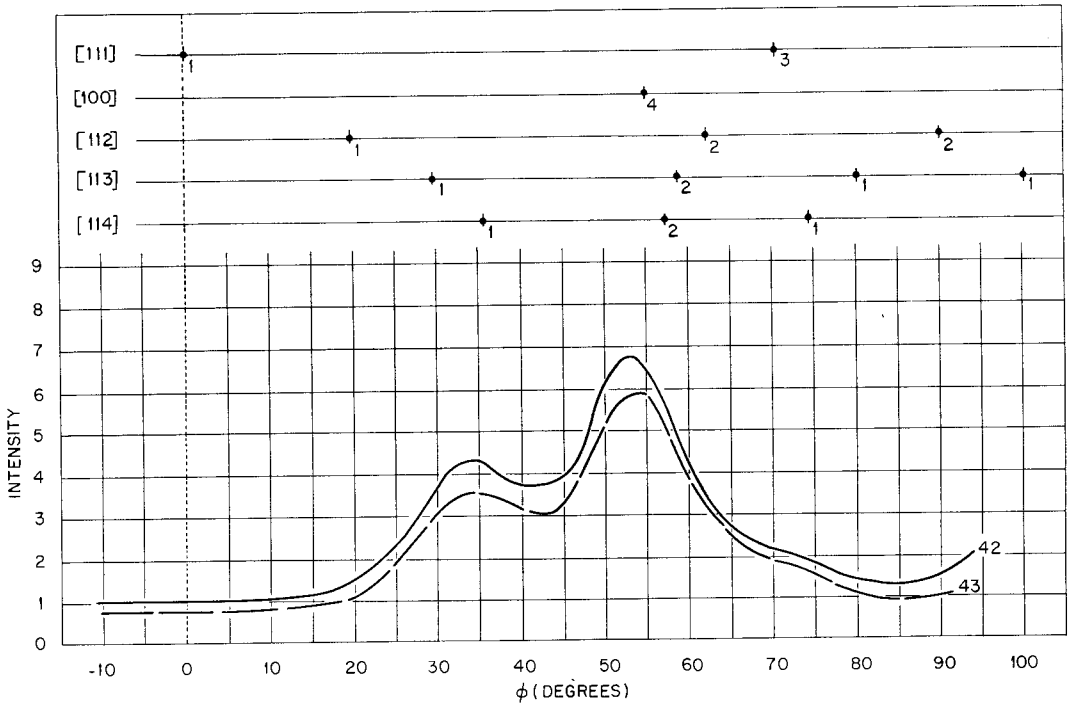

Fig. 29. Preferred Orientation Plot – (111) – 1-in.-dia Extruded Thorium Rod.

[redacted]

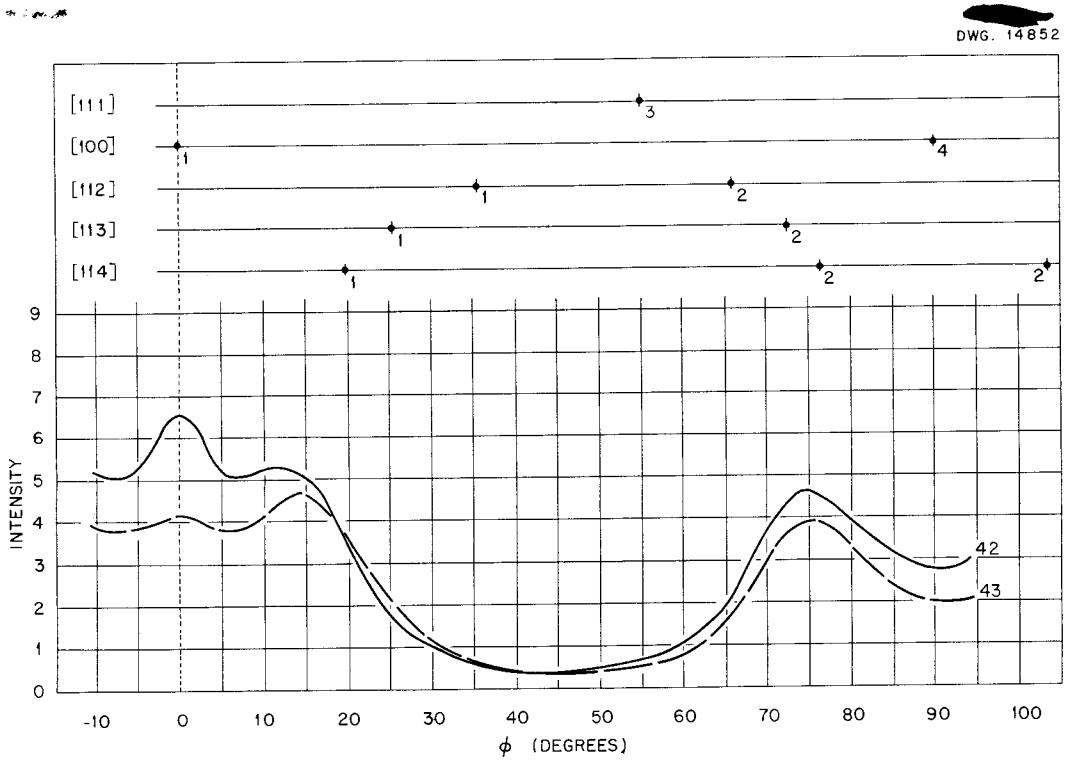

Fig. 30. Preferred Orientation Plot – (200) – 1-in.-dia Extruded Thorium Rod.

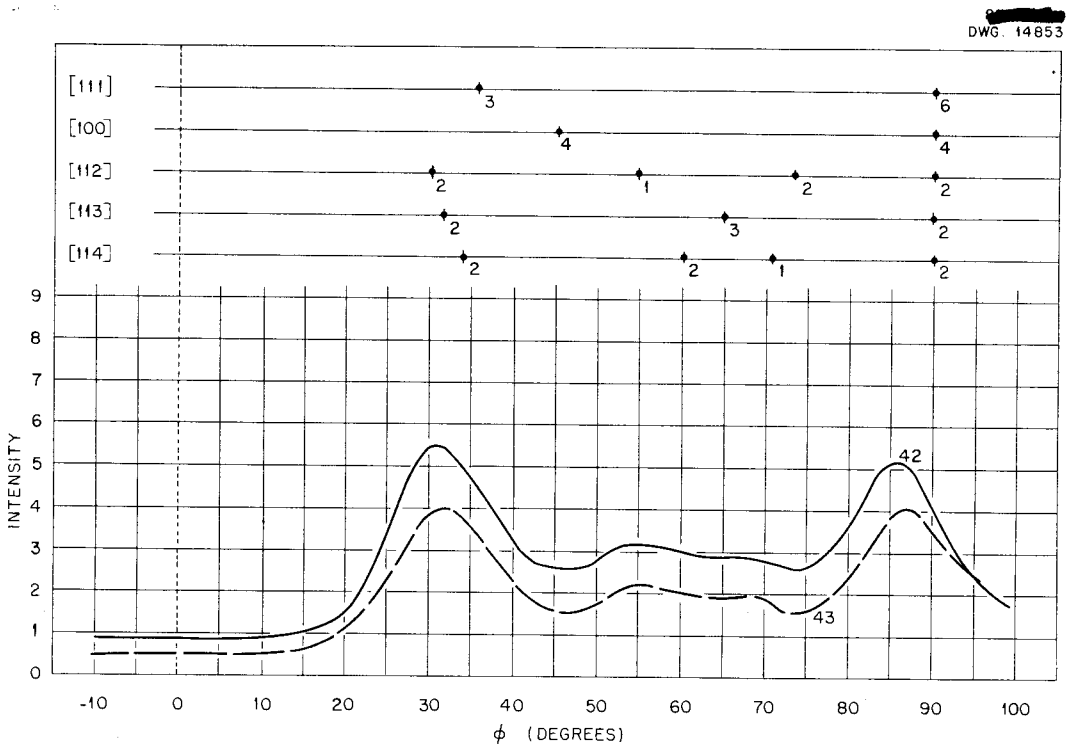

Fig. 31. Preferred Orientation Plot - (220) - 1-in.-dia Extruded Thorium Rod.

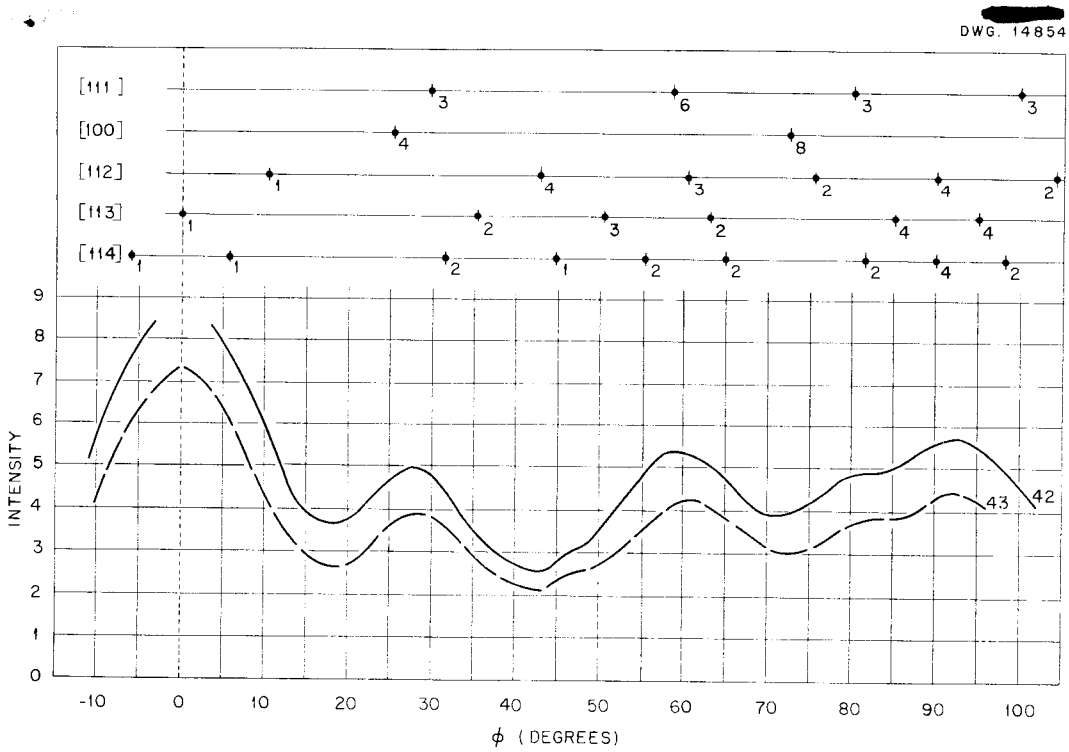

Fig. 32. Preferred Orientation Plot - (311) - 1-in.-dia Extruded Thorium Rod.

[redacted]

DWG. 14855

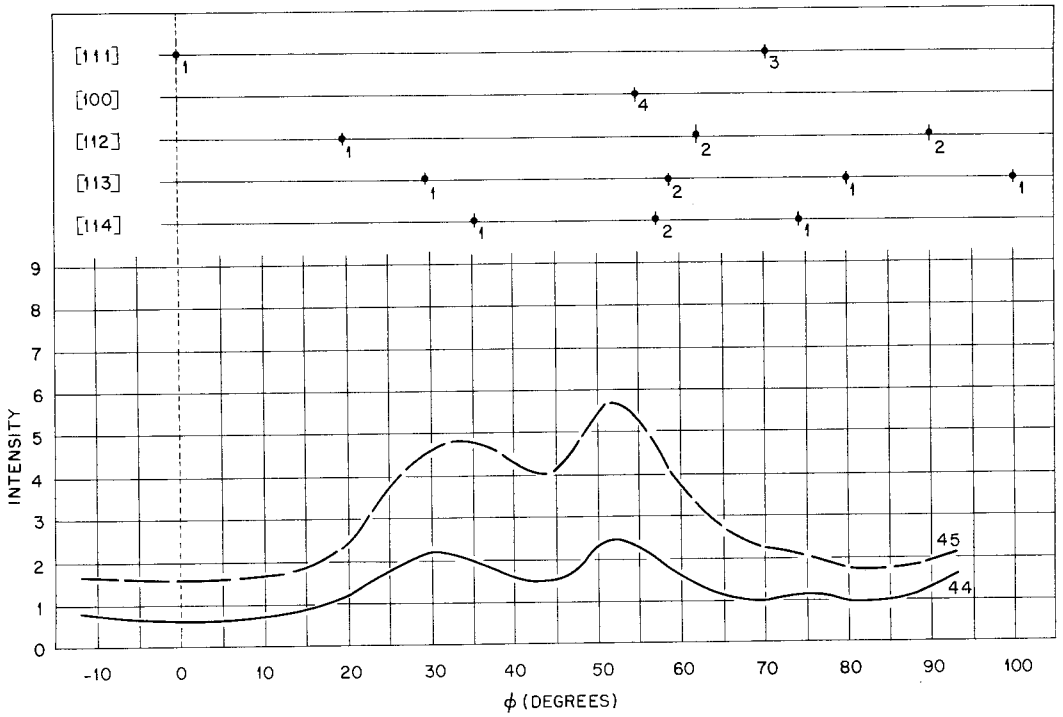

Fig. 33. Preferred Orientation Plot - (111) - 1-in.-dia Extruded Thorium Rod.

[redacted]

DWG. 14856

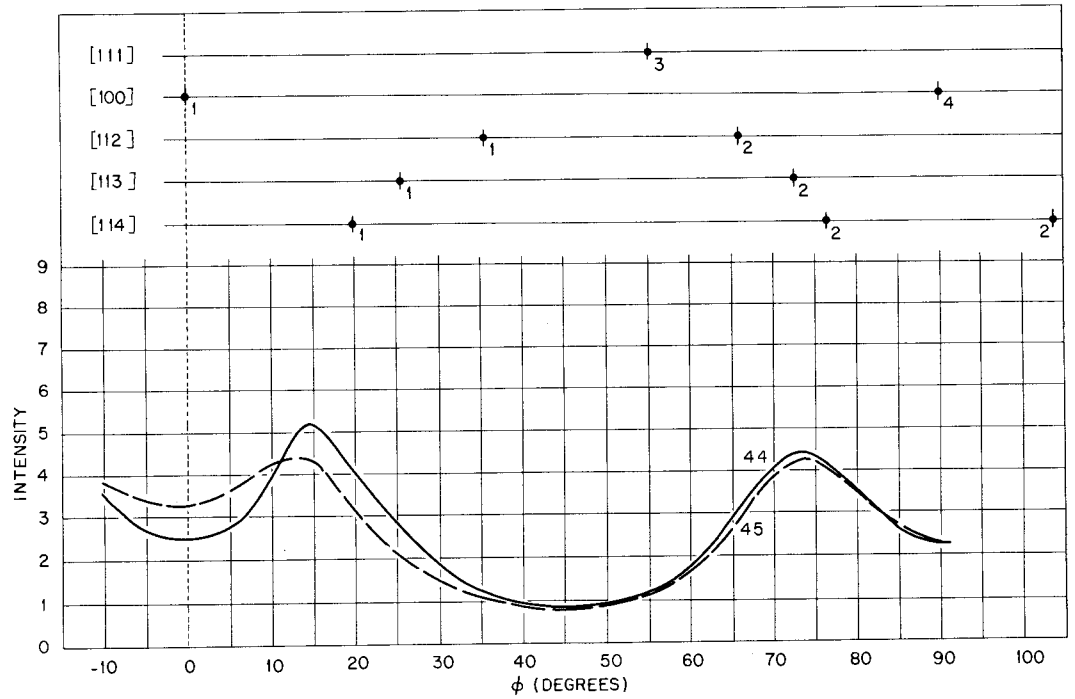

Fig. 34. Preferred Orientation Plot - (200) - 1-in.-dia Extruded Thorium Rod.

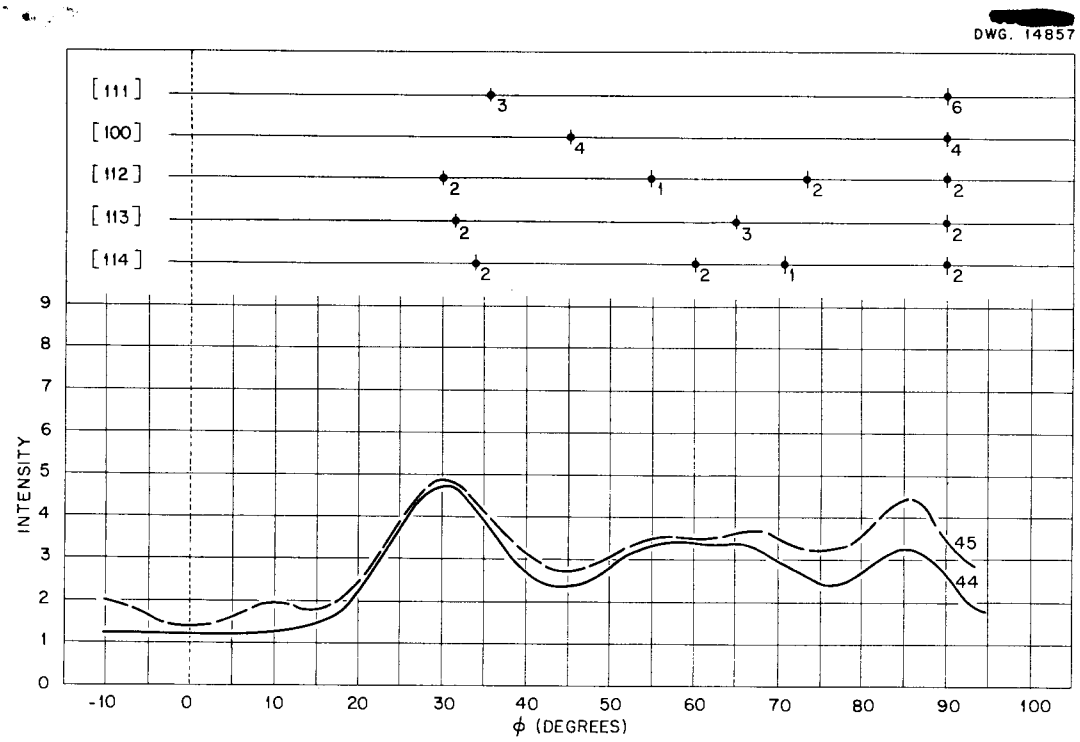

Fig. 35. Preferred Orientation Plot - (220) - 1-in.-dia Extruded Thorium Rod.

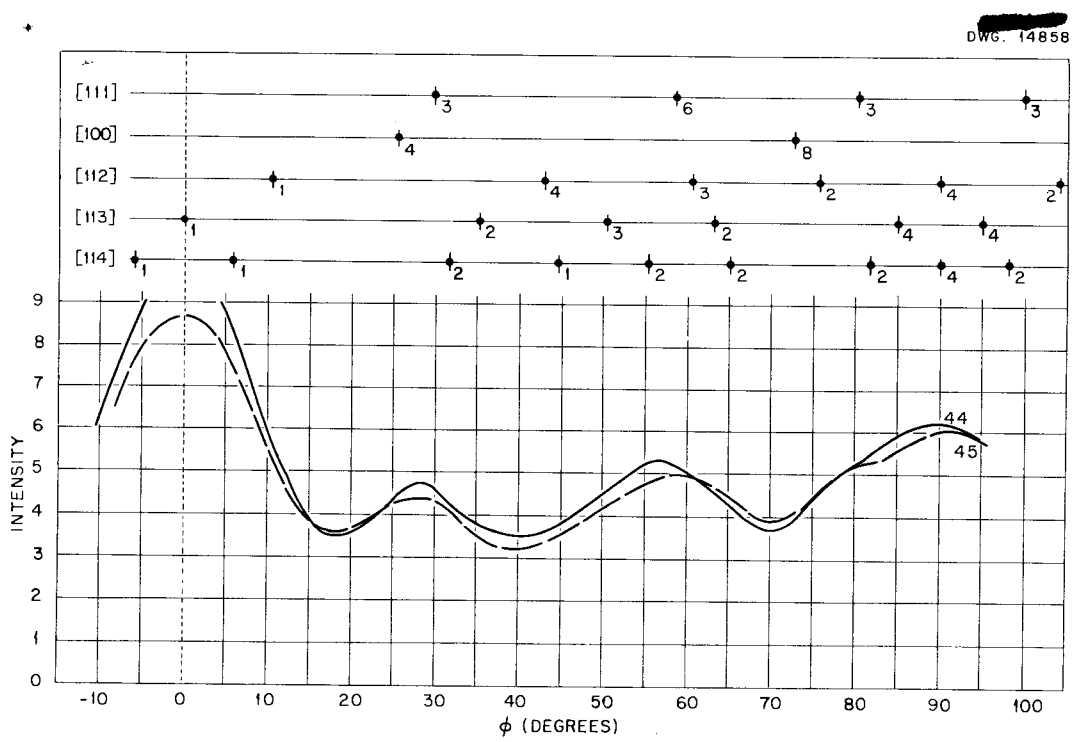

Fig. 36. Preferred Orientation Plot - (311) - 1-in.-dia Extruded Thorium Rod.

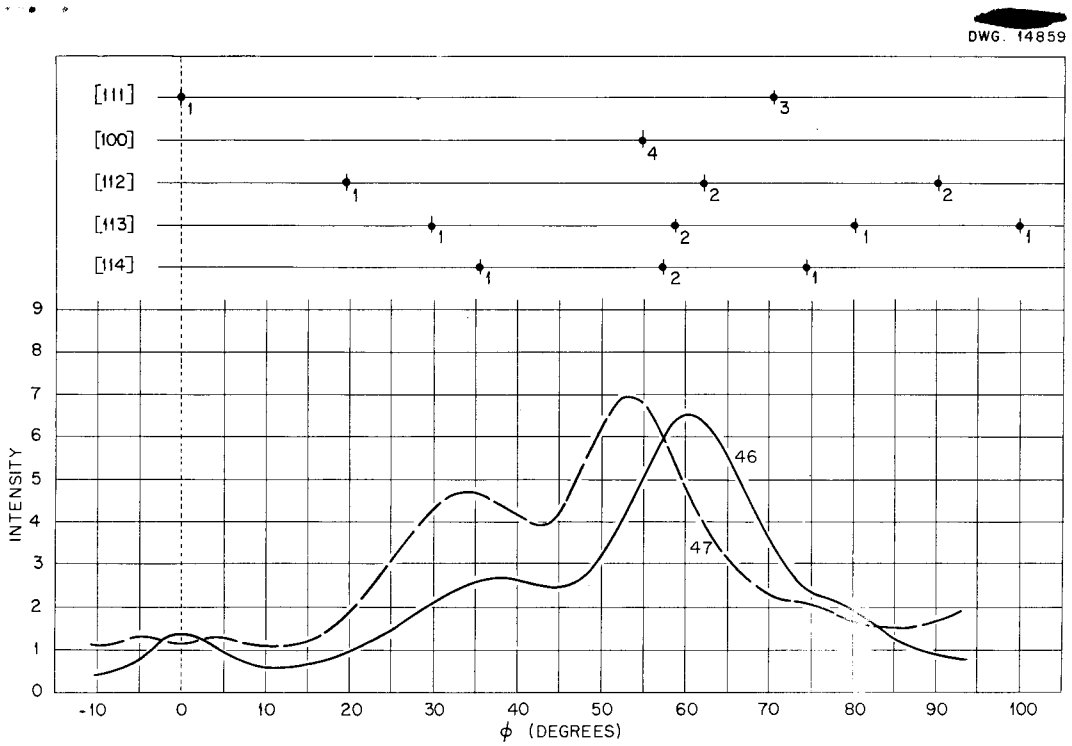

Fig. 37. Preferred Orientation Plot - (111) - 1-in.-dia Extruded Thorium Rod.

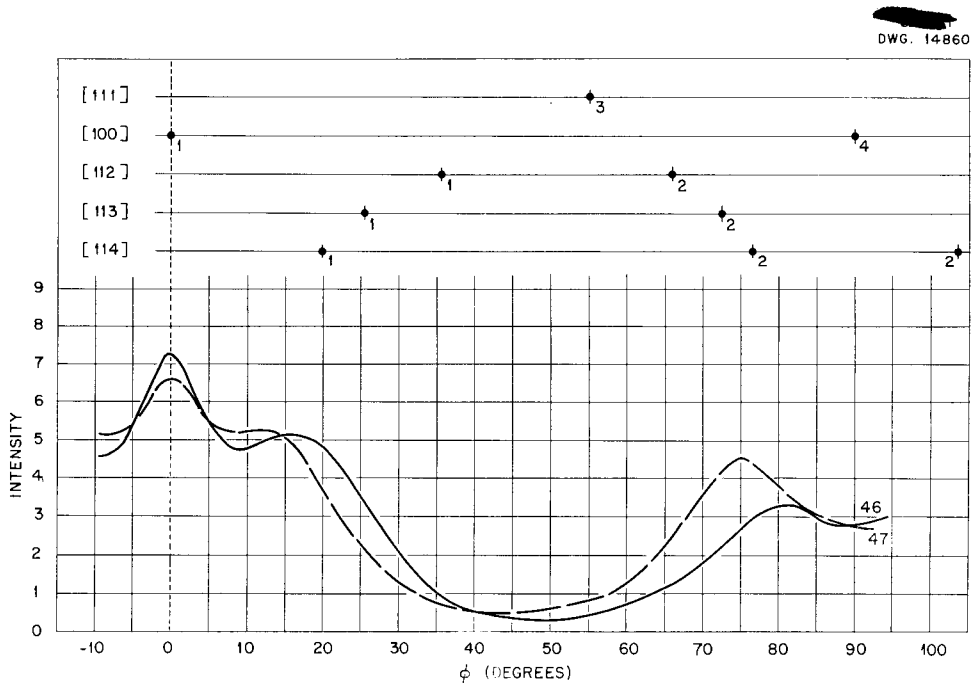

Fig. 38. Preferred Orientation Plot - (200) - 1-in.-dia Extruded Thorium Rod.

[redacted]

DWG. 14861

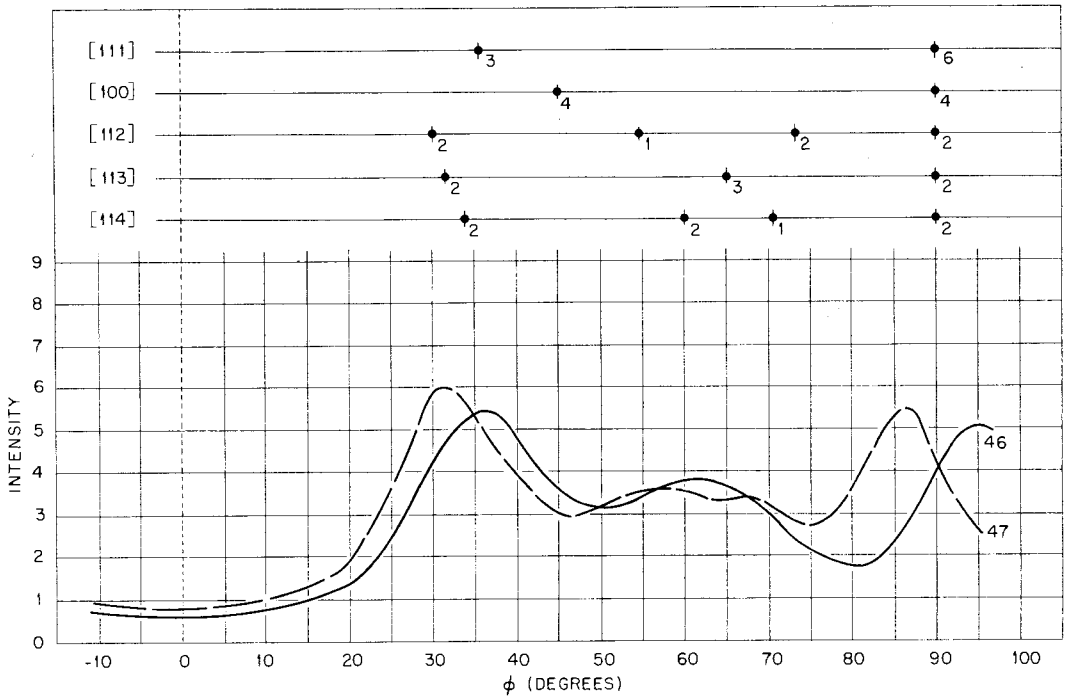

Fig. 39. Preferred Orientation Plot – (220) – 1-in.-dia Extruded Thorium Rod.

[redacted]

DWG. 14862

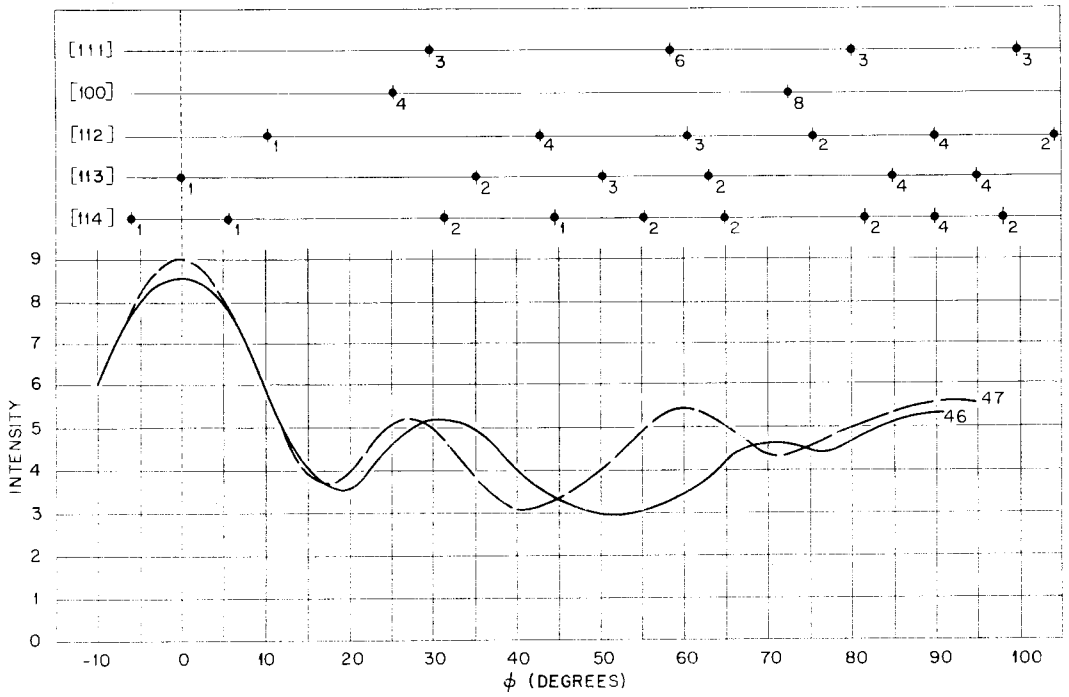

Fig. 40. Preferred Orientation Plot – (311) – 1-in.-dia Extruded Thorium Rod.

FUNDAMENTAL STUDIES OF ALLOYING

J. O. Betterton T. M. Kegley, Jr.

The study of the group IV*a* elements titanium, zirconium, and hafnium has begun with the binary phase diagrams of the systems silver-zirconium, cadmium-zirconium, indium-zirconium, tin-zirconium, and antimony-zirconium. These *B* subgroup solute elements extend along the same horizontal row in the periodic table as zirconium, and the metallic valences of these elements are usually considered to be 1, 2, 3, 4, and 5, respectively. The mixing of zirconium in these elements will therefore show the influence of changing solute valency in the phase diagrams.

The study of zirconium alloys involves certain difficulties in experimental technique. Earlier work indicated that titanium and zirconium react in the liquid state with graphite and all the usual refractories. Furthermore, in both the liquid and solid state, titanium and zirconium react readily with oxygen, nitrogen, and hydrogen gas at elevated temperatures.

One method for avoiding some of these difficulties is that of arc melting the reactive metal on a water-cooled copper plate such as that first used by von Bolton[1] for melting tantalum. This method was chosen for casting the zirconium alloys. In the present experiments the arc furnace designed by the Thorium Research Group is used.[2] The argon gas used inside the glass bell jar unit of the furnace is purified with zirconium machinings maintained at about 800°C, and the arc casting is done at a pressure of one-half atmosphere. The Vickers hardness of a typical, pure-zirconium casting melted in this way was found to be in the range of 80 to 100 VPN for a 10-kg load, which may be compared with the original crystal bar hardness of 64 to 84 VPN. This small increase in hardness during casting is probably partly owing to gas contamination, since the hardness of zirconium is known to increase rapidly when oxygen or nitrogen is added. However, since the weight gains of the ingots during casting were small, ranging from 0.0001 to 0.002%, a second part of the hardness increase is thought to result from changes in grain structure of the cast ingot as compared with the iodide-deposited bar

When the first alloys prepared by this method were annealed, the zirconium alloy reacted with the silica annealing container, and the alloy hardened to such an extent that a new container material was desirable. Also, the vacuum system used to evacuate the container was suspected of being inadequate. Experiments were therefore started to determine (1) the appropriate container material, and (2) the degree of evacuation required for heating pure zirconium at 1000°C for long times without gas contamination. These annealing experiments were done in a mullite combustion tube that was continuously evacuated with a glass diffusion pump. Small pieces of iodide-deposited zirconium, weighing 2 to 3 g, were annealed in various types of combustion boats and at different pressures. The results of

(1) W. von Bolton, "Das Tantal, Seine Darstetlung und Seine Eigenschaften," *Z. Electrochem.* **11**, 45 (1905); C. W. Balke, "The Story of Tantalum," *Chemistry & Industry*, p. 83 (1948).

(2) "Thorium Alloy Development," *Metallurgy Division Quarterly Progress Report for Period Ending July 31, 1951*, ORNL-1108, p. 10.

these experiments, after annealing for two days at temperatures between 960 and 1060°C, are shown in terms of weight changes and hardness changes on Fig. 41. It is readily seen from examination of these graphs that a vacuum of the order of 1×10^{-6} mm Hg is required for satisfactory annealing of pure zirconium for long periods of time at 1000°C. The effect of the different boat materials was not so great at this temperature as that of the pressure, and the differences observed were thought to be within the limit of experimental error.

Long-time heat treatments in phase diagram investigations usually involve the use of quartz or glass capsules, rather than a continuously evacuated tube, so that several capsules, each containing a different alloy, may be annealed in a simple muffle furnace without interchange of alloy constituents or maintenance of a continuous pumping system. This method was used for a series of survey experiments on small, 2 to 3 g, samples of iodide-deposited zirconium. The variables tested were:

1. use of interface materials (molybdenum foil, zirconium foil, and stabilized zirconia) between the specimen and the quartz tube,

2. use of a purified argon atmosphere inside the capsule,

3. use of a prolonged degassing treatment under vacuum prior to sealing off the capsule.

The results of these experiments are shown in Table 9. It was found that weight changes in the capsule annealing did not correlate so well with hardness changes as in the anneals

UNCLASSIFIED
DWG. 14863

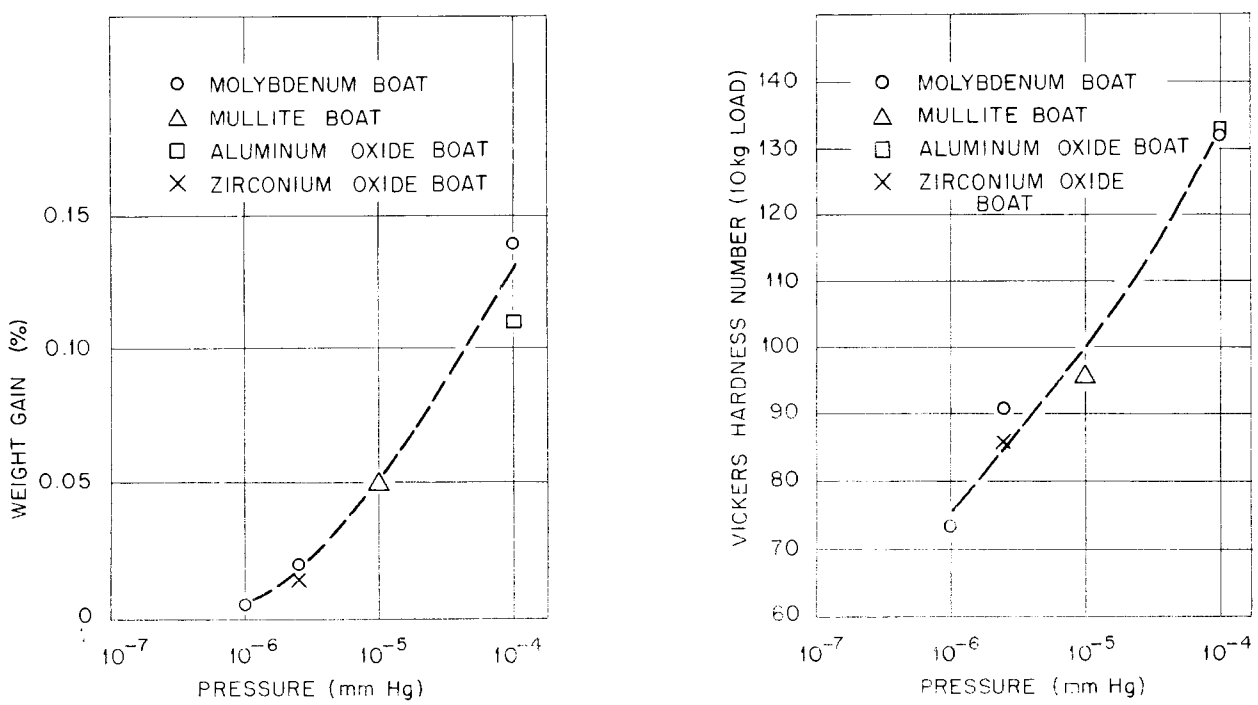

Fig. 41. Effect of Vacuum Pressure on Hardness and Weight Change of Zirconium Specimens Annealed for Two Days at 1000°C.

in the continuously pumped muffle tube. Some of the hardest specimens, for example, actually lost weight. This curious phenomenon is not fully understood but may be attributable to a volatile reaction product containing zirconium within the capsule, since the vapor pressure of pure zirconium is very small at this temperature.

The hardness of the iodide-deposited crystal bar used in these experiments varied with grain orientation between 65 and 85 VPN. The specimens degassed at 1000°C were slowly heated for 2 to 6 hr under a vacuum (always less than 0.3 micron) at a temperature of 1000°C. They were then cooled to room temperature and the capsules were sealed under vacuum or filled with purified argon and sealed.

Of the interface materials tested, zirconium foil proved to be the most effective in producing a specimen of low hardness. The next best material was molybdenum foil. Both the zirconium foil and the molybdenum foil tend to adhere to the specimen at sharp contact points, and some diffusion occurs in this region. For example, a spectroscopic analysis of a contact point on a silver-zirconium alloy, from which adhered molybdenum foil had been stripped after an eight-day anneal at 1000°C, showed that the contact point contained several weight per cent of molybdenum at the surface and approximately one-half as much 0.002 in. below the surface. On areas of the surface to which the foil had not adhered, no molybdenum was detected. The molybdenum at the contact points was removed by grinding and an

TABLE 9

Weight Change and Hardness of Small Zirconium Specimens After Annealing for Two Days at 1000°C in Quartz Capsules Under Various Conditions

CRUCIBLE OR JACKET SEPARATING ZIRCONIUM FROM QUARTZ	VACUUM DEGASSED AT 1000°C BEFORE SEALING		VACUUM DEGASSED AT 20°C BEFORE SEALING	
	VICKERS HARDNESS (10 kg load)	WEIGHT CHANGE (%)	VICKERS HARDNESS (10 kg load)	WEIGHT CHANGE (%)
	Argon Atmosphere with Capsule			
None	106	+0.004	155	-0.30
Molybdenum	97	-0.019	106	-0.10
Zirconia	104	-0.05	165	-0.13
Zirconium	83	+0.01		
	Evacuated Capsules			
None	109	+0.003	104	-0.20
Molybdenum	96	-0.036	99	-1.0
Zirconia	110	-0.345	135	-1.1
Zirconium	88	-0.008		

TABLE 10

Hardness and Weight Changes in 2- to 3-g Specimens of Iodide-Deposited Zirconium That Were Degassed Only

MAXIMUM PRESSURE REACHED DURING DEGASSING (microns)	CONDITIONS	VICKERS HARDNESS (10 kg load)	WEIGHT CHANGE (%)
3	Heated for 30 min to maximum temperature of about 800°C in zirconia crucible	77	+0.01
0.16	Slowly heated for 3 hr to a maximum temperature of 1003°C in zirconium-foil envelope	69	−0.0003

apparently satisfactory specimen was obtained. For the present, the specimens for the investigation of alloys will be wrapped in pure-zirconium foil. The extent to which depletion of the solute from the alloy occurs at the points of contact will be determined as the experiments are done.

The effects of the other variables (shown in Table 9) are that (1) degassing at 1000°C results in somewhat lower hardness and a smaller weight loss and (2) the use of an argon atmosphere results in a slightly lower hardness in the case of the specimens degassed up to 1000°C. When the degassing was done only at room temperature, the relatively small and questionable effect of argon was to increase the resulting hardness. The latter effect may be an experimental error since the evacuation of the capsules in the argon tests was done at 0.1 micron; whereas, in the tests without argon, the evacuation was done at 0.004 to 0.01 micron.

In connection with the above, it was of interest to examine the hardness and weight changes of two specimens that were degassed but not annealed. The results are given in Table 10 and it can be seen that even in the case where the degassing pressure rose to 3 microns the hardening of the zirconium was not great. The usual procedure, illustrated by the specimen with a maximum degassing pressure of 0.16 micron, resulted in a lowering of the hardness. This shows, with reasonable certainty, that the hardening effects shown in Table 9 occurred after the capsules were sealed off. Future experiments will be done to determine whether the effects are attributable to a slight permeability of the quartz to gases at 1000°C or whether a still more thorough removal of gases from inside the capsule would be advantageous.

SILVER-ZIRCONIUM SYSTEM

The silver-rich end of the silver-zirconium system has been investigated by Raub and Engel.[3] They found the solid solubility of zirconium in silver to be very restricted, with the maximum being less than 0.12 at. %

[3] E. Raub and M. Engel, "Die Legierungen des Zirkoniums mit Kupfer, Silber und Gold," *Z. Metallkunde* **39**, 172 (1948).

of zirconium at 955°C. The liquidus curve initially rises rapidly, with increasing zirconium content, from the eutectic point at 3 at. % of zirconium and 955°C to 5.4 at. % of zirconium at 1050°C. The liquidus curve then levels off and is remarkably flat in the region where the first intermediate phase, AgZr, forms congruently from the melt at 1135°C. The crystal structure of the compound, according to the powder pattern of Raub and Engle, is face-centered tetragonal with a gold-copper ordered arrangement of atoms. The only work that has been done in the zirconium-rich part of the phase diagram is a preliminary investigation of alloys of up to 6.6 at. % of silver by Anderson, Hayes, Roberson, and Kroll.[4] The alloys were hot swaged in an iron sheath at 850°C and then examined microscopically. They were found to have the typical acicular microstructure of the decomposed beta-zirconium phase.

In the present study, the alloys were prepared by the arc-casting method from iodide-deposited zirconium of 99.4% purity[5] and silver of 99.999% purity, supplied by Handy and Harmon, Inc. The following compositions (expressed in atomic per cent of silver) were made: 0.2, 0.4, 0.6, 0.8, 1, 2, 3, 4, 5, 6, 7, 8, 9, 10, 15, 33.3, 36.2, 40, 50, and 66.67. It was found that a small amount of silver vaporized from the alloys during casting. The observed specimen weight losses would amount to reductions in silver content of between 0.1 and 1.3 at. %. These weight losses were greatest in alloys 10 and 15 and were much smaller (0.2 to 0.3%) in alloys of 33 to 67 at. % of silver. These differences show a possible influence of stable compound formation in the alloys.

The buttons of the alloys between 0.2 and 15 at. % of silver were found to be quite ductile, and buttons of each of the alloys were cold pressed between flat dies (about 10 to 20%) to decrease the time required to reach equilibrium upon annealing.

Alloys 1, 3, 5, 10, and 15[6] were wrapped in molybdenum foil and annealed for two days in the range 973 to 1011°C within an argon-filled quartz capsule. Alloy 10 was annealed for two days and for nine days at 978°C, and since the relative proportion of the two phases present in this alloy was the same after both anneals equilibrium was considered to be reached in all the alloys after two days at 978°C. These alloys were then reannealed for 12 days at 802°C.

The results of these anneals showed that the beta phase of the silver-zirconium system decomposes eutectoidly at some temperature below 802°C and that the solid solubility of the alpha phase is restricted to about 0.8 at. % of silver at 800°C, whereas the beta phase dissolves considerably more zirconium. The solid solubility limit of the beta phase at 1000°C, for example, is somewhat greater than 5 at. % of silver, and the eutectoid composition appears to be only slightly less than 3 at. % of silver. The microstructures of some of these alloys are illustrated in Figs. 42 through 46.

---

(4) C. T. Anderson, E. T. Hayes, A. H. Roberson, and W. J. Kroll, *A Preliminary Survey of Zirconium Alloys*, Bureau of Mines, Report of Investigations 4658, March 1950.

(5) Typical impurities (at. %) in the zirconium are 0.008 Al, 0.3 C, 0.003 Cr, 0.002 Cu, 0.04 Fe, 0.09 H, 0.005 Hf, 0.01 N, 0.02 Ni, 0.07 O, 0.02 Si, and 0.003 Ti. These same figures expressed in terms of weight percentage give, by difference, zirconium of 99.85% purity.

(6) For convenience, the alloys are represented by the number indicating their composition in atomic per cent of silver.

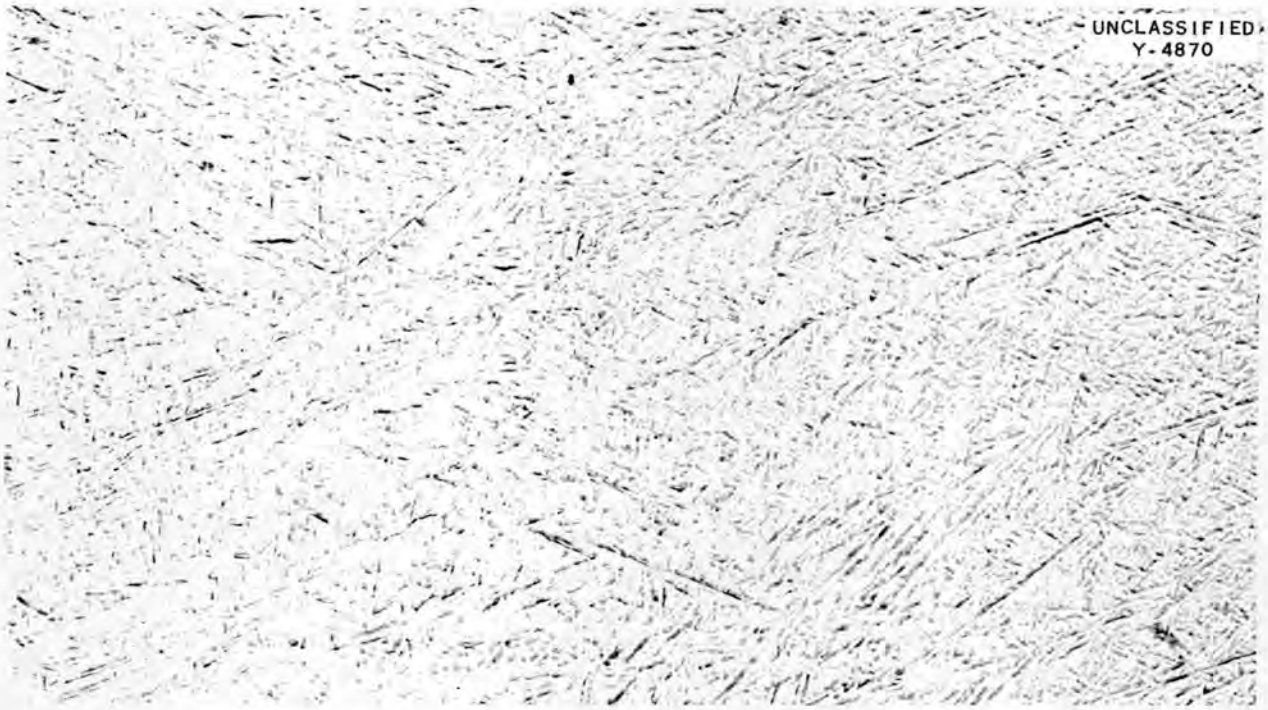

Fig. 42. Microstructure of Silver-Zirconium Alloy, 3.8 at. % Silver, Annealed 64 hr at 975°C, Showing Decomposed Beta Phase. Bright field. 250X.

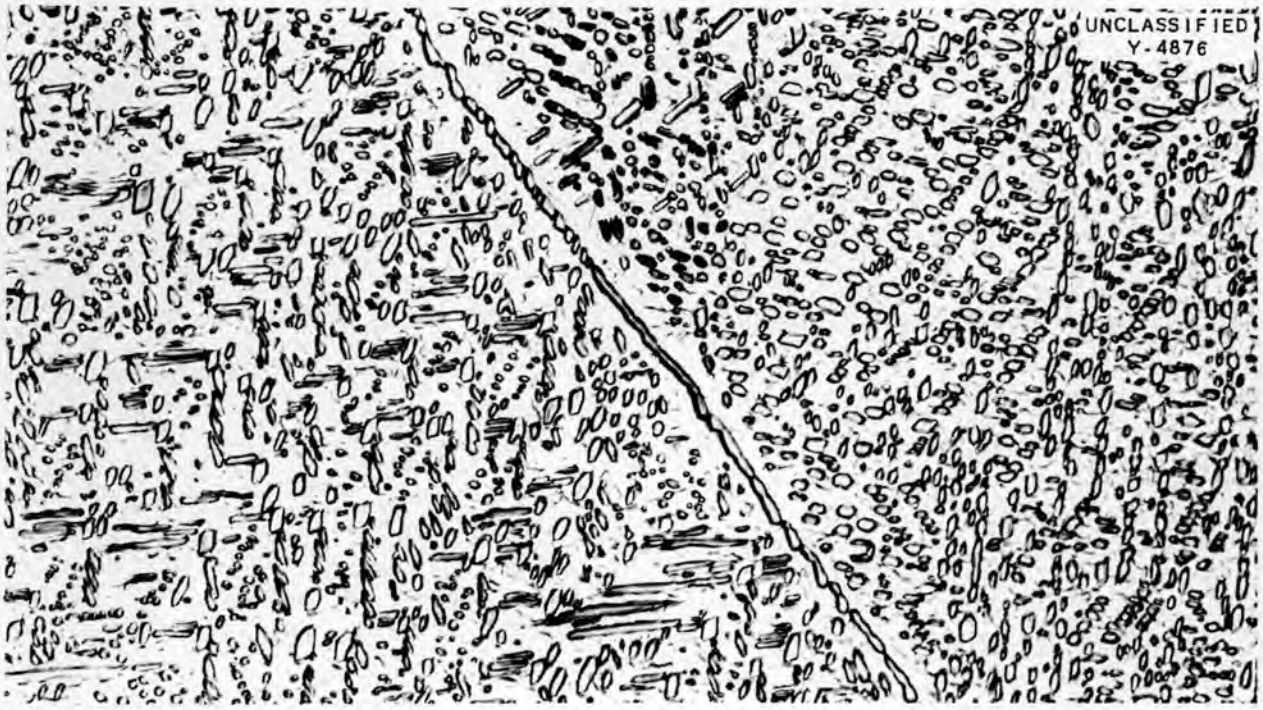

Fig. 43. Microstructure of Silver-Zirconium Alloy, 8.7 at. % Silver, Annealed 8 3/4 Days at 978°C, Showing Particles of Compound, Probably Ag_3Zr, Arranged in a Widmansatten Pattern on a Matrix of Decomposed Beta Phase. Bright field. 250X.

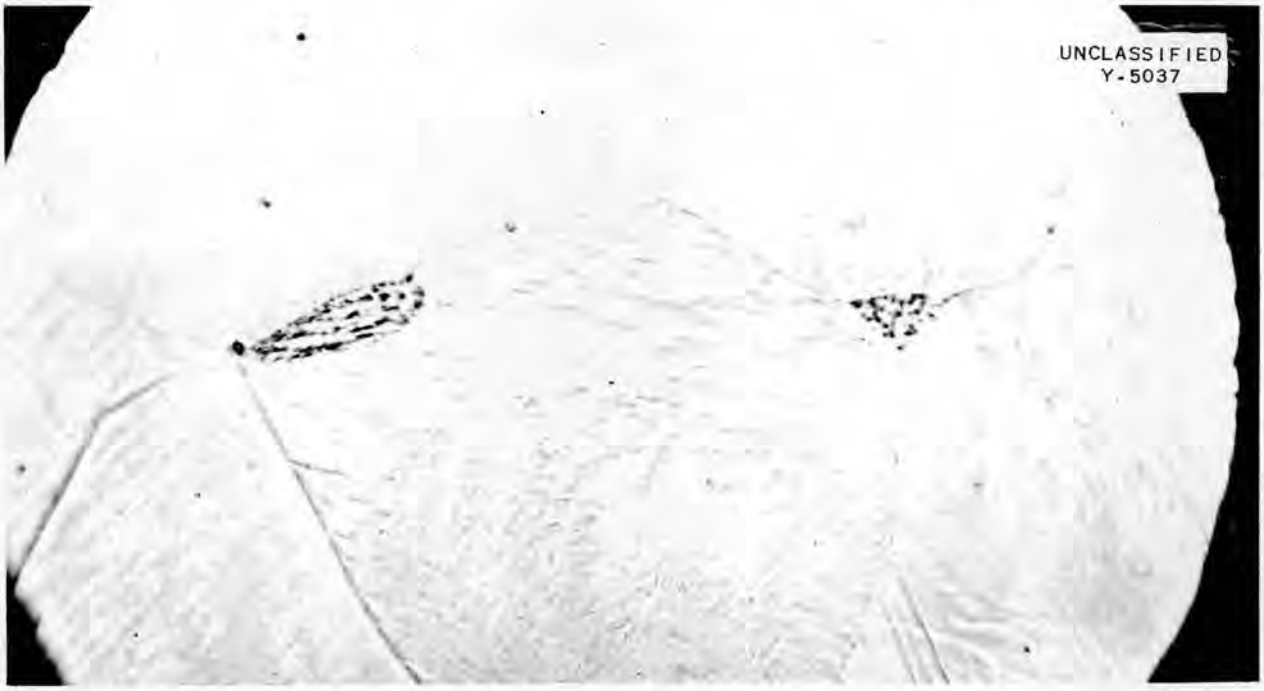

Fig. 44. Microstructure of Silver-Zirconium Alloy, 0.77 at. % Silver, Annealed 12 Days at 802°C, Showing Two Eutectoid Areas in Alpha-Phase Matrix. Bright field. 150X.

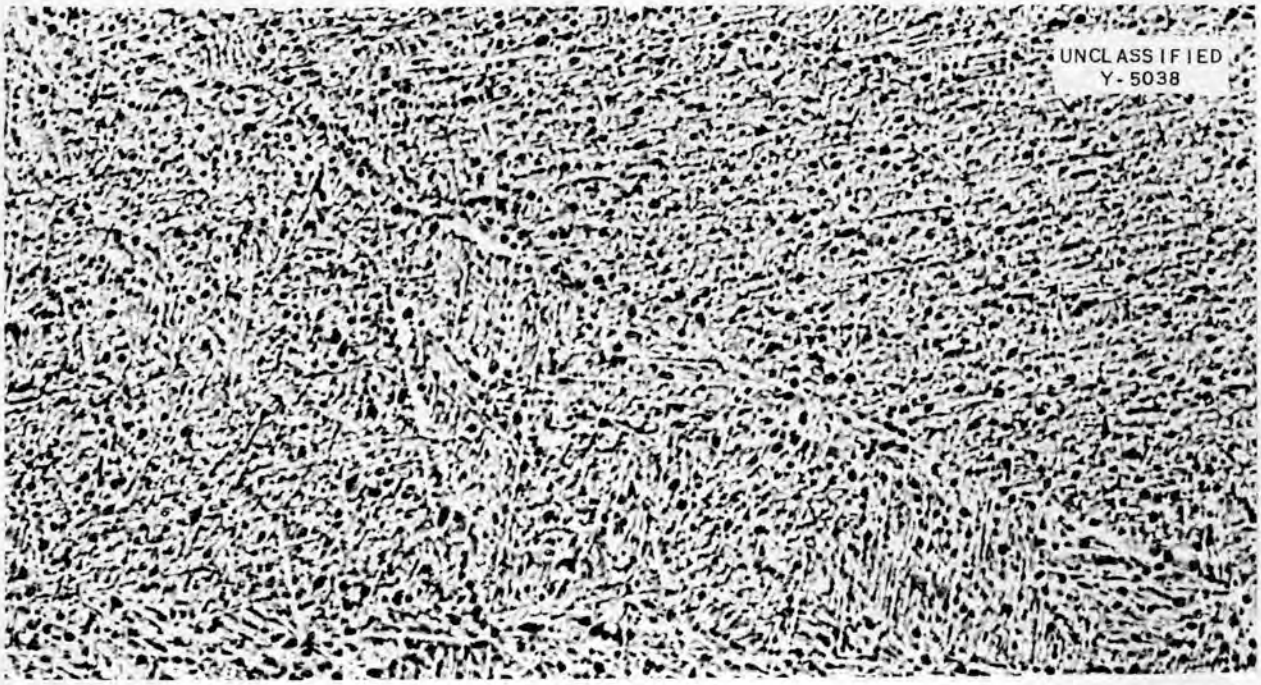

Fig. 45. Microstructure of Silver-Zirconium Alloy, 2.9 at. % Silver, Annealed 12 Days at 802°C, Showing Small, Dark Particles of Compound, Probably Ag_3Zr, in a Matrix of Decomposed Beta Phase. Bright field. 250X.

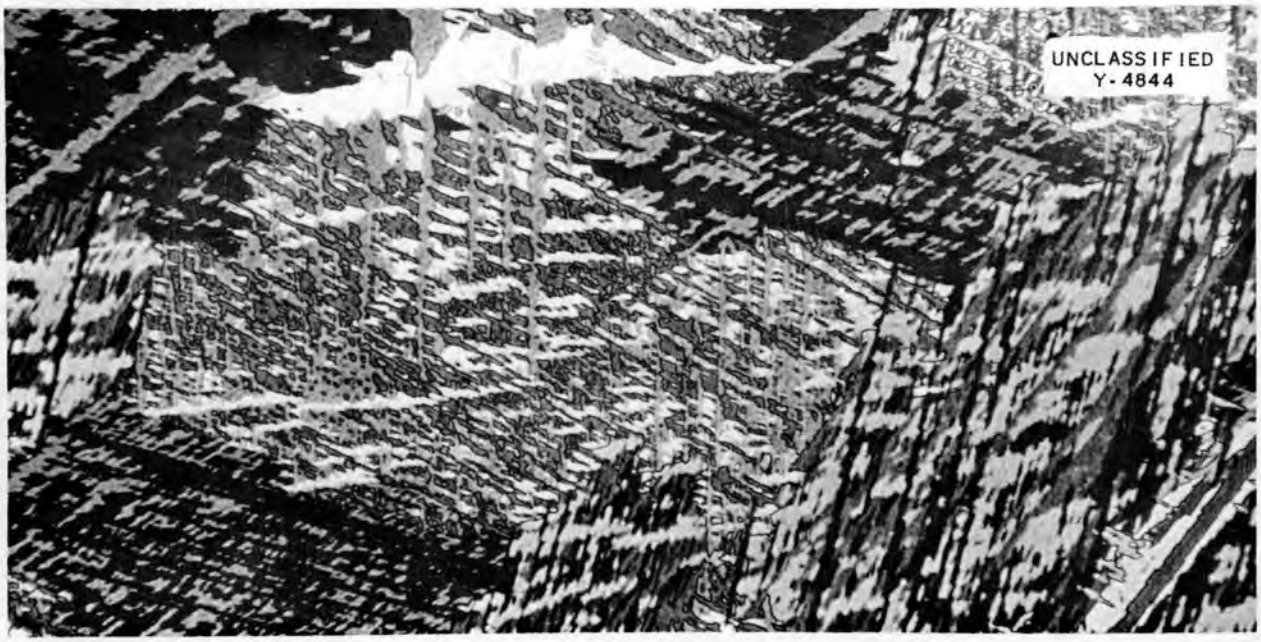

Fig. 46*a*. Silver-Zirconium Alloy, 0.77 at. % Silver, Annealed 48 hr at 1011°C, Quenched from the Beta Region, Showing the Decomposed Beta Phase and the Acicular or Basket-Weave Structure Typical of the Zirconium Reaction $\beta \rightleftharpoons \alpha$ During Quenching.

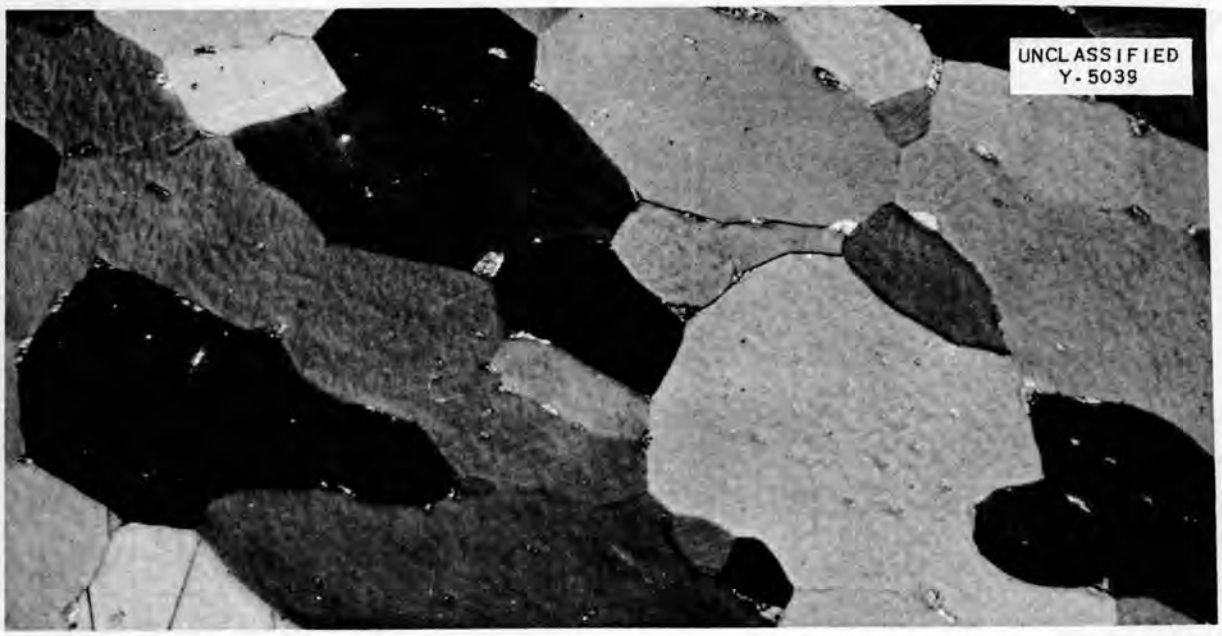

Fig. 46*b*. Silver-Zirconium Alloy, 0.77 at. % Silver, Annealed 12 Days at 802°C, Quenched from the Alpha Region, Showing the Alpha Phase with a Small Amount of Eutectoid. The shape of the alpha grains is typical of a phase that is annealed to equilibrium and quenched without transformation. Polarized light. 250X.

The first anneal of alloys 33 through 67 was for ten days at 779°C. The microscopic examination of these alloys was in agreement with the work of Raub and Engle[4] in that an intermediate phase occurs close to the composition 59 at. % of silver and no other intermediate phase appears at this temperature between the AgZr phase and the silver-rich solid solution.

Alloys 33, 36, and 40 did not appear to be fully in equilibrium after ten days at 779°C. This may possibly be a result of the omission of the cold working before heat treatment because these higher silver-content alloys were brittle. Two phases were predominant in these alloys, that is, the AgZr phase and another intermediate phase presumably near the composition $AgZr_3$. In the next series of experiments, an ingot of alloy 40 will be cast, and all the alloys will be heat treated for longer times.

The solidus investigation of the silver-zirconium alloys will begin after a vertical quenching furnace of the type described by Shramm, Gordon, and Kaufmann[7] has been constructed. Meanwhile, the capsule anneals of silver-zirconium alloys will be continued to determine the low-temperature parts of the phase diagram more exactly.

INDIUM-ZIRCONIUM SYSTEM

A review of the literature has not revealed reports of previous investigation of indium-zirconium alloys. In the present experiments, alloys were arc cast from iodide-deposited zirconium and 99.99+% pure indium supplied by the American Smelting and Refining Company. Zirconium-base alloys of 9.6, 19.3, 23.0, and 33.5 at. % of indium were cast, with small weight losses. The weight losses, if assumed to be entirely by vaporization of indium, would have reduced the indium concentration of these alloys by amounts between 1.1 and 2.4 at. % of indium.

At this time, only the cast microstructures have been examined. The beta phase of the system appears to dissolve somewhat less than 7.8 at. % of indium, and at least one intermediate phase was observed. Additional information about the structure in this region will be obtained after the alloys have been annealed to an equilibrium condition.

ANTIMONY-ZIRCONIUM SYSTEM

Russi,[8] in a preliminary attempt to make antimony-zirconium alloys, showed that remelting the alloy made by simultaneous bomb reduction of zirconium and antimony in vacuum resulted in considerable loss of antimony. Russi also reported that the same considerable loss of antimony occurred when a block of zirconium was immersed in an antimony melt under helium for 2 hr at 1200°C. From these results it would appear that considerable difficulty may be encountered in maintaining the antimony content of the alloys during casting and annealing.

In the present experiments, antimony of 99.95% purity, from Johnson, Matthey and Company, Ltd., was arc

(7) C. H. Schramm, P. Gordon, and A. R. Kaufmann, "The Alloy Systems Uranium-Tungsten, Uranium-Tantalum, and Tungsten-Tantalum," *J. Metals* **188**, 197 (1950), Fig. 2.

(8) R. F. Russi, Jr., "The Zirconium-Antimony System," *Some Investigations Into Zirconium Alloy Systems* (B. A. Rogers and P. Chiotti, ed.), ISC-132, p. 10, Nov. 28, 1950.

cast in the usual manner with iodide-deposited zirconium. Alloys of 1, 3, and 5 at. % of antimony were made with practically no weight loss in the 1 at. % alloy and with only small weight losses, mainly from volatilization of the antimony, in the other two alloys. If the entire weight loss were assumed to be antimony, the antimony content of alloys 3 and 5 would be reduced by 0.3 to 0.4 at. % of antimony.

At present, only the cast microstructures of these alloys have been examined. The microstructures suggest that the solubility of the beta phase is restricted to about 1 at. % antimony. The beta phase appears to decompose eutectoidally. The microstructures of alloys 3 and 5 show the peritectic formation of a new intermediate phase, apparently high in zirconium, that occurs by reaction between the beta phase and the liquid during solidification of the casting. This is illustrated by Fig. 47. A more certain interpretation will be made after annealed specimens have been examined.

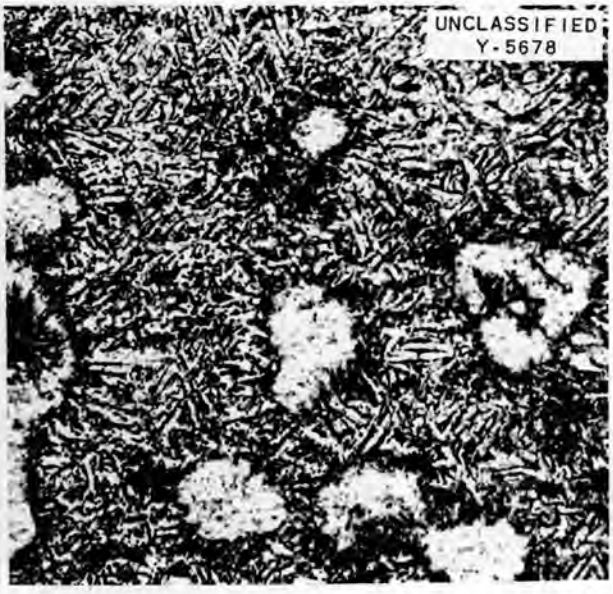

Fig. 47. Microstructure of a Zirconium Alloy Containing About 2.7 at. % Antimony in the As-Cast Condition. The dark-colored matrix is a eutectoid resulting from decomposition of the beta phase. The light-colored grains within this matrix appear to be a peritectic phase formed by a reaction between the beta phase and the liquid. The last part of the liquid to solidify appears as a eutectic in the center of the peritectic phase. 250X.

MAGNESIUM-ZIRCONIUM SYSTEM

Earlier work on the magnesium-zirconium system was concerned with magnesium-rich alloys. The most recent work of this type is that of Mellor,[9] who found that solid magnesium dissolves a maximum of 0.20 to 0.25 at. % of zirconium at 650.5°C and that the solid solubility decreases to lower amounts of zirconium at lower temperatures. At 650.5°C the magnesium-rich solid solution forms peritectically from magnesium-rich liquid and an unknown phase that is richer in zirconium. The only investigation made of alloys of higher zirconium content was a preliminary investigation by Nowotny, Wormnes, and Mohrnheim[10] using impure zirconium metal. These authors regarded the hexagonal phase of zirconium as dissolving up to 90 at. % of magnesium at 700°C. They also suggested that a superstructure may occur in this solid solution as Mg_2Zr. The extensive solid solution of magnesium is, however, questionable

[9] G. A. Mellor, "The Constitution of Magnesium-Rich Alloys of Magnesium and Zirconium," *J. Inst. Metals* **77**, 163 (1950).

[10] H. Nowotny, E. Wormnes, and A. Mohrnheim, "Untersuchungen in den Systemen Aluminium-Kalzium, Magnesium-Kalzium und Magnesium-Zirkon," *Z. Metallkunde* **32**, 39 (1940).

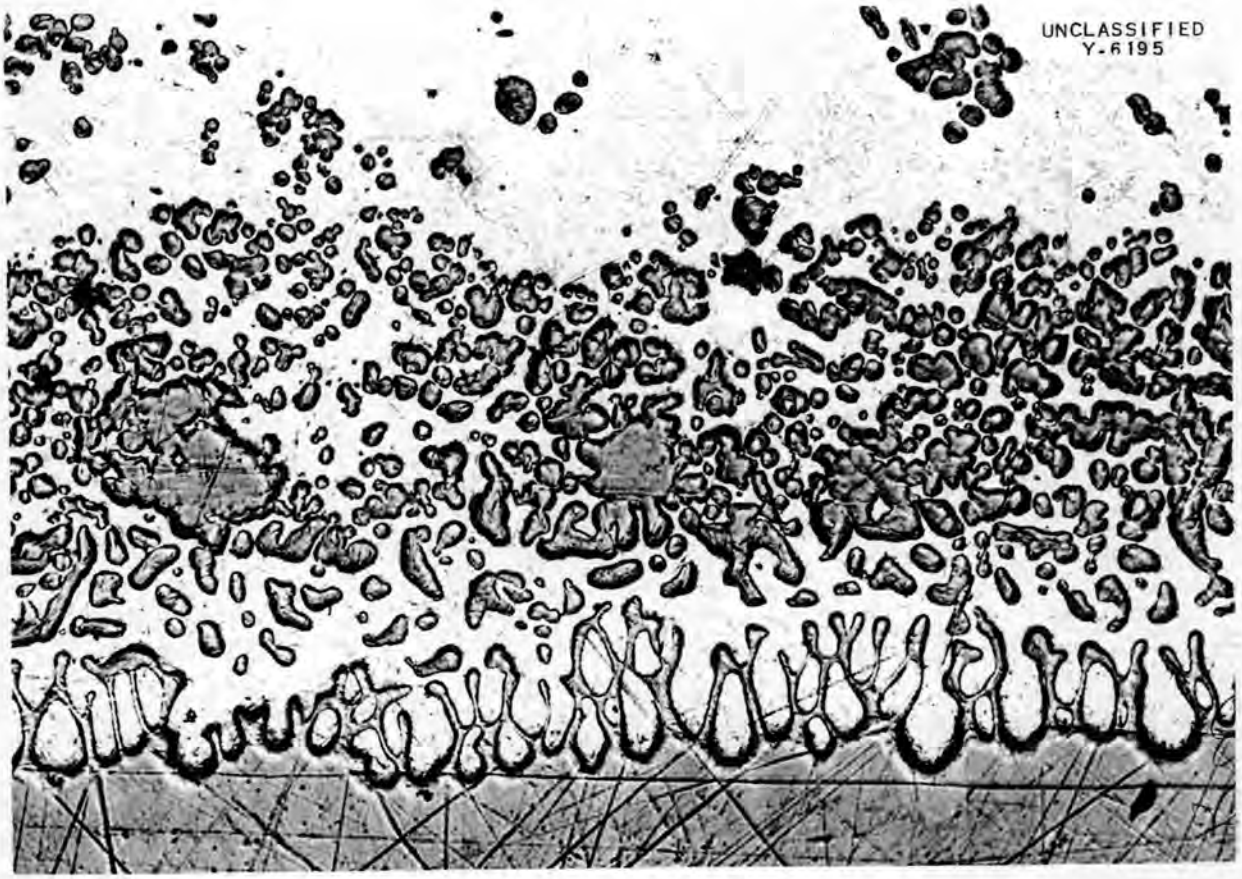

Fig. 48. Zirconium-Magnesium Diffusion Couple Quenched After 5 Days at 762°C. As polished. 250X.

on the basis of the two diffusion-couple experiments is described below.

The arc-casting method was not used to make magnesium-zirconium alloys because of the high vapor pressure of magnesium. In order to obtain some preliminary information about the phase diagram, distilled magnesium crystals[11] were placed inside zirconium cyclinders to which zirconium caps were welded in a purified argon atmosphere. These cans were then heated to 300 to 400°C in vacuum and sealed off in quartz capsules under an argon atmosphere. One can containing 29 at. % of magnesium was then annealed for five days at 762°C, and another can containing 7 at. % of magnesium was annealed for 11 days at 986°C. Both cans were quenched and examined metallographically. The magnesium region in the center of the zirconium cylinder remained, for the most part, unalloyed in both cases. In the region at the interface, shown in Fig. 48, the liquid magnesium penetrated the zirconium-phase grain boundaries and, in many cases, whole grains of zirconium phase were found suspended. No intermediate phase was found between these two phases, and it is probable that the phase diagram

[11] The distilled magnesium crystals were presented by the Dow Chemical Company and were of better than 99.97% purity. The zirconium cans were made of iodide-deposited crystal bar.

at these temperatures consists only of a zirconium-rich solid solution of limited solubility for magnesium. and a magnesium-rich liquid phase.

A recent experiment with a diffusion-couple of zirconium and magnesium has been reported by McPherson and Hansen.[12] These authors have also attempted to make magnesium-zirconium alloys by immersing solid pieces of zirconium in a magnesium melt. The results agree with those of the present experiments in that it was found that zirconium does not dissolve readily in molten magnesium; however, an intermediate phase was found in the diffusion-couple, and this result does not agree with those of the present experiments. The reason for this difference is not understood at the present, but the difference is most likely the result of the preliminary nature of both sets of experiments.

The investigation of the magnesium-zirconium system will be continued by further anneals of diffusion cylinders and analysis of the different parts of the quenched specimens. Methods will later be developed for powder-metallurgical preparation of the specimens, since alloys prepared in this manner would require less time to reach equilibrium by diffusion and would be more uniform in composition than alloys made by diffusion couples.

[12] D. J. McPherson and M. Hansen, *Phase Diagrams of Zirconium-Base Binary Alloys*, Illinois Institute of Technology Progress Report No. 5 to AEC, Nov. 27, 1951.

ANP PROGRAM

W. D. Manly

STATIC CORROSION

D. C. Vreeland L. D. Dyer
R. B. Day E. E. Hoffman

Low Melting Point Alloy Coolants. Interest has been expressed in the utilization of a low melting point alloy as a coolant in a secondary heat exchanger. Several eutectic compositions of these low melting point alloys have been used as corroding media in static corrosion tests with types-310 and -317 stainless steel and Inconel. The compositions and melting points of the eutectic alloys used are listed below.

COMPOSITION (%)	MELTING POINT (°C)
44 Pb, 56 Bi	124
43 Sn, 57 Bi	138.5
60 Bi, 40 Cd	144
68 Sn, 32 Cd	176
38 Pb, 62 Sn	183
82 Pb, 18 Cd	248

In these experiments, which were run for 100 hr at 816°C under vacuum, all the low melting point alloys containing tin proved to be extremely vigorous in their attack on the metals tested except the 68% tin-32% cadmium alloy on Inconel. An example of the attack is shown in Fig. 49. It is believed that the attack in these media can be classified either as intergranular, as in Fig. 50, which shows the characteristic penetration along the grain boundaries sometimes accompanied by voids, or as an alloying attack in which the attacked surface actually alloys with the molten coolant being tested, as shown in Figs. 49 and 51. Inconel showed very little promise in the tests. Type-317 stainless steel was unattacked by the 82% lead-18% cadmium alloy and only slightly attacked by the 60% bismuth-40% cadmium alloy, as shown in Fig. 52. The results of these tests are summarized in Table 11. It is planned to test other structural materials in the low melting point alloys that proved least corrosive in these initial tests.

Corrosion by Sodium-Lead Alloy Coolants. A series of tests of several stainless steels and Inconel in two different sodium-lead mixtures (50% Na-50% Pb and 80% Na-20% Pb) have been run at 816°C for 100 hr under vacuum. None of the specimens or tubes were severely attacked; all attack was 1/2 mil or under in depth. All specimens were ductile on bending 180 degrees. It was noted that some of the specimens that had been tested in the 80% sodium-20% lead mixture had apparently become carburized. This phenomenon has been observed before in testing materials in media containing sodium.[1] No carburization was noted in any of the tests with the 50% sodium-50% lead mixture, which indicates that the possibility of carburization taking place is enhanced by the presence of higher percentages of sodium in the bath metal. Table 12 shows the results of the examination of these specimens in detail. Future plans include running static corrosion tests with lower percentages of sodium in the bath metal.

Corrosion by Fluorides. A short series of tests on Inconel and type-309 stainless steel were run using molten fluoride mixture No. 14 as the corroding

[1] *Liquid Metals Handbook*, p. 90.

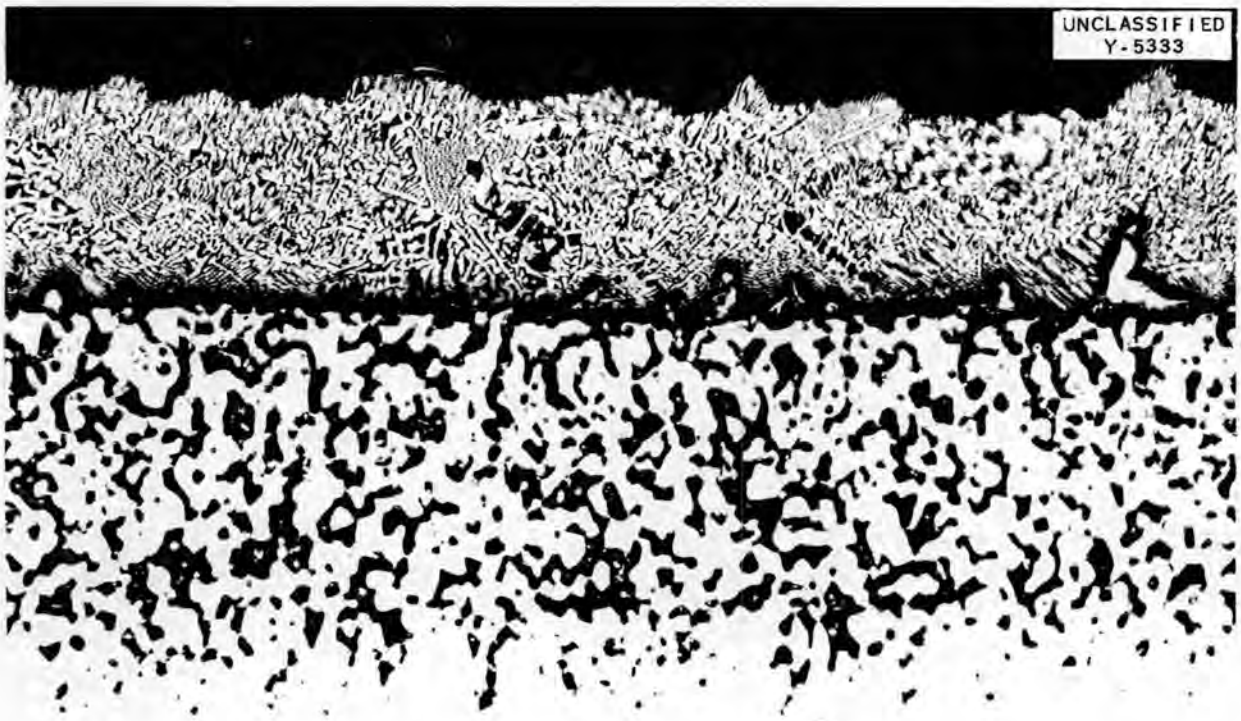

Fig. 49. Type-310 Stainless Steel Tested in 43% Sn-57% Bi Alloy for 100 hr at 816°C in Vacuum. Nital etch. 250X.

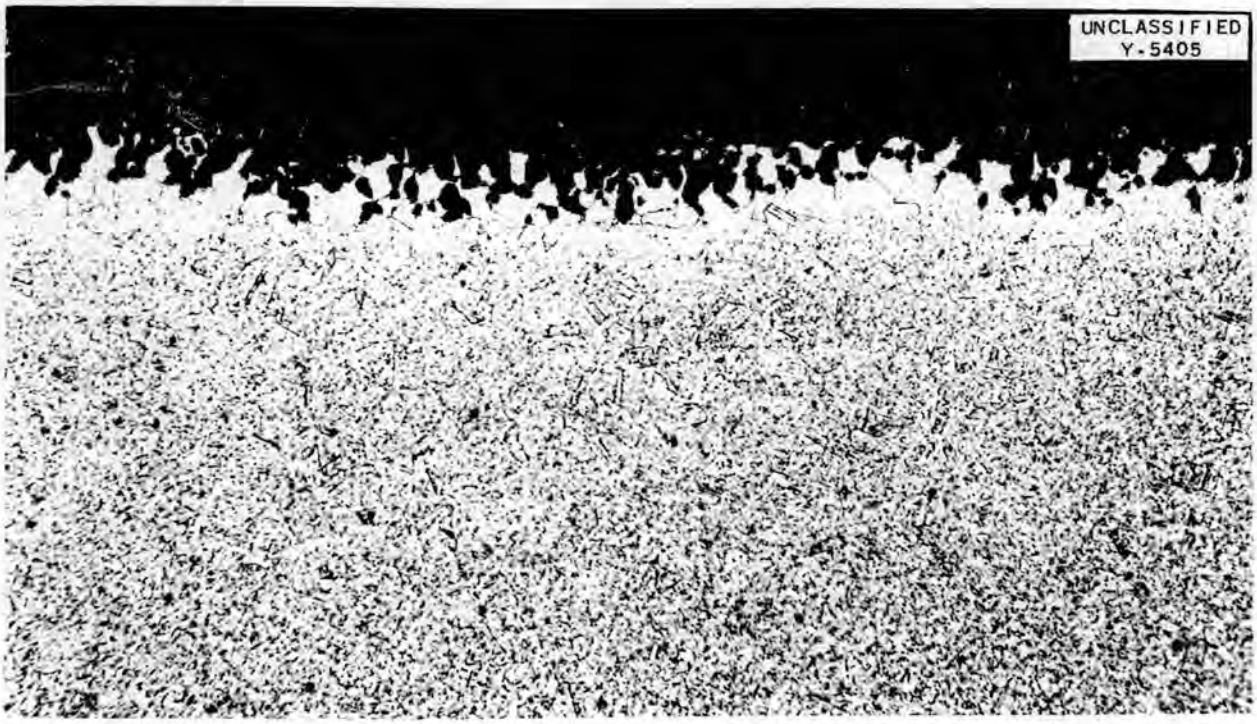

Fig. 50. Type-310 Stainless Steel Tested in 44.5% Pb-55.5% Bi Alloy for 100 hr at 816°C in Vacuum. Aqua regia and glycerin etch. 200X.

Fig. 51. Inconel Tested in 43% Sn-57% Bi for 100 hr at 816°C in Vacuum. No etch. 100X.

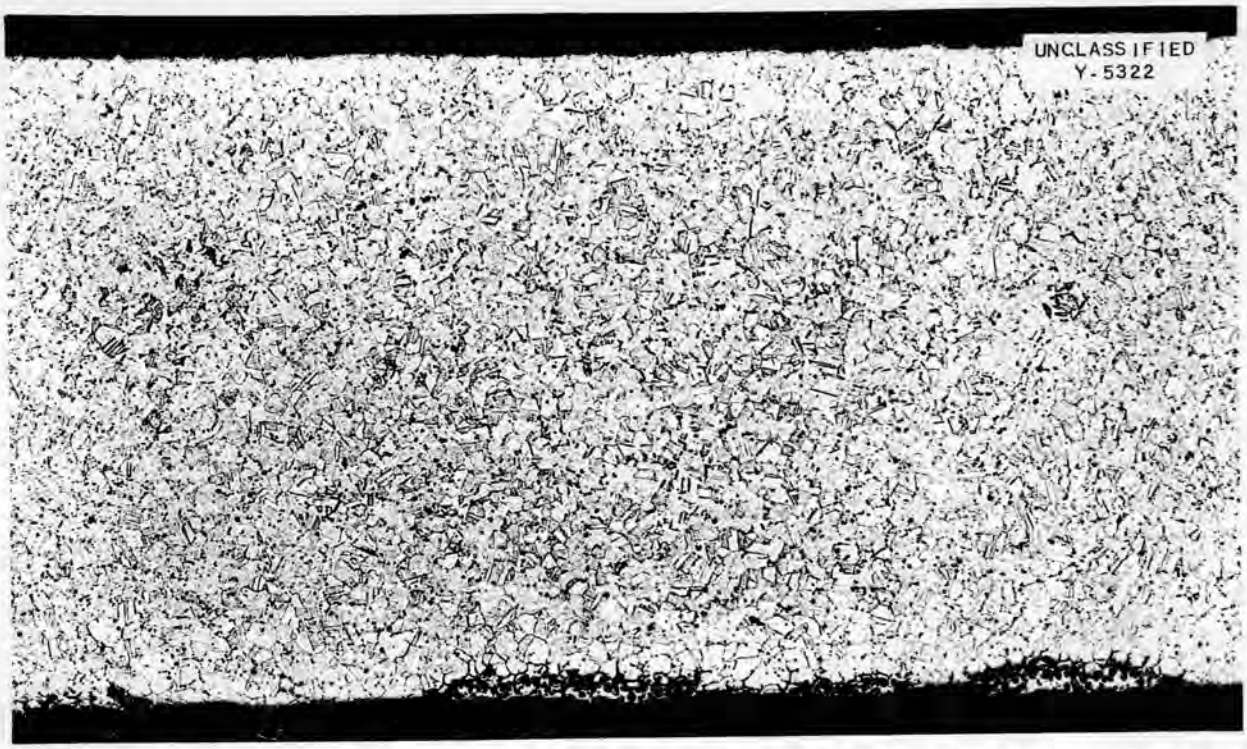

Fig. 52. Type-317 Stainless Steel Tested in 60% Bi-40% Cd for 100 hr at 816°C in Vacuum. Aqua regia and glycerin etch. 100X.

TABLE 11

Corrosion of Types-310 and -317 Stainless Steel and Inconel Tested in Various Low Melting Point Eutectic Alloys for 100 hr at 816°C in Vacuum

MATERIAL	DEPTH OF METAL AFFECTED (mils)	METALLOGRAPHIC NOTES
BATH: 43% Sn-57% Bi		
Type-310 stainless steel	10	Many large voids
Type-317 stainless steel	11	Irregular attack; many voids
Inconel	8	Five mils of a uniform layer on surface with an underlying layer of voids 3 mils in thickness
BATH: 60% Bi-40% Cd		
Type-310 stainless steel	15	Attack very irregular, varying from 0 to 15 mils; both grains and grain boundaries attacked in some cases
Type-317 stainless steel	2	Intergranular penetration and voids in a few areas
Inconel	Complete penetration of specimen	Voids throughout entire specimen; tube attacked to a depth of 20 mils
BATH: 38% Pb-62% Sn		
Type-310 stainless steel	Complete penetration of specimen	Erratic attack
Type-317 stainless steel	Complete penetration of specimen	Erratic attack; only 2 mils affected in places
Inconel	8	Erratic attack
BATH: 68% Sn-32% Cd		
Type-310 stainless steel	Complete penetration of specimen	Erratic attack; tube failed by penetration of wall
Type-317 stainless steel	Complete penetration of specimen	Erratic attack
Inconel	2	Uniform attack
BATH: 82% Pb-18% Cd		
Type-310 stainless steel	2	Intergranular attack
Type-317 stainless steel	0	No attack on specimen or tube
Inconel	10	Intergranular attack
BATH: 44% Pb-56% Bi		
Type-310 stainless steel	6	Intergranular attack varying from 2 to 6 mils
Type-317 stainless steel	15	Intergranular attack
Inconel	4	Irregular intergranular attack varying from 1 to 4 mils

media. The composition of fluoride mixture No. 14 is 43.5 mole % KF, 44.5 mole % LiF, 10.9 mole % NaF, and 1.1 mole % UF_4. The tests were run with the as-received or unpretreated fluoride mixture, the pretreated fluoride mixture from Y-12, and the unpretreated fluoride mixture plus additions of magnesium and zirconium. Magnesium and zirconium were added to the tests in the form of turnings. As would be expected, the pretreated fluoride appeared to be less corrosive than the unpretreated, as shown in Figs. 53, 54, 55, and 56. Figures 57 and 58 show how additions of magnesium apparently increased the corrosiveness of the unpretreated fluoride toward both type-309 stainless steel and Inconel. Additions of zirconium appeared to lessen the attack of the fluoride on these metals. In the tests with the zirconium additions it was noted that built-up surface layers of 1 1/2 to 2 mils and 1/2 mil in thickness were present on the Inconel and type-309 stainless steel, respectively, as shown in Figs. 59 and 60. An attempt is being made to identify these layers by spectrographic methods. A summary of the results of these tests is presented in Table 13.

Molybdenum, Timken alloy No. 6 (16% Cr, 26% Ni, 6% Mo, balance Fe), Timken alloy No. 3 (16% Cr, 13% Ni, 3% Mo, balance Fe), and a 74% nickel-26% molybdenum alloy have been tested in pretreated fluoride mixture No. 2 (composition: 46.5 mole % NaF, 26.0 mole % KF, 27.5 mole % UF_4) for 100 hr at 816°C. Molybdenum was not attacked

TABLE 12

Corrosion of Types-316, -317, and -446 Stainless Steel Tested in Sodium-Lead Alloy for 100 hr at 816°C in Vacuum

MATERIAL	DEPTH OF METAL AFFECTED (mils)	WEIGHT CHANGE (mg/in.^{2})	METALLOGRAPHIC NOTES
BATH: 50% Na-50% Pb			
Inconel		-3.9	Specimen had slightly irregular edges
Type-446 stainless steel	<1/2	+1.6	Attack irregular, only one end of specimen affected
Type-446 stainless steel			No attack
Type-316 stainless steel	1/2	+12.0	Surface crevices appeared to be filled with bath metal
Type-317 stainless steel	<1/2	+7.5	Attack irregular, concentrated on one end of specimen
BATH: 80% Na-20% Pb			
Inconel	<1/2	+0.9	Tube and specimen appeared to be carburized
Type-446 stainless steel	<1/2	+2.5	Slight attack
Type-317 stainless steel	<1/2	+1.8	Tube and specimen appeared to be carburized

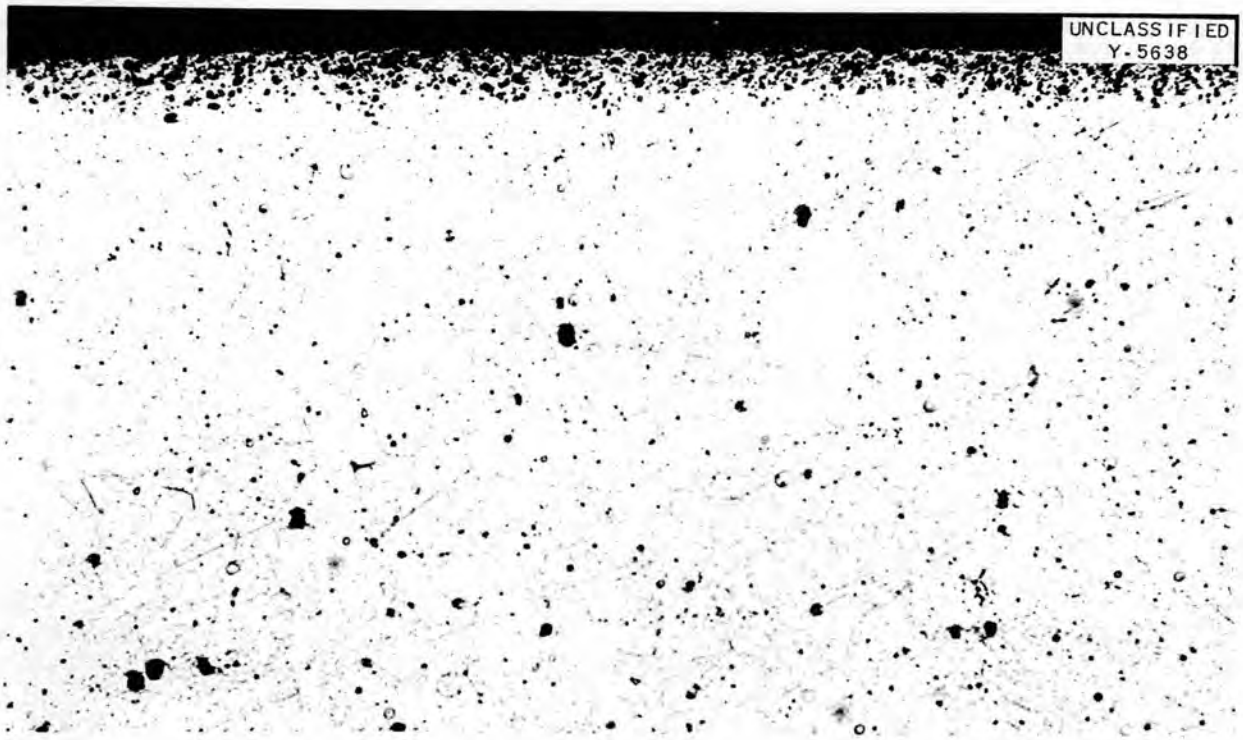

Fig. 53. Inconel Tested in Unpretreated Fluoride Mixture No. 14 for 100 hr at 816°C in Vacuum. Aqua regia and glycerin etch. 200X.

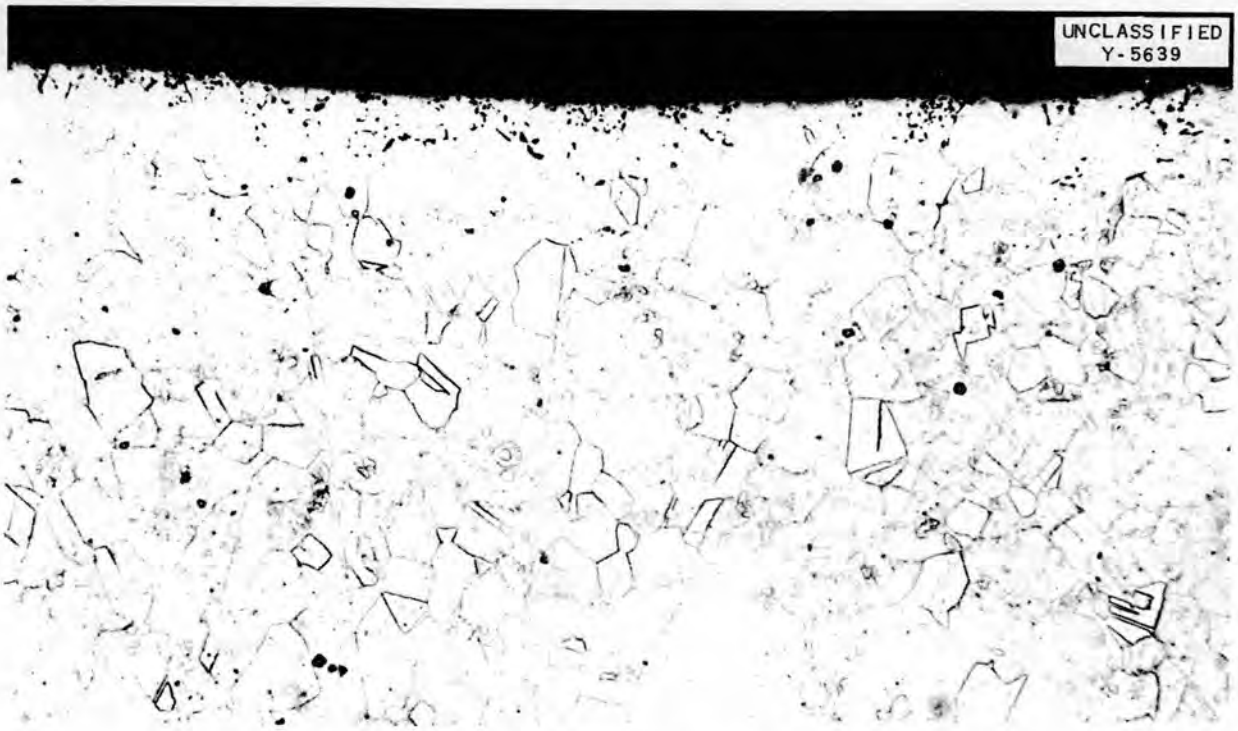

Fig. 54. Inconel Tested in Pretreated Fluoride Mixture No. 14 for 100 hr at 816°C in Vacuum. Aqua regia and glycerin etch. 200X.

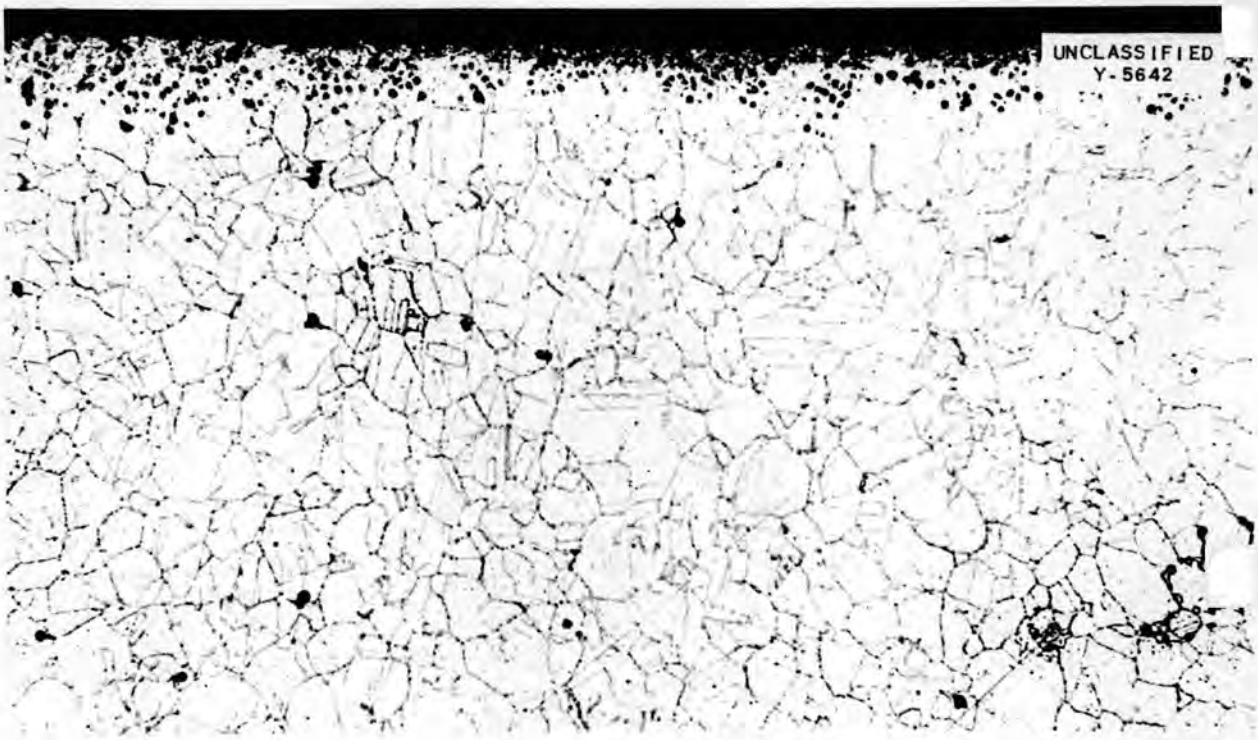

Fig. 55. Type-309 Stainless Steel Tested in Unpretreated Fluoride Mixture No. 14 for 100 hr at 816°C in Vacuum. Aqua regia and glycerin etch. 200X.

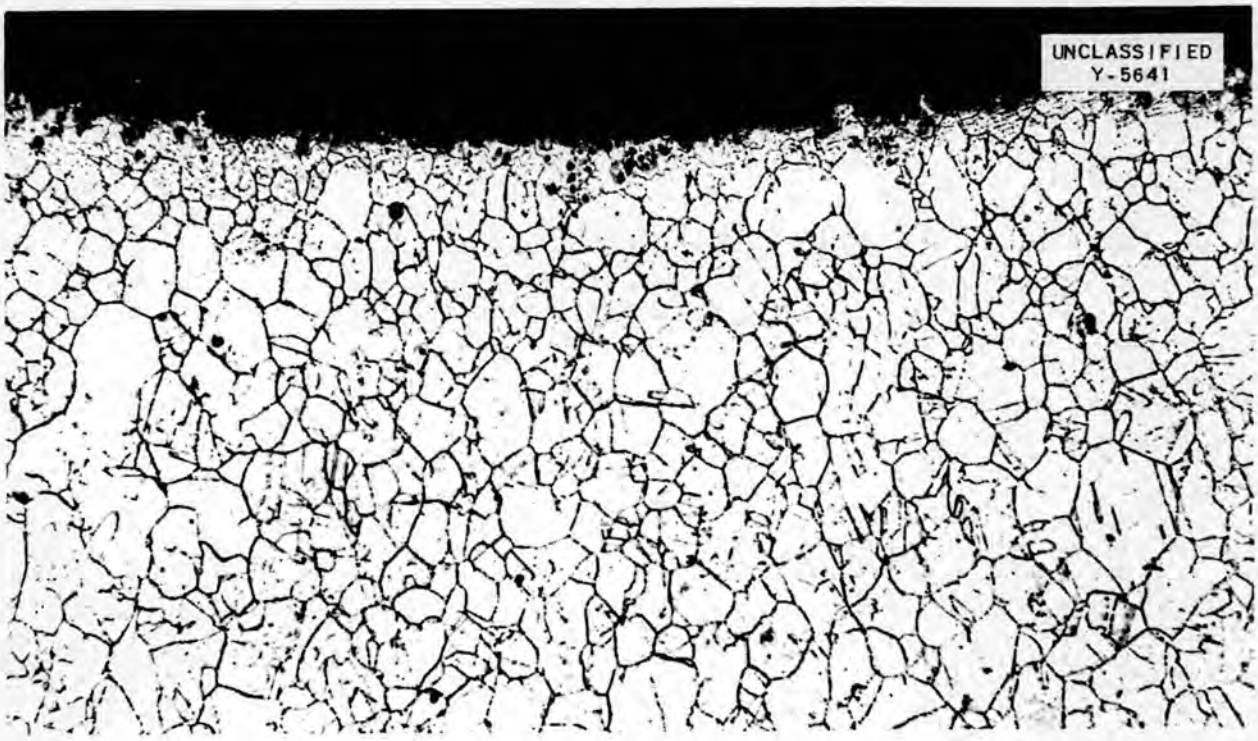

Fig. 56. Type-309 Stainless Steel Tested in Pretreated Fluoride Mixture No. 14 for 100 hr at 816°C in Vacuum. Aqua regia and glycerin etch. 200X.

Fig. 57. Inconel Tested in Unpretreated Fluoride Mixture No. 14 plus 2% Magnesium for 100 hr at 816°C in Vacuum. Aqua regia and glycerin etch. 200X

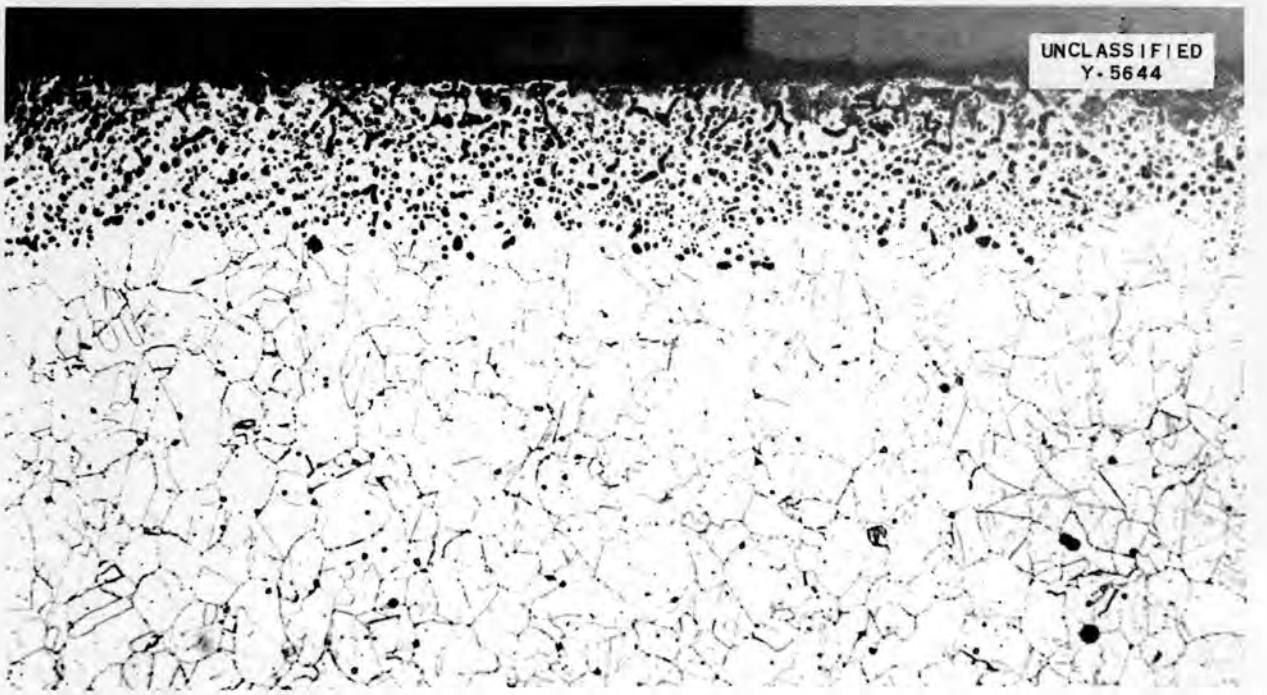

Fig. 58. Type-309 Stainless Steel Tested in Unpretreated Fluoride Mixture No. 14 plus 2% Magnesium for 100 hr at 816°C in Vacuum. Aqua regia and glycerin etch. 200X.

Fig. 59. Inconel Tested in Unpretreated Fluoride Mixture No. 14 plus 2% Zirconium for 100 hr at 816°C in Vacuum. Aqua regia and glycerin etch. 200X.

Fig. 60. Type-309 Stainless Steel Tested in Fluoride Mixture No. 14 plus 2% Zirconium for 100 hr at 816°C in Vacuum. Aqua regia and glycerin etch. 300X.

and the Timken alloys and molybdenum-nickel alloy were attacked only slightly. In Table 14 are the details of these tests and the results of static corrosion tests run on specimens of as-received and approximately 20% cold-worked Inconel and types-316 and -310 stainless steel in fluoride mixture No. 2 at 816°C for 100 hours. This amount of cold working appeared to have no significant effect on the corrosion properties of these materials under the testing conditions used.

Temperature-Dependence Tests. One-hundred-hour tests of Inconel and types-310 and -317 stainless steels in fluoride mixture No. 2 have been run at 850, 900, and 1000°C. No definite correlation between temperature of test and amount of attack could be established. Apparently these materials are insensitive to test temperatures within the temperature range that was used. Detailed results are presented in Table 15. There was irregular attack, with subsurface voids, and intergranular attack of each specimen.

Corrosion by Sodium Hydroxide. A series of tests were run using various additives in sodium hydroxide. The additives used in these tests included zirconium, sodium, sodium carbonate, sodium cyanide, and sodium hydride. The addition of approximately 50% sodium cyanide appeared to lessen attack and change the mode of attack on type-316 stainless steel and Inconel from oxidation to intergranular penetration, as shown in Figs. 61 and

TABLE 13

Corrosion of Inconel and Type-309 Stainless Steel Tested in Fluoride Mixture No. 14 for 100 hr at 816°C in Vacuum

BATH	DEPTH OF METAL AFFECTED (mils)	METALLOGRAPHIC NOTES
MATERIAL: INCONEL		
Unpretreated fluoride	2	Subsurface voids in both specimen and tube
Pretreated fluoride	1 1/2	No attack on specimen; subsurface voids to 1 1/2 mils in tube
Unpretreated fluoride plus 2 wt % magnesium	5	Large voids in both specimen and tube
Unpretreated fluoride plus 2 wt % zirconium	1	Surface layer 1 1/2 to 2 mils thick, 1/2 to 1 mil of attack beneath surface layer
MATERIAL: TYPE-309 STAINLESS STEEL		
Unpretreated fluoride	2	Subsurface voids
Pretreated fluoride	2	Subsurface voids; attack irregular in occurrence
Unpretreated fluoride plus 2 wt % magnesium	5	Subsurface voids; attack irregular in occurrence
Unpretreated fluoride plus 2 wt % zirconium		No attack on specimen or tube; specimen has a surface layer 1/2 mil deep

62. In the test with type-304 stainless steel, additions of 10% zirconium and 30% sodium carbonate resulted in a 6-mil oxide layer on the test specimens. A specimen run at the same time in sodium hydroxide without additions developed a 5-mil oxide layer. In a previous test of type-304 stainless steel in sodium hydroxide a 22-mil oxide layer was noted on the specimen at the conclusion of the test period. It is planned to recheck these tests in an effort to discover the source of this discrepancy.

A few tests of special alloys in sodium hydroxide have been run. A 26% molybdenum-74% nickel alloy showed light attack to a depth of 2 mils. Alloys composed of iron-nickel, iron-nickel-cobalt, and nickel-cobalt have also been tested in sodium hydroxide. The data on the depth of affected metal, given in Table 16, may be somewhat misleading. None of these alloys was severely corroded and attack was quite erratic. The capsules and specimens were machined from as-cast bars without prior working or

TABLE 14

Corrosion of Various Metals Tested in Fluoride Mixture No. 2 for 100 hr at 816°C in Vacuum

MATERIAL	DEPTH OF METAL AFFECTED (mils)	METALLOGRAPHIC NOTES
Molybdenum		No attack
74% Ni-24% Mo	<1/2	One side of specimen had some pits to a depth of <1/2 mil
Timken alloy No. 3		Some signs of slight penetration along stringers near the surface
Timken alloy No. 6	1	Shallow voids to 1 mil in depth
Type-316 stainless steel, as-received	1	Intergranular attack
Type-316 stainless steel, 20% cold worked	2 1/2	Intergranular attack, heavier on one end of specimen
Type-310 stainless steel, as-received	1 1/2	Subsurface voids, irregular in occurrence
Type-310 stainless steel, 21% cold worked	1 1/2	Subsurface voids, irregular in occurrence
Inconel, as-received	2 1/2	Subsurface voids, irregular in occurrence
Inconel, 26% cold worked	1/2	Subsurface voids, irregular in occurrence

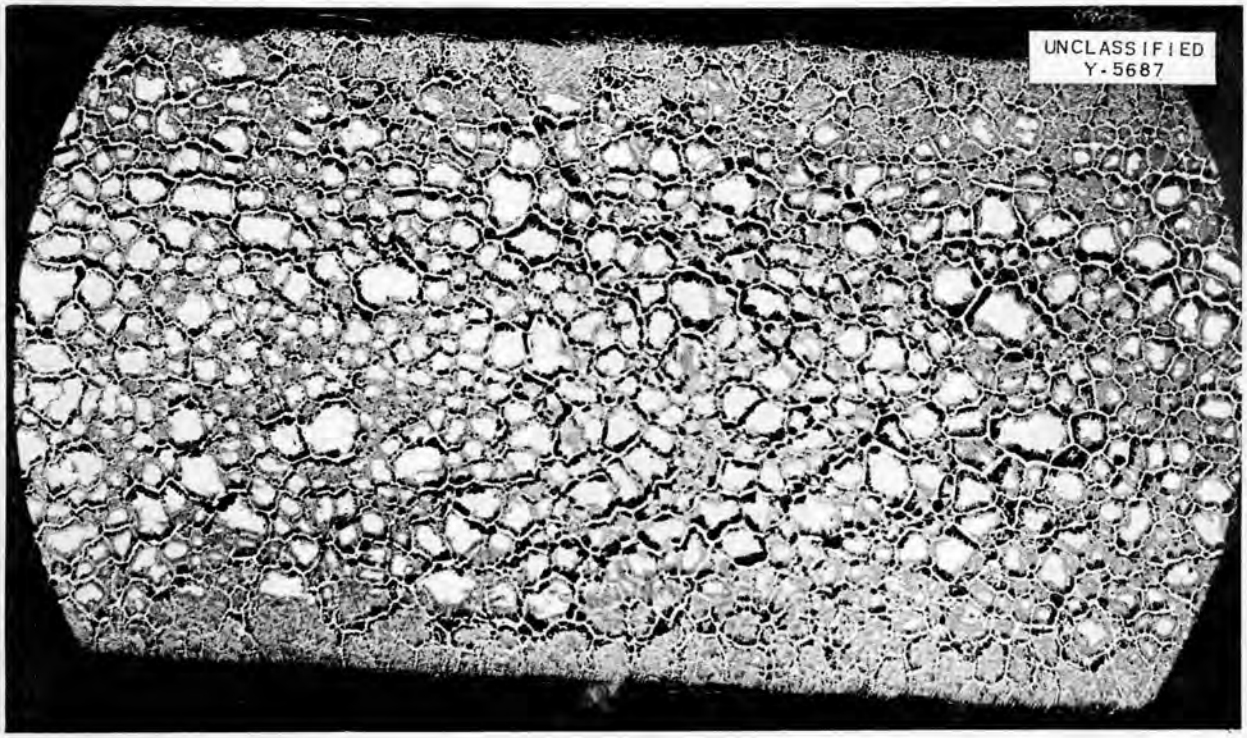

Fig. 61. Inconel Tested in Sodium Hydroxide for 100 hr at 816°C in Vacuum. No etch. 75X.

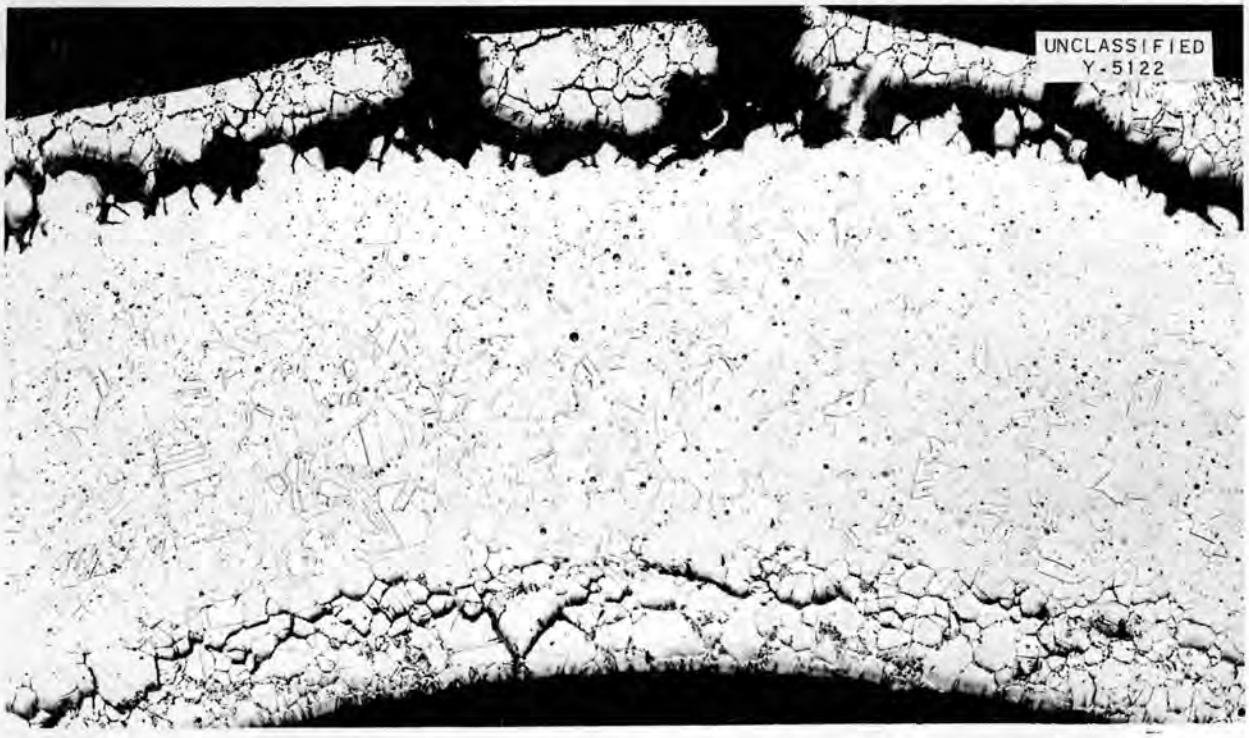

Fig. 62. Inconel Tested in 51% NaOH-49% NaCN for 100 hr at 816°C in Vacuum. Aqua regia and glycerin etch. 100X.

annealing. It is believed possible that the cast structure of these materials may have had some effect in influencing this type of attack, and that if the material were hot worked and annealed to a more uniform structure, corrosion resistance might be increased. It is planned to test materials of similar compositions that have been hot worked and annealed.

DYNAMIC CORROSION

G. M. Adamson K. W. Reber

Under the joint sponsorship of the Metallurgy Division and the Experimental Engineering Section of the ANP Division a program for dynamic testing of various fluoride mixtures in containers of various materials is being conducted. During this period the emphasis has been on screening tests to determine which alloys are the most feasible. At present none of the stainless steels or Inconel appear to be satisfactory container materials for mixed fluorides under dynamic conditions at 1500°F.

The preliminary dynamic screening tests are being made in thermal convection loops; Table 17 summarizes the results obtained. All loops have been of the same design and have been fabricated from 1/2-in.-IPS, schedule-40 pipe. It is evident from Table 17 that Inconel and nickel are the only loops that have not plugged in a short time when fluorides are circulated at 1500°F. Figure 63 is of a section of the tube wall from the hot leg of Inconel loop No. 210. If thin-walled tubes are to be used this attack cannot be tolerated. Figure 64 is from the cold leg of the same loop and shows very little, if any, attack. The mechanism and nature of the plugging in the stainless steel loops have not yet been determined. Metallic dendrites can be found in these loops but as yet it is not certain that they are present in sufficient quantities to cause the plugging. The attack in the type-316 stainless steel loops is

TABLE 15

Temperature-Dependence Tests in Fluoride Mixture No. 2 for 100 hr in Vacuum

MATERIAL	TEMPERATURE (°C)	DEPTH OF METAL AFFECTED (mils)
Inconel	850	4
Inconel	900	5
Inconel	1000	5
Type-317 stainless steel	850	3
Type-317 stainless steel	900	4
Type-317 stainless steel	1000	3
Type-310 stainless steel	850	2
Type-310 stainless steel	900	4
Type-310 stainless steel	1000	3

TABLE 16

Corrosion of Various Metals Tested in Sodium Hydroxide and Sodium Hydroxide Plus Additions for 100 hr at 816°C in Vacuum

MATERIAL	ADDITION TO NaOH BATH	WEIGHT CHANGE (mg/in.^{2})	DEPTH OF METAL AFFECTED (mils)	METALLOGRAPHIC NOTES
1/3 Ni, 1/3 Co, 1/3 Fe		-21.6	20	Intergranular voids, average depth about 5 mils
1/3 Ni, 1/3 Co, 1/3 Fe		-13.7	20	Intergranular voids, average depth about 5 mils
1/4 Ni, 3/4 Fe		None	1	Intergranular voids in some areas
1/4 Ni, 3/4 Fe		+57.2	4, on specimen 15, on tube	Intergranular voids
1/2 Ni, 1/2 Co		None	25	Intergranular voids, average about 8 mils
Type-304 stainless steel			2	Five-mil oxide layer
Type-304 stainless steel	10% Zr		2 1/2	Six-mil oxide layer
Type-304 stainless steel	30% Na_2CO_3		3	Six-mil oxide layer
A-Nickel	7% Zr			No attack
Inconel	12% Zr		3	Eleven-mil oxide layer
Type-316 stainless steel	48% NaCN	-286.61	2	Intergranular attack
Inconel	49% NaCN	-207.31	7	Intergranular attack
Inconel	7.4% Na		Complete penetration	Specimen converted completely to oxide
Inconel	50% Na		Complete penetration	Specimen converted completely to oxide
A-Nickel	14% Na	+51.1		No corrosion product, but edge of specimen rough
A-Nickel	54% Na	-2.5		No attack
Inconel	31% NaH		Complete penetration	Specimen converted completely to corrosion product
Type-304 stainless steel	31% NaH	-24.9	4 1/2	Oxide layer

TABLE 17

Results of Preliminary Dynamic Screening Tests in Thermal Convection Loops

LOOP NO.	MATERIAL	COOLANT	TIME OF CIRCULATION (hr)	REASON FOR TERMINATION	HOT LEG TEMP. (°F)	MIN. TEMP. AT START (°F)	MIN. TEMP. AT TERM.[a] (°F)	X-RAY STUDIES	METALLOGRAPHIC NOTES	
									HOT LEG	COLD LEG
78	Inconel	Flinak[b]	1000	Scheduled	1500	1220	1220		Intermittent layer of pits, 5 mils; intergranular attack of 10 mils	No attack; no mass transfer
111	Type-316 stainless steel	Flinak	173	Leak	1525	1210	1150		Very coarse-grained metal; intergranular attack of 10 mils; some reduction of wall	Very coarse-grained metal; continuous layer of 1 mil; no attack
112	Type-316 stainless steel	Fulinak[c]	82	Plug	1500	1210	960	Second phase in hot leg and possibly in cold leg	Intergranular attack of up to 8 mils	Intermittent mass transfer layer
113	Type-316 stainless steel	Fulinak	123	Plug	1600[d]	1250	?		Intergranular attack of 8 mils; some pitting	Thin mass transfer layer
210	Inconel	Fulinak	500	Scheduled	1500	1245	1245		Layer of pits of 10 mils, with maximum of 15 mils; layer on surface of 2 mils	Slight surface roughening
211	Inconel	Fulinak	500	Scheduled	1500	1250	1245	Second phase in hot horizontal and cold legs		
212	Inconel	Fulinak	38	Leak	1500	1230	1230		Intermittent layer of pits of 5 mils	
40	Type-410 stainless steel	Fulinak	9	Plug	1500	1240	1115	Second phase in hot horizontal and cold legs and possibly in hot leg		
43	Type-410 stainless steel	Fulinak	12	Plug	1500	1230	1160	Second phase in both parts of hot leg		
48	Type-430 stainless steel	Fulinak	8	Plug	1500	1250	?	Second phase found in all sections		
49	Type-430 stainless steel	Fulinak	9	Leak	1500	1250	1150			
275	Type-347 stainless steel	Fulinak	39	Leak	1500	1250	1100	Second phase in horizontal part of hot leg		
251	Type-310 stainless steel	Fulinak	73	Plug	1500	1260	1140	Second phase in horizontal hot leg and possibly in cold leg		
104	Nickel	Fulinak	500	Scheduled	1500	1260	1185	Second phase in all parts of hot leg and possibly in cold leg		

[a] Last recorded temperature usually 1 to 2 hr before termination.

[b] Flinak: 11.5 mole % NaF, 42.0 mole % KF, 46.5 mole % LiF.

[c] Fulinak: 10.9 mole % NaF, 43.5 mole % KF, 44.5 mole % LiF, 1.1 mole % UF_4.

[d] This loop was held at 1500°F for 70 hr and then turned up to 1600°F for the remainer of the test.

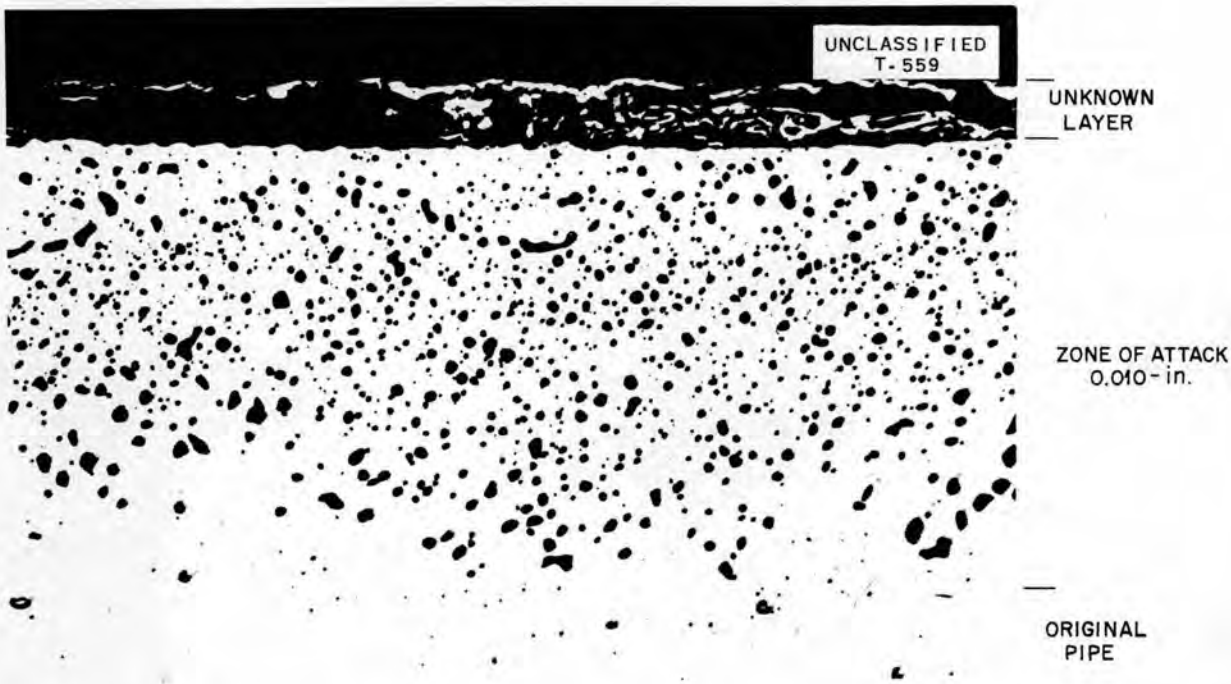

Fig. 63. Hot-Leg Section of Inconel Convection Loop After Circulating Fulinak at 1500°F for 500 Hours. 250X.

Fig. 64. Cold-Leg Section of Inconel Convection Loop After Circulating Fulinak at 1500°F for 500 Hours. 250X.

not quite so deep or so general as that found in Inconel. Examination of the remaining stainless steel loops has been held up until a satisfactory sampling technique for the fluoride mixture is worked out.

Additional loops of Nimonic, Monel, nickel, iron, hydrogen-cleaned Inconel, and type-316 stainless steel, all to run at 1500°F, and loops of Inconel and type-316 stainless steel to be run at 1300°F are being prepared or are awaiting filling.

A second phase of this work is to obtain data on physical properties of metals in the fluorides. The apparatus for this work has now been modified and calibrated so that fluorides may be used instead of sodium. Two tube-burst tests have been completed. An Inconel tube withstood a stress of about 1200 psi for 1000 hr in Fulinak at 1500°F with an increase in diameter of 1.7%. A type-316 stainless steel tube showed an increase in diameter of 0.7% with a stress of 1600 psi under similar conditions.

PHYSICAL METALLURGY OF LIQUID METAL CORROSION

A. deS. Brasunas L. S. Richardson

An effort is being made to obtain an understanding of the phenomenon of mass transfer, in which solid metal is gradually removed from one portion of the liquid metal system and deposited elsewhere. The molten metal acts as the carrier.

The mass transfer process is not understood, as yet, but most of the observations (there are few exceptions) suggest that solid metal is taken into solution in the hot zone, perhaps as a compound, and redeposited as a metal in the form of metallic crystals in the cold zone. In a few cases, the cold zone crystals were observed to be metal oxides.

Tests have been made in containers having thermal gradients. For one test, referred to as a seesaw test, an evacuated and sealed horizontal metal tube approximately one-third full of molten material is used. One end of the tube is heated to approximately 800°C and the other end is maintained at some lower temperature that is above the melting point of the molten medium. The tube is gently rocked, in a manner resembling a seesaw, so that the molten material flows by gravity to either end of the tube. After several thousand cycles, the tube is sectioned for examination. In a second type of test, referred to as a standpipe test, a similar tube completely filled with the molten material is maintained in a vertical position. In this type of test, the thermal gradient is maintained in two directions - that is, it is hottest at the center and cooler at the top and bottom. After a suitable time, this tube is also examined for mass transfer and corrosion effects.

Seesaw Tests. The apparatus used in making seesaw tests is shown in Fig. 65. The specimens and furnaces rock back and forth 20 deg off horizontal in either direction so that the fluid which partly fills the sealed metal tube flows from one end to the other. The hot end is maintained at approximately 800°C and the cold end at some suitable lower temperature.

The metal tube and fluid both undergo cycling; the hot end is cooled by the cool fluid, and the cold end is heated by the relatively hot fluid. Temperatures at either end are obtained with Chromel-Alumel thermocouples spot welded to the tube ends and subsequently coated with Sauereisen insulating cement, as shown in Fig. 66.

UNCLASSIFIED
Y-5660

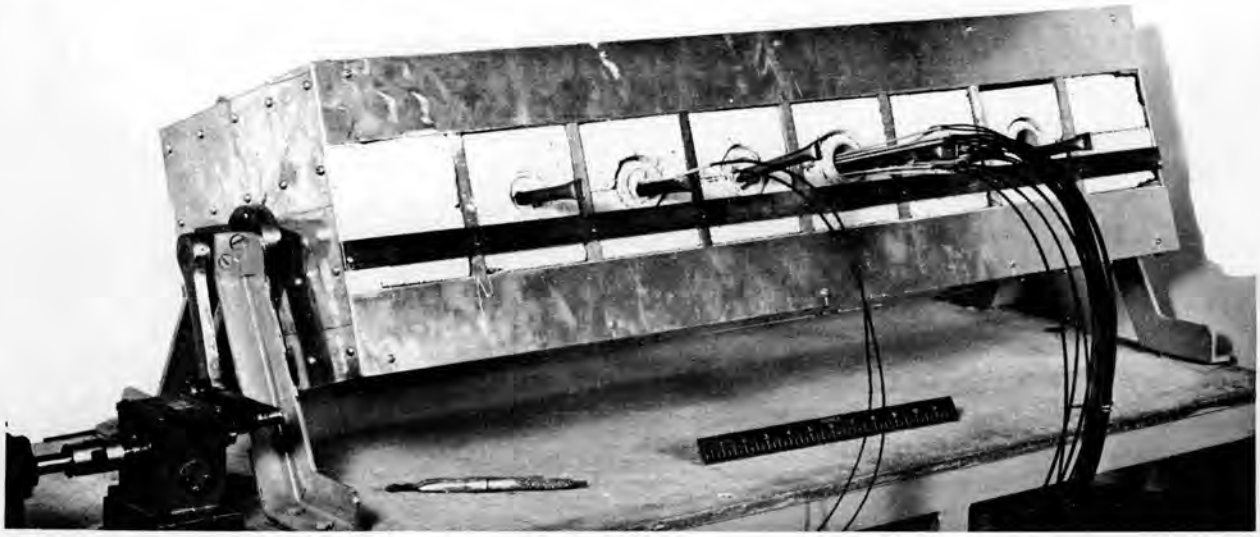

Fig. 65. Rocking Furnace used in Making Seesaw Tests. Furnace tilts 20 deg off horizontal in either direction at 260 cycles per hour.

Several tests have been made with a small seesaw unit, and the tests with nickel tubing containing dehydrated sodium hydroxide were consistent in the formation of metal crystals in the cold zone and a polished surface in the hot zone. A sectioned view of a test specimen is illustrated in Fig. 67. The nature of the metal crystals and the polished surface are shown in Figs. 68 and 69. The crystals have well-developed faces and many have a hexagonal shape. The structure of the polished metal surface, however, is not typical of a grain-boundary structure but rather suggests a subgrain structure.

UNCLASSIFIED
Y-5596

HOT END COLD END

Fig. 66. Typical Seesaw Test Specimen. Sealed tube (usually evacuated) one-third full of liquid medium; thermocouples spot welded to tube indicate hot- and cold-end temperatures.

UNCLASSIFIED
Y-5598

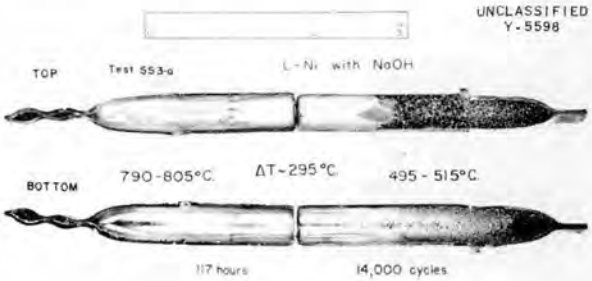

Fig. 67. Sectioned View of Nickel Tube Containing Sodium Hydroxide After 14,000 cycles (117 hr) in Seesaw Unit. Note polish on wall of hot end and crystalline deposit on wall of cold end; hot end at 790 to 805°C, cold end at 495 to 515°C, ΔT ~295°C. Test SS-3a.

Fig. 68. Nickel Crystal Observed on Wall of Cold End of Nickel Tube Containing Sodium Hydroxide (Fig. 67). Note stepwise development of crystal. 250X.

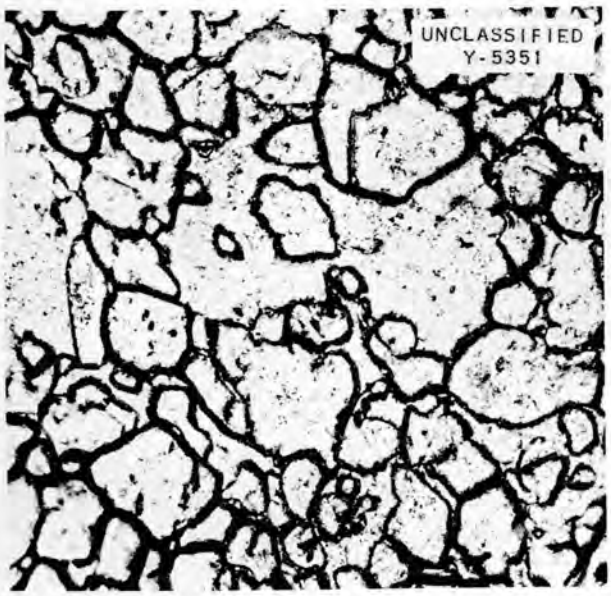

Fig. 69. Polished Nickel Surface on Wall on Hot End of Nickel Tube (Fig. 67). Developed pattern does not appear to be that of ordinary grain-boundary structure. 150X.

A second such test was made with sodium hydroxide and nickel, but a lower maximum temperature was used and the thermal gradient was reduced. In this test, in addition to the metal crystals, a black, comblike crystalline deposit was formed in the cold zone. These crystals were definitely identified as nickel oxide by x-ray diffraction. A few tiny platelets of a green, translucent material were also found, but these have not yet been identified. These nonmetallic crystals are shown in Fig. 70. Metal crystals deposited on the tube wall in the usual fashion and also formed on the black, nickel oxide crystals, as shown in Fig. 71. The oxygen involved in the formation of nickel oxide is believed to have come from impurities, since the decomposition of sodium hydroxide by nickel is quite unlikely and has not occurred in previous tests. Future tests with sodium

hydroxide will be made in an attempt to develop inhibitors for the suppresion of mass transfer and to obtain a better understanding of the conditions under which crystal formation occurs.

Two seesaw tests were made with fluoride mixture No. 14 contained in Inconel tubes. The hot-zone temperature was approximately 800°C and a gradient of 120 and 180°C was maintained. After 162,000 cycles (450 hr) the tubes were opened. Many tiny metal dendrites were observed to be embedded in the fluoride at the hot and cold ends of the tubes. These were, presumably, attached to the wall prior to the solidification of the fluoride. They have been identified as face-centered cubic metal having a lattice parameter of 3.541 Å, and they were analyzed as 81.5% nickel, 13.6% iron, and 4.9% chromium. Figure 72 shows metal crystals at the surface of the hot zone tube where some of the fluoride bath was retained intact. The cold zone also contained dark, red-brown crystals of high melting point, which were identified as UO_2 by x-ray diffraction. These are shown in Fig. 73. Here, again, the oxygen is presumed to have come from impurities.

The metal crystals formed in fluoride were much smaller and apparently formed much more slowly than those formed in caustic under similar thermal conditions. The hot zones of the caustic-containing tubes were polished, whereas the hot zones of the fluoride-containing tubes had roughened surfaces, which indicated that a corrosive reaction had occurred or that crystal deposition occurred throughout the tube. Formation of

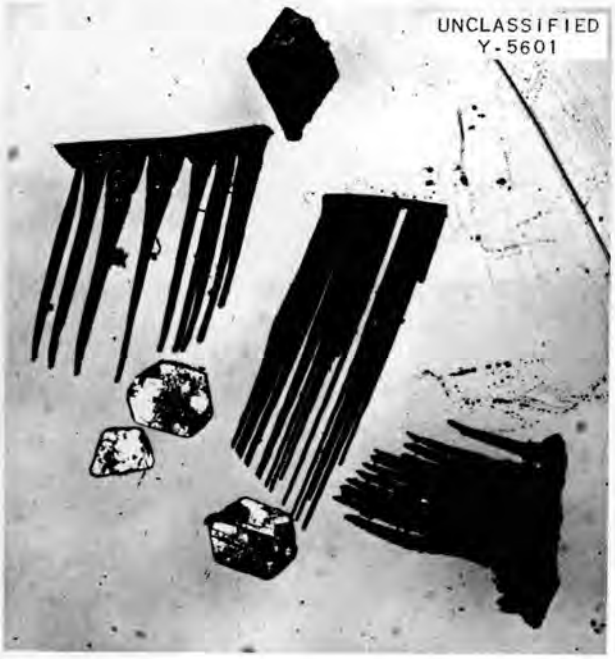

Fig. 70. Nonmetallic Crystals Obtained from Cold End of Nickel Tube Containing Sodium Hydroxide. Black comb-like crystals identified as nickel oxide by x-ray diffraction; translucent, green, hexagonal platelets not yet identified. Test SS-4a. 70X.

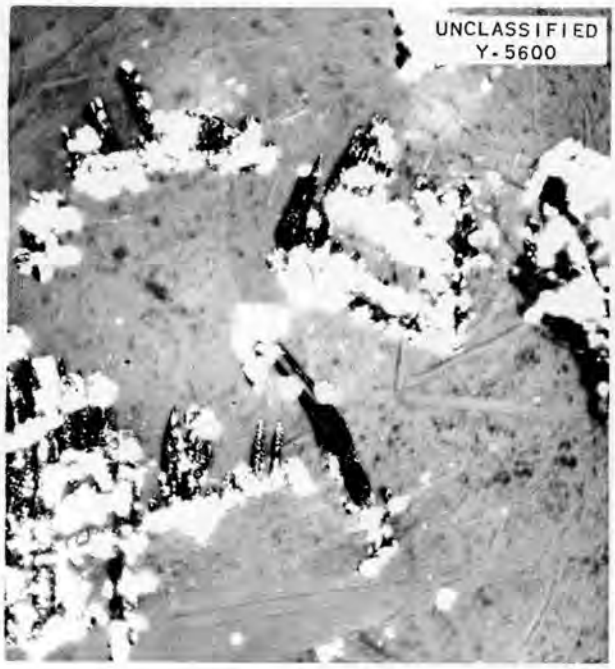

Fig. 71. Metal Crystals Deposited on Comb-like Nickel Oxide Crystals in Cold End of Test SS-4a (Fig. 70). 70X.

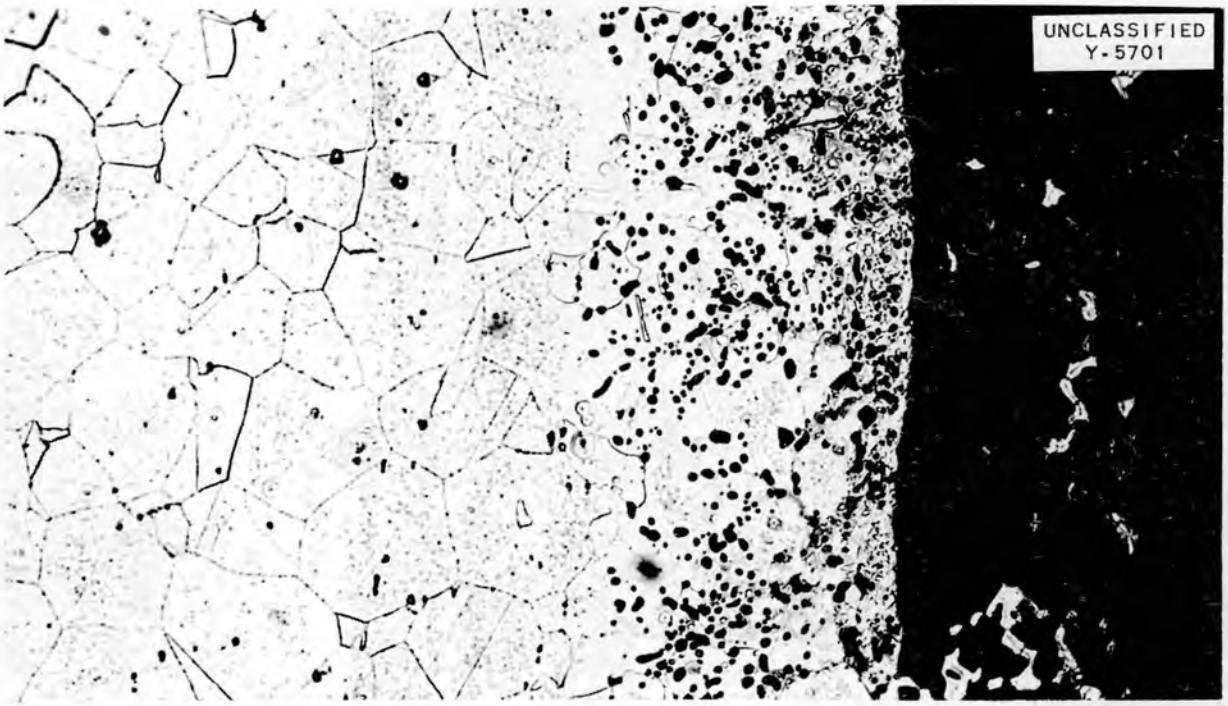

Fig. 72. Metal Crystals at the Surface of the Hot Zone Tube.

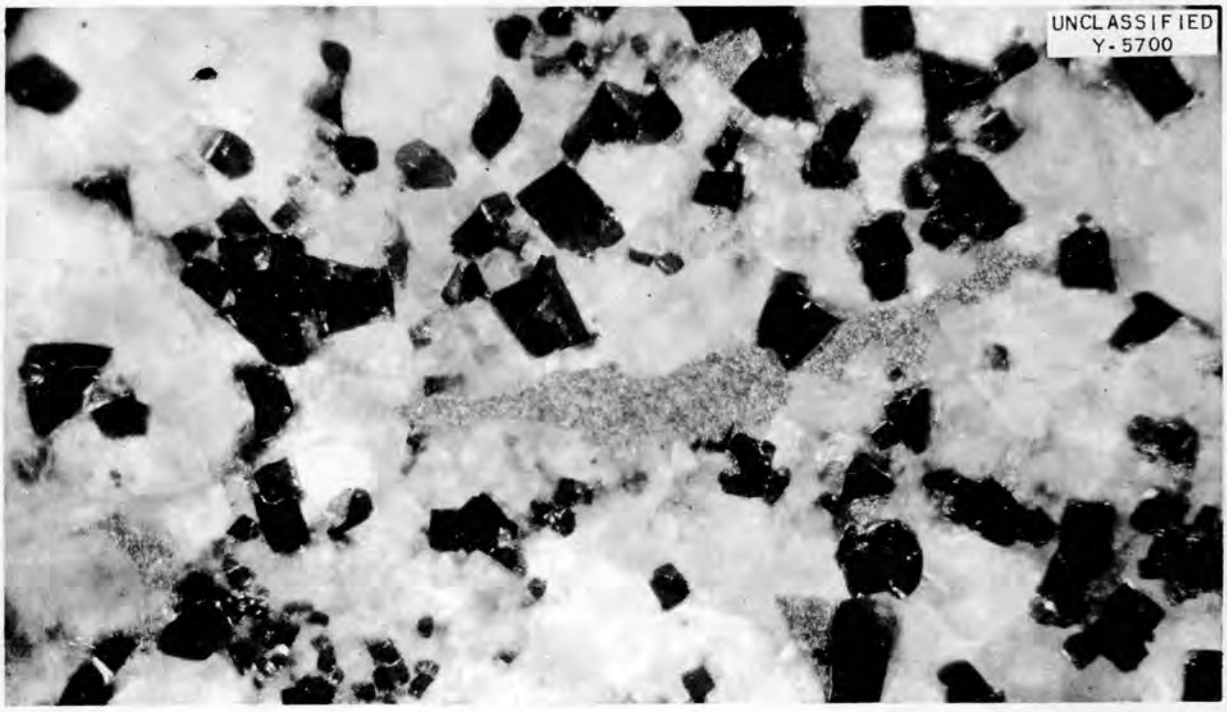

Fig. 73. Crystals in the Cold Zone.

oxide crystals in molten fluoride or caustic could probably be eliminated by removing oxygen from the bath material, metal tube, and/or atmosphere.

Standpipe Tests. A sectional view of the apparatus used in making standpipe tests is shown in Fig. 74. The specimen, an 18-in. metal tube, is inserted inside a quartz tube and the entire assembly placed in a furnace constructed so that the temperature at the center and ends can be separately controlled. The tubing, previously hydrogen fired to remove impurities, is filled with the fluid to be studied. The temperature gradient is measured by means of thermocouples that are spot-welded or brazed to the tube and connected to a multipoint recorder. Tests have been run under either of several atmospheres or under vacuum and with the use of a sealed evacuated tube produced by the tubulating technique of the Static Corrosion group.

The following results were obtained with a nickel tube and sodium hydroxide bath: (1) By using the tubulating technique, a maximum temperature of 820°C, and a temperature difference of 140°C a moderate amount of mass transfer and oxidation of the interior of the tube were observed; (2) and by using a hydrogen atmosphere, a maximum temperature of 740°C, and a temperature difference of 140°C no attack or mass transfer was observed.

The following results were obtained with Inconel tubes and a fluoride mixture No. 14: By using the tubulating technique in duplicate tests, a maximum temperature of 815°C, and a temperature difference of 165°C one test showed very slight mass transfer and the other showed none. In both of these tests, however, separation of a second, reddish-black phase occurred. This was assumed to be the same phase as the UO_2 observed in the seesaw tests.

PHYSICAL CHEMISTRY OF LIQUID METALS

G. P. Smith J. V. Cathcart
W. H. Bridges

There is experimental evidence that the presence of free oxygen, metallic oxides, and, perhaps, water may contribute significantly to mass transfer in hydroxide-metal systems. This statement is based on the results obtained from studies made by the National Advisory Committee for Aeronautics, the International Nickel Company, and by the Physical Chemistry and Physical Metallurgy Sections of the Metallurgy Division at the Oak Ridge National Laboratory. The experiments conducted by NACA consisted of heating, under a thermal gradient, metal crucibles containing hydroxides. Although argon formed the atmosphere above the crucibles, the experimental techniques used made it plain that oxygen contamination must have occurred. Considerable mass transfer was observed in these experiments. In a comparable study conducted at the International Nickel Company, a nonreducing atmosphere was used over the hydroxide and again mass transfer occurred. The work done at the Oak Ridge National Laboratory was described in detail in the last quarterly report.[2] Essentially, the work at ORNL consisted of heating sodium hydroxide in nickel crucibles in air and under purified hydrogen. Copious quantities of nickel crystals and nickel oxides formed in the hydroxide in the tests conducted in air; however, with a hydrogen atmosphere, not only was mass transfer completely eliminated but no corrosion of any sort could be

[2] "Physical Chemistry of Liquid Metals," *Metallurgy Division Quarterly Progress Report for Period Ending October 31, 1951*, ORNL-1161, p. 35.

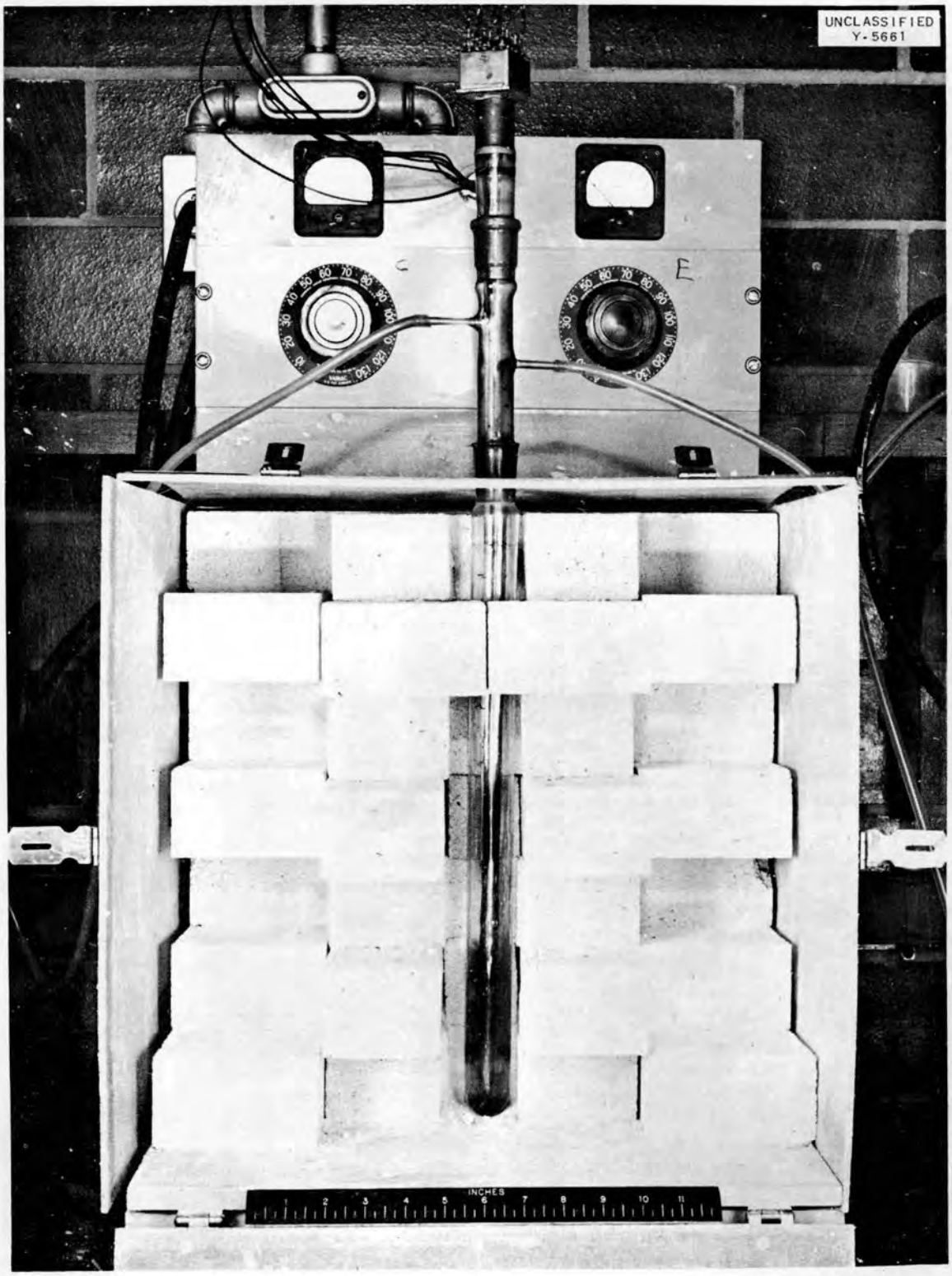

Fig. 74. Sectional View of Thermal-Gradient Furnace for Standpipe Tests.

detected. These experiments were carried out at 500°C. Similar results were obtained by the Physical Metallurgy Section for tests run at temperatures of 740 to 815°C. That group also carried out a series of static tests with Inconel-potassium hydroxide systems. These experiments were conducted at 537, 704, and 815°C under atmospheres of air and hydrogen. Under the air atmosphere, heavy intergranular penetration (greater than 0.035 in.) was noted at all temperatures; under the hydrogen atmosphere, the greatest penetration observed was 0.008 inch.

It was felt that these experimental results gave strong indication that the nature of the atmosphere above a hydroxide-metal system might be a factor of prime importance in controlling mass transfer. A successful conclusion to a study of the effect of atmosphere on mass transfer would immediately solve many of the problems that have arisen in connection with the heat transfer apparatus for the aircraft reactor; such a study has been undertaken.

Small thermal convection loops were used in these experiments, since this type of apparatus afforded the simplest and most direct means of studying mass transfer – the characteristics of the loops accentuate the effects that lead to mass transfer. It was found that the loops could be modified to exclude oxygen, water vapor, and, to some extent, metallic oxides from the system.

Inconel loops containing potassium hydroxide and nickel loops filled with sodium hydroxide have been investigated. These systems are referred to as Inconel-potassium hydroxide and nickel-sodium hydroxide loops. Four nickel-sodium hydroxide and five Inconel-potassium hydroxide loops have been operated.

Description of Apparatus. Both the Inconel and nickel loops were made by bending appropriate 1/2-in. tubing, 0.035-in. nominal wall thickness, into the form of a rectangle, 7 by 17 in., with a loading tube extending above the hot leg of the loop (Fig. 75). In Inconel-potassium hydroxide loops 4 and 5 and in nickel-sodium hydroxide loop 4, a dehydration pot was attached to the loops. This pot was made of standard 3-in. pipe with 1/8-in. cover plates welded into the top and bottom and a loading pipe 1 in. in diameter welded into the top cover plate. The dehydration pot was connected with the loop by standard 1/4-in. tubing. Glass tubing was attached at the tops of the loading legs of both the loop and the dehydration pot by means of Kovar seals, and vacuum and hydrogen lines were attached through appropriate side arms. Hydroxide pellets were dumped into the dehydration pot from a glass bulb. This bulb was attached to the glass tube at the top of the dehydration pot by means of a short length of Tygon tubing.

The furnaces for heating the loops were constructed from heating coils mounted in split, cylindrical ceramic forms that fitted around sections of the loop, as shown in Fig. 75. The coils were insulated with fire bricks. Temperatures at various points on the loop were measured with thermocouples; the thermocouples on the cold leg were welded to the loop and the rest were tied in place.

Particular care was exercised during the construction of the loops to clean out the metal tubes and to avoid excessive oxidation during welding. For example, the 1/2-in. tubing was cleaned mechanically with a dry cloth both before and after bending and after the necessary holes had been drilled in the tubing. The tubing was then rinsed with ethyl

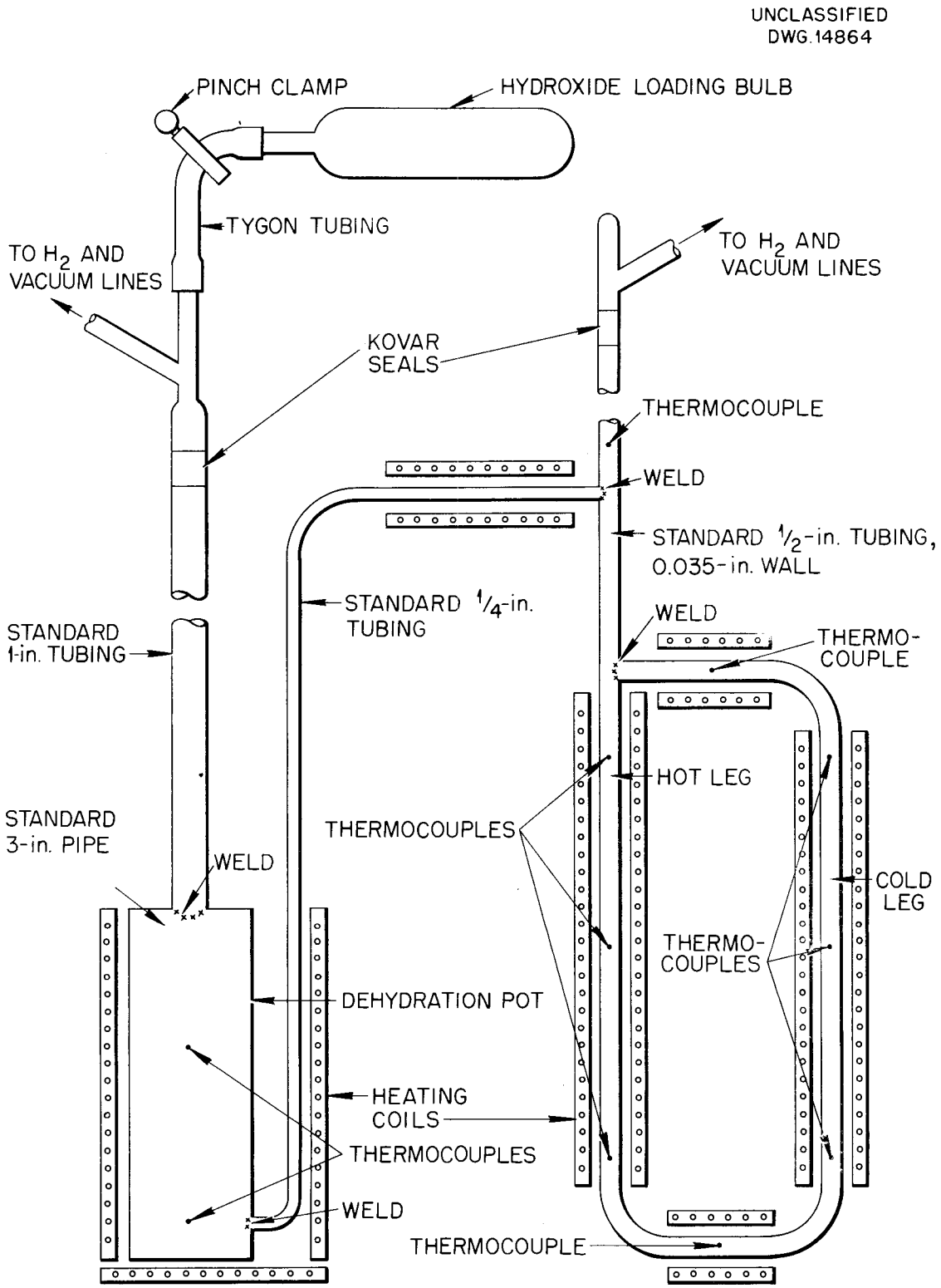

Fig. 75. Thermal Convection Loop.

alcohol to remove any dirt or metal chips that might have been left. No bending compound was used in bending either the 1/2- or the 1/4-in. tubes. The other metal parts were cleaned with soap and water, rinsed, and dried. The necessary welding was done without the use of a flux, and during welding argon was passed through the loop. Finally, the entire apparatus was tested for vacuum leaks.

The hydrogen used in this work was purified by passing it through a Deoxo unit to remove oxygen and then through successive tubes of Dehydrite, Ascarite, and Dehydrite. The hydroxides used were Baker's C. P. Analyzed Grade. Except for dehydration they were not further purified.

Experimental Procedure. The operation of the loop was divided into five steps.

1. *Hydrogen-firing.* After the loading bulb had been filled with hydroxide pellets and attached to the top of the dehydration pot, as described above, the entire apparatus was evacuated and thoroughly flushed with hydrogen. The Tygon tubing connection between the bulb and pot was then closed with a clamp, and the loop and dehydration pot containing hydrogen were heated at temperatures ranging from 500 to 750°C.

2. *Dehydration of the Hydroxide.* After hydrogen-firing, the entire apparatus was allowed to cool to room temperature while filled with hydrogen. The hydroxide pellets were then dumped into the dehydration pot and the system evacuated. The temperature of the dehydration pot was slowly increased over a period of 48 hr to 500°C. The hydroxide was maintained at this temperature for another 24 hr, and a vacuum of 0.04 mm was obtained in the system during this time. This procedure was made necessary by the large amounts of water in the hydroxides (about 15 wt % in the case of KOH). The water was removed from the vacuum system with a liquid nitrogen trap.

3. *Hydrogen-refiring.* After the dehydrated hydroxide had cooled below its melting point, the loop was again filled with hydrogen and its temperature raised to 600 to 750°C. The system was evacuated several times during this process in an effort to remove any water formed in the hydrogen-firing. In nickel-sodium hydroxide loop 4, this procedure was changed to the extent that the dehydrated sodium hydroxide was kept molten during the hydrogen-refiring, and the hydrogen, which entered through the top of the loading tube of the loop, left the system by bubbling through the hydroxide and out the top of the dehydration pot through a mercury manometer. In this case not only was the oxide in the loop reduced, but oxides in the sodium hydroxide were also subjected to reducing conditions.

4. *Loading.* The loading of the loop itself was carried out by evacuating the entire system and then applying a small pressure of hydrogen above the molten hydroxide in the dehydration pot. This caused the hydroxide to be pushed through the small connecting tube between the pot and the loop. The extent to which the loop was filled at any moment was judged by the temperature changes recorded by the thermocouples around the loop.

5. *Operation.* After the loop was loaded and the hot-leg temperature increased to the desired temperature, the furnace bricks and heating coil around the cold leg were removed so that the cold leg was completely exposed and heated entirely by the circulation of the hydroxide.

The procedure outlined above allowed a loop, which was relatively free of easily reducible oxide films, to be loaded with dehydrated hydroxide without the interior of the loop or the hydroxide coming into contact with air or moisture once the process was begun. It was realized that chromic oxide, unlike the nickel and iron oxides, could not be reduced under the conditions of hydrogen-firing used in this study; therefore, it is not correct to say that the Inconel loops were oxide-free. However, it was felt that the procedure used was the best one available without resorting to very elaborate furnace arrangements and hydrogen purification systems.

Although the procedure outlined here has become the standard operating practice, several important changes have been made since the first loop was run. For example, nickel-sodium hydroxide loop 1 was loaded and run under vacuum (the details of its operation were described in the previous quarterly report[1]). Nickel-sodium hydroxide loops 2 and 3 and Inconel-potassium hydroxide loops 1, 2, and 3 were set up without the dehydration pot attached. In these cases the operating procedure was similar to that described, except that the hydroxide pellets in the glass loading bulb were dehydrated in a separate furnace before being attached directly to the loading leg of the loop. Since the loading bulb was made of glass, the dehydrations in these cases had to be carried out at temperatures below the melting points of the hydroxides; this method proved unsatisfactory because higher temperatures are required to remove all the water from the hydroxides.

The operation of nickel-sodium hydroxide loop 3 was unique in that, after hydrogen firing and loading in the manner described, the loading leg above the loop was filled with air rather than hydrogen. This was done to provide a basis for comparison between runs made under reducing conditions and those made with oxygen present.

The hot-leg temperature in the nickel-sodium hydroxide loops was maintained at about 825°C, whereas the hot-leg temperature in the Inconel-potassium hydroxide loops was about 700°C. Hot- and cold-leg temperatures of all the loops are listed in Table 18.

Results. Several loops failed for various reasons, and no significant results could be obtained from them. Nickel-sodium hydroxide loop 2 failed because a leak developed in the hot leg after 24 hr of operation. A similar failure occurred with Inconel-potassium hydroxide loop 4 when a leak developed at one of the thermocouple welds after only 1 hr of operation. Inconel-potassium hydroxide loops 1, 2, and 3 were discontinued because of clogging of the loading legs with potassium hydroxide The clogging was caused by a failure to remove all the water from the potassium hydroxide before loading the loops. This difficulty was removed when the dehydration pot was incorporated into the system.

Nickel-sodium hydroxide loops 1, 3, and 4 were run under vacuum, air, and hydrogen, respectively. The temperatures of the hot and cold legs and the temperature distribution around the loops are shown in Table 18 and in Figs. 76, 77, and 78. In all three loops a considerable amount of mass transfer occurred between the hot and cold legs. In nickel-sodium hydroxide loop 1 most of the removal of nickel occurred in a 3-in. section in the hot leg where the temperature was highest. To the eye the wall surface in this region appeared to be highly polished (Fig. 79); however,

TABLE 18

Summary of Test Conditions for Nickel-Sodium Hydroxide Loops

LOOP	HOT-LEG TEMP. (°C)	COLD-LEG TEMP. (°C)	ATMOSPHERE	TIME OF OPERATION (hr)	REMARKS
Ni-NaOH 1	705	465	Vacuum	317	Considerable mass transfer; small amounts of black and greenish powders noted (probably nickel oxides); run terminated on schedule
Ni-NaOH 2	825	425	Hydrogen	24	Leak developed in hot leg after 24 hr of operation
Ni-NaOH 3	835	380	Air	117	Run terminated by leak in hot leg; considerable mass transfer occurred; heavy oxidation of loop surface
Ni-NaOH 4	825	535	Hydrogen	296	Considerable mass transfer; no oxidation of inside of loop except for small amount in loading leg; heavy plug of nickel crystals formed in loading leg above loop
Inconel-KOH 1					Loop failed because of clogging of loading tube
Inconel-KOH 2					Loop failed because of clogging of loading tube
Inconel-KOH 3					Loop failed because of clogging of loading tube
Inconel-KOH 4	700	450	Hydrogen	1	Operation terminated because of leak at a thermocouple weld
Inconel-KOH 5	715	440	Hydrogen	135	Operation halted by failure of temperature controller; no mass transfer and no corrosion occurred

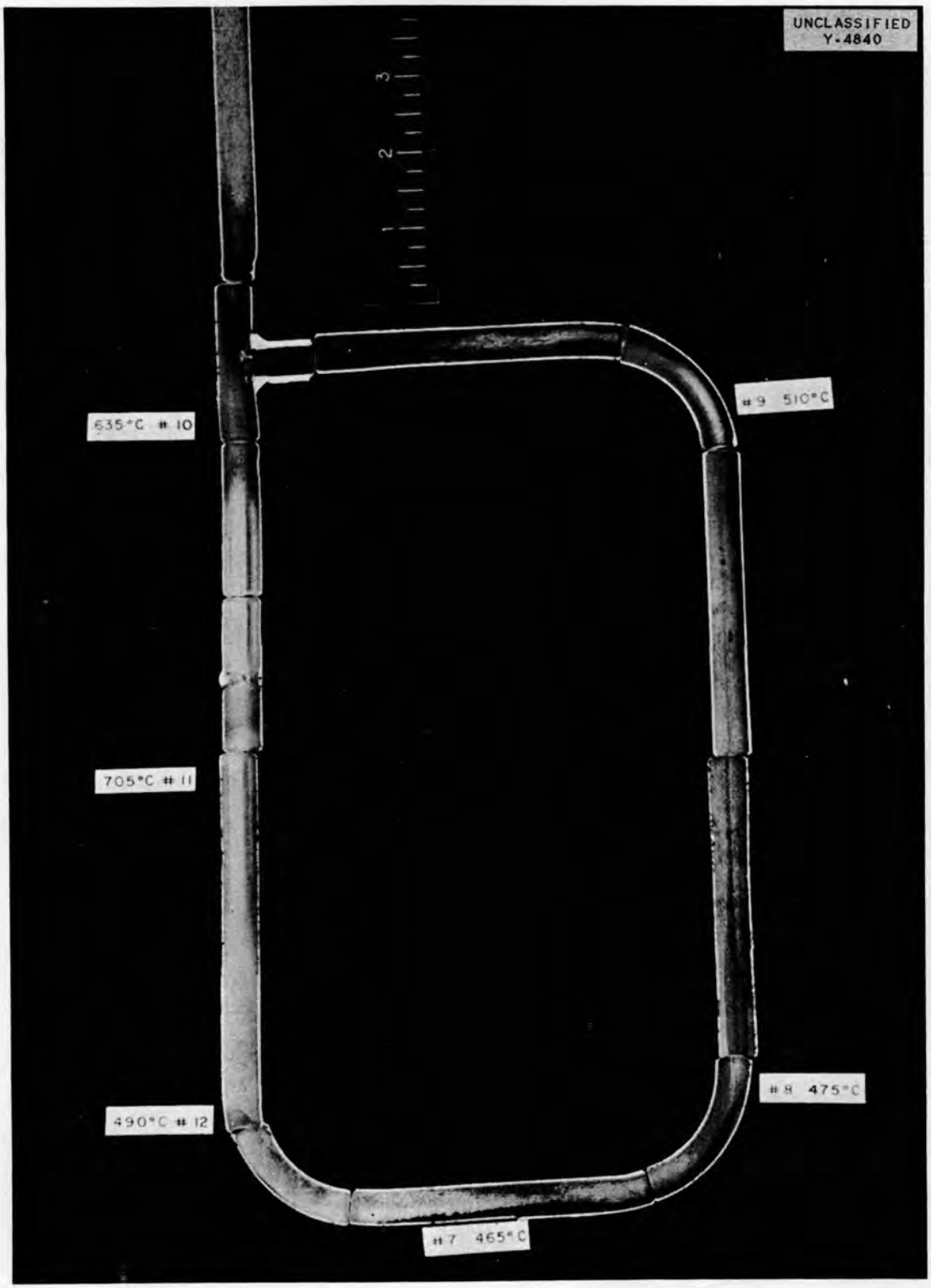

Fig. 76. Nickel-Sodium Hydroxide Thermal Convection Loop No. 1.

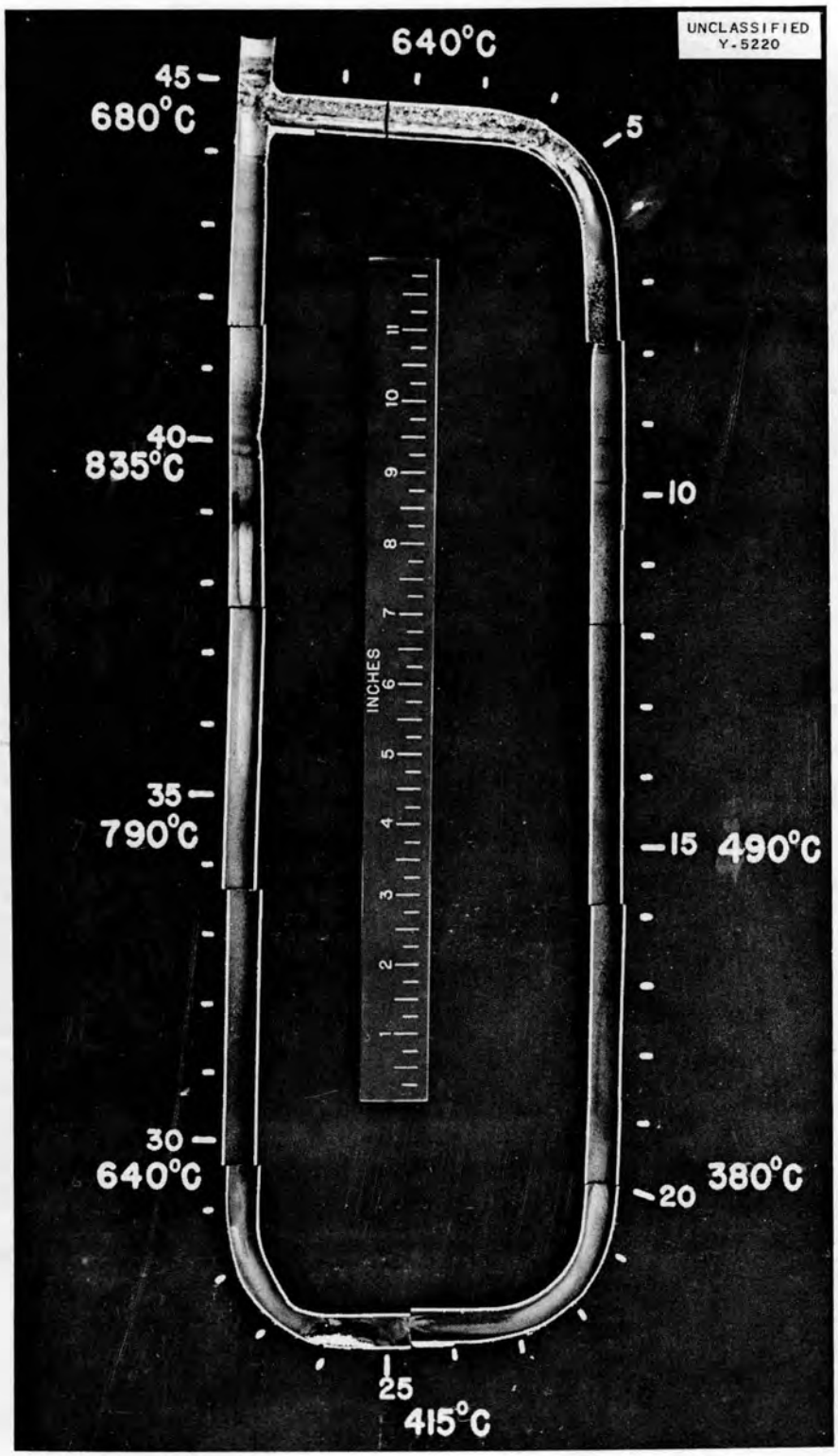

Fig. 77. Nickel-Sodium Hydroxide Thermal Convection Loop No. 3

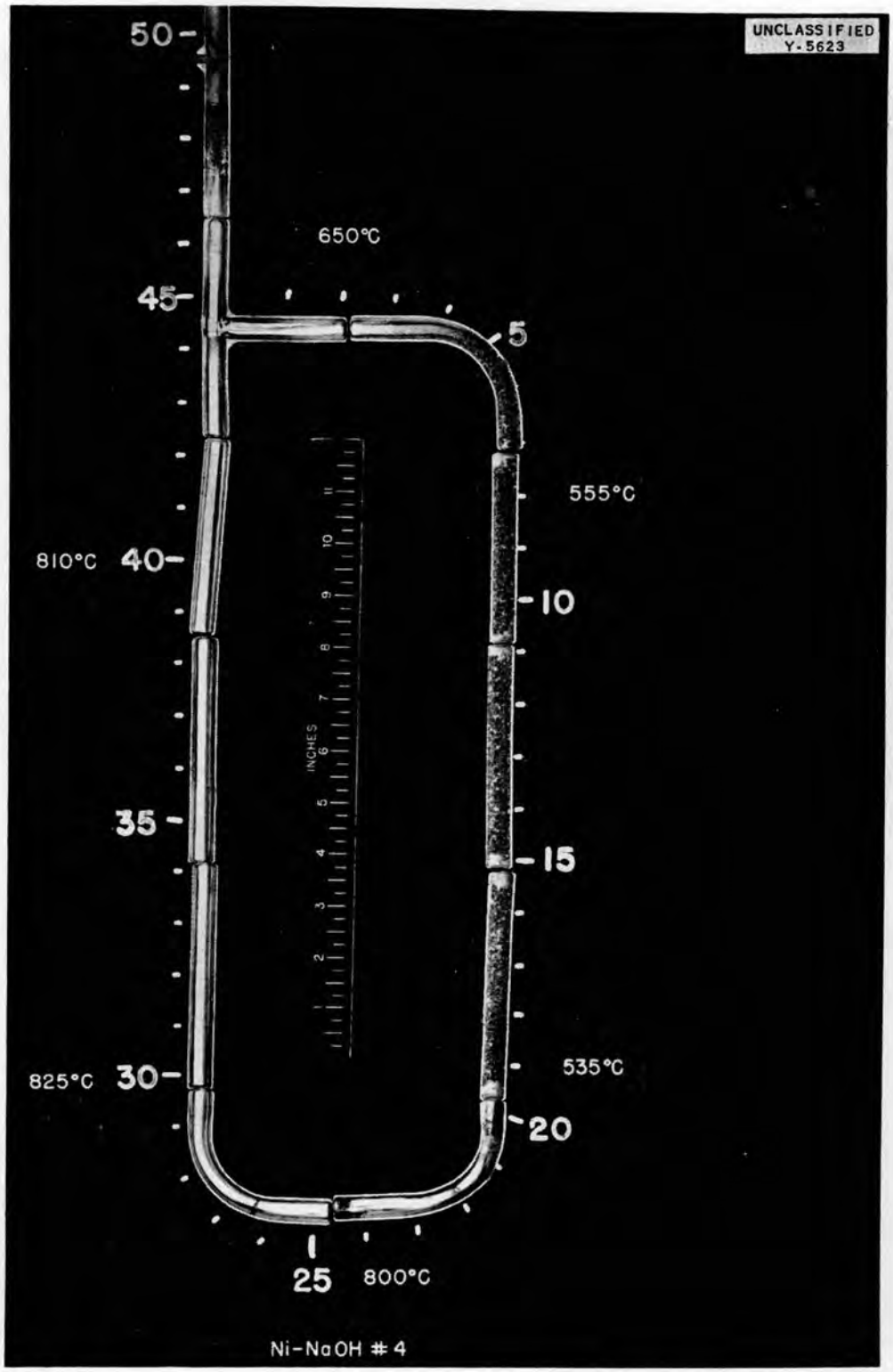

Fig. 78. Nickel-Sodium Hydroxide Thermal Convection Loop No. 4.

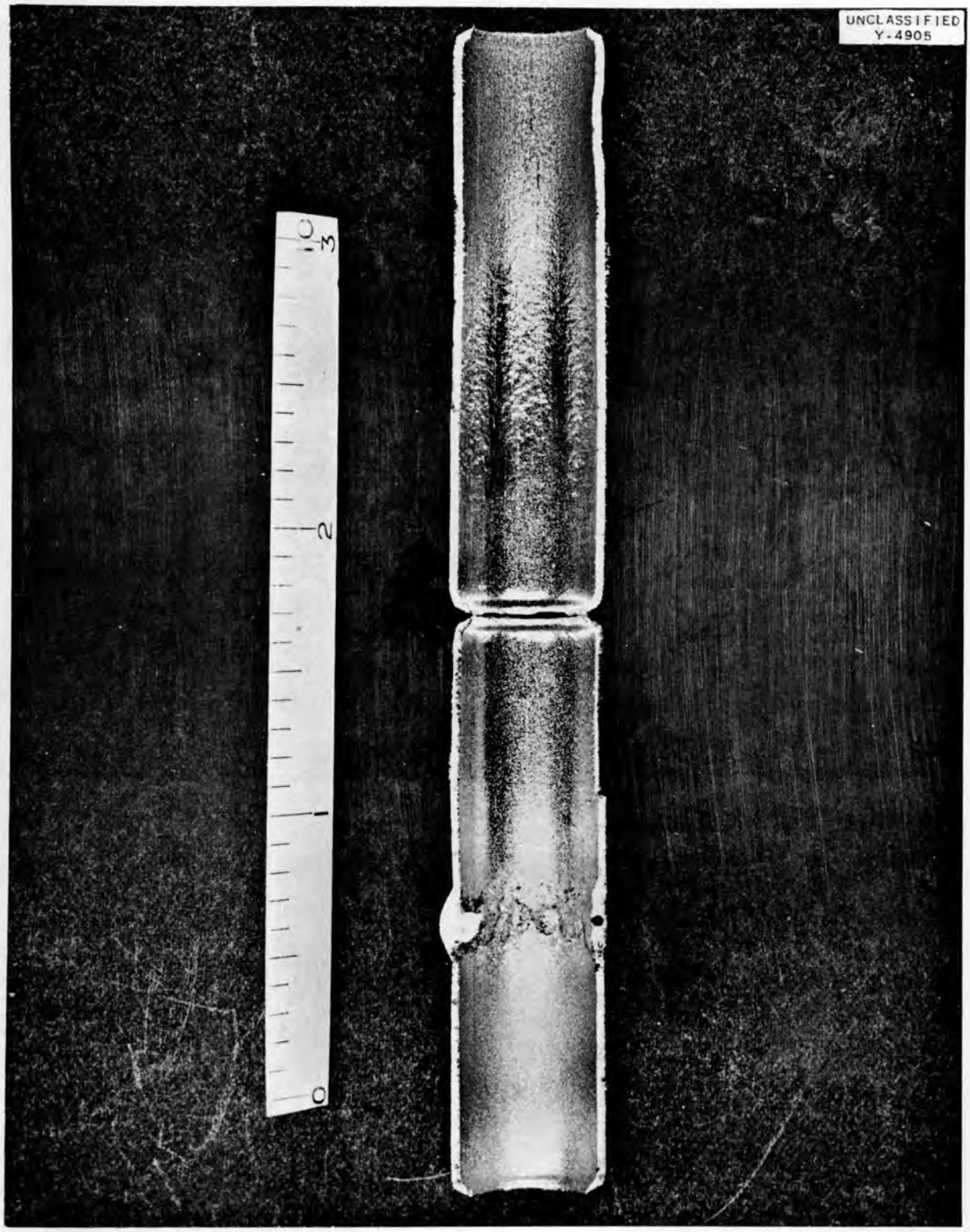

Fig. 79. Hot Leg of Nickel-Sodium Hydroxide Loop No. 1 Showing Polished Surface.

microscopic examination of the surface showed that although most of the grains were polished, a few were etched (Fig. 80). As may be seen from this photograph, there was no significant grain-boundary attack in this region. The polished region gradually merged with the rougher surfaces at its ends. Moderately heavy deposits of nickel occurred in the cold leg of this loop both as dendritic needles and as a dense, compact layer on the loop walls. In some cases grains in this layer appeared to have the same orientation as the grains of the underlying surface, as can be seen in Fig. 81 (note the line of demarkation between the original surface and the deposited layer). Small amounts of black and greenish-brown powders were also found in the cold leg. These were examined by x-ray diffraction and found to be largely nickelous oxide. On the average, about 0.008 in. of metal was removed from the surface of the walls in the polished region in the hot leg, and a deposit averaging 0.001 in. formed in the cold leg.

Nickel-sodium hydroxide loop 3, which was run under an oxygen atmosphere, showed no polished regions even in the hot leg (Fig. 77). The wall surfaces of the entire inside of the loop were covered with a heavy black powder. This black powder was examined by x-ray diffraction and found to contain nickelous oxide, metallic nickel, and an unidentified constituent that gave moderately strong diffraction lines. In the cold leg, crystals of nickel could be distinguished. An extremely heavy deposit of nickel crystals occurred in the top cross piece of the loop (Fig. 82) along what appeared to be the sodium hydroxide-gas interface. This deposit was about 0.1 in. in thickness. Approximately 0.005 in. of metal was removed in the hot leg (sec. 40 in Fig. 77), but there was almost no change in the wall thickness in the other sections of the loop except for the deposit in the top cross leg, as noted above. There was no evidence of intergranular attack.

Nickel-sodium hydroxide loop 4 was carefully hydrogen-fired, and, in contrast to the two previous loops, it was run under an atmosphere of hydrogen. Again considerable mass transfer occurred between the hot and cold legs (Fig. 78). As in the case of nickel-sodium hydroxide loop 1, the hot region showed a high surface polish; however, this polished region extended over the entire high-temperature region. The deposition of nickel crystals in the cold leg was somewhat heavier than in either of the two previous loops, and a heavy plug of nickel crystals, which virtually stopped up the loop, formed in the loading leg at the hydroxide-gas interface (sec. 48, Fig. 78). It was significant that no oxidation occurred inside the loop, as evidenced by a complete absence of black powder; however, a small amount of a black, powdery substance was found in the loading leg above the plug. Since this region was not heated to a high temperature during hydrogen-firing, it is possible that this black powder (presumed to be an oxide of nickel) formed as a result of the presence of unreduced nickel oxide on the tube walls.

The greater extent of mass transfer in this loop, as compared with the previous two, may have been influenced by at least three factors: time of operation, temperature, and the atmosphere above the loop. This loop was operated at a higher temperature than nickel-sodium hydroxide loop 1 and for a longer time than nickel-sodium hydroxide loop 3. Either or both of these factors may have been responsible for the increase in mass

Fig. 80. Polished Surface in Hot Leg of Nickel-Sodium Hydroxide Loop No. 1. Original magnification 250X, reduced 29%.

Fig. 81. Cross Section of Cold Leg of Nickel-Sodium Hydroxide Loop No. 1. Original magnification 250X, reduced 29%.

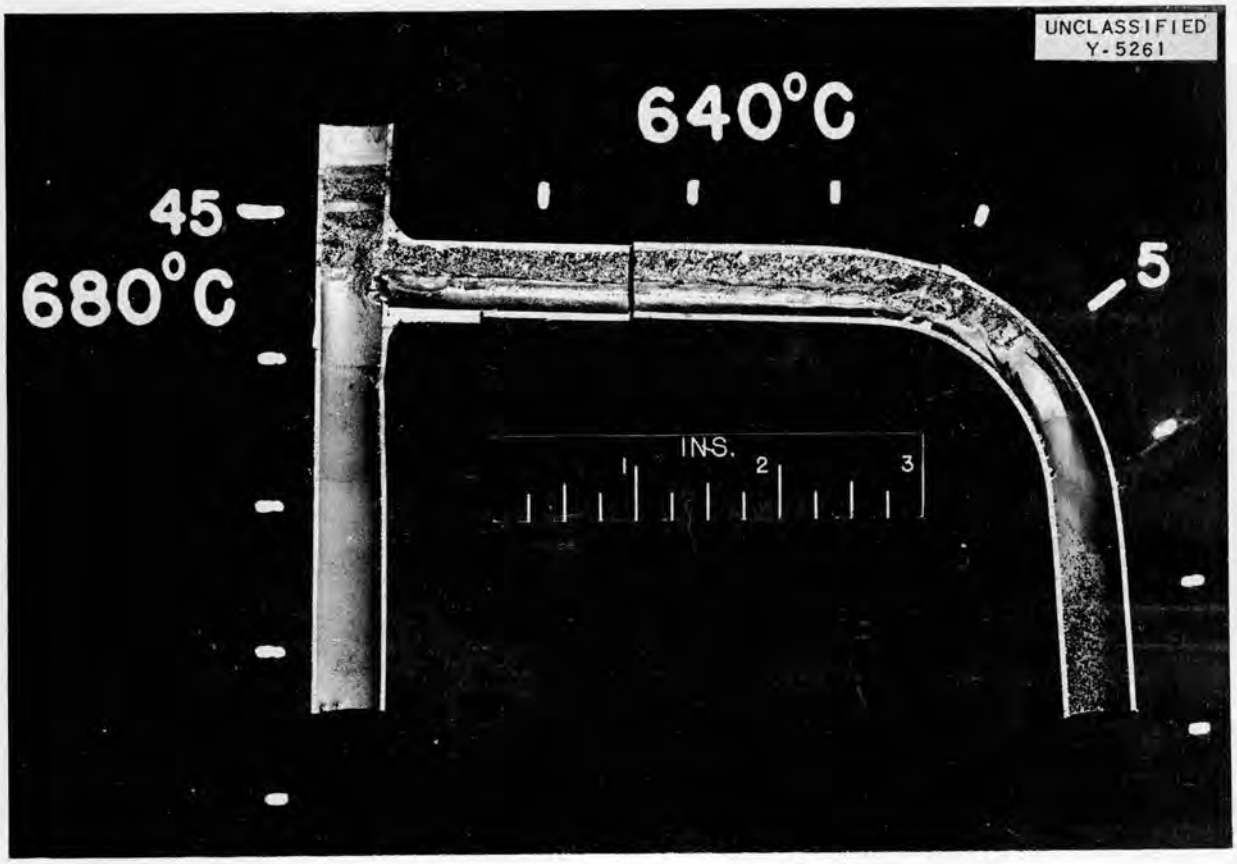

Fig. 82. Heavy Deposits in Top Cross Piece of Nickel-Sodium Hydroxide Loop No. 3.

transfer. The third factor, the nature of the atmosphere above the loop, may possibly be more important than the other two. Because of the formation of the plug of nickel crystals in the loading leg, the effect of the hydrogen atmosphere above the loop is still not clear. It is thought that this plug may have prevented free access of the hydrogen to the sodium hydroxide in the loop, and thus the influence of a reducing atmosphere may not have been felt. As has already been suggested, this plugging may have been the result of the presence of unreduced nickel oxide in the loading tube of the loop.

Metallographic examination of nickel-sodium hydroxide loop 4 has not been completed; hence, no information is available concerning the extent of removal of metal from the hot-leg walls.

The Inconel-potassium hydroxide loop 5 (Fig. 83) was operated for 135 hr with hot- and cold-leg temperatures of 715 and 440°C, respectively. The run had to be stopped at the end of this time because a failure of the temperature controller allowed the cold leg to freeze solid. No mass transfer occurred in this loop. Virtually no change could be noted in the wall thickness of either the hot or the cold legs as compared with the original wall thickness before exposure to the hydroxide. A slight smoothing out of the irregularities in the loop wall was noted in both the hot and cold legs (Figs. 84 and 85) as compared with the untreated surface (Fig. 86), but other than this there was little evidence of corrosion.

Conclusions. Very appreciable mass transfer occurred in the three nickel-sodium hydroxide thermal convection loops operated. The presence of oxygen definitely increased the oxidative corrosion in the loop, and this type of corrosion was completely eliminated if the loop was operated under an atmosphere of hydrogen.

On the basis of the results of Inconel-potassium hydroxide loop 5, it appeared that neither mass transfer nor appreciable corrosion occurred in an Inconel-potassium hydroxide thermal convection loop if the maximum hot-leg temperature was no higher than 715°C. It should be pointed out that this is a tentative conclusion based on the result of a single experiment; further testing is required for its final verification.

Future Experiments. The results with the Inconel-potassium hydroxide loop at 715°C will be rechecked. If it is again found that no mass transfer occurs at 715°C, an attempt will be made to establish the highest temperature at which an Inconel-potassium hydroxide loop can be run without appreciable mass transfer or corrosion. It is planned to test nickel-sodium hydroxide loops at lower temperatures and to run some Inconel-sodium hydroxide loops.

STRUCTURES OF LIQUID LEAD AND LIQUID BISMUTH

G. P. Smith J. V. Cathcart
W. H. Bridges P. C. Sharrar

The structures of liquid lead and of liquid bismuth each at two temperatures have been studied with the aid of neutron diffraction. The experimental work was done during the summer of 1951; however, the calculations of structure based on these measurements were carried out during the quarter covered by this report. The purposes of this study and the general method of conducting these measurements were given in the previous quarterly progress report.[2]

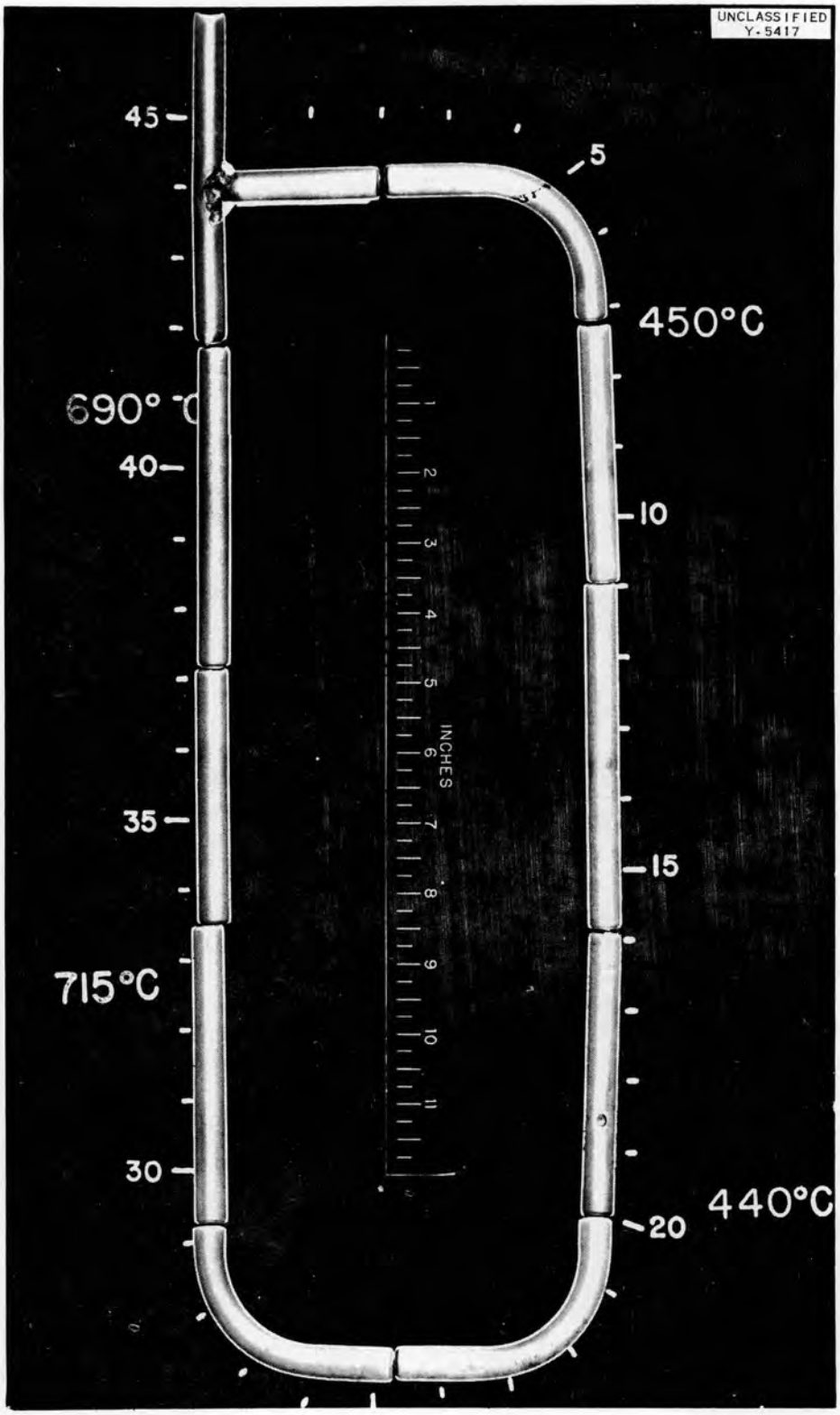

Fig. 83. Inconel-Potassium Hydroxide Convection Loop No. 5.

Fig. 84. Surface of Hot Leg of Inconel-Potassium Hydroxide Loop No. 5. 250X.

Fig. 85. Surface of Cold Leg of Inconel-Potassium Hydroxide Loop No. 5. 250X.

Fig. 86. Surface of Untreated Section of Inconel-Potassium Hydroxide Loop No. 5. 250X.

Experimental Procedure and Results. Table 19 gives a summary of the neutron-diffraction runs that have been made in connection with the studies on liquid lead and liquid bismuth. All the runs were made with cylindrical sample holders having an inside diameter of about 1 centimeter.

Five satisfactory graphs were obtained by using liquid bismuth and three by using liquid lead. Two of the satisfactory runs on bismuth were made with a 24S aluminum sample holder and two with a quartz sample holder. A number of attempts to use 2S aluminum for holding the liquid bismuth failed. Quartz was the only type of sample holder used for liquid lead. Only the results obtained with quartz sample holders have been analyzed.

All the runs were made by using a wavelength of 1.16 Å except number 9, for which a value of 0.71 Å was used. This gave experimental intensity data out to larger values of $(\sin\theta)/\lambda$. However, the latter graph was essentially constant from $(\sin\theta)/\lambda = 0.7$ to the end, and the accuracy was not sufficient to place much significance in some small variations or broad peaks that were present beyond this value. For this reason, data beyond 0.7 for $(\sin\theta)/\lambda$ were not used in this work. The 0.71 Å beam was much weaker than the 1.16 Å beam. [A copper crystal reflecting from (220) planes was used for 0.71 Å and from (111) planes for 1.16 Å.]

Other satisfactory runs were made with empty sample holders and with nickel powder. These data are necessary in evaluating the results obtained with the liquid metals. A run with an empty iron capsule showed that diffraction peaks from iron are too strong for this material to be useful as a sample holder.

Analysis of Diffraction Patterns. The atomic distribution in the liquid elements can be determined through an analysis of the diffraction patterns produced by the liquid. The equation that relates the atomic distribution function or atomic density, ρ, to the experimental results may be placed in either of the following forms:

$$4\pi R^2\rho(R) = 4\pi R^2\rho_0 + \frac{2R}{\pi}\int_0^{S_0} S\, i(S)\, \sin(RS)\, dS \qquad (1)$$

or

$$4\pi R^2\rho(R) = 4\pi R^2\rho_0 + \frac{2R}{\pi}\int_0^{S_0} S\left[\frac{4\pi}{\sigma_s}\frac{d\sigma}{d\omega} - 1\right] \sin(RS)\, dS\,. \qquad (2)$$

The first form is the one customarily used in x-ray work,[3] the second is similar to a form that has been used for neutron studies on liquids.[4]

[3] N. S. Gingrich, "The Diffraction of X-Rays by Liquid Elements," *Rev. Modern Phys.* **15**, 90 (1943).

[4] O. Chamberlain, "Neutron Diffraction in Liquid Sulfur, Lead, and Bismuth," *Phys. Rev.* **77**, 305 (1950).

TABLE 19

Summary of Neutron-Diffraction Runs for Determining the Structures of Liquid Lead and Liquid Bismuth

RUN NO.	MATERIAL	TEMPERATURE (°C)	SAMPLE DIAMETER (mm)	SAMPLE HOLDER			FULL SCALE OF INSTRUMENT (cpm and variance)	SCANNING RATE (deg/hr)	CHART SCALE (deg/in.)	REMARKS
				MATERIAL	HOLDER NO.	THICKNESS OF WALL (mm)				
1*	Bismuth	300	9.17	24S Al	3P	0.3	2000 (0.3)	4	4	
2	Bismuth	300		24S Al	3P	0.3				Sample holder failed
3	Aluminum holder	Room	9.17 ID	24S Al	4P	0.3	500 (0.6)	4	4	
4*	Bismuth	300	9.17	24S Al	4P	0.3	2000 (0.6)	8	8	
5	Bismuth	300	9.17	24S Al	4P	0.3	2000 (0.6)	8	8	Scanning direction reversed at end of run 4
6	Bismuth	300	9.17	24S Al	4P	0.3	2000 (0.6)	8	8	Sample holder failed
7	Bismuth	300	9.17	2S Al	4A1	0.3	2000 (0.6)	8	8	Sample holder failed
8	Iron holder	Room	9.17 ID	Globe	1020 Iron	0.15	2000 (0.6)	8	8	Peaks too high for use as sample holder
9	Bismuth	300	9.17	2S Al	5A1	0.3	200 (0.6)	2	2	Sample holder failed after 2 1/2 hr
10	Aluminum holder	Room	9.17 ID	2S Al	5A1	0.3	200 (0.6)	2	2	
11*	Bismuth	300	10 ± 0.4	Quartz	Q1	~0.5	200 (0.6)	2	2	Count register used simultaneously (peaks on chart shifted due to long time-constant set on electronic circuit)
12*	Lead	350	10.6 ± 0.4	Quartz	Q2	~0.5	2000 (0.6)	8	8	
13*	Lead	500	10.6 ± 0.4	Quartz	Q2	~0.5	2000 (0.6)	8	8	
14*	Lead	350	10.6 ± 0.4	Quartz	Q2	~0.5	2000 (0.6)	8	8	
15	Nickel powder	Room	9.17	2S Al	6A1	0.15	5000 (0.6)	8	8	Scale 16
	Nickel powder	Room	9.17	2S Al	6A1	0.15	1000 (0.6)	8	8	Scale 8
16*	Bismuth	300	10.6 ± 0.4	Quartz	Q3	~0.5	2000 (0.6)	8	8	
17*	Bismuth	550	10.6 ± 0.4	Quartz	Q3	~0.5	2000 (0.6)	8	8	
18	Quartz holder	Room	10.6 ± 0.4	Quartz	Q3	~0.5	500 (0.6)	8	8	
19	Bismuth	300	~4	Quartz	Q3	~0.5	500 (1.2)	8	8	
20	Quartz holder	300	10.6 ± 0.4 ID	Quartz	Q3	~0.5	500 (0.6)	8	8	

*Indicates a satisfactory liquid metal run over the full range of angle.

The symbols in Eqs. 1 and 2 have the following significance:

$$S = 4\pi(\sin\theta)/\lambda,$$

$$i(S) = \frac{I - K}{K},$$

where

I = experimental diffraction curve corrected for background, absorption, and incoherent scattering;

K = scattering intensity to be expected if no interference effects are present and is assumed to approach the measured scattering at large values of $\sin\theta/\lambda$;

R = distance from any given atom in the liquid when that atom is considered as the origin;

ρ_0 = average density of the atoms in the liquid (atoms/cubic angstrom) determined from the known density and atomic weight;

$\rho(R)$ = atomic density or probability distribution function;

S_0 = maximum value of S to which the experimental diffraction curve extends;

σ_s = scattering cross section of a bound atom;

$d\sigma/d\omega$ = differential scattering cross section determined experimentally and given by the following equation:

$$\frac{d\sigma}{d\omega} = \frac{n(\phi)}{N'\left[\frac{a}{r^2}\right] n_0 A}, \qquad (2a)$$

where

n_0 = incident beam strength (neutrons per minute);

N' = number of atoms in the sample;

a = area of the detector slit;

r = distance from the sample to the detector;

A = absorption correction factor, for a cylindrical specimen such as used in this work;[5]

$n(\phi)$ = measured counting rate as a function of the scatter angle ϕ;

ϕ = scattering angle (angle between detector and incident beam).

The dimensions and constants used are given in Table 20.

The integrated intensity (cpm) in the (111) reflection from nickel was used as a standard in determining the differential cross-section scale used for runs 12, 13, and 14 for lead and runs 16 and 17 for bismuth. One method made use of a wide slit (5/8 in.) on the detector, which was set to cover the complete reflection and, after correcting for the background of 350 cpm, gave 2210 cpm integrated intensity. The second method made use of a narrow slit (1/16 in.) on the detector, which was made to scan the peak, and an integrated intensity of 2470 cpm was obtained. The equation for the integrated intensity from a powdered sample is given below (ref. 5, p. 562).

$$\frac{P}{I_0} = \frac{N^2\lambda^3 l V_p F^2}{16\pi r \sin^2\theta \cos\theta} A\left[\frac{\rho'}{\rho}\right] \qquad (3)$$

[5] *Internationale Tabellen zur Bestimmung von Kristallstrukturen*, Vol. I and II (Gebrüder Borntraeger, Berlin, 1935).

where

P = total power (cpm) diffracted;

I_0 = intensity of the incident beam (counts/cm^2/min);

N = number of unit cells per unit volume;

λ = the wave length of the neutrons (1.16×10^{-8});

l = height of the detecting slit;

V = volume of the sample;

(ρ'/ρ) = ratio of apparent density of the powder to that of the solid (2.24/8.9);

p = multiplicity of the reflecting planes;

F = crystal structure factor;

A = absorption factor tabulated for different angles and values of R for cylindrical samples completely bathed in x rays.[5]

Figures 87 and 88 show the intensity curves that were obtained from the experimental curves after correcting for the absorption of neutrons by the sample and by the quartz sample holder. The latter correction was obtained from run 20.

The distribution curves were calculated from the intensity curves by the use of Eq. 2. The integrals involved in these calculations were evaluated by the Mathematics Panel, who used the IBM method of harmonic analysis. These distribution curves are given in Figs. 89 and 90.

TABLE 20

Dimensions and Constants Used

Collimating slit	3/8 by 1 1/4 in.
Detector slit	5/8 by 1 3/4 in.
Detector distance	9.4 cm
Diameter of sample	0.916 cm
Scattering cross sections (bound)	
Bismuth	10 barns
Lead	11.6 barns

Scattering amplitudes for nickel

$f = 1.03 \times 10^{-12}$ cm

$F(111) = 4f \exp(-M)$, where $\exp(-M)$ is the temperature factor[5]

$F^2 = 16.3 \times 10^{-24}$ cm^2 (including temperature correction)

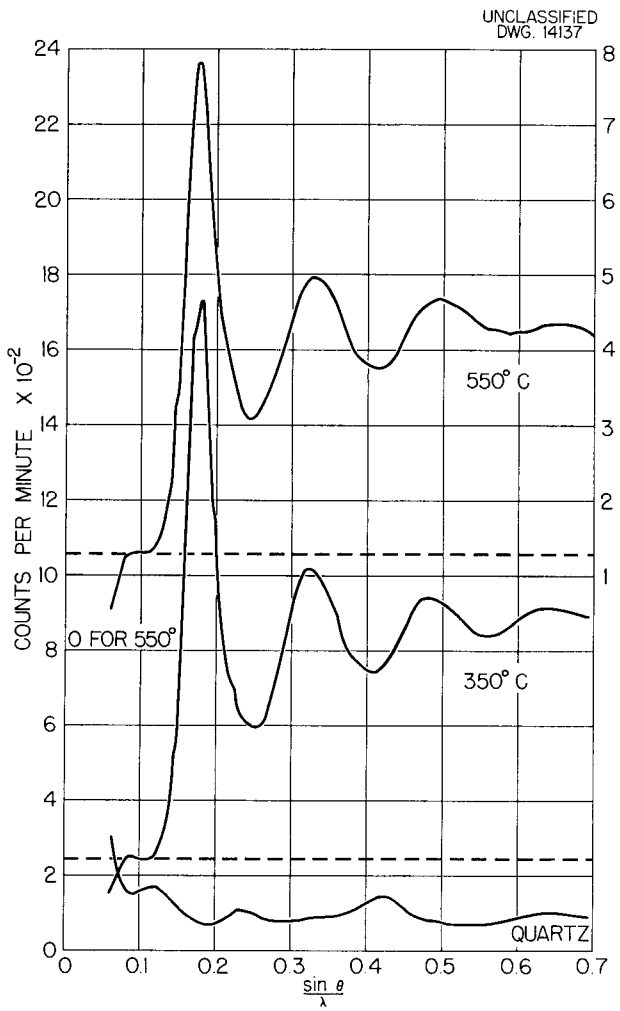

Fig. 87. Intensity Curves for Liquid Lead.

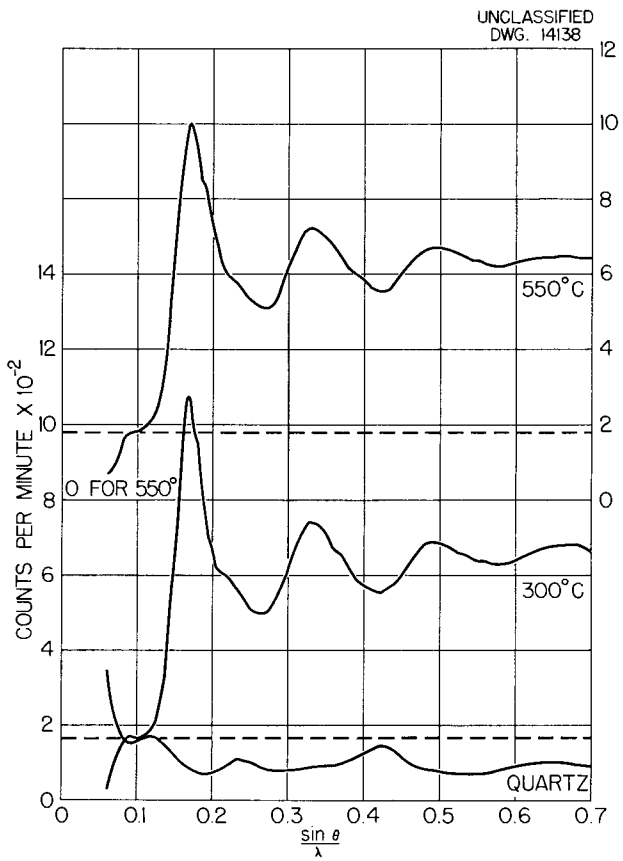

Fig. 88. Intensity Curves for Liquid Bismuth.

Extensive calculations were made to determine whether the intensity curves were properly normalized. The calculations were based on the assumption that the density of atoms at a distance R from one atom approaches zero as R approaches zero. This is a method of normalization used by Chamberlain[4] in previous neutron diffraction studies of liquid metals and is similar to the method common in x-ray diffraction. The results of these calculations showed that the error in the distribution curves because of improper normalization was exceedingly small. When the corrected distribution curves were plotted, it was found that the difference between these curves and the uncorrected curves was too small at nearly all points to be discernible on the scale of Figs. 89 and 90.

Figures 91 and 92 represent the Menke W function, which shows the probability of finding an atomic center in the interval r to $r + dr$ from the central atom, based on an average probability of 1 if the liquid were a continuum.

The calculated results of the experiments appear to be in excellent agreement with the best x-ray diffraction work on liquid lead and

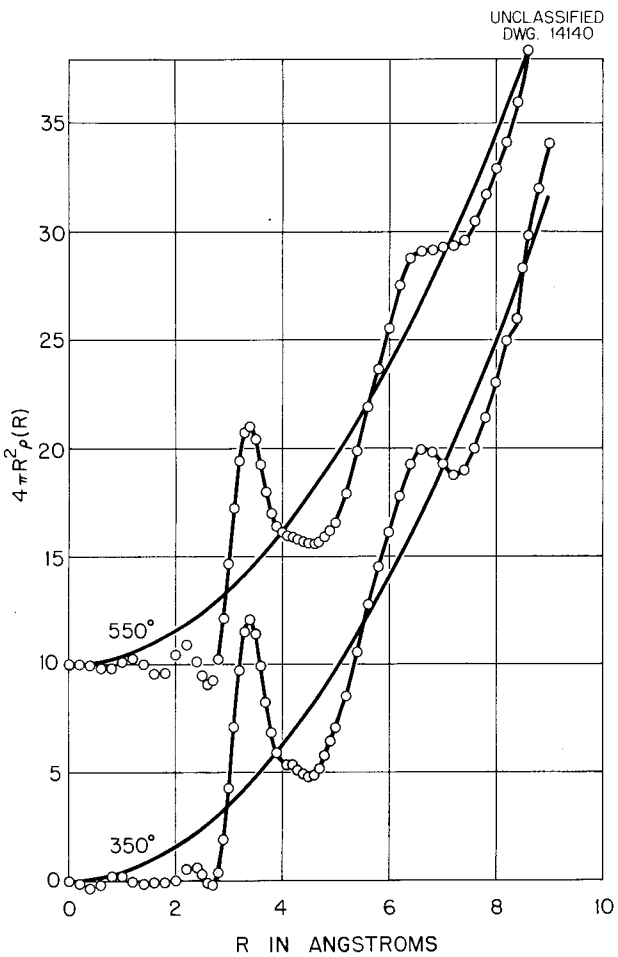

Fig. 89. Distribution Curves for Liquid Lead.

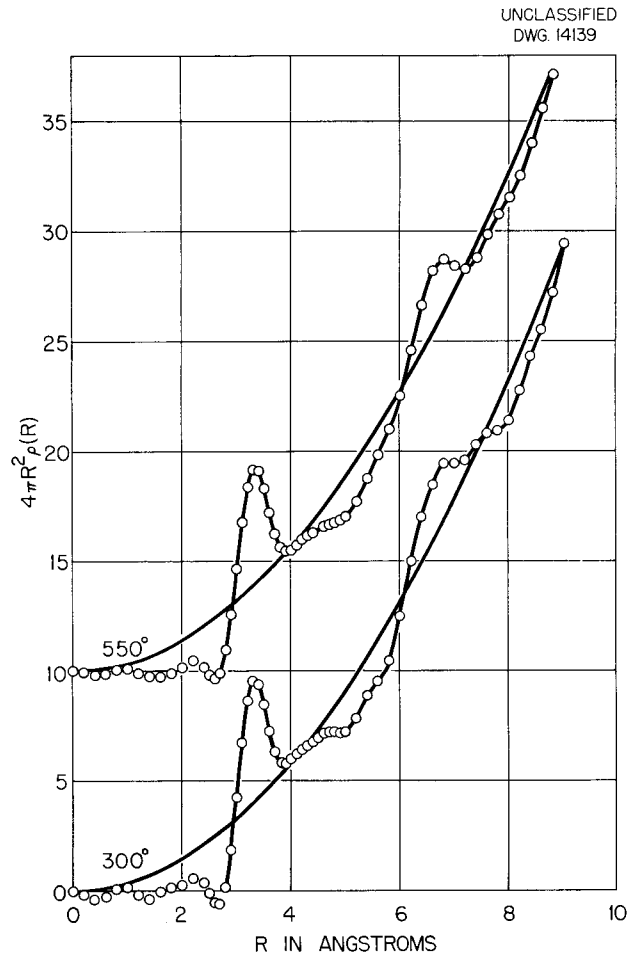

Fig. 90. Distribution Curves for Liquid Bismuth.

liquid bismuth[6] and to represent a considerable improvement over the previous neutron-diffraction work.[4] Furthermore, this work shows some new details, not previously reported, of the structure of these liquid elements. A detailed analysis of the distribution curves and a quantitative comparison with previous work on the structure of liquid metals will be given in the next Metallurgy Division quarterly progress report.

[6] H. Hendus, "Die Atomverteilung in den flüssigen Elementen Pb, Tl, In, Au, Sn, Ga, Bi, Ge, und in flüssigen Legierungen des Systems Au-Sn," *Z. Naturforsch.* **2A**, 505 (1947).

FABRICATION

E. S. Bomar J. H. Coobs

Fuel Elements. Tubular elements fabricated by joining two semicircular plates with seam welds or by rubber-static-pressing methods were subjected to cold-drawing operations at the Superior Tube Company. All the samples, except the one prepared by rubber-static pressing, were given an initial hot reduction of 62 to 75% to bond pressed core, picture frame, and cladding. This operation was carried out on the flat stock before forming into tubes. Table 21 gives the core composition of the various tubes.

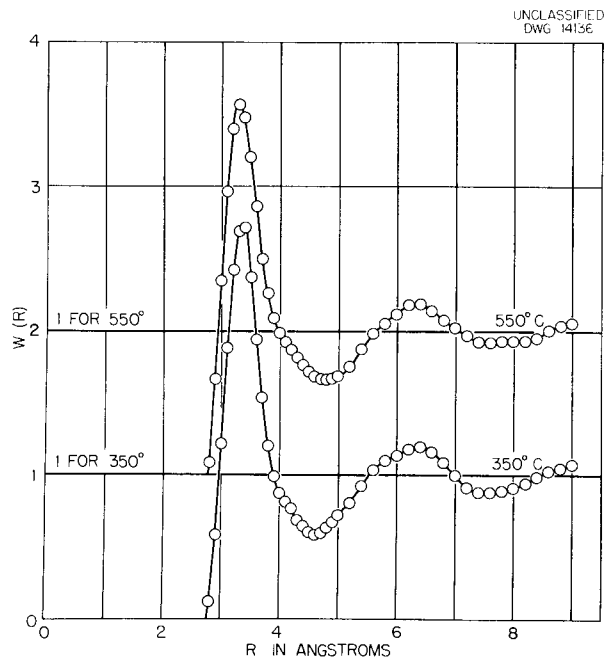

Fig. 91. $W(R)$ Functions for Liquid Lead.

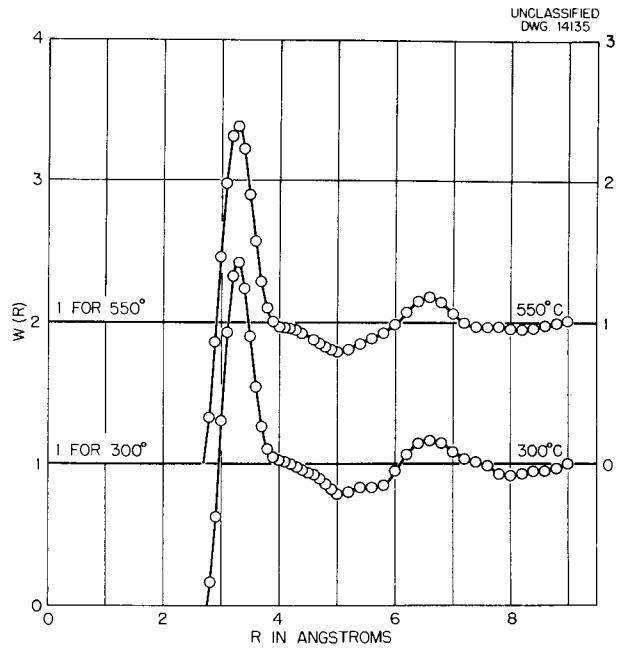

Fig. 92. $W(R)$ Functions for Liquid Bismuth.

A reduction schedule based on commercial practice was set up, and tubes 1 through 11 were given an initial reduction of 26% to smooth the weld seams. Inspection after the first pass showed that the seams had been flattened satisfactorily. A second pass was made with a reduction of 38% on tube 1. The tube failed, however, so subsequent reductions on the remaining tubes were made at values less than 32%, without further difficulty.

Table 22 is a summation of the reduction schedule.

TABLE 21

Core Compositions of Various Tubes

TUBE NO.	CORE MATERIAL	
	METALLIC 70 vol %	UO_2 30 vol %
1, 2, 3	Type-302 stainless steel, -325 mesh	-100 mesh, as received
4, 5, 6	Iron, 10-microns mesh	-100 mesh, as received
7, 8, 9	Type-302 stainless steel, -325 mesh	-100 + 325 mesh, high fired
10, 11	Nickel, -325 mesh	-100 mesh, as received
12	Type-302 stainless steel, -325 mesh	-200 + 325 mesh, high fired

TABLE 22

Summation of the Reduction Schedule

TUBE NO.	REDUCTION PASSES	REDUCTION (%)	TOTAL REDUCTION (%)
1 through 11	1	26	
3	2	38 (failed)	54
1 through 11	2	23	
	3	24	
	4	25	
	5	28	
	7	22	87.5
5, 8, and 10	8	18	
	9	28	
	10	24	94

Each reduction was followed by a bright anneal at 1950°F for 20 minutes. This program yielded two sets of tubes - one 1/4 in. OD by 0.015-in. wall thickness and a second set 1/8 in. OD by 0.015-in. wall thickness. All were mandrel drawn through the sixth pass by using lubricants specified for processing stainless steel. The seventh pass was a sinking operation, or reduction in diameter without a mandrel, and resulted in some surface wrinkles on all tubes except 4, 5, and 6, which had very good surface finishes. The degree of wrinkling varied from very slight in 7, 8, 9, and 10 to severe in 1, in which the weld folded in.

Metallographic examination of specimens taken from the tubes showed that bonding and UO_2 distribution varied from very poor in 1 to fair in 6. These structures are shown in Fig. 93 for sections transverse to the direction of drawing at reductions of 87.5% (1/4-in.-OD tubes). In general, further reductions to 94% (1/8-in.-OD tubing) only exaggerated the defects found in the 1/4-in.-OD stock.

Tube 12 was prepared as a seamless, laminated tube by rubberstatic pressing and sintering at 1300°C. This procedure is outlined in the previous quarterly report. The tube was reduced to 1/4 in. OD by using a slightly modified version of the schedule outlined above. The primary change was the use of a plug for the final pass instead of a mandrel. The tube failed three times during the initial part of this pass and broke completely at the die. The final reduction was then completed as a sinking operation during which the tube behaved well. A transverse section of this sample, Fig. 94, shows that the UO_2 distribution is reasonably good. However, the inside cladding was very poorly bonded to the core and was easily broken away from the core when a longitudinal section was cut.

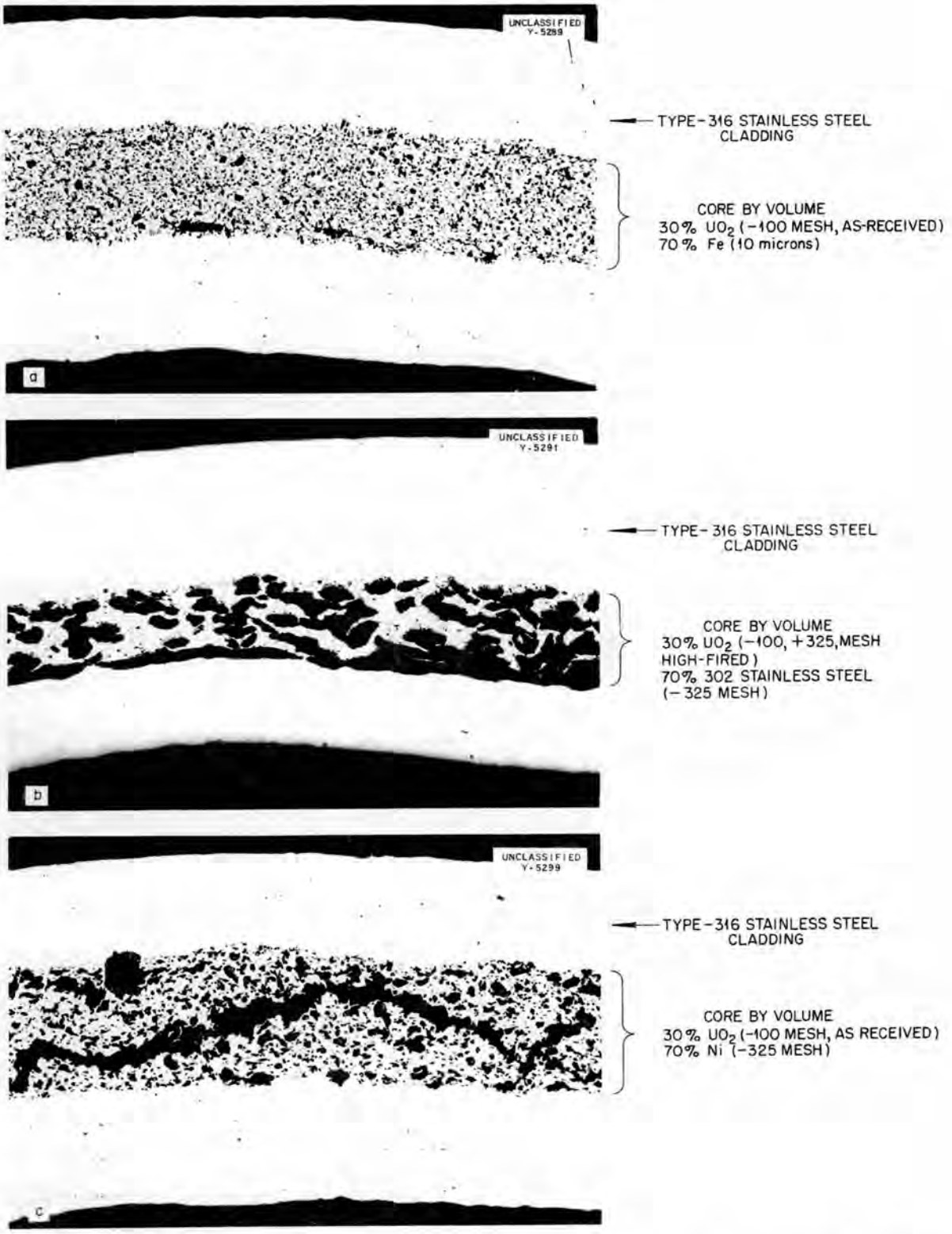

Fig. 93. Transverse Section Through 1/4-in.-OD Tubes Prepared from Rolled Plate. Original magnification 200X, reduced 37%.

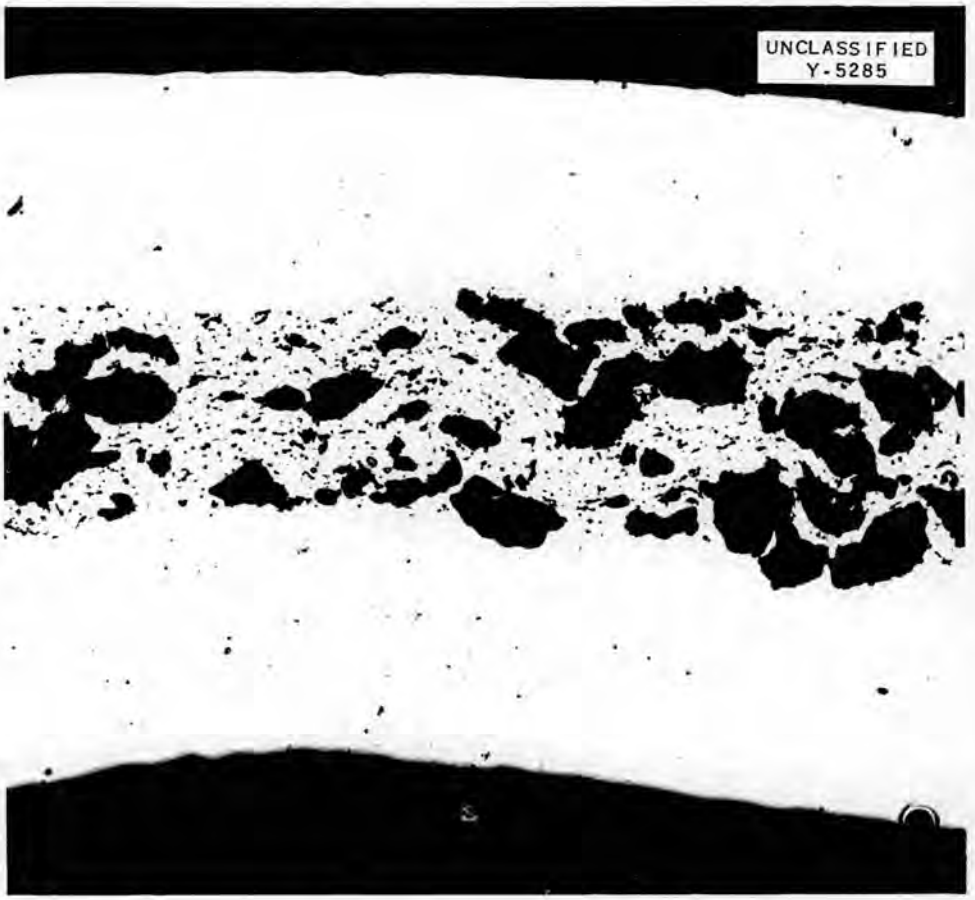

Fig. 94. Transverse Section Through 1/4-in.-OD Tube Prepared by Rubberstatic Pressing.

It is unfortunate that plug drawing was not tried on at least one of the composite tubes. Consultation with some of the technical staff at Superior Tube Company produced the opinion that plug drawing would not disturb the core of a laminated structure so much as drawing on a mandrel. It was argued that rod drawing produces more slip cracks in the core because of slightly uneven reduction of the two cladding layers, whereas plug drawing should give uniform reduction. A poor original bond between the inner cladding and the core of the rubber-statically pressed tube may be the reason that plug drawing appeared to be too severe.

Variation of the reduction schedules used for these tubes will be tried by using the Metallurgy Division draw bench and emphasizing less severe reductions. Mandrels are now on order to supplement dies already on hand. Equipment for plug drawing is not available at present.

ARE Control Rod. At the operating temperature of the ARE there exists the possibility of solid phase bonding of metallic components that are in close contact. This phenomenon could possibly lead to malfunctioning of the control rods if it occurred between the control rod cladding and the walls of the tubes in which they are housed.

Several tests have been made with the equipment shown in Fig. 95. Samples made of two different metals were tested at the same time. The end plates were polished with fine emery paper, and 1/8-in.-dia specimens were arranged in three columns with two metallic samples in each. For example, if one end plate was made of metal *A*, the three small samples bearing on it would also be made of metal *A*. The same arrangement would exist at the opposite end composed of metal *B* with its adjoining samples of *B*. The interface at the junction of the 1/8-in.-dia pieces would be of the dissimilar metals *A* and *B*. A refractory disk with holes drilled to receive 1/8-in. samples with a snug fit was used to assure alignment. Pressure was applied to the metal samples through refractory inserts by using a weight of sufficient size to create contact pressure of 250 psi in the 1/8-in. columns used. The pressure selected was arbitrary, but it was chosen so that it would probably be higher than would be encountered radially at the control rod and control-rod-tube contact points.

The tests were initiated with type-316 stainless steel and Inconel in various atmospheres. However, results of compatibility tests made available after a portion of the welding tests had been run indicated a fair amount of reaction between the systems boron carbide–type-316 stainless steel and boron carbide–Inconel. The exposures were made for 100 hr at 800°C. A less marked interaction was found when boron carbide was contained in type-430 stainless steel. The solid phase welding schedule was revised to include the type-430 stainless steel–type-316 stainless steel and type-430 stainless steel–Inconel systems.

Atmospheres of purified H_2, purified He, and tank He were selected to create conditions ranging from those conducive to welding to those actually present in the reactor. Tank H_2 was purified by using a platinum catalyst followed by an activated alumina column; dew points of −80°F have been obtained regularly with this equipment. Removal of moisture and oxygen from the helium was accomplished by using a column of activated alumina followed by two columns of magnesium turnings heated to 500°C. Subsequent examination of samples exposed to the above atmospheres indicated that a portion of the study of the effect of purity of the atmospheres was nullified by the outgassing of the refractory support in the hot zone.

The gaseous atmosphere was introduced at the bottom of the refractory tubes containing the test pieces. The portion of the tube containing the samples was heated to a temperature of 815°C with a 1400-watt, split-type, Hevi-Duty tube furnace. A thermocouple located inside the tube and adjacent to the self-weld samples controlled the furnace output. Exposures were made for 100 hours.

After completion of a high-temperature exposure, the samples were allowed to cool before removal for examination. The degree of bonding was evaluated in a qualitative manner and can be classified as (1) no bonding, (2) slight bonding – removed with finger pressure, and (3) severe bonding – could not be removed without pliers. The results of four runs are summarized in Table 23.

In two instances bonding occurred in only one column of samples. This could possibly be the result of nonuniform loading of the samples, since the long cylindrical geometry of the test rig is not conducive to a maximum of stability. However, every care was exercised in loading to avoid an unbalanced condition. The presence of a nonuniform load would not invalidate

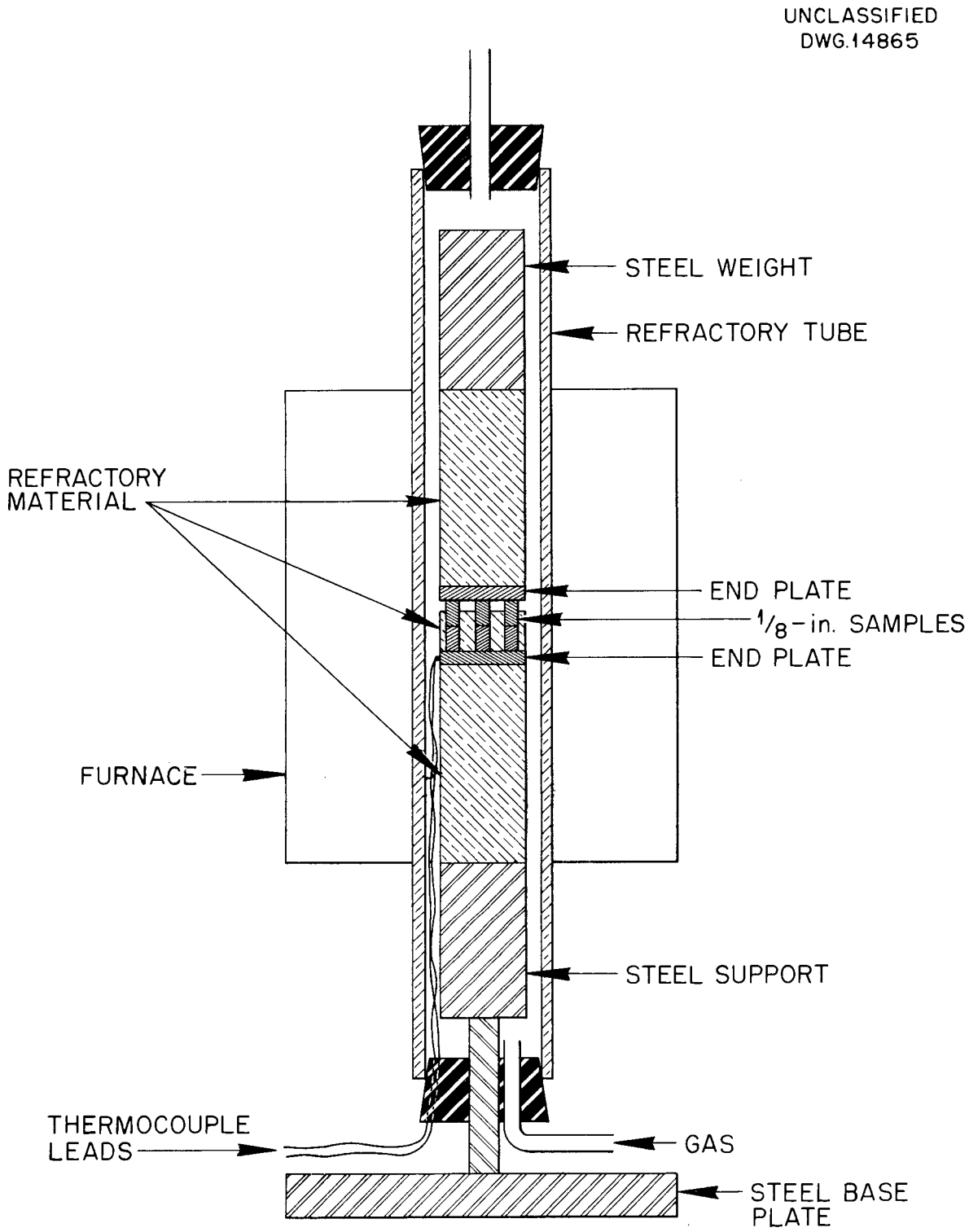

Fig. 95. Solid-Phase-Welding Test Equipment.

the tests run but would increase the severity of the tests, because the unit loading in one or two columns would rise above the 250-psi pressure selected.

Tests of the type-430 stainless steel–type-316 stainless steel systems with a tank He atmosphere are now being conducted. Exposure to the other atmospheres will be carried out

TABLE 23

Results of Bonding Tests

ATMOSPHERE	INTERFACE	BONDING	REMARKS
	TEST 1		
Purified H_2	Type-316 stainless steel–type-316 stainless steel	One, slight Two, severe	Thin oxide film on all samples
	Type-316 stainless steel–Inconel	Three, none	
	Inconel–Inconel	One, slight Two, none	
	TEST 2		
Purified He	Type-316 stainless steel–type-316 stainless steel	One, slight Two, none	Fairly heavy oxide film on all samples
	Type-316 stainless steel–Inconel	Three, none	
	Inconel–Inconel	One, severe Two, none	
	TEST 3		
Tank He	Type-316 stainless steel–type-316 stainless steel	One, slight Two, none	Heavy oxide film on all samples
	Type-316 stainless steel–Inconel	One, slight	
	Inconel–Inconel	One, severe One, slight One, none	
	TEST 4		
Tank He	Type-430 stainless steel–type-430 stainless steel	One, severe Two, none	Flaky oxide film on type-430 stainless steel; continuous film on Inconel
	Type-430 stainless steel–Inconel	Three, none	
	Inconel–Inconel	One, severe Two, none	

if examination of results indicate that this is desirable.

MECHANICAL PROPERTIES OF METALS

R. B. Oliver J. W. Woods

Thorium. Four creep testing units have been used for measurements with thorium during the previous quarter. All testing of thorium has been conducted at 300°C. The early test results were determined with an external dial gage for sensing the movement of the pull rod. These data show elongations that are much greater than the true elongation of the specimen. During the past quarter all specimens tested were equipped with scribed platinum strips, and the elongation was measured with a micrometer microscope.

Figure 96 summarizes the work on thorium. The strains indicated were measured with dial gages so that all tests could be compared. These specimens were from several billets of Ames thorium with carbon content varying from 0.040 to 0.076%. For high-carbon thorium, it is apparent that at some stress, a little greater than 19,000 psi, there is a great increase in the strain rate with increasing stress. The same change appears for the low-carbon thorium at a stress between 16,000 and 19,000 psi.

Another behavior of thorium appears in the shape of the strain-time curves for specimens loaded to stresses under 16,000 psi. Instead of exhibiting a constant rate, a decelerating rate is observed even after 1000 hr in test.

Figure 97 shows the strain-time behavior of three test bars taken from adjacent positions in the original extruded bar. All three bars were tested at 300°C and 16,000-psi stress. One bar was tested with no prior treatment and the test chamber was maintained at a pressure of 0.05 microns; another bar was previously pulled 5% in tension and then tested under the same conditions as the first bar; a third bar was given a heavy silver plate and tested in air. The prior cold work, all other variables being the same, resulted in a decreased creep-rate and a smaller initial elongation. The silver plate appears to have failed at about 200 hr, so a comparison of the creep rates cannot safely be made, but it is significant that this specimen showed a much greater initial elongation. The microstructure of this specimen shows severe intergranular oxidation.

Considerable out-gassing is observed during the initial heating and pumping of a thorium specimen. It is planned to conduct several tests with controlled amounts of the several possible gaseous constituents of the metal for evaluating the individual effects on the strength properties at elevated temperatures.

The creep rate for extruded thorium containing 0.040% carbon and tested at 300°C, 16,000 psi, and 0.05 microns averages about 0.0003% per hr for the period between 900 and 1200 hours.

Uranium. Figure 98, a logarithmic plot of stress vs. rupture time, summarizes the work on uranium to date. The main points determining the curve are the results from test bars made of alpha-rolled uranium. One point at 4500 psi lies above the curve and is from alpha-rolled stock, which was heated to 680°C for several hours because of a malfunction of the temperature controller; this treatment resulted in a very large grain size. Several points falling below the curve represent rupture times for specimens from the same alpha-rolled stock that were given a 40-sec beta treatment at 725°C.

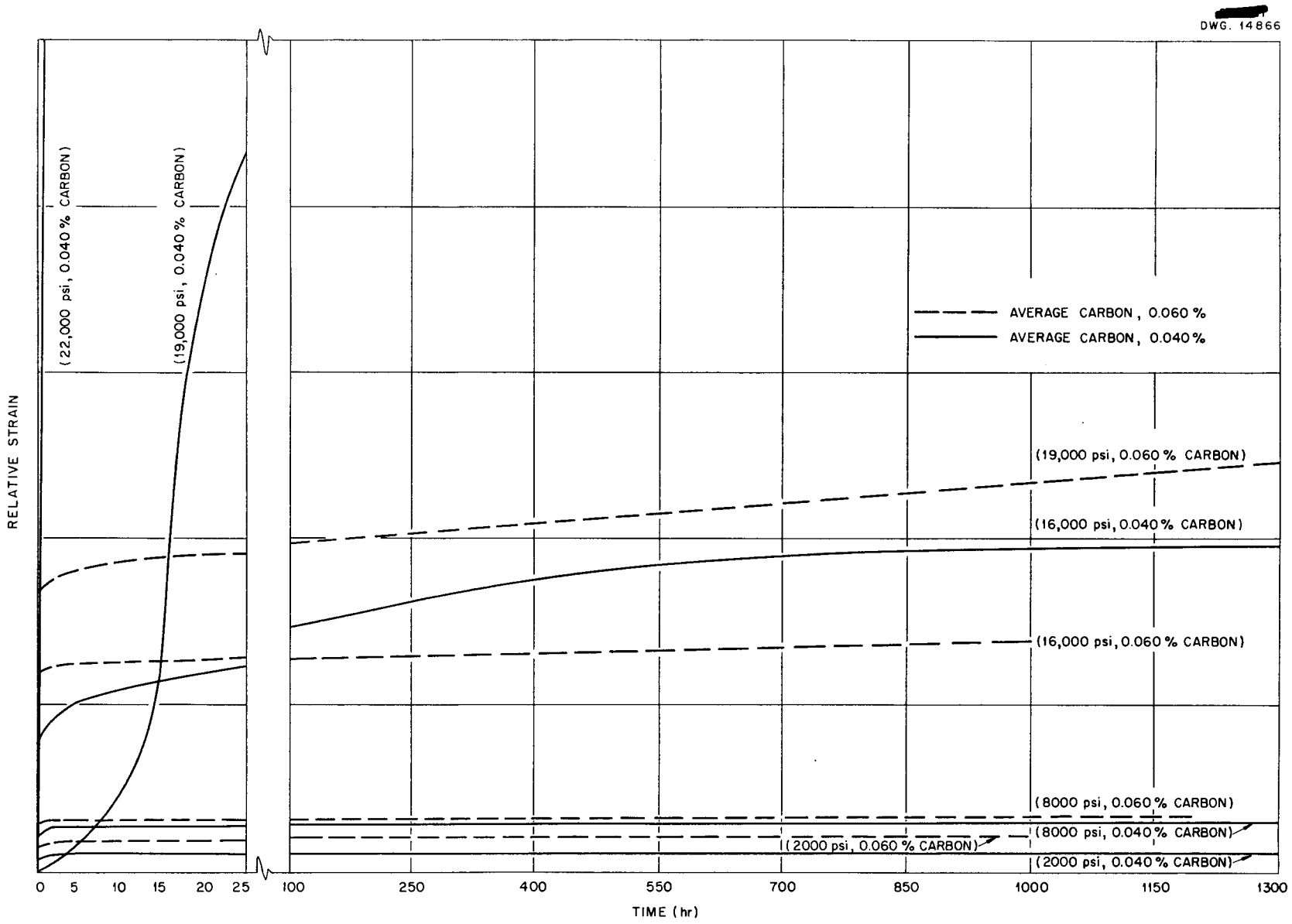

Fig. 96. Creep of Thorium.

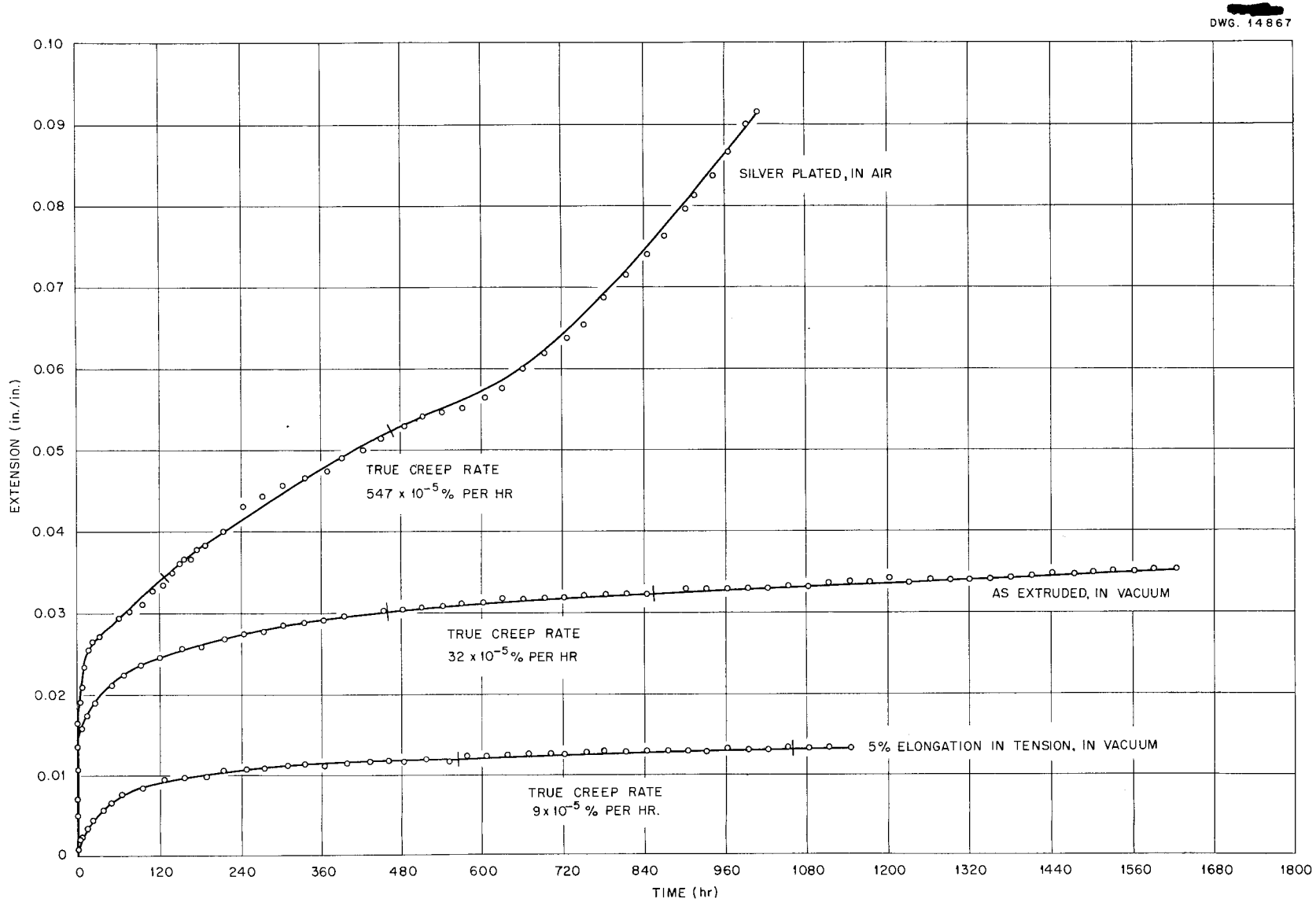

Fig. 97. Creep Rate of Thorium.

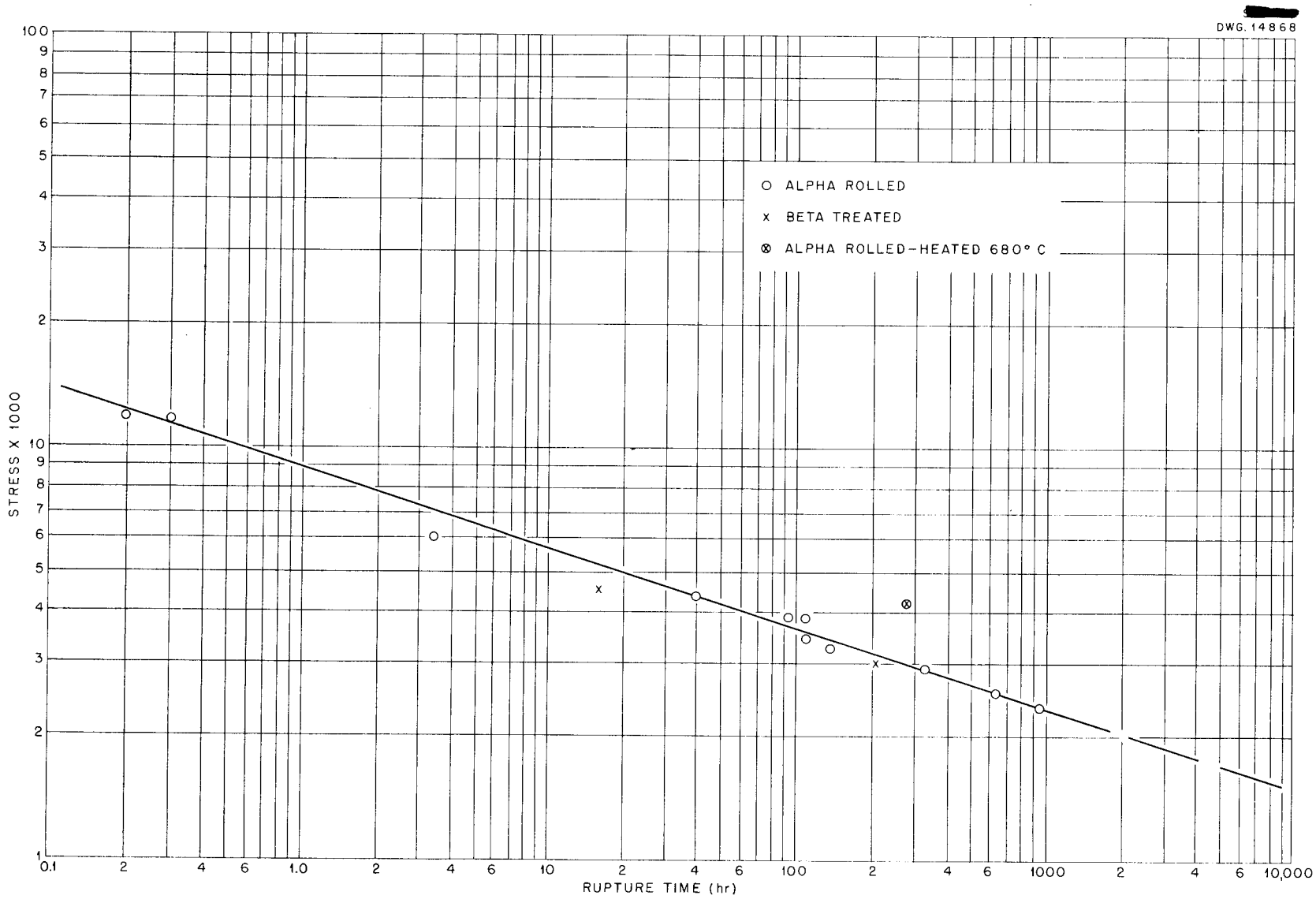

Fig. 98. Stress-to-Rupture Plot for Normal Uranium.

Figure 99 compares the strain-time behavior of ORNL and BMI test specimens at 500°C and 0.05 microns and at stresses of 2220 and 1720 psi. The uranium used for the ORNL specimens was rolled at 600°C from the 5-in. billet to 7/8-in. bar and machined to give a standard 0.505-in. test bar. The BMI stock was rolled at 600°C from the original 5-in. billet to a 1 3/8-in. round bar, forged to a 1 1/8-in. square, and rolled to 1/2-in. round bar, which was then machined to produce a 0.252-in. test bar and annealed for 12 hr at 600°C and furnace cooled. The strain ordinate represents the strain as measured with an external dial gage; the indicated creep rates were optically measured on platinum strips fastened across the gage of the specimens. BMI reported a creep rate of 9×10^{-4} %/hr at 1720 psi (0.252-in. bar); ORNL determined a rate of 11×10^{-4} %/hr for the same material. Under the same conditions but with the 0.505-in. bar from ORNL stock a creep rate of 40×10^{-4} %/hr was observed. The discontinuity observed in the bottom curve is associated with an air leak in the vacuum chamber.

Inconel. Five Inconel specimens have been tested from 40 to 100 days, and the data being obtained will be reported upon completion of the tests. Present data indicate that sheet Inconel has a considerably smaller rupture strength than is reported in the literature for round Inconel bars. Severe, coarse, edge cracking is observed for the sheet specimens but has not been observed on the round specimens. This cracking is probably a function of the shape; the shape may also account for the observed difference in strength.

Stainless Steel. Testing of type-316 stainless steel has been suspended during this quarter pending completion of the Inconel testing. Figure 100 compares the stress-rupture data on type-316 stainless steel sheet specimens tested in air by the Cornell Aeronautical Laboratory with sheet specimens from a different heat tested in argon atmosphere at 815°C at this Laboratory. Six specimens of type-310 stainless steel have been tested in air as a service to the General Electric ANP Program.

WELDING LABORATORY

P. Patriarca G. M. Slaughter

Cone-Arc Welding. The feasibility of the use of the cone-arc welding process for production of tube-to-header joints has been demonstrated by previous investigations.[7] The welding group of the Metallurgy Division has undertaken an investigation to determine the applications and limitations of the process, since the need for a reliable automatic or semiautomatic process for production of the multitude of tube-to-header joints required by ANP core and heat exchanger designs is evident.

Equipment. Figure 101 is a schematic diagram of the welding circuit being used in the investigation. The apparatus consists of a G-E 200-amp, direct-current welding generator with the addition of a resistor circuit that enables the use of currents as low as 3 amp when desired. A Miller Electric Company high-frequency spark-gap oscillator provides the high frequency required for starting the inert welding arc without the necessity of having to touch the 1% thoriated tungsten electrode to the work. The apparatus has been provided with a timer and contactor control circuit to make the arc timing an automatic

(7) E. R. Mann, *Means for Making Uniform Circular Heliarc Welds by Deflecting the Ion Beam Continuously*, ANP-63, Apr. 9, 1951.

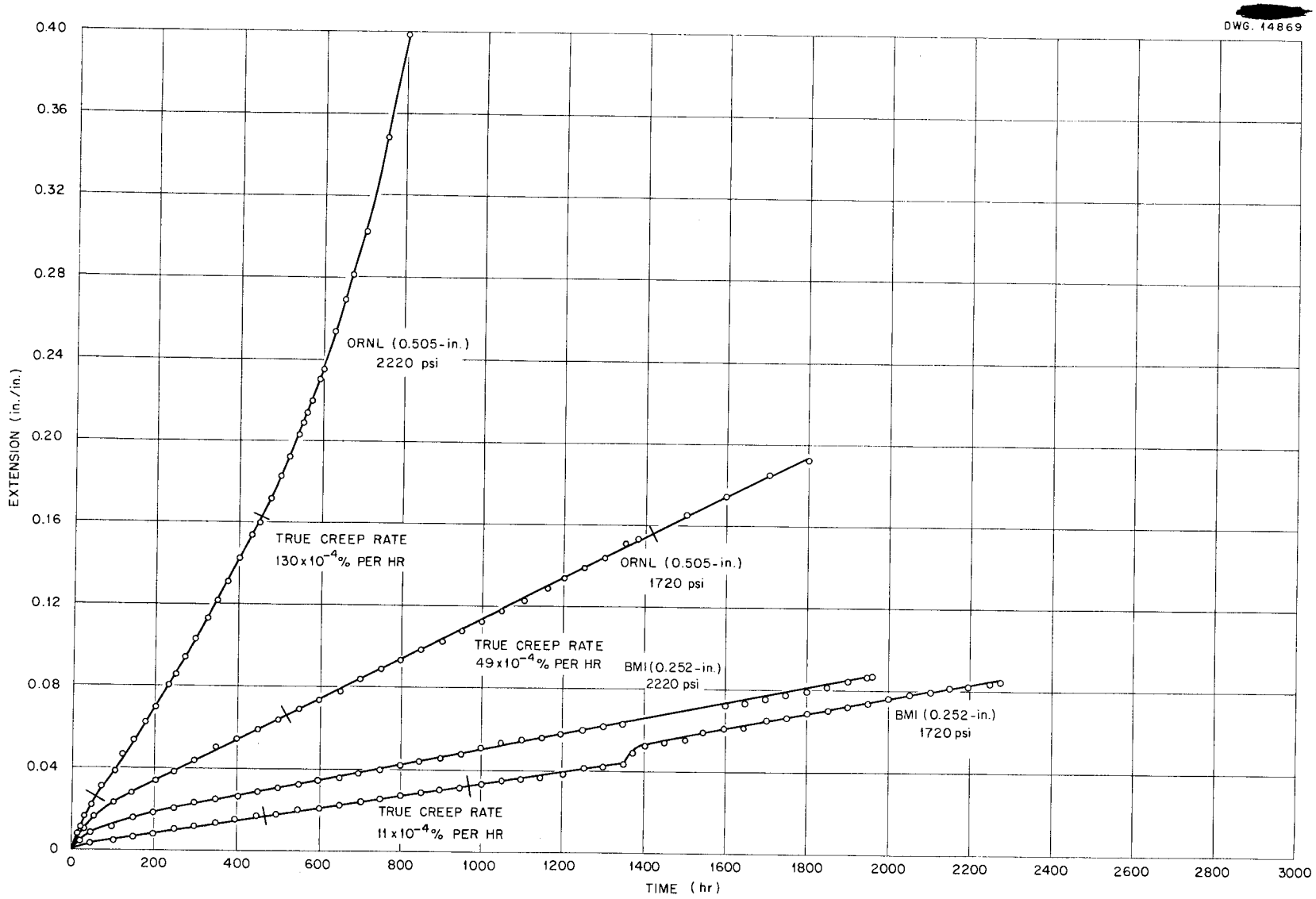

Fig. 99. Creep Rate of Normal Uranium.

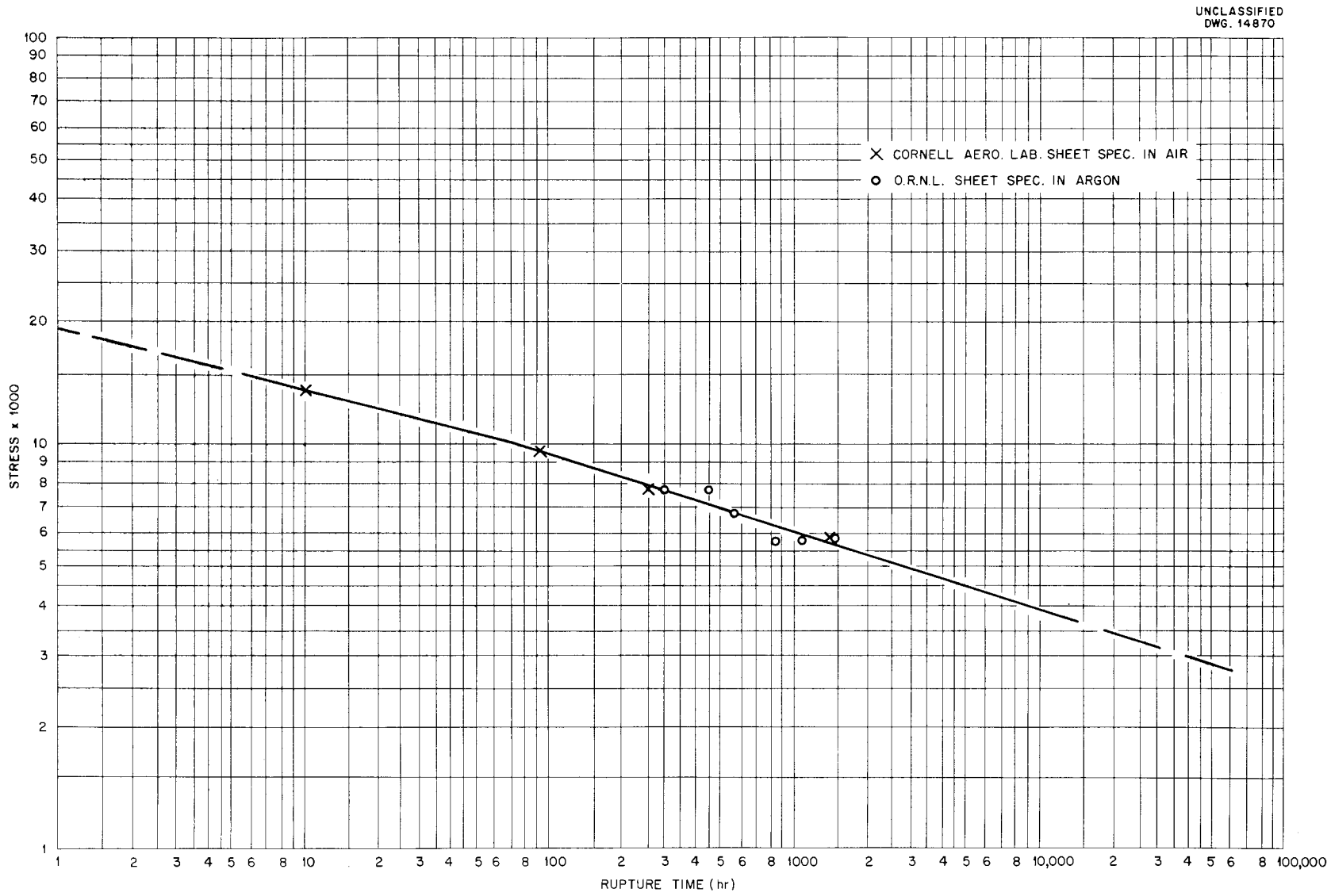

Fig. 100. Stress-to-Rupture Plot for Type-316 Stainless Steel.

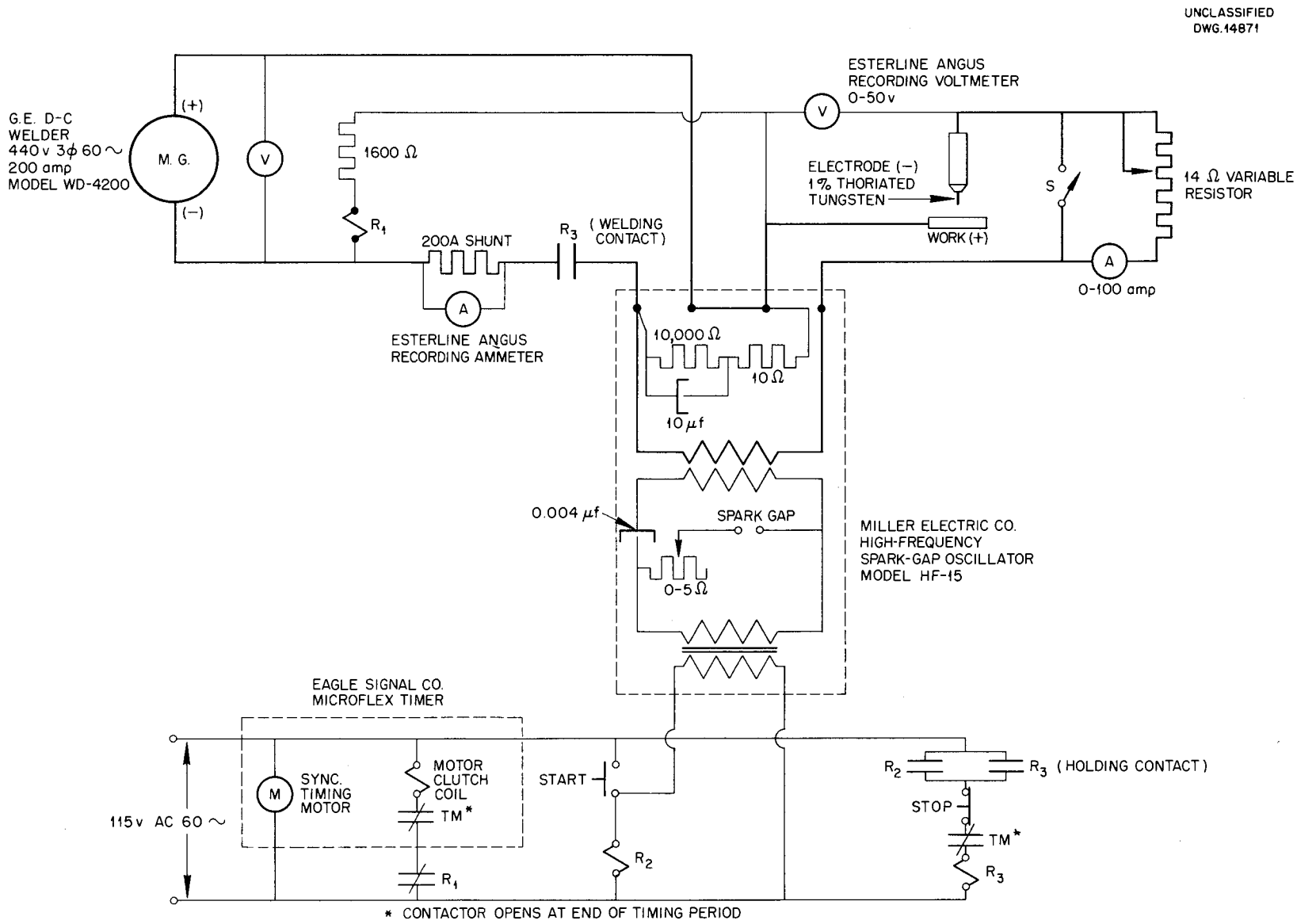

Fig. 101. Schematic Diagram of Cone-Arc Welding Circuit.

operation. The sequence of operation is as follows:

1. Upon starting the welding generator, the open circuit voltage reaches a preset value of 50 to 70 volts. (This voltage range has been determined by experiment to be ample for argon arc-striking with high frequency.) The relay R_1 operates to open contact R_1, which de-energizes the clutch coil of the Eagle Signal Company Microflex timer, which mechanically holds contacts TM closed.

2. The starter button is depressed to energize the high-frequency circuit. Relay R_2 is also energized and closes contact R_2. This contact in turn energizes coil R_3, which closes the main welding contact R_3 and the holding contact R_3. Since the welding circuit is complete, the high frequency is permitted to strike the welding arc, and at that time the starter button is released by the operator.

3. When the welding arc has struck, the voltage drop across relay R_1 reduces to 10 to 15 v with knife switch S closed, depending on the electrode or arc distance and the type of inert gas. Relay R_1 permits contact R_1 to close and energize the clutch coil of the timing motor, and a preset timing period begins. At the end of the timing period the contacts TM are opened to de-energize the clutch coil and relay R_3 and open welding contactor R_3 to extinguish the arc.

4. The normally closed stop button is provided to stop operation before the end of the timing period if desired.

Principle of Operation. Figure 102 is an iron-filing pattern of the magnetic lines of flux of the permanent Alnico magnet nozzle being used in this investigation. This nozzle is manufactured by the Air Reduction Company for use with their inert-arc welding electrode holder. The portion of the nozzle directly above the Inconel tube-to-header work pieces is of soft iron and serves to concentrate lines of flux parallel to the welding electrode. The Alnico permanent magnet is directly above the soft iron, and the remainder of the nozzle is aluminum and plastic.

Since the welding arc will strike from the electrode tip to a point on the periphery of the tube, the arc stream is cut by the lines of flux at a small angle. The angle suffices to set up resultant forces tangential to the tube periphery and in the plane of the header sheet. These forces cause the arc to rotate around the tube at very high speeds. To the observer, the arc appears as a cone, hence the name "cone arc." The arc serves to raise the temperature of the tube edge and the complete header-hole periphery in a uniform manner until the melting point is reached and a circumferential weld results.

Experimental Procedure. Some of the variables that may affect the operation are:

1. arc current and time,
2. arc distance (affects arc voltage and the angle between the arc stream and the magnetic lines of flux),
3. magnetic nozzle to work distance,
4. choice of inert gas and rate of flow (affects arc voltage, which is higher for helium than argon, and turbulence),
5. work geometry including tubing size, header thickness, and heat transfer uniformity such as header hole-to-hole distance, hole-to-header edge distance, and centering of work and electrode.

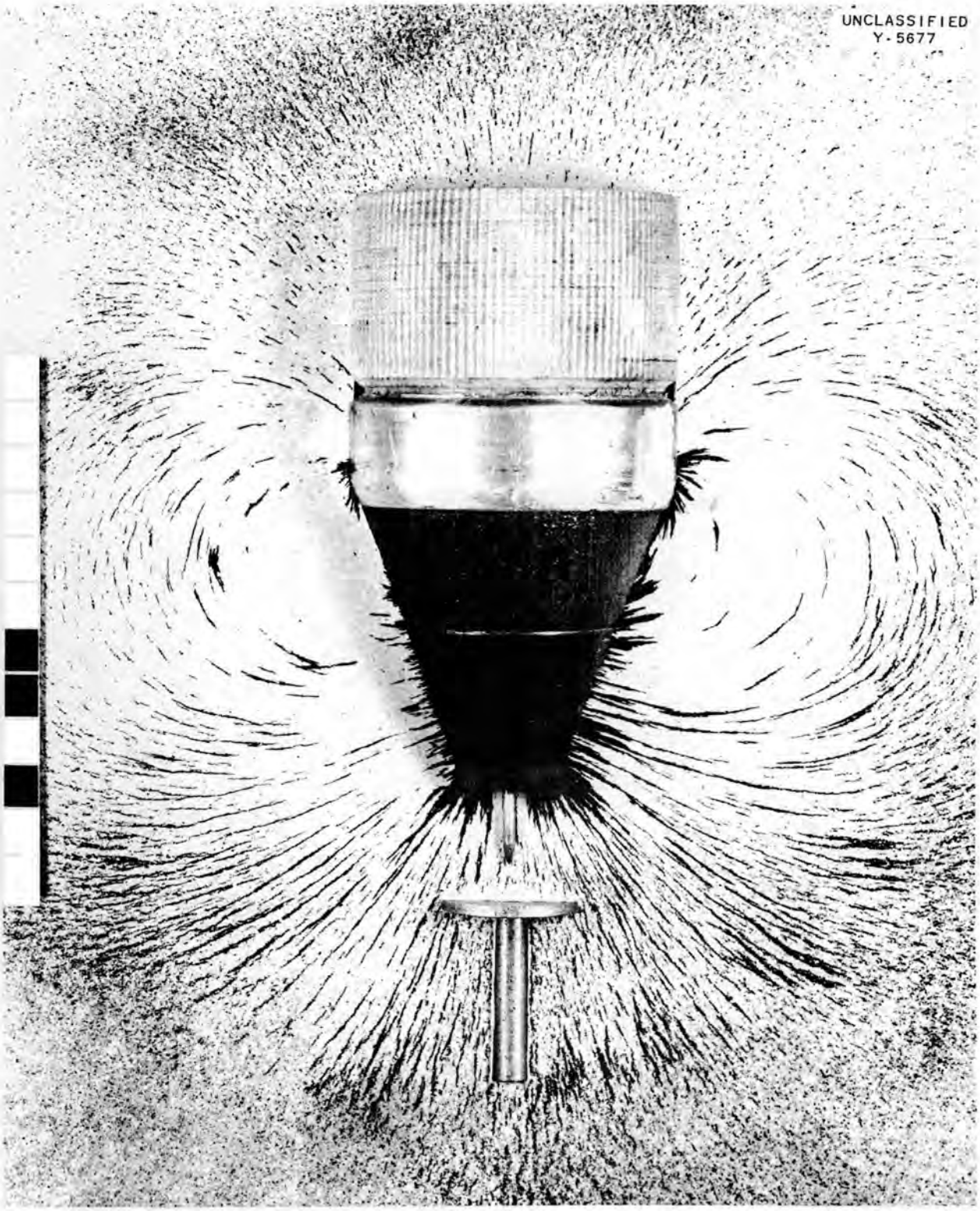

Fig. 102. Iron Filing Pattern of the Magnetic Lines of Flux of a Permanent Alnico Magnet.

On the basis of a few experiments, observations of the effect of arc current have been made. The initial experiments were performed by using header holes without tubing, since it was assumed that the behavior of the arc in the formation of a circumferential molten pool would yield representative information with or without a tube. The header material used was type-304 stainless steel sheet 1/8 in. thick. The holes were 3/16 in. in diameter and spaced 3/8 in. center to center. Welding conditions were:

1. electrode, 1/16 in. dia,
2. electrode to plane of work distance, 0.070 in.,
3. magnetic nozzle (tip of soft iron) to plane of work distance, 0.41 in.,
4. argon flow, 30 cu ft/hr,
5. open circuit voltage, 70,
6. arc voltage, 11,
7. current, variable,
8. time, variable.

Current was varied and the arc permitted to exist for a maximum of 30 sec during the observation period. A minimum current of 48 amp was necessary before significant observations could be made. At currents less than 48 amp, the formation of one, and often two, small but distinct molten pools were noted at equally spaced points on the hole periphery. These pools appeared to be attempting to rotate in a counterclockwise direction around the periphery of the hole. When a current of 48 amp was used two, and sometimes three, distinct pools formed that appeared to rotate around the periphery at a finite rate of approximately one rotation per second after a time interval of about 20 seconds. The pool sizes were observed to grow peripherally and radially until the operation was stopped at 30 seconds. A further increase in current to 56 amp resulted in the formation of two distinct puddles within 15 sec that began to rotate. Growth of the puddles within the next 5 to 10 sec resulted in the formation of a single peripheral pool. It would appear from these observations that the transition time from individual molten pools to a single complete pool increases with increasing current. Experiments with a current of 75 amp resulted in the formation of a single peripheral pool with a transition time of approximately 3 seconds. The use of higher currents and shorter times will be the subject of future work.

As would be expected, the size of the heat-affected zone, as determined by the size of the heat tint surrounding the header hole, diminishes with increasing current and decreasing arc time. The limiting value of permissible hole-to-hole distance will probably be a function of the arc current and time for a given header thickness and hole size. Experiments will be conducted to determine these limiting values, since ANP designs may require as small a hole-to-hole distance as possible to permit the maximum number of heat exchanger tubes per unit area of header sheet.

The experiments have been limited and are inconclusive. It is expected that work during the coming quarter may yield sufficient information to enable a comprehensive study of the quality of cone-arc welded tube-to-header joints as a function of the welding variables.

Brazing. It is quite probable that brazing may be used extensively in the fabrication of the ANP type of heat exchangers, so experiments were made to determine the feasibility of using

this process in the construction of several small assemblies similar to that shown in Fig. 103. The tubes had a 0.100-in. OD with a 0.010-in. wall thickness and the baffle plates were 0.020 in. in thickness. Preliminary work on such assemblies seems to indicate that brazing can be used advantageously in the production of sound joints if proper control of the brazing variables is exercised. Typical important variables are joint fit, joint geometry, degree of base-metal cleanliness, and quality of the furnace atmosphere during the brazing process. Further investigations of the fabrication of these and other types of assemblies will be conducted in future developmental operations.

A relatively long-range research program on the evaluation of various brazing alloys for the high-temperature ANP type of applications is being conducted because of the promising results attained from fabricating assemblies by brazing. A major consideration is the minimum temperature at which the various brazing alloys flow readily; a test for determining this temperature was developed. The test specimen consisted of a moderate amount of brazing alloy placed at one end of a T joint, 6 in. in length. Both legs of the T joint were 0.062-in. Inconel strips, one of which was milled flat on the mating surface to facilitate the production of a tightly fitting joint. The specimens were then heated until the temperature was found at which the brazing alloy was observed to have flowed freely up the total joint length of 6 inches. A series of such tests were conducted for several brazing alloys, and more will be run on other alloys as they are developed.

UNCLASSIFIED
Y-5664

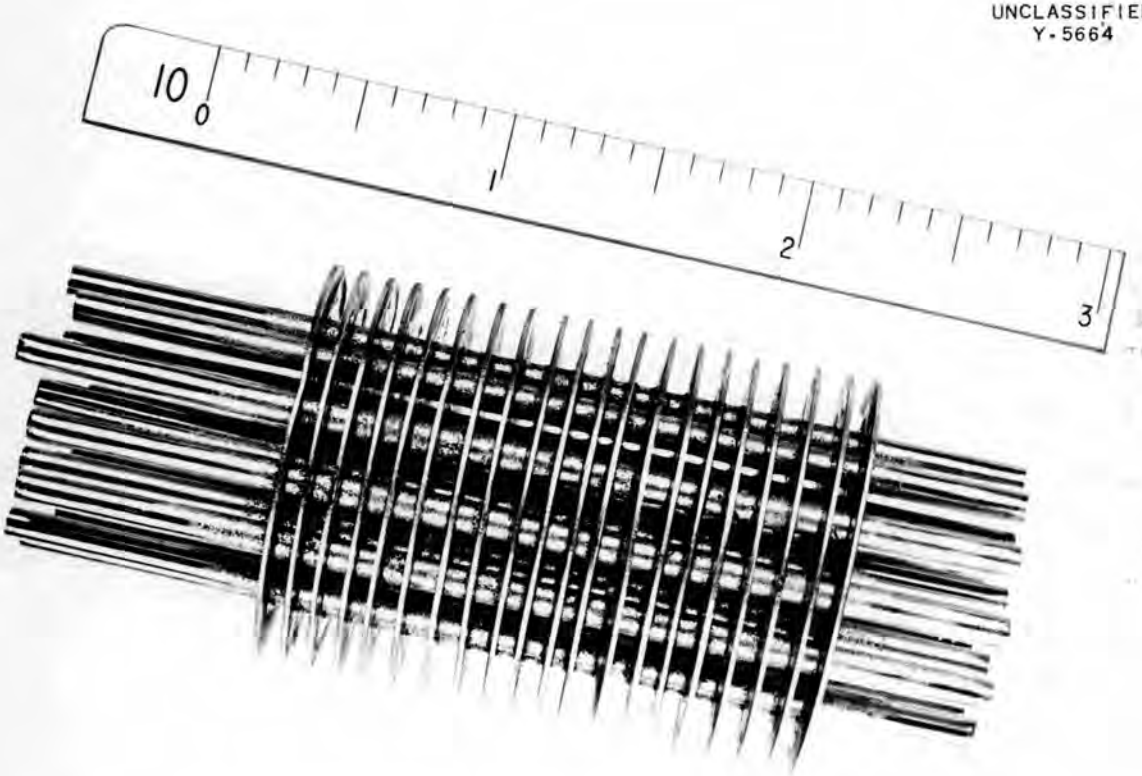

Fig. 103. Typical Heat Exchanger Component Fabricated by Brazing.

It became apparent during the experiments that any tendency towards oxide-scale formation on the metal specimens was highly undesirable. The brazing alloy does not easily wet scaled surfaces; therefore flow around a joint is impeded. Since a very dry, hydrogen atmosphere, with a dew-point in the range of -60°F or below, prevents scaling in most cases, moisture was apparently the prominent factor in scale formation.

A series of experiments proved the hypothesis that if the hydrogen continuously reduces any oxide, with subsequent moisture formation in the hydrogen atmosphere, the exit dew point of the hydrogen should decrease with increasing flow rate. With an inlet gas dew point of -78°F, tests showed that low hydrogen flow rates resulted in exit dew points of only -34°F, but with higher flow rates exit dew points approximating those at the inlet were attained. These experiments were significant because they made it obvious that a relatively large hydrogen flow rate was extremely desirable when furnace brazing.

Resistance to corrosion of the various brazing alloys, alone and in combination with various base metals as in joints, is very important in the selection of suitable joining media; therefore emphasis has been placed on the results of corrosion tests in fluorides and hydroxides. Nicrobraz alloy containing boron is excellent for use in conventional high-temperature applications and was tested extensively. Samples of the pure alloy were subjected to corrosion experiments in fluorides and hydroxides and the baths later chemically analyzed for boron. A photomicrograph of a typical section of one of these samples before being tested in corrosion is shown in Fig. 104.

Figure 105, which is a photomicrograph taken at the surface of a sample of Nicrobraz tested in sodium hydroxide for 100 hr at 1500°F, illustrates the heavy corrosive attack characteristic of this medium. There is a general surface attack and severe local attack, as shown by the large dark area in the center of the photomicrograph. The sample tested in the fluoride mixture No. 14 bath for 100 hr at 1500°F was subjected to moderate pitting in some areas, particularly near the intermetallic components. Other surface areas were relatively untouched. A section of the sample showing areas of both light and heavy pitting is shown in Fig. 106. Results of the chemical analyses on the contents of both the fluoride and hydroxide baths indicate that boron is preferentially leached from the alloy. Further research will be conducted to determine the actual percentage loss of the boron from the alloy.

Preliminary experiments have been conducted on the resistance to corrosion of Nicrobrazed tube-to-header joints with Inconel as the base metal. Sodium hydroxide was severely corrosive to these joints, but the fluoride mixture No. 14 salt had a relatively mild effect. The degree of attack of these two substances is illustrated in Fig. 107. Chemical analyses of the baths and photomicrographs of sections of the corroded joints will be shown in later reports.

Similar tests will be conducted with other high-temperature brazing alloys of current interest, including 60% palladium-40% nickel, 60% manganese-40% nickel, 60% palladium-37% nickel-3% silicon, 16.5% chromium-73.5% nickel-10% silicon, 16.5% chromium-71.5% nickel-10% silicon-2.5% manganese. No data are yet available on the resistance to corrosion of these

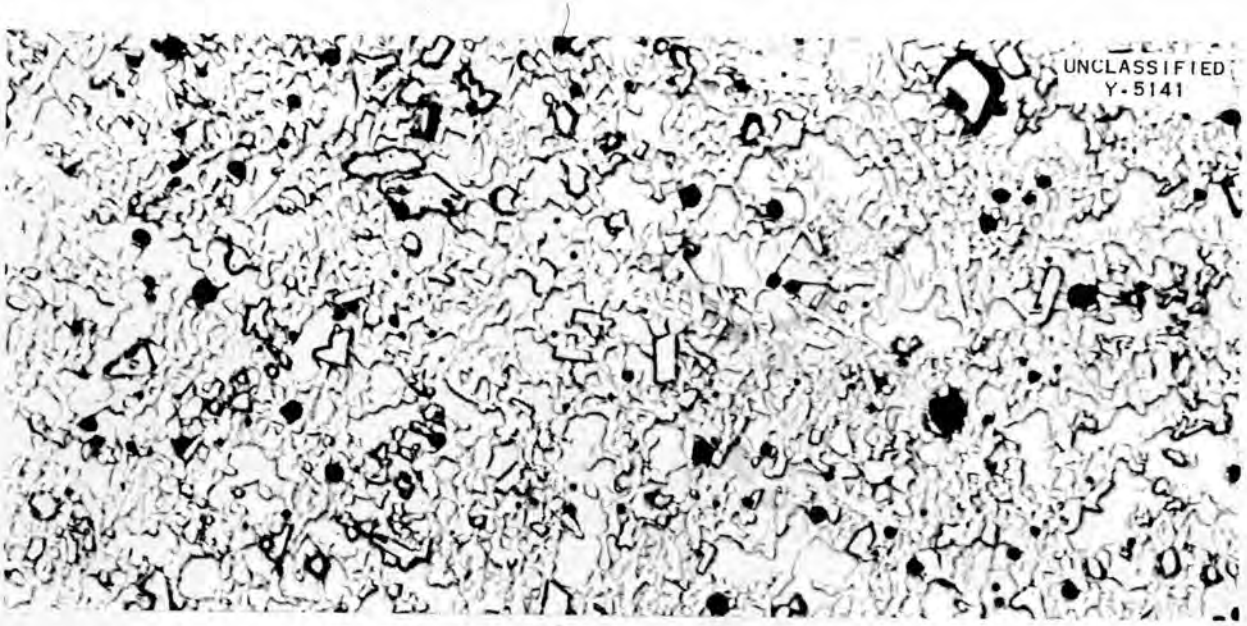

Fig. 104. As-Polished Nicrobrazed Slug Showing Various Intermetallics. 250X.

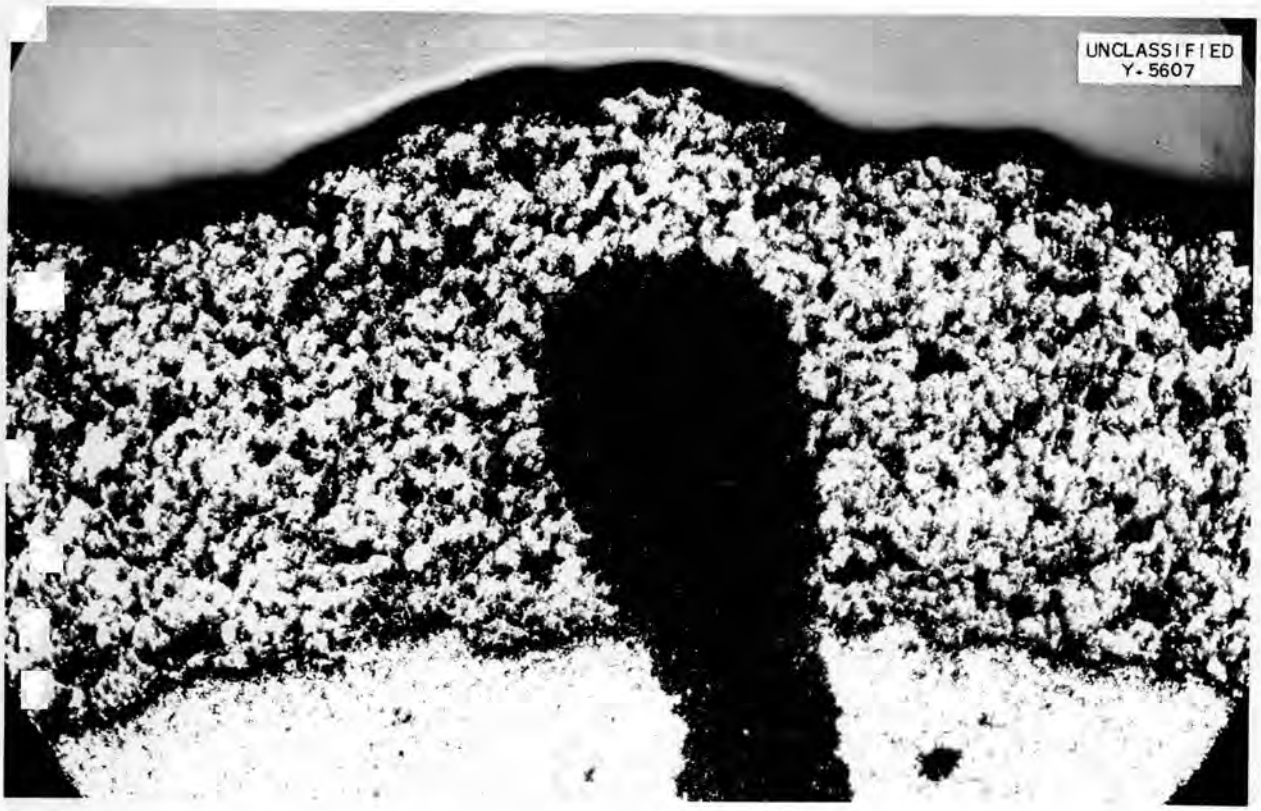

Fig. 105. As-Polished Nicrobrazed Slug After Corrosion Testing in Sodium Hydroxide for 100 hr at 1500°F. Severe corrosion over entire surface plus extremely intense localized attack. 50X.

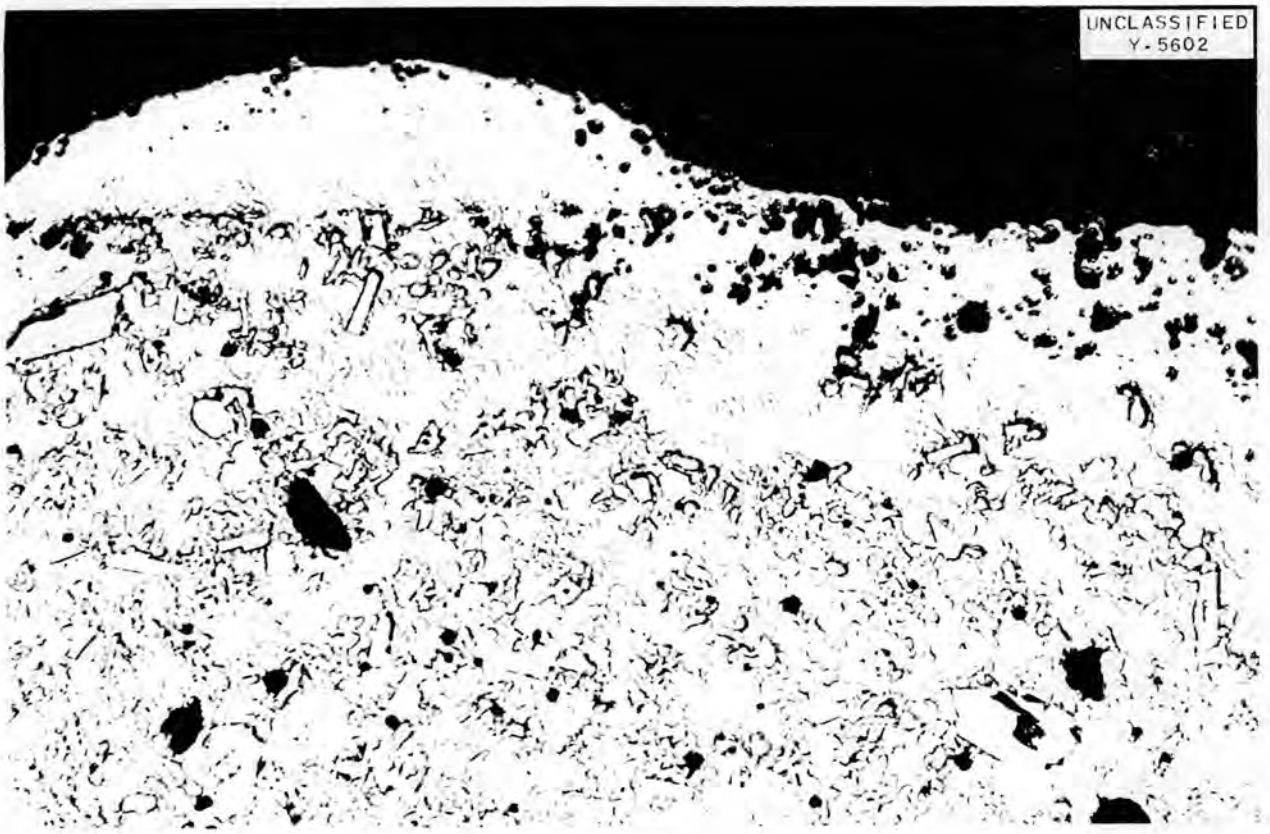

Fig. 106. As-Polished Nicrobrazed Slug After Corrosion Testing in Unpretreated Fluoride Mixture No. 14 for 100 hr at 1500°F. Areas of light and mederate pitting can be seen, with the pitting type of attack apparently concentrated in the areas containing intermetallics. 250X.

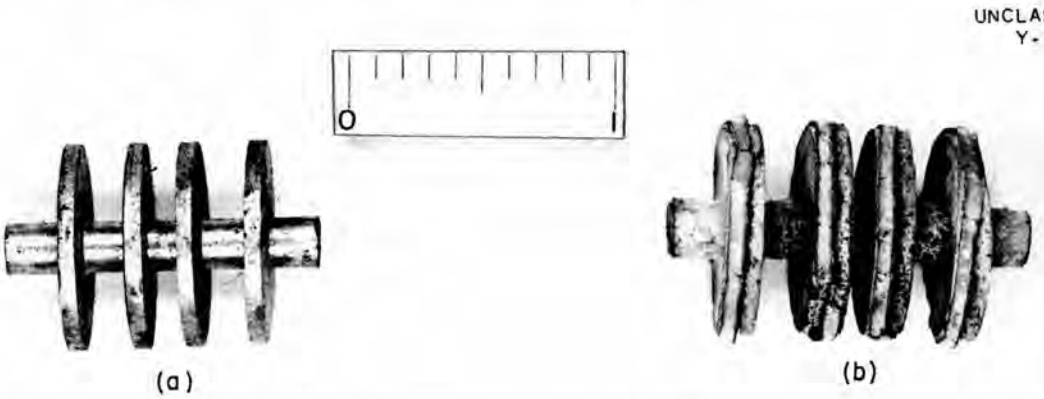

Fig. 107. Nicrobrazed Inconel Tube-To-Header Joints Corrosion Tested for 100 hr at 1500°F. (*a*) Tested in fluoride mixture No. 14. (*b*) Tested in sodium hydroxide. The samples tested in sodium hydroxide were severely corroded at the joint, whereas those tested in the fluoride mixture were much less attacked.

alloys. Methods have been devised for coating the inside of the standard nickel test capsules with brazing alloy so that corrosion resulting from dissimilar metal combinations can be eliminated when testing samples of the pure brazing alloy. When brazed joints are tested for corrosion, a capsule of the same metal as that of the joint base-metal is used to eliminate dissimilar metal combinations.

CERAMICS

S. D. Fulkerson	J. R. Johnson
C. E. Curtis	A. J. Taylor
L. M. Doney	G. D. White

The organization of the new ceramic laboratory is nearly completed. Two of the remaining three openings are filled, and the men are awaiting clearance. Much of the equipment that could be ordered from outside sources has been received and installed. Some heavy equipment will not be on hand until late in 1952, and other equipment that must be designed and built will not be completed before July 1. The laboratory should be essentially complete and operating at full capacity by the end of 1952. A number of projects have been started and some results should be available in the near future. The laboratory will continue to perform necessary service work for other groups.

The primary accomplishments of the past quarter are as follows:

1. Additional personnel have been procured.

2. Laboratory equipment and facilities have been installed.

3. Service work and consultation have been performed.

4. A research program has been developed.

5. Special equipment has been designed and fabricated.

6. Research has been started on diverse projects, including a study of hafnia and the development of coatings.

7. A cooperative program with the Norris Electrotechnical Laboratory of the Bureau of Mines has been established for producing beryllium oxide shapes.

Since so many interests must be served by the laboratory, it was designed to be versatile with respect to equipment and personnel. It is felt that considerable progress has been made toward this end.

A major job of installation of facilities such as water, gas, air, and electricity throughout the laboratory was completed late in this quarter, and thus it has been possible to begin some project work.

Service work and consultation have been carried out to the limit of the ability of the laboratory and personnel. Now that facilities are installed, it is expected that a considerably greater service can be rendered. The making or processing of ceramic shapes, such as crucibles and tubes, and advising in their use was part of the service given by the laboratory. Other work has included petrographic examination of UO_3 for the HRE group and the study of glass coatings for protection of radiators for the ANP group.

After considerable discussion with interested groups and a survey of earlier ceramic work, a program of research has been established which, it is believed, will serve the best interests of ORNL and the AEC. The program is broad in scope and designed to accommodate projects of immediate interest and those with long-range objectives. Considerable emphasis has been placed on the systematic and

reliable measurement of physical properties of ceramic materials of interest.

The laboratory is now equipped with most of the usual standard machines and devices, including fabricating and forming equipment, driers, kilns, and other miscellaneous items. In addition, many highly specialized devices are installed, are in the design stage or being fabricated, or are on order from commercial producers.

A study of hafnia has been started and some experience in fabricating and processing has been gained. A preliminary thermal expansion study is in progress. The melting point of the unpure material has been determined to be of the order of 2750°C. X-ray investigation has shown it to be monoclinic; the β angle is 80° 48'; and the cell dimensions are

$\breve{a}$	0.508
b	0.515
c	0.533

A coating program for stainless steels is well under way. Successful coatings of the type developed by the National Bureau of Standards have been applied to stainless steels for radiators for the ANP project. Some preliminary work has been done in the development of aluminum phosphate glass coatings for protecting steels against fluorides.

HRP METALLURGY

E. C. Miller, Metallurgy Division
F. J. Lambert, Research Engineering, Y-12
A. R. Olsen, Reactor Experimental Engineering Division
W. E. Taylor, Solid States Division

The Metallurgy Division has been asked to coordinate the metallurgical phases of the Homogeneous Reactor Project, with particular reference to the long-range experimental and development effort that will extend beyond the HRE stage. A small group is being formed within the Metallurgy Division to carry out this work, and other groups will participate as necessary. Since the long-range program is in the formative stage, the work of this new group has thus far been largely that of evaluating the problems, planning experimental work, and furnishing day-to-day assistance and recommendations concerning metallurgical problems that arise in connection with the current experimental work of other groups of HRP.

Austenitic stainless steel, particularly type 347, which is being used in the HRE work, is high on the list of potential constructional materials. Investigations are being carried out that will lead to the development of specifications and procedures for fabricating, welding, and relieving stress, if any, of the 18-8 series stainless steels, particularly where heavy sections and difficult joints are involved. In addition to type 347, other stainless steels, such types as 304 ELC, 316, 316 ELC, 329, and the high-chromium 400 series, are being considered. Other alternate materials requiring evaluation include titanium, zirconium, tantalum, and some of the precious metals, such as platinum. Some of these materials, if used, would have to be used sparingly because of both economic and mechanical property considerations. Therefore considerable investigation of methods and feasibility of cladding and lining would be required.

Another requirement is for hard and hardenable materials to be used for valve trim, bearings, and journals; this requirement calls for an investigation of such materials as Stellite and various metal-ceramic combinations.

Metallurgical assistance will be provided to the corrosion section of HRP in the recommendation of materials, the preparation of corrosion test specimens, and the interpretation of results from the metallurgical viewpoint.

The operation of a high-pressure, elevated-temperature engineering system makes stringent demands on materials and their fabrication and requires very rigid inspection procedures. The Y-12 Engineering Department has set up a nondestructive testing group that has carried out radiographic and penetrant inspection on HRE and other experimental components and structures. The long-range work of this type will be conducted by the same group. Their work will be extended to include additional nondestructive testing with ultrasonic and magnetic-induction test procedures.

All reactor construction involves the relatively unknown factor of radiation damage, which affects all structural materials. The Solid State Division is participating in the

metallurgical effort by investigating radiation damage effects on stainless steels and other potential pressure vessel materials. Of particular interest in connection with the pressure vessel materials is the effect of radiation on notched-bar impact, transition temperature.

A great deal of service work has been and is being done, particularly in the metallographic examination of components removed from experimental systems. Several metallographic examinations will be reported in greater detail in the next quarterly report.

The mechanical testing group is setting up a bend test to assist in the evaluation of materials.

The rolling and fabrication group will be actively engaged in the preparation of special alloys as soon as the investigation of titanium is started.

The powder metallurgy group furnishes facilities for heat treatment and has been actively engaged in the development and fabrication of safety plates for the HRE.

The welding group has assisted with the preparation of test specimens and has worked on other fabrication problems.

The ceramics group will be called on to prepare coated specimens and metal-ceramics for test purposes.

HRE CONTROL ROD

E. S. Bomar J. H. Coobs

The active portion of the HRE control rod is a mixture of approximately 35 wt % boron carbide and 65 wt % aluminum, called Boral. This core material is clad with type-347 stainless steel. The fabrication group was asked to determine a schedule of assembly that would result in a continuous stainless steel cladding and a metallurgical bond at the Boral-stainless steel interface.

The preliminary experimental work was done on samples measuring about 1 1/2 in. on a side, which were prepared in the following manner: Pressed Boral cores of -100, +200 mesh boron carbide and -100 mesh atomized aluminum were consolidated by using pressures of 50 tons per square inch. These cores were placed in picture frames, divided into three groups, and given various treatments.

Group 1. Type-302 stainless steel powder was sintered at 1150°C to inside surface of cladding.

Group 2. Copper powder was sintered at 1020°C to inside surface of cladding.

Group 3 (plain, bright-annealed cladding). The cladding and picture frames were spot welded to hold them together, heliarc welded around the edges, and given the treatment listed in Table 24.

Samples were taken from each group for metallographic examination, thermal cycling, and autoclave tests.

Metallographic examination indicated that the Boral and cladding were well bonded in all groups. No core-to-cladding reaction zone was evident in the samples rolled at 500°C. Samples reduced entirely at 600°C did show a region of interaction between the Boral and stainless steel. Bonding of cladding to picture frame occurred with the group containing the copper layer.

Thermal cycling had no observable effect on any of the three groups.

TABLE 24

Treatment of Pressed Boral Cores

GROUP	ROLLING TEMPERATURE (°C)	TOTAL REDUCTION (%)
1	600	32.5
1	600, 1 pass 500, 2 passes	31
2	600	35
2	600, 1 pass 500, 2 passes	34
3	600	33
3	600, 1 pass 500, 2 passes	37

Figure 108 shows the Boral-stainless steel interface of a group 3 sample after 25 cycles between room temperature and 500°F.

The results of the autoclave tests were not available at the time this report was written.

Very little extrusion of the aluminum between cladding and picture frame occurred in any of the samples and the core reduced at nearly the same rate as the cladding.

Based on the results of the above tests, it would seem possible to fabricate the required control plates by using stainless steel with a sintered coating of copper powder. The bond obtained at the cladding-picture

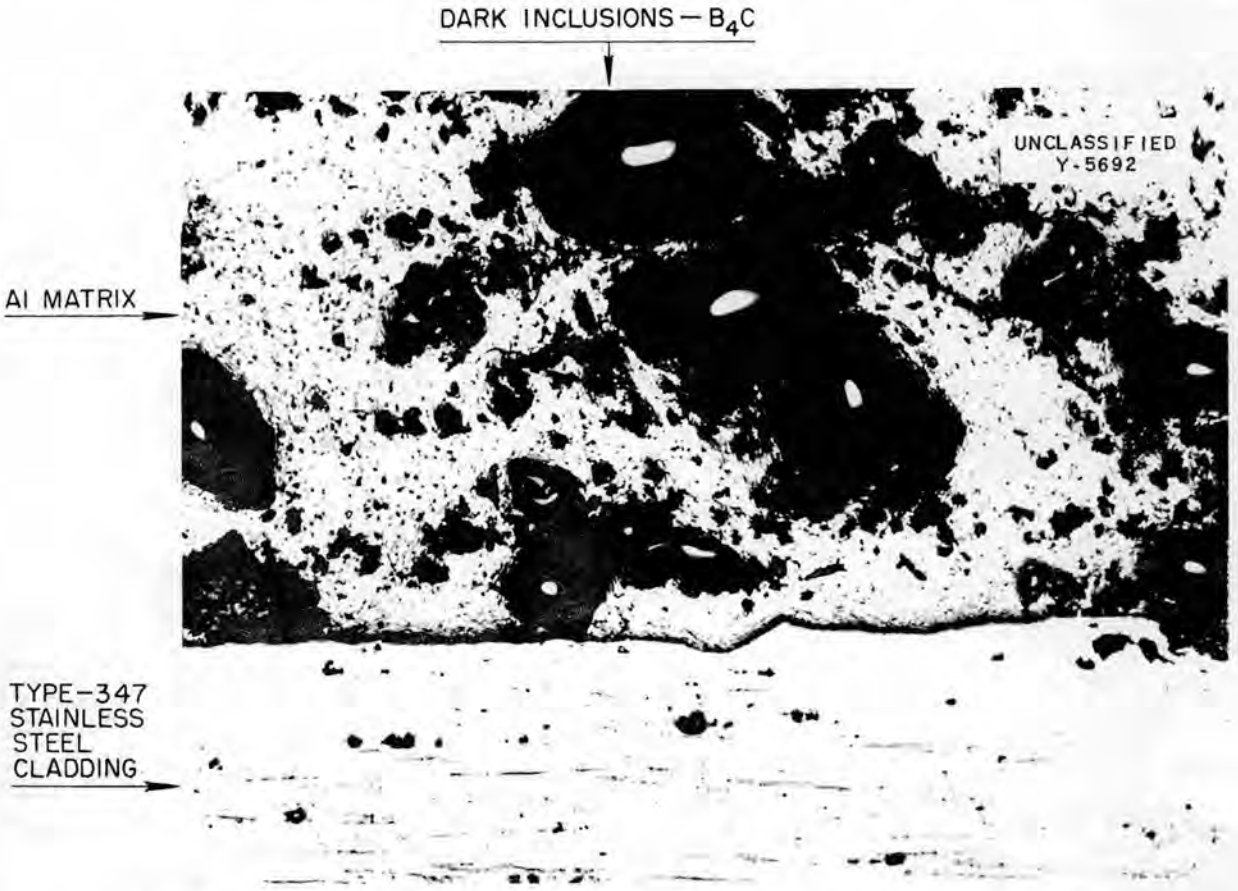

Fig. 108. Boral-Stainless Steel Interface of Thermally Cycled Sample. 250X.

frame interface would permit shearing off excess edge stock, submerging all but an edge of the plate in water for cooling, and sealing the edge with a heliarc weld. In this way the stainless steel stock at the edge of the Boral might be held close to the maximum of 1/8 in. desired without melting the aluminum in the core.

Dilution of the stainless steel with copper would be very small, approximately 2 to 3%. Copper is added to the stainless steel, in some grades, in higher percentages than this to improve corrosion resistance to solutions that reduce rather than oxidize.

A clad plate that is intermediate in size between that of the samples used for this investigation and the full scale size is now being fabricated. Its properties should prove or disprove the conclusions based on the above series of tests.

X-RAY LABORATORY

B. S. Borie, Jr. R. M. Steele

LOW-TEMPERATURE X-RAY DIFFRACTION

The low-temperature-specimen holder for use with the North American Philips high-angle spectrometer has been completed and is now in use. A photograph of the specimen holder disassembled is shown in Fig. 109. It is shown assembled and mounted on the spectrometer in Fig. 110.

The apparatus consists of a liquid nitrogen containing tank on which a specimen properly oriented for spectrometer focusing is mounted. The tank and specimen are contained within an outer shell, which has a beryllium window for the transmission of x rays. The outer shell is evacuated through a tube that is concentric with the spectrometer axis. Evacuation is intended to prevent ice formation on the specimen and to minimize convection losses to the nitrogen reservoir. Temperature control is accomplished by a small heater built into the base of the specimen mount. It has been found that some degree of temperature control may be obtained by adjusting the vacuum and thus changing the convection losses of the specimen.

The specimen temperature is measured by a copper-constantan thermocouple. Kovar seals are used to take the thermocouple leads through the outer vacuum-tight shell. They are shown in Fig. 109 on the left of the shell. The terminals to the right are used for the heater leads and other accessory equipment. The connector shown at the right in Fig. 109 screws onto the end of the tube that extends through to the back of the spectrometer. It accommodates a lead to the vacuum pump, a leak valve, and a G-E thermocouple vacuum gage.

The apparatus has been used to investigate the possibility of a low-temperature transformation in thorium similar to that reported for cerium.[1] In cerium the transformation involves no change in crystal structure but there is a sudden change in the lattice constant. To date, no transformation of this type has been observed in thorium. Further experiments are planned in which heavily cold-worked thorium will be used.

TABLE 25

Lattice Constants of Ammonium Bromide as a Function of Temperature

TEMPERATURE (°C)	a (Å)	c (Å)	c/a
21	4.052 (cubic)		
-100	5.711	4.054	0.7099
-124	5.703	4.048	0.7098
-144	5.695	4.043	0.7099

The low-temperature-specimen holder has been used in measuring the lattice constants of the tetragonal phase of ammonium bromide, which is of interest to the neutron-diffraction group of the Chemistry Division. The tetragonal phase is reported to occur at temperatures below -70°C. The results of the measurements are given in Table 25. Similar measurements on a deuterized sample of ammonium bromide are planned.

[1] A. F. Schuch and J. H. Sturdivant, "The Structure of Cerium at the Temperature of Liquid Air," *J. Chem. Phys.* **18**, 145 (1950).

UNCLASSIFIED
Y-5593

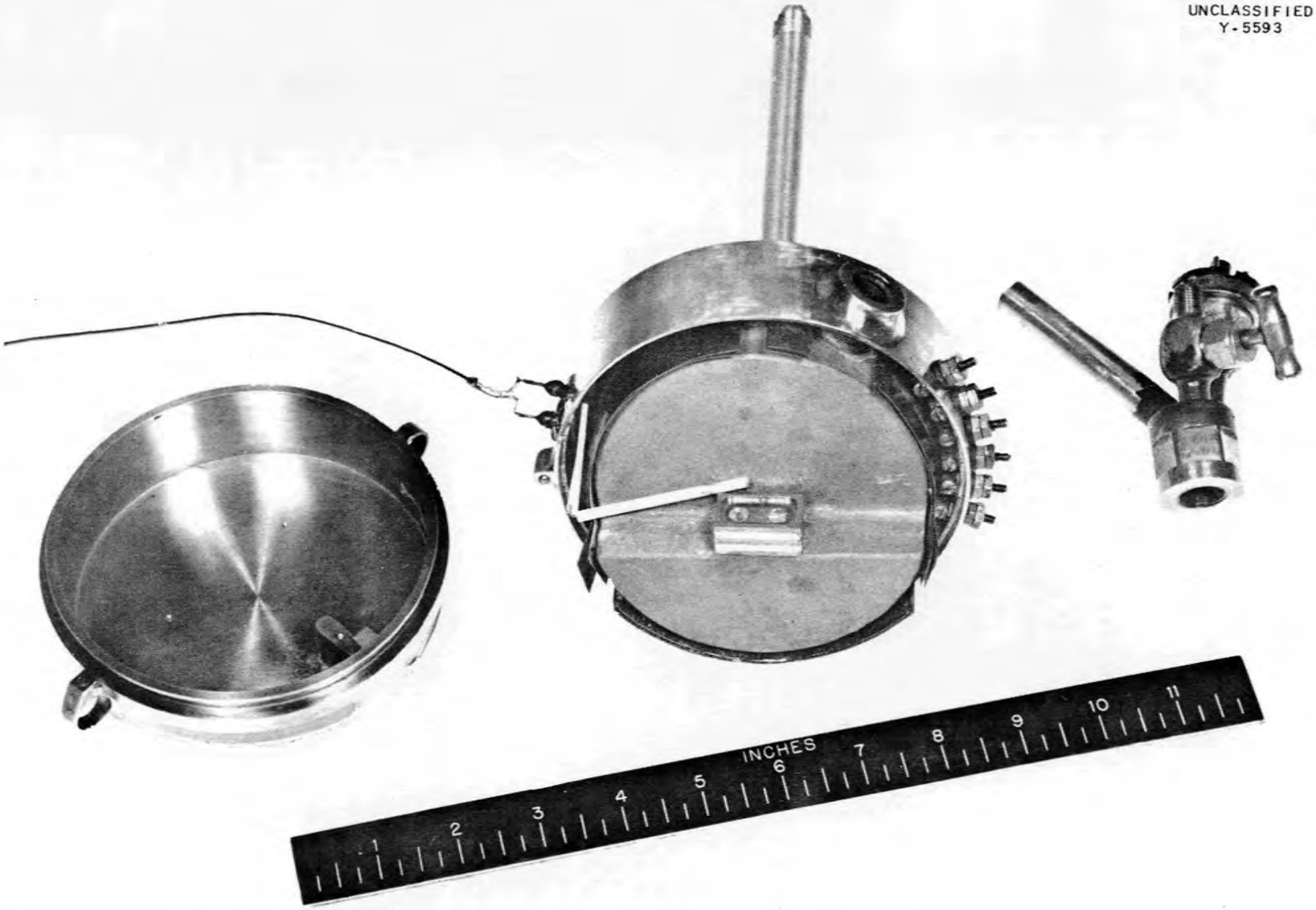

Fig. 109. Low-Temperature Specimen Holder for High-Angle X-Ray Spectrometer.

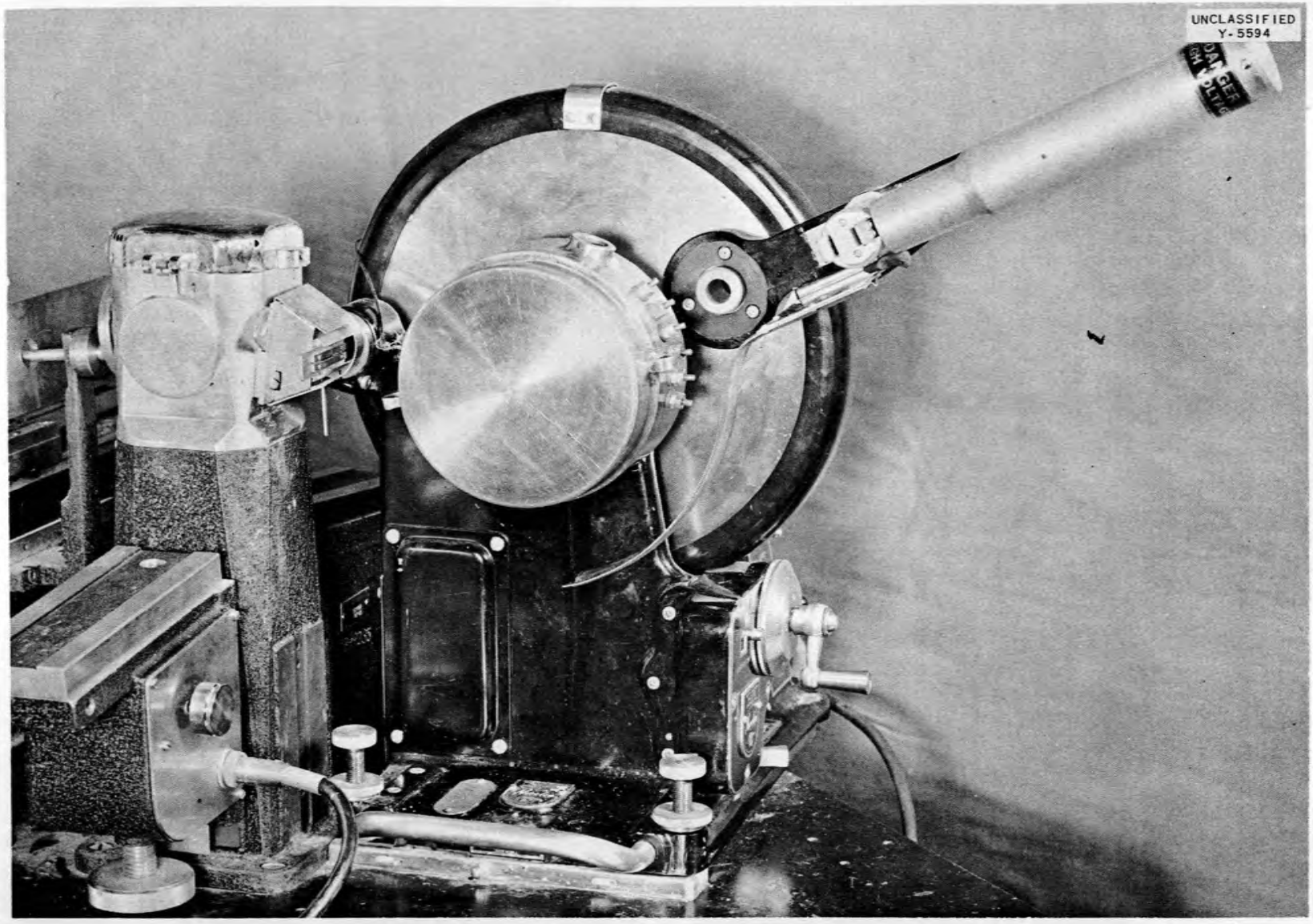

Fig. 110. Low-Temperature Specimen Holder in Place on X-Ray Spectrometer.

SERVICE WORK

During this quarter 156 diffraction patterns were measured by the x-ray laboratory for other research groups. Although this is less than the total number of specimens submitted to the x-ray laboratory in most previous quarters, a larger fraction of the problems have involved more than routine powder techniques.

The distribution of the service work has also changed during the past quarter. Previously, approximately two-thirds of the samples were from Metallurgy Division sources. During this quarter over one-half the work has come from research groups outside the division – about one-half of the problems were from the Chemistry and Physics Division, and a small number of patterns were taken for the Solid State Division.

A large number of identification problems concerned with the corrosion products occurring in hydroxide convection loops have been submitted by groups both inside and outside the Division. These specimens are usually in the form of a few small single crystals and identification requires the use of the Weissenberg camera or the precession camera.

A series of samples of $Nd(C_2H_5SO_4)_3 \cdot 9H_2O$ was submitted for composition checks by L. D. Roberts of the Physics Division. Since most of the samples were prepared with enriched neodymium isotopes, only small quantities were available and it was necessary to use single-crystal techniques for the composition checks.

An interesting specimen of a copper-beryllium alloy (5.23 wt % Be) has been studied for W. E. Taylor of the Solid State Division. The sample was a small, single crystal that had been quenched from the beta field to the alpha plus gamma field. Although the specimen was predominantly beta copper-beryllium alloy, the alpha and gamma phases were observed. The alpha phase was polycrystalline, but it had a high degree of preferred orientation. A cubic structure, $a_0 \simeq 9.1$Å, was also observed. The cube faces were parallel to those of the beta phase. Several other unindexed reflections were observed. All of the spots were quite broad and diffuse and indicated a high degree of strain in the sample. It is hoped that a careful examination of the photograph may indicate the nature of the beta decomposition.

METALLOGRAPHY LABORATORY

R. J. Gray R. S. Crouse
T. K. Roche

METALLOGRAPHY OF ZIRCONIUM AND ITS ALLOYS

The metallography laboratory completed its part of a joint AEC-installation program on the investigation of zirconium and its alloys.

A consumable-electrode method of preparing the zirconium-tungsten alloy was not successful because of insufficient melting of the tungsten-wire addition. Nonconsumable-electrode melting with the addition of tungsten powder in an argon atmosphere was more successful; however, some undissolved powder was evident in two master melts of 4.91 and 5.72 wt % tungsten.

A 1.01 wt % tungsten alloy was made by using sections of the 4.91 wt % tungsten alloy for further dilution. Homogeneity was good after repeated sectioning and remelting. A blank melt and three alloys of 1.01, 4.91, and 5.72 wt % tungsten additions were analyzed for O_2, N, and H_2, as shown in Table 26.

Heat treatments were made of the blank melt and the three tungsten alloys. Diamond pyramid hardness values were obtained in the as-cast condition and after heat treatment; hardness increased rapidly with increasing tungsten addition (Table 27).

Specimens were electrolytically polished in an electrolyte of 1 part perchloric acid and 10 parts glacial acetic acid. An etch was devised to show the structure of the 1.01 wt % tungsten alloy, and it was examined at 1000X. The etch was 5% HF, 10% HNO_3, and 85% glycerol.

The structure appeared to be very close to the eutectoid composition of alpha zirconium and ZrW_2. Some primary ZrW_2 was evident in a very irregular shape in the as-cast specimen (Fig. 111) and also in a specimen heated at 800°C for 1 hr (Fig. 112). The specimen heated at 900°C and slowly cooled apparently had a small segregated area that was lower in tungsten and resulted in a hypoeutectoid composition.

TABLE 26

Analyses of a Blank Melt and Three Alloys of Tungsten

	ANALYSES (wt %)			
	W	O_2	N	H_2
One-in. crystal-bar		0.009 ± 0.003	**	**
Zr, as cast		0.025 ± 0.003		
Zr + W (1% nominal)*	1.01 (0.50 at. %)	0.060		0.016
Zr + W (4% nominal)*	4.91 (2.49 at. %)	0.015 ± 0.002	**	**
Zr + W (11% nominal)*	5.72 (2.92 at. %)	0.040 ± 0.004	**	**

*Nonconsumable electrode, repeated melting.

**None detected.

Some alpha zirconium patches were present with the eutectoid (Figs. 113 and 114). The major part of the specimen had a eutectoid structure. A specimen heated at 900°C and water quenched had scattered patches, which might be small amounts of eutectoid that developed on the rapid quench. The matrix could be alpha zirconium and ZrW_2 produced by decomposition of the beta phase (Fig. 115).

A homogenization treatment of 990°C for 4 1/2 hr and cooling to 800°C for 1 hr followed by a water quench showed only a eutectoid structure (Fig. 116).

The 4.91 and the 5.72 wt % tungsten alloys were electrolytically polished and examined at a lower magnification (250X) in the unetched condition. A primary precipitate was present in a veining pattern at grain boundaries (Figs. 117 through 125).

Some acicular structure present in the 4.91 wt % tungsten alloy was identified as the eutectoid composition.

X-ray identification showed all the samples to be alpha zirconium and ZrW_2.

REMOTELY CONTROLLED POLISHING UNIT

It was requested that the metallography section assist S. E. Dismuke and M. J. Feldman of the Solid State Division and A. E. Zulliger of the Engineering Division in the development of a remotely controlled polishing unit. This unit was to be for polishing metallographic specimens with radiation levels too high for the usual manual technique.

It was decided that the best approach would be to purchase a commercial polishing machine and remodel it for specimen polishing so that the specimens could be held and moved over a polishing wheel by some mechanical device.

A polishing unit obtained from Buehler, Ltd., was covered by a stainless steel plate. An aluminum rotator, with a diameter about the same as the

TABLE 27

Hardness Values* of a Blank Melt and Three Alloys of Tungsten

Nonconsumable-electrode method

HEAT TREATMENT	DIAMOND PYRAMID HARDNESS (10 kg load)			
	BLANK	1.01 % W	4.91 % W	5.72 % W
As cast	60 to 68	213 to 221	317 to 336	437 to 455
800°C for 1 hr, slowly cooled	59 to 61	199 to 206	249 to 253	264 to 276
900°C for 1 hr, slowly cooled	52 to 61	173 to 176	129 to 134	133 to 146
900°C for 1 hr, water quenched	78 to 90	216 to 221	139 to 146	199 to 207

*Hardness of as-received crystal-bar zirconium = 48 to 53.

radius of the polishing wheel, was provided that held four specimens and rotated on a bearing on the steel plate. The four hollow cylinders, with screw cap covers, contained lead shot to obtain a desired weight variation. A permanent magnet was located at the base of each cylinder to hold the plastic mount, which was molded with a steel washer on the side opposite the specimen (Fig. 126).

Since the materials to be examined might vary from hard and abrasion resistant to soft and susceptible to development of a cold-worked surface, it was decided that the abrasive should be capable of handling any such materials. The abrasive also should be a type that could be added easily to the polishing wheel, since the polishing unit holding the wheel would be positioned in a hot cell.

Diamond paste, available as a commercial product, was found to be the best abrasive to meet these requirements. A desirable feature of the diamond paste was the wide range of particle size, and an applicator gun with replaceable cartridges (Fig. 127) was available for use with the paste. The applicator gun could be secured outside the hot cell so that it was convenient for an operator to use, and a stainless steel capillary tube could carry the abrasive to the polishing wheel. Also, cartridge replacements could be made when necessary from outside the cell.

A liquid thinner, necessary for cooling and lubricating the specimen during polishing, could be added in drop amounts by a capillary tube from outside the cell.

It was considered possible to accomplish the necessary polishing step by using three units. For the trial runs, one polishing unit was used with two lead-tin polishing laps and one cloth wheel.

Four specimens were first run on a lead-tin lap with a 600 mesh (20 to 40μ) diamond particle size. The lap was removed, the polishing unit cleaned, and a second lap was used with a 60,000 mesh (0 to 1μ) diamond particle size. A third step followed in which a cloth-covered wheel and the finer diamond paste was used.

Six trial specimens were polished with only about 100 ml of liquid and abrasive accumulated from the drain. This was another notable feature, since there is a waste disposal problem when polishing hot samples.

Using only one unit, it was possible that the cleaning operations were not sufficiently thorough to prevent some contamination of the final polish. This would not happen with the three units and even better results could be expected than with the trial method.

An Inconel specimen was polished to show evidence of rounding the specimen when making edge examinations (Fig. 128). A stainless steel specimen subjected to a corrosion test was also examined for edge preservation and revelation of the type of corrosion (Fig. 129). An Inconel tube brazed to copper was polished to show polishing results on various compositions in close contact (Fig. 130). A mild steel specimen showed the ability of this polishing method to retain inclusion (Fig. 131). A tungsten specimen that was difficult to polish by manual methods showed clear structure delineation (Fig. 132). A molybdenum specimen coated with a $MoSi_2$ layer was polished with no evidence of cold-worked metal (Fig. 133). A molybdenum specimen usually requires an electrolytic polish for best results.

The specimens described were prepared completely by the proposed polishing methods. No wear was apparent on the laps or cloth. Etching was done by the usual manual methods.

As shown by the illustrations, with reasonable care the proposed polishing procedures will prepare specimens of quality comparable to those prepared manually for metallographic examination.

Some changes were made to the polishing unit, and some suggestions have been made for improving the functioning of the proposed apparatus. The changes and suggestions are as follows:

1. An "oilite" bearing was machined and pressed onto the stainless steel plate. This bearing was made with a 1/16-in. shoulder on the inside to reduce contamination of the polishing wheel. The other bearing surface was made of cast iron and secured to the aluminum rotator. These bearing changes were necessary because of scoring of the original two surfaces—aluminum vs. stainless steel.

2. The cylindrical weights were reduced in diameter by 0.005 in. to allow more freedom for them to turn in the rotator. A close fit and the presence of some abrasive working in between the two surfaces did not allow the weights and specimen mount to turn as desired.

3. An additional device should be provided for rotating the weight and specimen. A possibility would be to provide an arm on the polishing machine to reproduce about 1/4 turn with each rotation of the rotator.

4. Another line should run to each machine to carry carbon tetrachloride, or a similar solvent, to wash the polishing wheel when necessary.

5. Since the motor in the unit becomes quite hot after a long running time, it should be cooled by an air jet, a fan, or some other device.

6. Specimens should be washed in some manner between polishing steps with different size abrasives and prior to etching. This could be accomplished with one, small, vapor-degreasing unit; the specimen would be washed by the condensate.

Fig. 111. As-Cast Zirconium-Tungsten Alloy. Bright field. Original magnification, reduced 22%.

Fig. 112. Zirconium-Tungsten Alloy Heated at 800°C for 1 hr and Slowly Cooled. Bright field. Original magnification 1000X. reduced 22%.

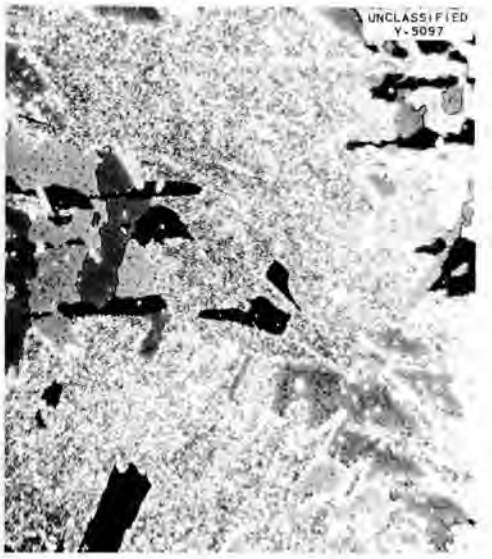

Fig. 113. Zirconium-Tungsten Alloy Heated at 900°C for 1 hr and Slowly Cooled. Segregated section of hypoeutectoid composition showing alpha zirconium and a eutectoid of alpha zirconium and ZrW_2. Polarized light. Original magnification 1000X, reduced 38%.

Fig. 114. Section Shown in Fig. 113. Bright field. Original magnification 1000X, reduced 22%.

Fig. 115. Zirconium-Tungsten Alloy Heated at 900°C for 1 hr and Slowly Cooled. Bright field. Original magnification 1000X, reduced 21%.

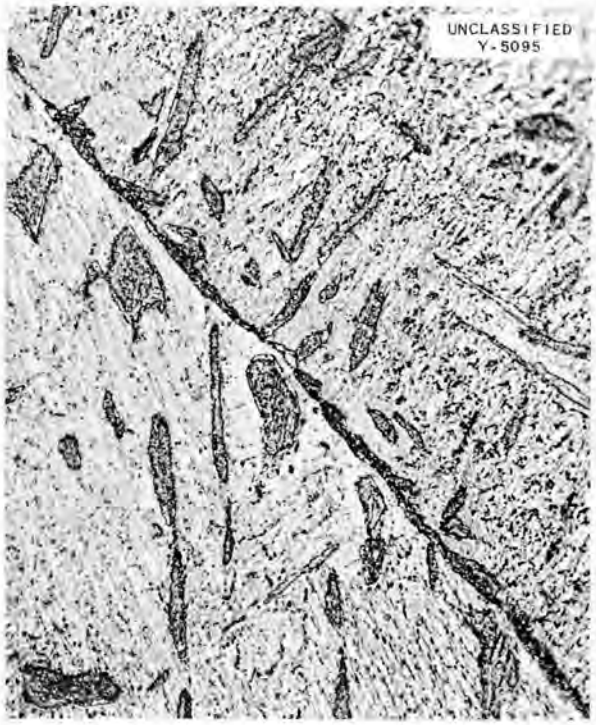

Fig. 116. Zirconium-Tungsten Alloy Heated at 900°C for 1 hr and Water Quenched. Bright field. Original magnification 1000X, reduced 21%.

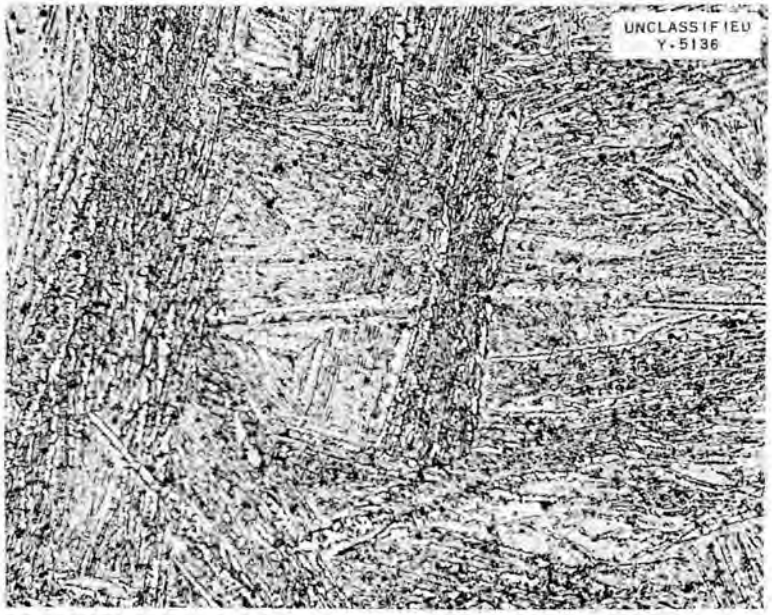

Fig. 117. Zirconium-Tungsten Alloy Heated at 990°C for 4 1/2 hr, Slowly Cooled for 1 hr, and Water Quenched. Bright field. Original magnification 1000X, reduced 21%.

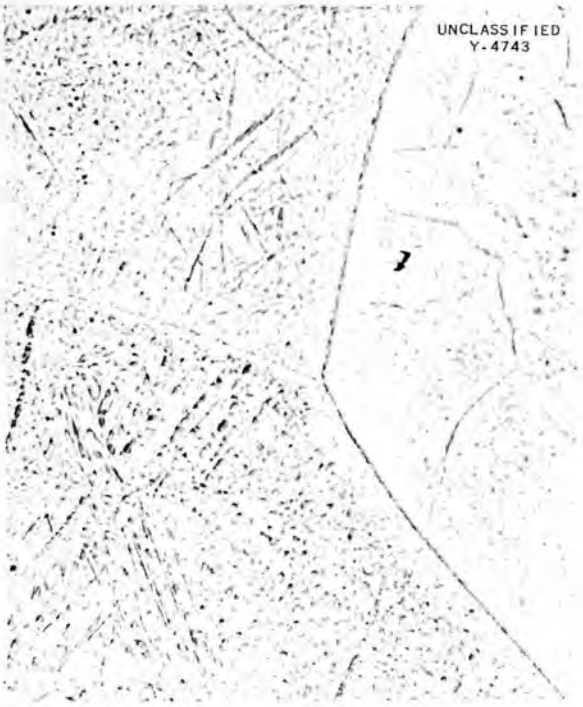

Fig. 118. As-Cast Zirconium-Tungsten Alloy (4.91 wt % W). Bright field. Original magnification 250X, reduced 24%.

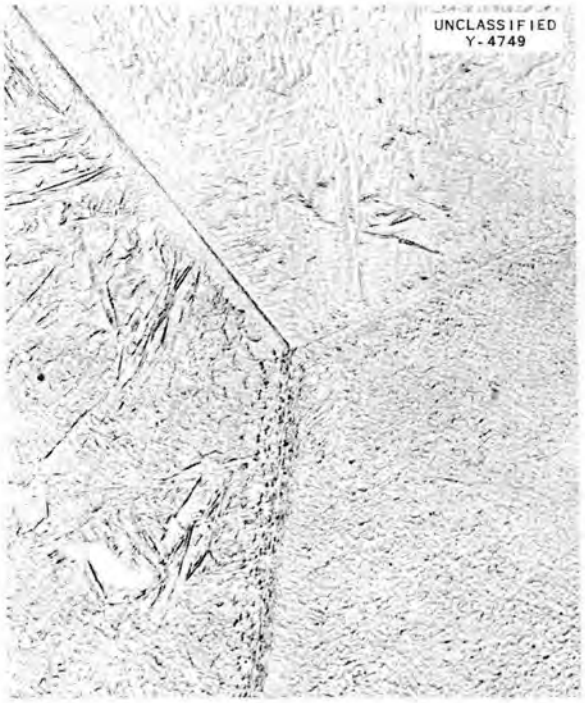

Fig. 119. Zirconium-Tungsten Alloy (4.91 wt %W) Heated at 800°C for 1 hr and Slowly Cooled. Bright field. Original magnification 250X, reduced 24%.

Fig. 120. Zirconium-Tungsten Alloy (4.91 wt % W) Heated at 900°C for 1 hr and Slowly Cooled. Bright field. Original magnification 250X, reduced 24%.

Fig. 121. Zirconium-Tungsten Alloy (4.91 wt % W) Heated at 900°C for 1 hr and Water Quenched. Bright field. Original magnification 250X, reduced 24%.

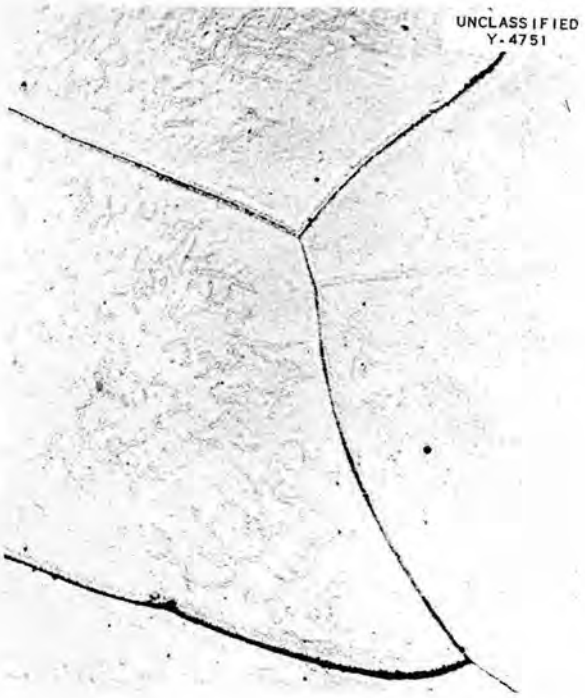

Fig. 122. As-Cast Zirconium-Tungsten Alloy (5.72 wt % W). Bright field. Original magnification 250X, reduced 24%.

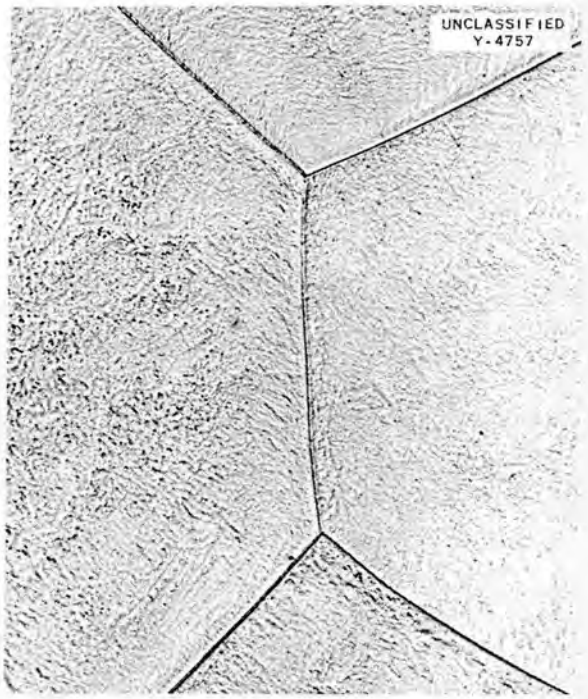

Fig. 123. Zirconium-Tungsten Alloy (5.72 wt % W) Heated at 800°C for 1 hr and Slowly Cooled. Bright field. Original magnification 250X, reduced 24%.

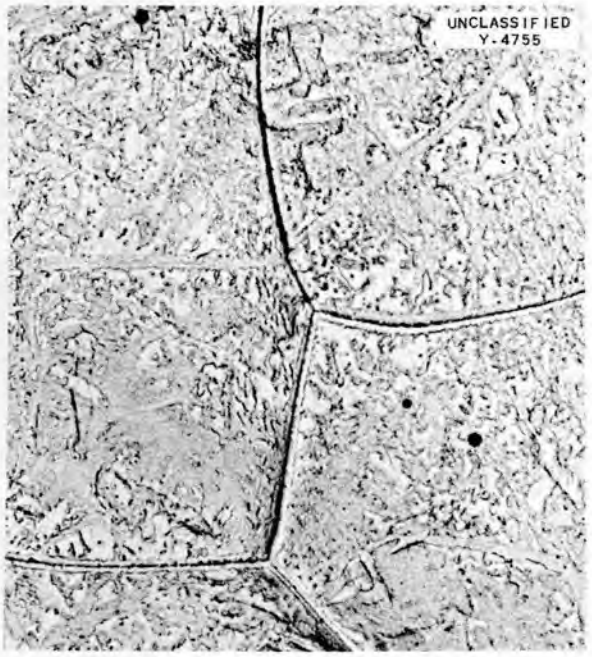

Fig. 124. Zirconium-Tungsten Alloy (5.72 wt % W) Heated at 900°C for 1 hr and Slowly Cooled. Bright field. Original magnification 250X, reduced 24%.

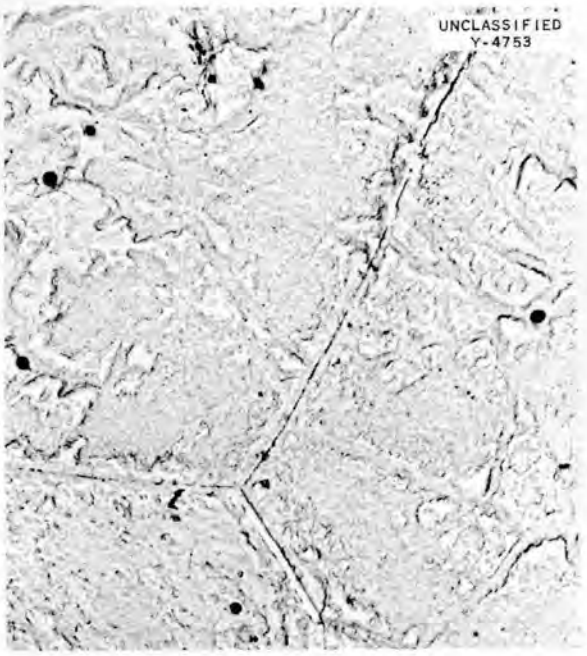

Fig. 125. Zirconium-Tungsten Alloy (5.72 wt % W) Heated at 900°C for 1 hr and Water Quenched. Bright field. Original magnification 250X, reduced 24%.

UNCLASSIFIED
Y-4878

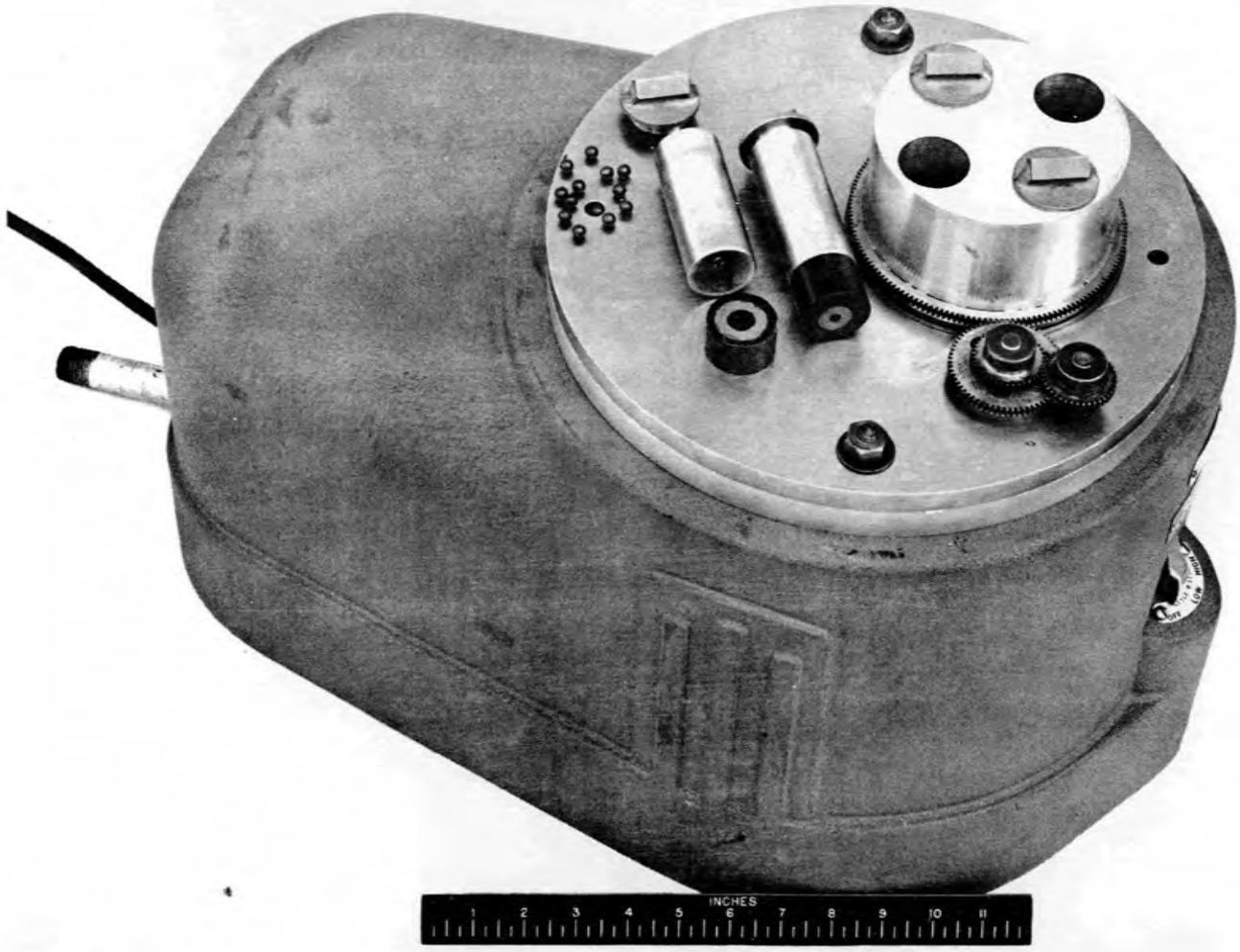

Fig. 126. Polishing Unit with Rotator for Holding Four Specimens; Specimen Mount with Steel Washer; Lead Shot for Weight Variation.

Fig. 127. Thinner, Applicator Gun, and Refill Cartridge.

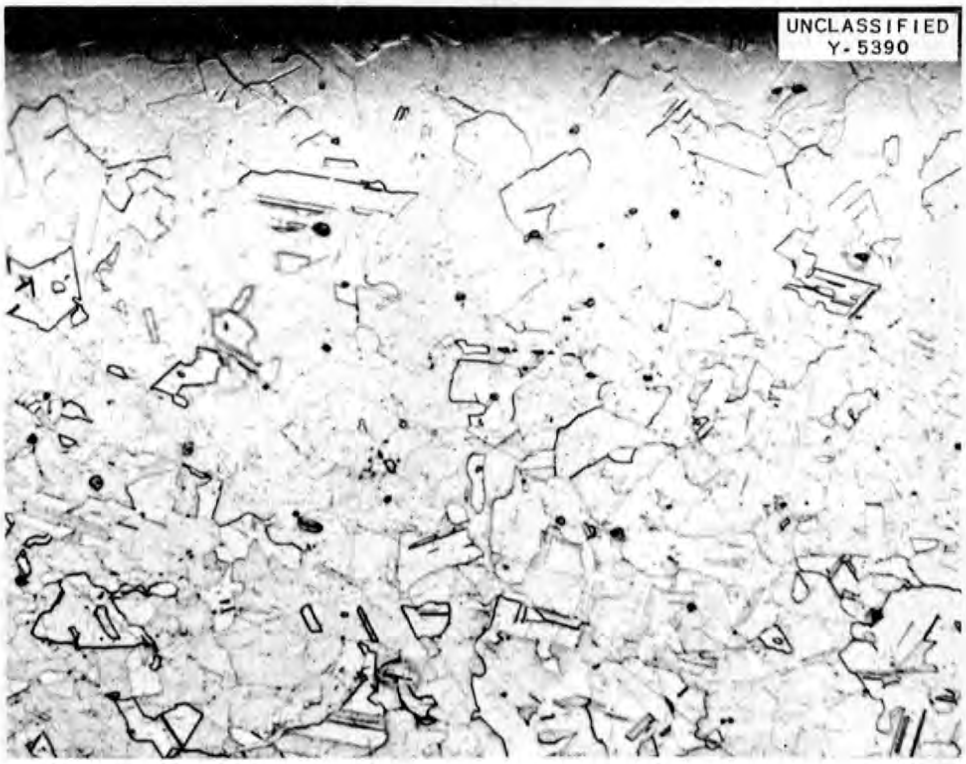

Fig. 128. Inconel. Edge shown at top. Aqua regia and glycerin etch. 250X.

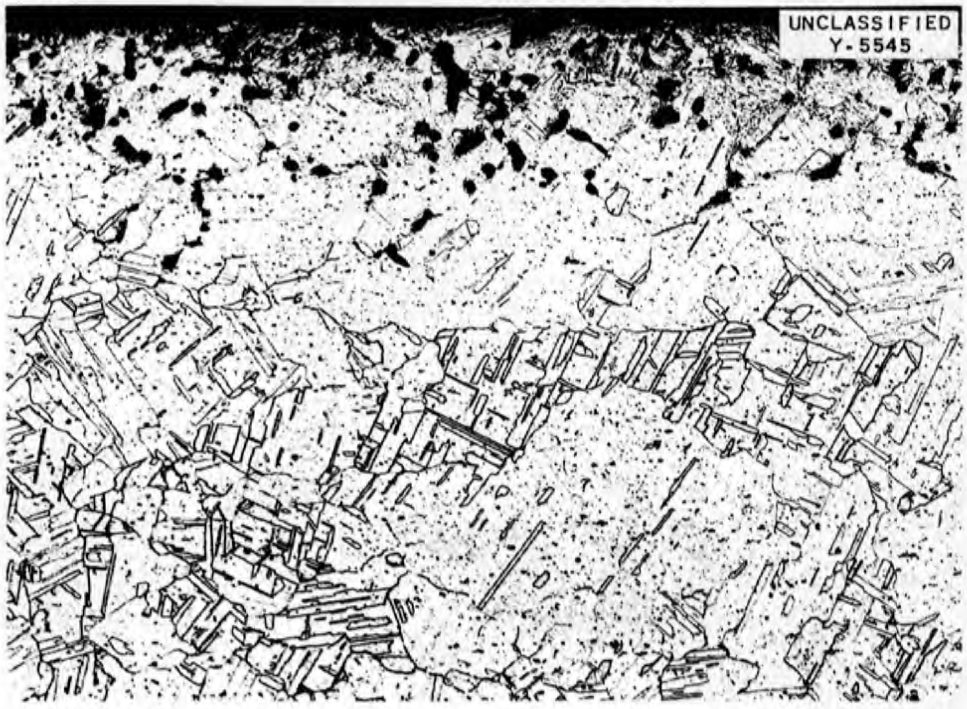

Fig. 129. Type-347 Stainless Steel After Corrosion Test. Exposed surface shown at top. Aqua regia and glycerin etch. 100X.

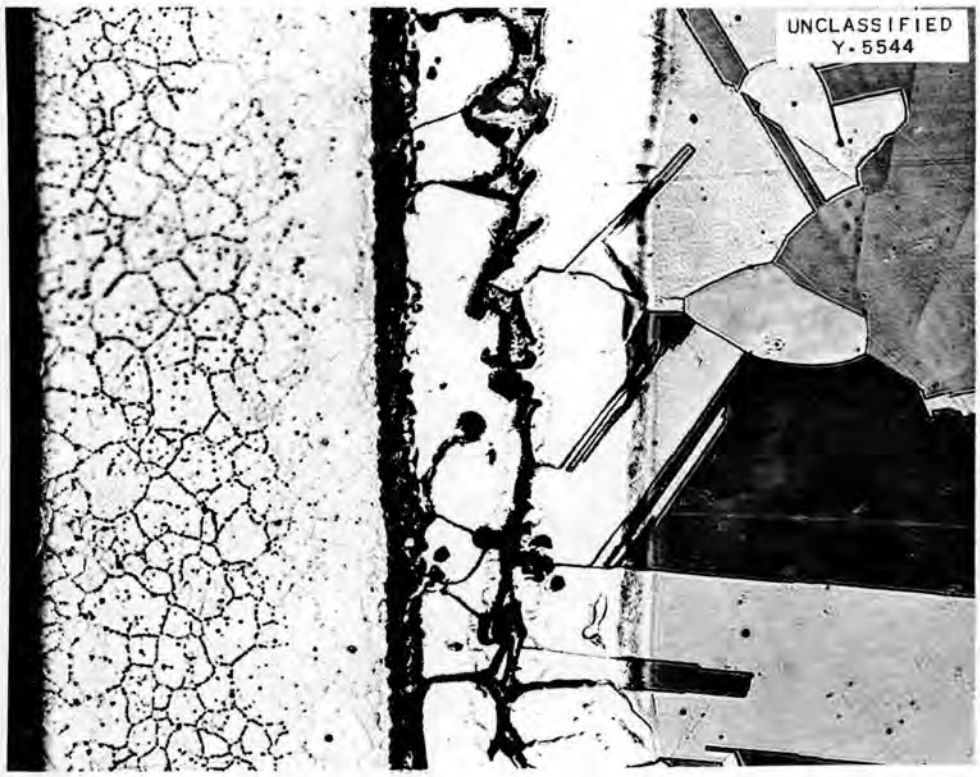

Fig. 130. Inconel Tube Brazed to Copper. Aqua regia and glycerin etch. 100X.

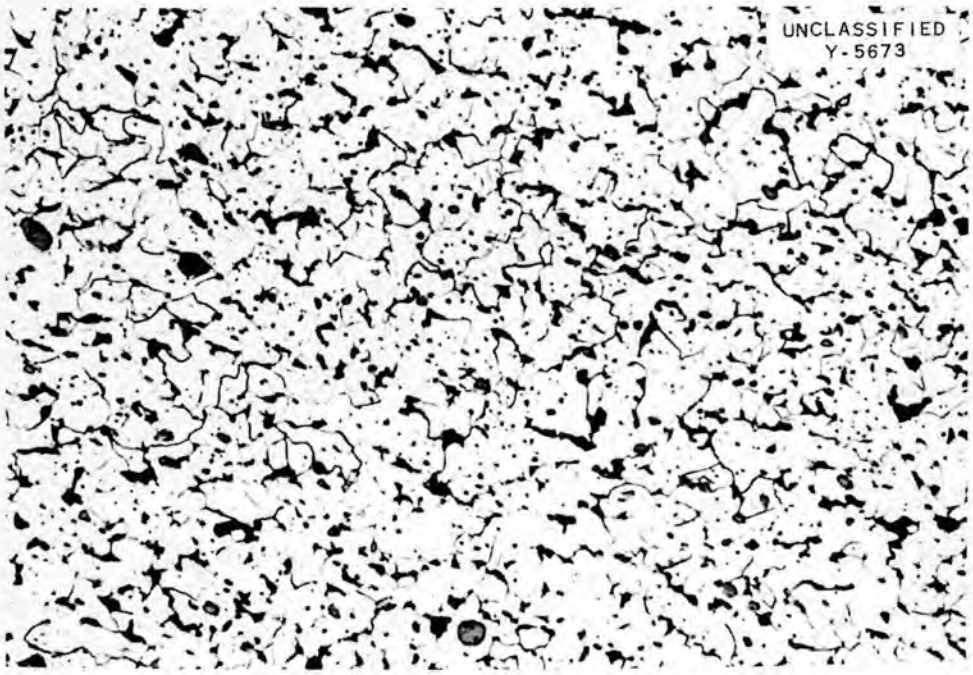

Fig. 131. Mild Steel Showing Dark Pearlite Patches in a Matrix of Alpha Ferrite. Note retention of grey, globular-shaped, MnS inclusions. Picral-nital etch. 250X.

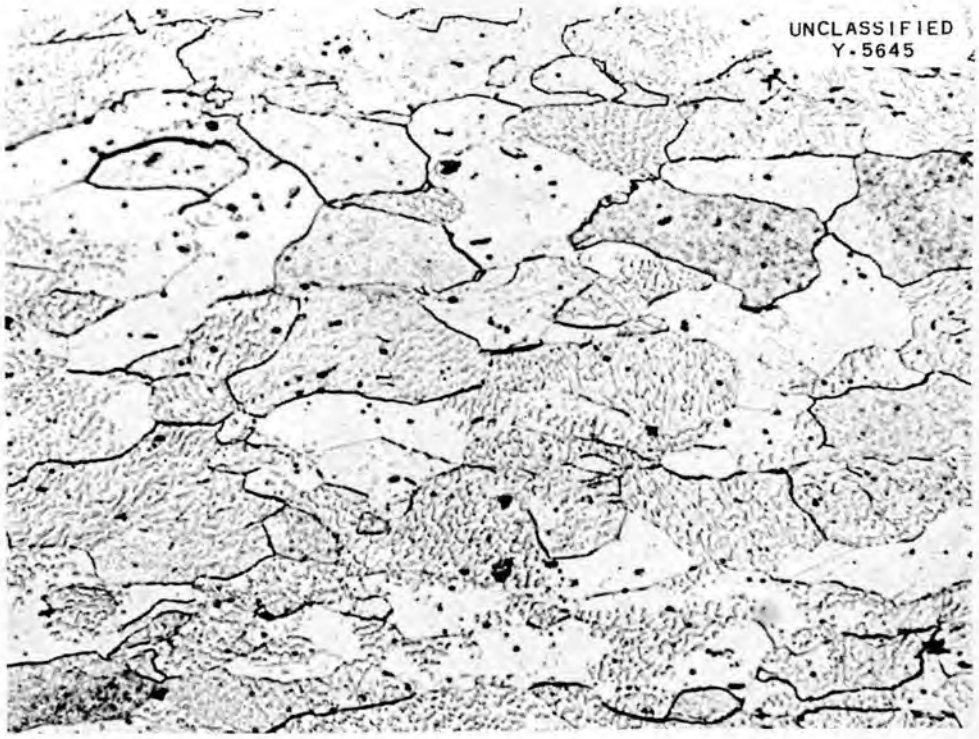

Fig. 132. Tungsten. Alkaline potassium ferricyanide etch. 250X.

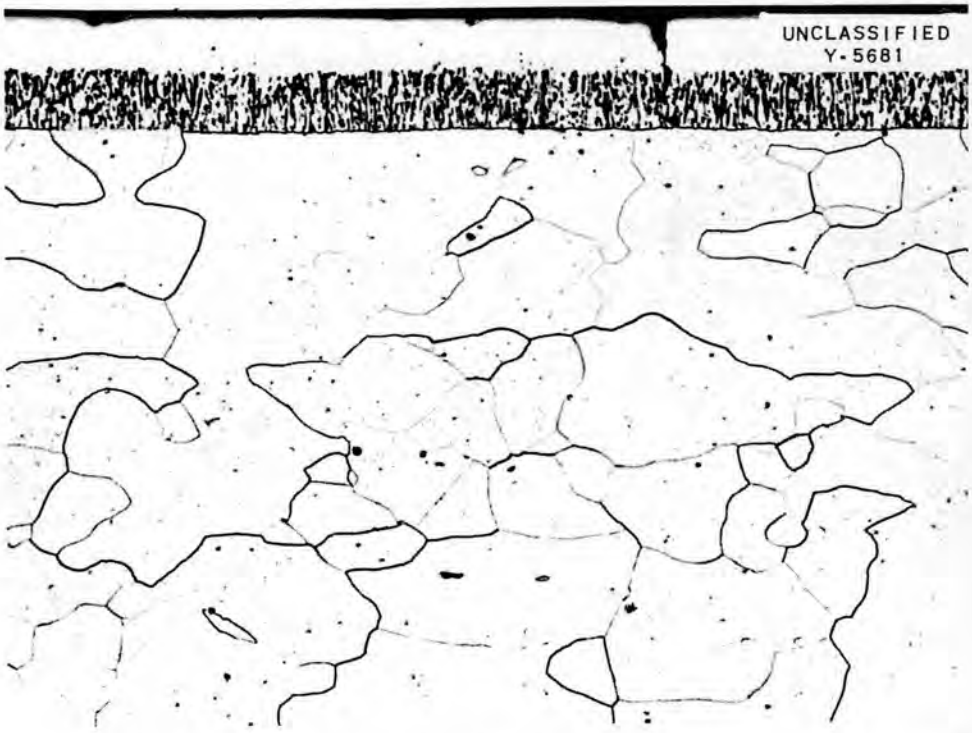

Fig. 133. Molybdenum with a Surface Layer of $MoSi_2$. Alkaline potassium ferricyanide etch. 250X.

FUEL PLATE DEVELOPMENT FOR GENERAL ELECTRIC

W. J. Leonard

Type-309 stainless steel sandwiches with cores of 25 wt % uranium oxide (UO_2) were used in the development of a suitable manufacturing process for the fuel elements for the proposed direct-cycle aircraft reactor. The samples, as received, were 2 3/4-in. squares, approximately 0.190 in. thick. The as-received samples had a perfect bond between cladding and core. The final desired thickness of the fuel elements was 0.012 to 0.016 inch. A two-high Mesta mill with rolls 20 in. in diameter and 30 in. wide of hardened, white, cast iron (primarily designed for hot-rolling work) was used.

The variables of temperature, reduction per pass, and ratio of hot work to cold work necessary in finishing to final dimensions were investigated and none were found to be critical. Temperatures could vary from 1950 to 2150°F during hot rolling with reductions per pass from 10 to 40%; the ratio of hot to cold work should be the maximum obtainable. Figure 134 shows the core of the as-received sample, and Fig. 135 shows a specimen hot rolled to 0.035 in. that exhibits the average structure after hot rolling to the minimum practical size (corresponding to about 80% reduction in thickness by hot working).

The plates were then cold rolled various amounts, as shown in Fig. 136. More than 30% reduction in thickness by cold working put the oxide particles in an undesirable condition and strain hardened the steel to such an extent that any further rolling without annealing would be difficult. Cleaned, hot-rolled specimens, 35 mils thick, were cold rolled to 0.025 in. (approximately 30% cold work), bright annealed at 1950°F, further cold worked to 0.018 in., bright annealed again, and cold rolled to the minimum possible thickness (0.015 in.) on the mill. Figure 137 shows the final specimen, which is considered to be in a satisfactory condition. The amount of steel at the edges is about 30 mils (average) in the finished sheet. Cold rolling below 22 mils would be very difficult and time consuming with the mill used for this work.

The following is a final, recommended schedule for rolling these samples at a furnace temperature of 2150°F with a controlled atmosphere:

1. Hot roll to approximately 0.065 in. in four passes at 30% reduction per pass with 1 hr preheat and 10 min reheat between passes;

2. Continue rolling to approximately 0.035 in. in three passes at 20% reduction per pass with 10 min reheat between passes;

3. Clean in salt bath containing "virgo" salt by using proprietary Hooker process with acid cleaning and a hot water rinse;

4. Cold roll to approximately 0.025 in. by taking the maximum possible reduction per pass (seven or eight passes required);

5. Bright anneal at 1950°F for 4 hr and cool rapidly to room temperature, clean if necessary;

6. Cold roll to approximately 0.018 in. by taking the maximum possible reduction per pass (seven or eight passes required);

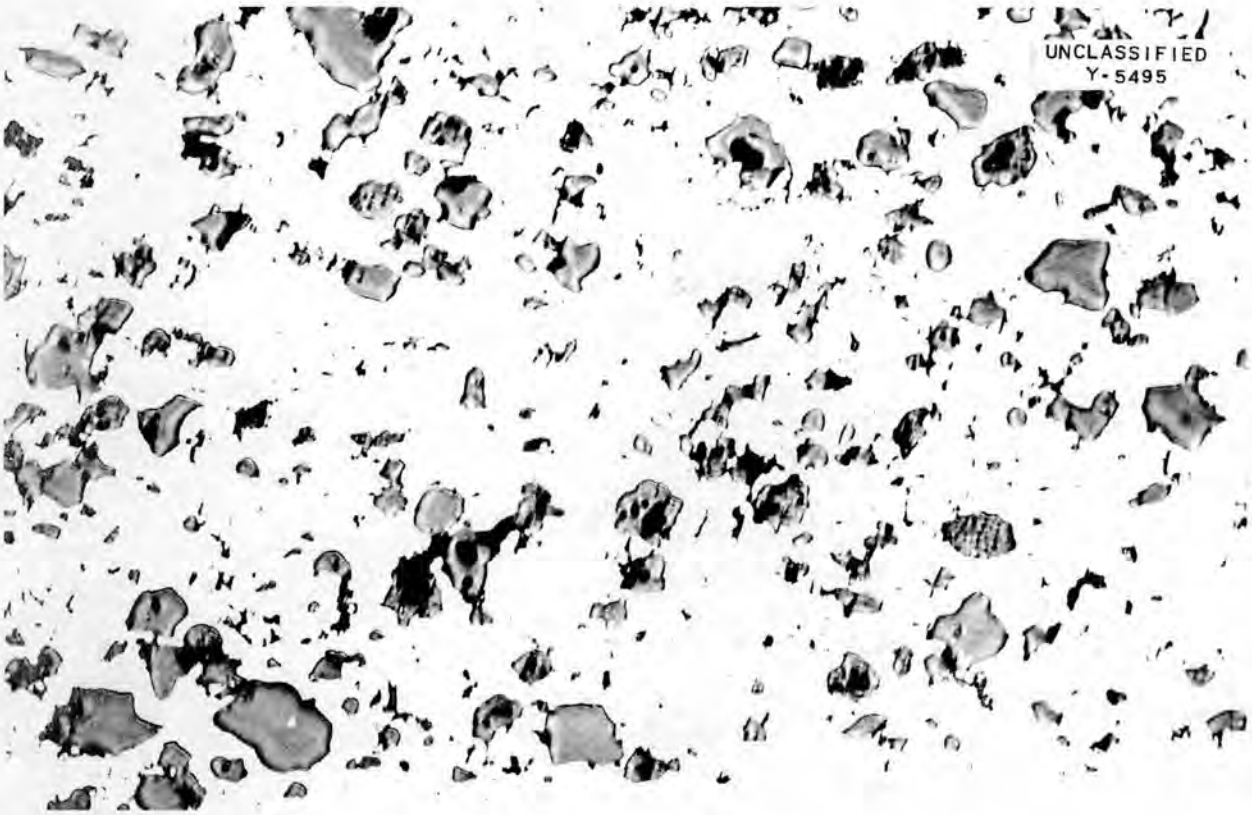

Fig. 134. **As-Received Stainless Steel Sandwich.** Specimen No. 3897. 200X.

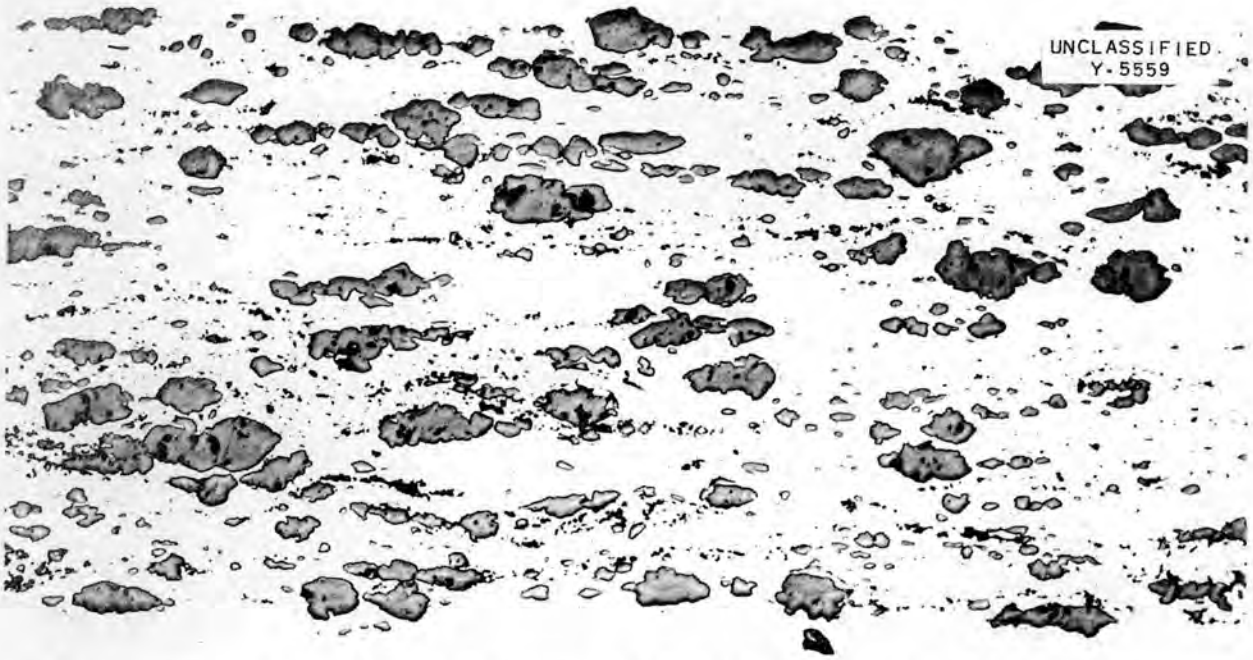

Fig. 135. **Effect of Hot Rolling on Stainless Steel Sandwich.** Specimen No. 3984. 200X.

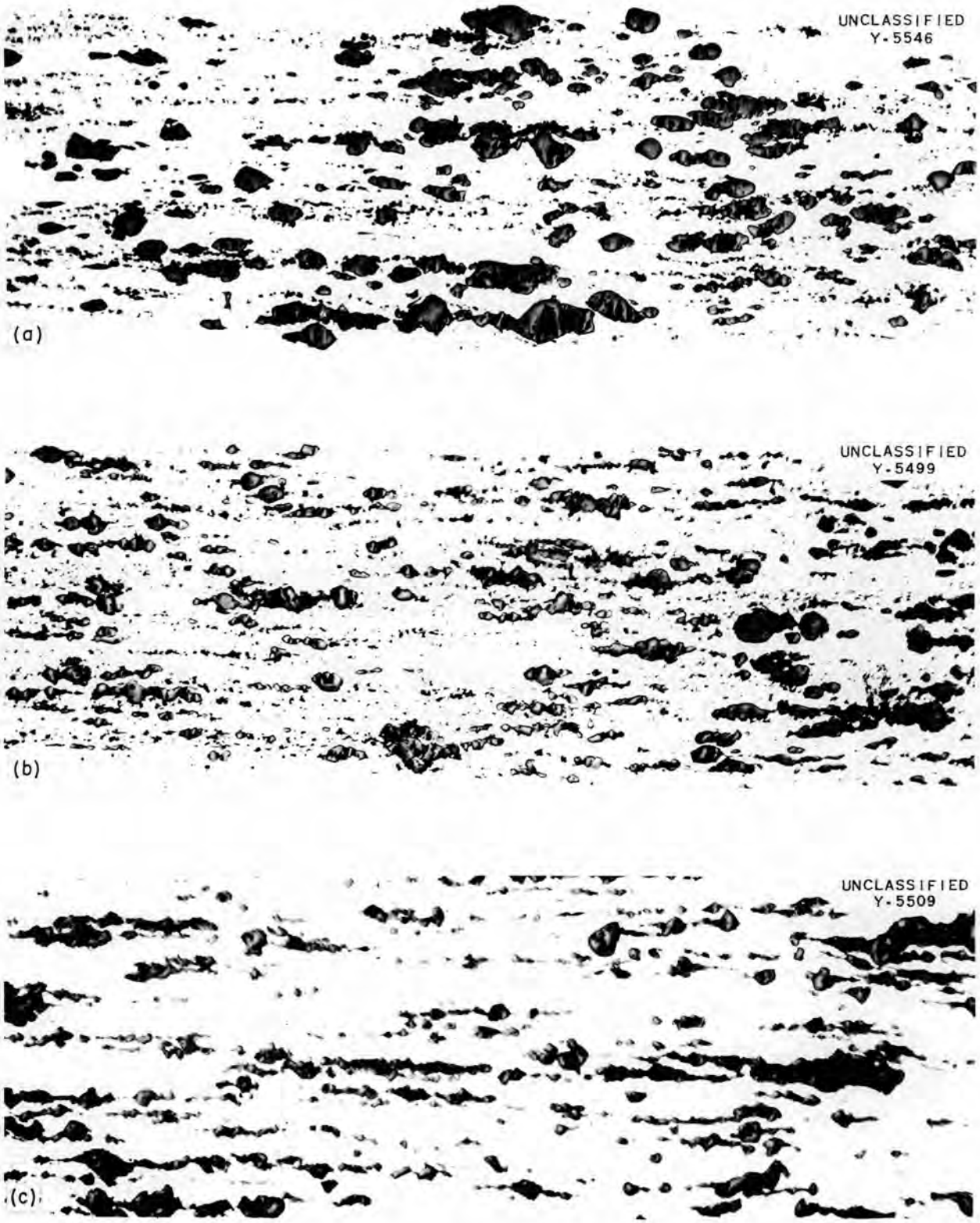

Fig. 136. Effect of Total Cold Reduction on Stainless Steel Sandwich. (*a*) 30%, (*b*) 45%, (*c*) 65%. 200X.

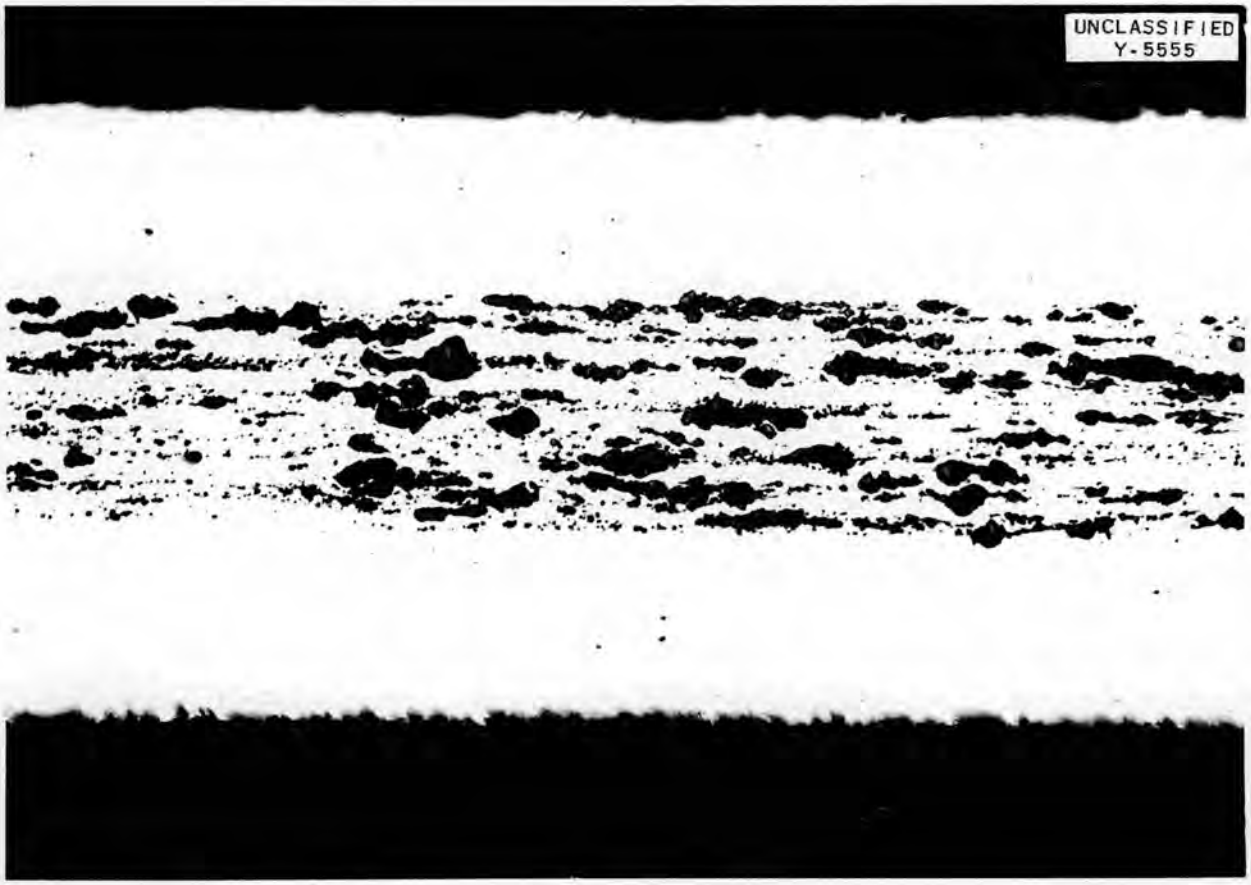

Fig. 137. Stainless Steel Sandwich 30% Cold Worked plus Annealed plus 24% Cold Worked plus Annealed plus 17% Cold Worked. Specimen No. 3979. 200X.

7. Bright anneal at 1950°F for 4 hr and cool rapidly to room temperature, clean if necessary;

8. Pack roll[1] two strips of 18 mils thickness to 0.014 inch;

9. Bright anneal, acid clean to remove any scale, hot water rinse, and degrease in "degreasol" bath.

(1) Simultaneous cold rolling of two strips together to desired dimension.

MTR FABRICATION

J. E. Cunningham R. J. Beaver
J. F. Delaney

FUEL UNIT AND CONTROL ELEMENT FABRICATION

Work in the metallurgy shop on the fabrication of fuel units and control rods for the MTR at Idaho continued. Twelve enriched uranium-aluminum alloy melts were prepared and fabricated into standard fuel plates. Thirty-one additional fuel units and four fuel sections for the shim-safety control rods were assembled and brazed according to specifications. Seventy-five units are now on hand and awaiting the arrival of sound end-box castings for completion. The spring, bevel ring, and snap retainer ring accessories are on hand.

In December, after repeated delays, the first shipment of 25 sets of the 356 sets of aluminum alloy end-box castings ordered were received from the Chemalloy Foundry Company. Visual and x-ray inspection revealed the presence of external cracks in 80% of the upper adapter castings and excessively large blow holes in the lower adapter castings. In many cases, the semipermanent mold (sand core) castings failed to conform properly to the mold. In January, another batch of castings, prepared with the new single-piece sand core, was received and inspected. Although the quality was somewhat improved, these castings were still not dimensionally acceptable for the intended use.

An emergency order was placed with the Aluminum Company of America for supplying the castings to prevent delaying start-up of the reactor in March. Procurement arrangements are complete and production is scheduled to start at the Cleveland Plant on February 4, 1952 and to be finished by February 16, 1952. If this foundry schedule can be met, there is an excellent possibility that the initial loading of 23 fuel units will be ready for shipment to the site on March 1, 1952.

Final machining and inspection work on nine cadmium shim control rods are in progress in the machine shop. Four completed rods are enroute to the site for pre-operational hydraulic and mechanical tests.

Containers for shipping both the fuel units and control rods to Idaho have been designed and constructed. Five control rod and ten fuel unit boxes are required to ensure continuous delivery of the reactor components to the site.

Both types of boxes are of wood encased in an angle-iron frame work. The control rod box is reinforced over the entire 14-ft length with a Tee section cut from an I beam to prevent loss of critical alignment during shipment. Each control rod box will carry two elements. The fuel unit box is designed to carry six units and has a built-in 0.040-in.-thick layer of cadmium, which is a safety feature in the event that several of the boxes were accidentally flooded with water. All shipments will be confined to less than 1 kg of U^{235}.

An over-all inventory has been completed on the first 9 kg of enriched metal processed. The accounting showed a gain of 0.36%. Balance was obtained only after all the graphite tools (crucibles, stirring, and sampling rods) used in preparing the melts were

leached and the dross dissolved for recovery of uranium. In spite of the fact that copper is being plated out prior to making the uranium determination, the chemical analysis data are running slightly higher than the intended melt composition, which can in part, if not totally, account for the recorded gain.

CLADDING OF THORIUM WITH ALUMINUM

Development work started on the problems of cladding thorium with aluminum for production of U^{233} by irradiation in the MTR. The problem is complicated by the fact that thorium exhibits a high chemical affinity for the nuisance gas, oxygen, and that at least two intermetallic compounds are present in the thorium-aluminum phase diagram. Several test billets were jacketed by various techniques and hot-rolled into alclad plate.

Preliminary inspection results are extremely encouraging – they indicate that a satisfactory metallurgical bond can probably be obtained for service in the MTR. Coupons cut from a test billet hot-rolled at 500°C with a total reduction in thickness of 20 to 1 appeared to possess a good bond over the flat area. The coupons withstood repeated 360-deg bend tests and showed good resistance to parting when chiseled.

The steps taken in preparation of the billet, prior to hot rolling, were:

1. mechanical removal of the surface oxide film,
2. immediate jacketing in an aluminum picture frame and cover,
3. welding and evacuating through attached tubular extension,
4. sealing and rolling.

Figure 138 shows a typical photomacrograph of a transverse section of the alclad thorium sample. Figure 139 is a photomicrograph of a similar section. As can be seen, the bond is continuous and an intermetallic compound, approximately 0.0002 in. thick, is present at the aluminum-thorium interface. The thickness of aluminum cladding on this particular sample is 11 mils. Test results on the other samples are incomplete.

SERVICE WORK

Boral Rolling. Alclad boral shielding material was fabricated for several AEC installations. Boral (50 wt % mixture of boron carbide and aluminum) ingots are prepared at Y-12 and forwarded to the metallurgy shop for cladding and rolling to the desired dimensions. Cladding is accomplished by hot-rolling at 1000°C with a total reduction in thickness of 6 to 1. Orders for the following were completed: eight of the remaining 20 sheets (26 by 108 by 0.250 in.) on order for Hanford, 20 strips (4 by 30 by 0.040 in.) for KAPL, and ten sample sheets (27 by 120 by 0.250 in.) for CP-5 at ANL.

Uranium Rolling. Three hundred and fifty pounds of normal uranium metal was rolled from bar stock into sheet of 10, 31, and 62 mils in thickness for cyclotron bombardment tests at UCRL. Also, several sheets of thorium metal were prepared and shipped to UCRL.

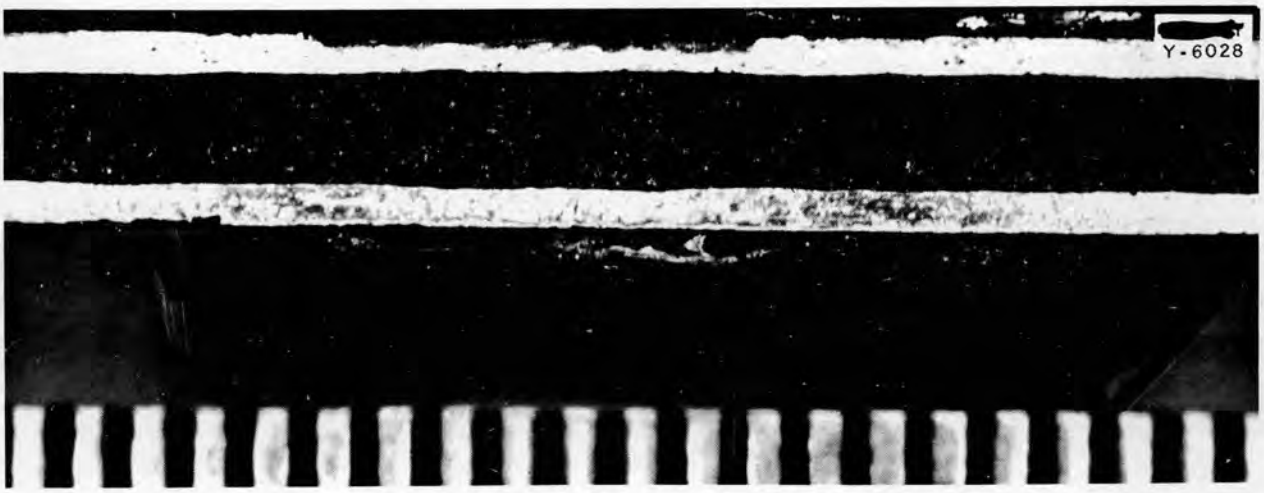

Fig. 138. Transverse Section of an Alclad Thorium Sample Showing Thickness of Aluminum Cladding. Aluminum appears white; thorium appears black. 27½X.

Fig. 139. Transverse Section of an Alclad Thorium Sample Showing Continuous Bond and Intermetallic Compound at Aluminum-Thorium Interface. Aluminum appears white. Alcohol and perchloric etch. 1000X.